Sayyad Nojavan
Kazem Zare *Editors*

Demand Response Application in Smart Grids

Operation Issues - Volume 2

Springer

Demand Response Application in Smart Grids

Sayyad Nojavan • Kazem Zare
Editors

Demand Response Application in Smart Grids

Operation Issues - Volume 2

Springer

Editors
Sayyad Nojavan
Department of Electrical Engineering
University of Bonab
Bonab, Iran

Kazem Zare
Faculty of Electrical and Computer Engineering
University of Tabriz
Tabriz, Iran

ISBN 978-3-030-32103-1 ISBN 978-3-030-32104-8 (eBook)
https://doi.org/10.1007/978-3-030-32104-8

This Springer imprint is published by the registered company Springer Nature Switzerland AG
The registered company address is: Gewerbestrasse 11, 6330 Cham, Switzerland

Preface

After restructuring and deregulation of the electricity industry, it is stated that the power system will be more efficient if the differences between peak and low load periods are kept as small as possible. It has been demonstrated that the perfect balance between the supply and demand in the real time is necessary for a reliable operation of electricity system. Demand response program is defined as changes in electric consumption patterns of end-user clients in response to changes of electricity price over time or to incentive payments designed to decrease high electricity usage at high wholesale market prices times or when the system reliability problems occur. In other words, the procedure through which consumers respond to the price signals inserted in tariffs by changing their consumption patterns is called the demand response programs (DRPs). Moreover, DRPs can help the independent system operator (ISO) to reduce the price volatility during peak demand hours. Different DRPs can be classified into two main categories: incentive-based programs (IBPs), which are further divided into classical programs and market-based programs, and price-based programs, (PBPs), which are based on the dynamic pricing rates in which the electricity tariffs are not flat. The rates fluctuate following the real-time cost of electricity. The ultimate objective of these programs is to flatten the demand curve by offering a high price during peak periods and lower prices during off-peak periods. These rates include the time of use (TOU) rate, critical peak pricing (CPP), extreme day pricing (EDP), extreme day CPP (ED-CPP), and real-time pricing (RTP). The basic type of PBP is the TOU rates, which are the rates of electricity price per unit consumption that differ in different blocks of time. The rate during peak periods is higher than the rate during off-peak periods. The simplest TOU rate has two time blocks: the peak and the off-peak. The rate design attempts to reflect the average cost of electricity during different periods. The CPP rates include a pre-specified higher electricity usage price superimposed on TOU rates or normal flat rates. CPP prices are used during contingencies or high wholesale electricity prices for a limited number of days or hours per year. On the other hand, EDP is similar to CPP in having a higher price for electricity and differs from CPP in the fact that the price is in effect for the whole 24 h of the extreme day. Furthermore, in ED-CPP rates, CPP rates for the peak and off-peak periods are called during extreme

days. RTPs are the programs in which the customers are charged hourly fluctuating prices reflecting the real cost of electricity in the wholesale market. RTP customers are informed about the prices on a day-ahead or hour-ahead basis. Many economists are convinced that RTP programs are the most direct and efficient DRPs suitable for competitive electricity markets and should be the focus of policymakers. In other words, PBPs have a wide range of planning horizon from a few minutes to many years. DRP can be categorized into long-term, midterm, and short-term programs based on their planning intervals. Programs with more than a day period are long-term or midterm programs. Finally, this book seeks to analyze economic and technical effects of demand response programs in smart grids in operation issues.

Bonab, Iran Sayyad Nojavan
Tabriz, Iran Kazem Zare

Contents

Chapter 1
Smart Grids and Green Wireless Communications

Farzad H. Panahi and Fereidoun H. Panahi

Nomenclature

AMI	Advanced metering infrastructure
AP	Access point
BS	Base station
CR	Cognitive radio
D2D	Device to device
DR	Demand response
DSM	Demand-side management
EE	Energy efficiency
EH	Energy harvesting
FQL	Fuzzy Q-learning
FSL	Fuzzy SARSA learning
GA	Genetic algorithm
GHG	Greenhouse gas
HetNet	Heterogeneous network
HPPP	Homogeneous Poisson point process
ICT	Information and communications technology
IoT	Internet of things
LTE-A	Long-term evolution advanced
M2M	Machine to machine
MNO	Mobile network operator
NE	Nash equilibrium
OPEX	Operational expenditure
PLC	Power line communications
PSM	Power saving mode

F. H. Panahi (✉) · F. H. Panahi
Department of Electrical Engineering, University of Kurdistan, Sanandaj, Kurdistan, Iran
e-mail: f.hpanahi@uok.ac.ir

S. Nojavan, K. Zare (eds.), *Demand Response Application in Smart Grids*,
https://doi.org/10.1007/978-3-030-32104-8_1

QoS	Quality of service
RES	Renewable energy source
RPS	Renewable power supplier
SEP	Smart energy profile
SG	Smart grid
SGFAN	Smart grid field area network
SGHAN	Smart grid home area network
SGNAN	Smart grid neighborhood area network
SGWAN	Smart grid wide area network
SINR	Signal to interference and noise ratio
UDN	Ultradense network
UE	User equipment
UMTS	Universal mobile telecommunications system
WSN	Wireless sensor network

1.1 Introduction

In a traditional electric grid, the main causes of power inefficiency are high-voltage, long-distance transmission, and large-scale centralized electricity generation [1]. To improve the power efficiency and reliability of the grid, the concept of smart grids (SGs) has been proposed by using information and communications technology (ICT). Demand response (DR), decentralized power generation, demand-side management (DSM), and price signaling are the key characteristics of a SG associated with green wireless communications. With DR and DSM, both power generators and consumers can interact to optimize the process of power supply and consumption. The power generation may be performed by small distributed power plants (e.g., small wind turbines and solar panels) and consumers using decentralized design. Therefore, this could help consumers to be less dependent on the main electrical grid. With price signaling, the consumers will know about the present power price. Moreover, the generators can encourage consumers to consume electrical energy when the demand is low, i.e., during the off-peak period, by giving them a lower price for electricity during those times. This will result in a lower investment for the infrastructure as the peak load will be reduced.

In recent years, the integration of wireless communications and SGs has attracted a significant research attention [2]. On one hand, wireless communication technologies will play an essential role in the revolution of SGs by communicating a variety of data and measurement over all nodes of the electrical grid. On the other hand, for a better power usage when providing a wireless service to mobile units, SGs can be used to support green wireless communications. In wireless networks, each wireless base station (BS) powered by a SG might be selfish in optimizing its own operation in terms of capacity or quality of service (QoS). In this chapter, how to design energy-efficient communication infrastructures without negative effects on the

performance is one of the main concerns. Indeed, the problems of power management, cost-function analysis, optimal network design, energy-harvesting (EH), and energy-efficient strategies are considered for green-powered communication networks in a SG environment and, in particular, we attempt to focus on efficient interaction between the RPS's random green power generations and the BS's dynamic of energy consumption via minimization of an energy-based cost function, considering the D2D and M2M impacts on efficient utilization of energy and bandwidth. In general, due to the unlimited growth of service demands and high load traffic, a green wireless communication system is considered with the aim of decreasing energy consumption of heterogeneous networks (HetNets). This system provides a proportion of required energy of BSs by employing some renewable power suppliers (RPSs), while user equipment (UE) and sensor nodes especially benefit from short device-to-device (D2D) and machine-to-machine (M2M) links as a promising technique to design energy-efficient HetNets.

1.2 Demand-Response Power Consumption Model

To meet today's rapid proliferation of data traffic, the cellular network operators are recently installing more and more BSs. As a result, the daily power cost adds up to a huge bit of the operational expenditure (OPEX). Therefore, the need for cellular operators to implement new energy-efficient solutions is critical in order to lower their energy costs [3–6]. In general, energy-efficient solutions can be employed by managing either the power supply or the data-traffic demand. On the supply side, energy-harvesting technologies, such as wind turbines and solar panels, at the BSs are considered as one of the most commonly adopted solutions. Using energy-harvesting devices, BSs can consume clean and affordable renewable energy to decrease or even substitute the energy purchased from the grid. It is clear that the power grid, as a reliable energy source to BSs, is still required. This is because the renewable energy is not always available when needed, and it is mainly distributed in both time and space in a random way. As a result, different BSs are hard to solely rely on the uncertain supply to power their units.

Power grid, in addition to being a reliable energy supply, can offer new capabilities for the BSs' cost-saving with its ongoing transformation from conventional grid to SG. A SG differs from the conventional grid in that it allows two-way data and energy flows between the grid and end users by deploying smart meters at end users, rather than a one-way flow. Energy cooperation in cellular networks, which allows the BSs to trade and share their harvested energy to support the nonuniform data traffic in a cost-effective way, will then be possible through the two-way delivery of energy-information flow in SG. On the demand side, to lower the energy consumption, different methods have been proposed across various layers of protocols for data transmission. Among these methods, communication cooperation, which enables the BSs to share the wireless resources and shift the traffic loads with each other, is the most appealing. However, the use of renewable energy sources at BSs

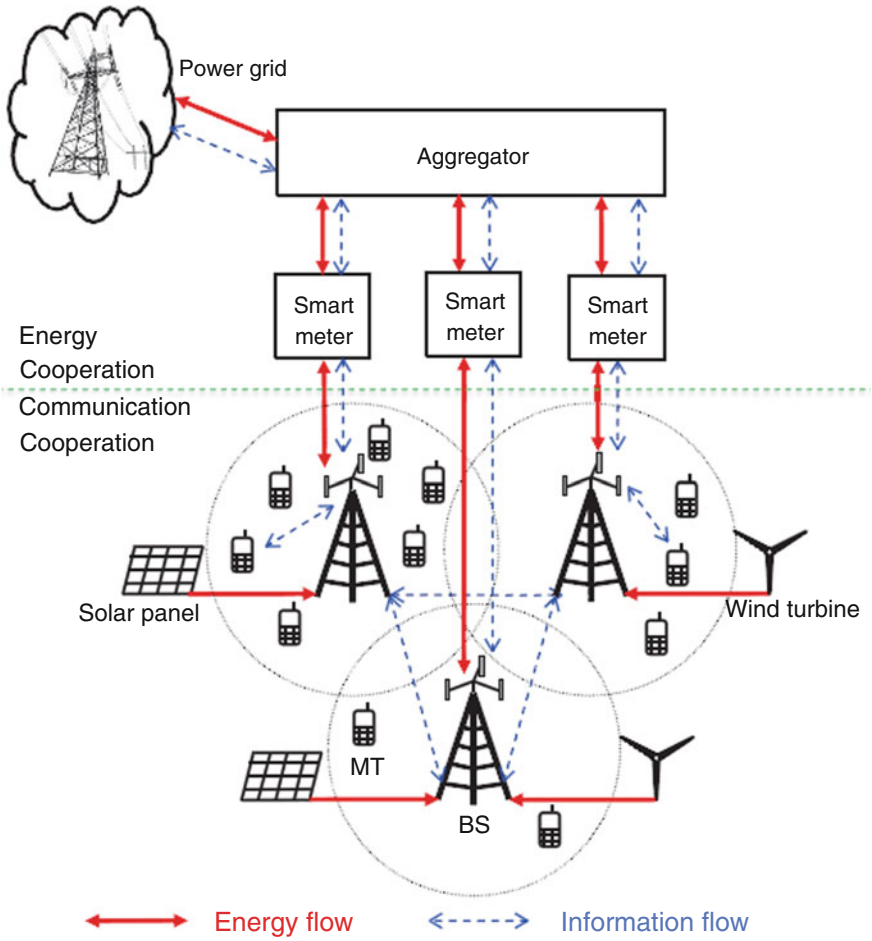

Fig. 1.1 A general model for integrated smart grids and green wireless communications [3]

would lead to a variety of new problems and challenges in the current communication cooperation design: the conventional design to save energy may no longer be cost-effective. In fact, although renewable energy is unreliable in supplying energy, in general it is way cheaper than the energy purchased from the grid and thus BSs should maximally harvest renewable energy to lower cost. However, under the energy-saving design, the harvested energy at BSs may not be efficiently exploited when serving a time-variant traffic load. To tackle this issue, the design of novel cost-aware communication cooperation schemes is desirable. This can be done by taking into consideration the cost differences between conventional and renewable energy sources [3]. In Fig. 1.1, we can see the general energy and communication cooperation model for cellular networks at the power supply and the communication demand layers, respectively.

1.3 Energy-Efficient Communication Infrastructures

In wireless networks, consisting of battery-powered nodes such as sensor nodes or mobile phones, energy efficiency (EE) has always been under consideration. However, until recently, the EE of network equipment powered from mains such as switches, routers, and BSs has not been caught in the spotlight of attention [7]. With the growing number of subscribers and their ever-increasing energy demands, electricity bills of service providers have been skyrocketing. Therefore, to reduce the energy consumption of core and access network equipment, significant efforts have been made in both academic and industrial projects. Besides the energy costs, the high level of greenhouse gas (GHG) emissions coming from the communication networks is expected to increase the expenses and costs of the operators with the forthcoming carbon taxes and caps. To lower energy costs and electricity bills, the communication infrastructure can employ the price-following demand management of SG. Indeed, on one side, the way energy-efficient communication technologies are implemented is influenced by SG-driven schemes. On the other side, SG is impacted from EE techniques as it involves dense communications.

In terms of communication coverage and functionality, we can roughly divide the SG into three interconnected communication networks: SG home area network (SGHAN), SG neighborhood area network (SGNAN), and SG wide area network (SGWAN). SGHAN basically corresponds to a network of signal-controlled appliances, consumer devices, and energy management devices. This will enable connected devices to send/receive signals from meter, displays, and other home management devices. Indeed, SGWAN covers home area monitoring, regulation, control, and management. SGNAN is applicable for distributed generation and distribution automation, and it is related to a group of houses possibly fed by the same transformer. SGWAN shelters SGHAN and SGNAN for monitoring and control of the entire communication network. SGWAN is a gigantic network covering the management of generation, transmission, distribution, and utilization of the entire grid. The communication facility for the electricity distribution systems is also formed by a SG field area network (SGFAN), which operates as a bridge between customer premises and substations. Since the geographical scale of a SGFAN is similar to SGNAN, similar communication techniques can be considered for both of them. A variety of communication technologies can be used to implement these network domains. For example, because of their wide-coverage fiber-optic, universal mobile telecommunications system (UMTS), long-term evolution (LTE)/LTE-advanced (LTE-A) can be more applicable for SGWAN, while IEEE 802.11 and IEEE 802.15.4 power line communications (PLC) could be more appropriate for SGNAN and SGHAN. The authors in [8] present a profound research on routing protocols and applications in the related fields. Generally, wireless communications have a broad range of applications in the SG including demand management, substation, meter data collection, and power line monitoring and protection. In the following subsections, wireless technologies that are applied in SGWAN, SGNAN, and SGHAN are described, respectively.

1.3.1 Energy-Efficient SGWAN

The EE, in wireless communications, is generally defined as the ratio of the total achievable data rate to the total power consumption, and it is quantified by the "bits-per-joule" metric [7]. The EE of OFDMA as the common multiple access scheme for 3G, 4G, and WIMAX networks has been studied in several works. Note that 3G, 4G, and WIMAX stand as strong candidates for SGWAN. An energy-efficient rate adaptation and resource allocation approach has been presented in [9]. Multiple input multiple output (MIMO) is another technique that is common in 3G, 4G, and WIMAX. In MIMO, higher throughput is often achieved at the cost of using more antennas and therefore higher circuit power consumption. The authors in [10] propose a selective model of active antennas in order to improve EE for MIMO according to the daily profile of traffic loads. In a SG environment, the implications of adaptively changing the number of antennas have been explored. Note that the effects of this adaptive approach on the performance of SG applications still remain as an essential challenge.

Finally, according to the IEEE 802.22 standard, cognitive radio (CR) is a technology that allows unlicensed users to access the blank frequency bands. Based on the concept of CR, underutilized resources that are facing scarcity are being used by unlicensed secondary users opportunistically when the primary users (licensed user) are idle, i.e., when the channels are not occupied by primary users. Thus, the spectrum is maximized and the channels are vacated before the primary users arrive since they have higher priority. The authors in [11] have suggested a CR network that senses not only the radio-frequency bands but also the SG resources. Under real-time pricing, the operating cost of the CR network is optimized. More specifically, BSs manage their power consumptions over the related cells according to the electricity costs. Although the main focus of those studies has not been energy conservation, they are providing a combinational model of CR networks and SG concepts. To this end, EE of CR has been investigated in [12]. The effects of EE techniques on the QoS of SG data and other related challenges in energy-efficient communications have been discussed in [7] as well.

1.3.2 Energy-Efficient SGNAN

SGNAN, one of the important fields, carries large volumes of data that come from heterogeneous data sources and supports a large number of devices. Indeed, 3G, 4G, and WIMAX can also be exploited in the SGNAN as they are strong candidates for SGWAN. In addition, promising deployments for urban SGNANs are offered by the IEEE 802.11 family of standards. Recently, power saving mode (PSM) has been adopted by several IEEE 802.11 standards in their operations. PSM is utilized by IEEE 802.11b and IEEE 802.11s to enable sleep mechanisms for wireless nodes when they are not in active mode, i.e., when they are not transferring data. IEEE

802.11b is also preferred for SGHANs because it is widely used for residential premises, while IEEE 802.11s, the mesh standard, is defined as a promising solution for electric vehicle networks. In [13], the authors consider an admission control scenario for electric vehicles to study the performance of IEEE 802.11s. In fact, PSM can be used for SGNAN communications; however, one bottleneck of the PSM is the extra delay which is the common issue in all sleep/wake-up mechanisms [14]. Because of this, it is necessary to further explore the impacts of PSM on the SG operation [7].

1.3.3 Energy-Efficient SGHAN

In general, ZigBee is considered a widely adopted protocol for home automation and smart energy standards in SGHANs. Recently, there exist different types of ZigBee-certified products for home automation. Some of the leading smart meter vendors have manufactured ZigBee-enabled smart meters. In addition, smart energy profile (SEP) has been developed by ZigBee Alliance to support the needs of smart metering and advanced metering infrastructure (AMI) and connects utilities and household devices. Indeed, ZigBee is a new technology of short-range, low complexity, low power consumption, low-cost, and duplex wireless communications that is based on the IEEE 802.15.4 standard. Initially, ZigBee was defined for power-constrained sensor networks; thus, EE is an intrinsic property of ZigBee. The authors in [15] propose to use a ZigBee-based wireless sensor network (WSN) for demand management in the SGHAN. Another strong candidate for wireless SGHAN communications is Wi-Fi. The use of Wi-Fi-enabled sensors in the SG has been researched in [16]. Particularly, it is expected that newly emerging ultralow-power Wi-Fi chips increase the adoption of Wi-Fi for WSNs and increase their interoperability at SGHAN. There is abundant literature relating to energy saving and EE in WSNs; however, those works are out of the scope of this chapter because they are independent of SG concepts such as demand management and dynamic pricing. Besides ZigBee and Wi-Fi, cellular technologies are also able to provide data-transmission links among residential premises distributed over small cells. To lower the energy consumption of the transmitters in SGHAN, femtocells and indoor picocells can be used as they are more energy-efficient than macrocells [17]. It should be noted that the total power consumption of a cellular network can be reduced by up to 60% in urban areas using the joint deployment of macro- and residential picocells. Moreover, the growth of small cell density and ultradense networks (UDNs) will increase the EE [18]. As a result, implementing small-cell-based SGHANs provides energy-efficient wireless communications [7].

1.4 Green Communications Model to Support Smart Grids

As already stated, due to the rapid growth of subscribers and the traffic loads, power consumption of the networks is rising [19]. Indeed, the main issues in correspondence to the rise in the number of sensors and devices need to be responded through an improvement in EE. The traditional networks provide capacity enhancement by focusing on the transmission power. However, such strategy is not always applicable from the economic perspective of the mobile network operators (MNOs). Therefore, modernization of cellular networks with green strategies is one of the most important goals which is realized by the 5G networks and the networks thereafter. This goal is met by reducing the power consumption which is not related to information transmission directly. The 5G green strategies which allow minimization of power consumption can be observed in Fig. 1.2.

Since the highest proportion of energy is consumed by the BSs, some practical strategies should be investigated in order to reduce power consumption and achieve the desired demand response without ignoring the acceptable QoS [20]. Meanwhile, employing renewable energy sources (RESs) has been suggested to reduce the overall grid energy consumption of HetNets, where the user equipment and machines are respectively allowed to use D2D and M2M communications to improve the capacity with little amount of energy in the presence of managing the interference [21]. In D2D communications, UEs are able to transmit information via direct links not through the BS, which offloads the traffic load of the core network. D2D users can either utilize different time/frequency resources from cellular ones (overlay mode) or reuse the same resources with them and transmit simultaneously (underlay mode) [22]. Considering environmental conditions and dependence on location and weather, the amount of supplied power of renewable power suppliers (RPSs) is variable. In addition, the reservation capacity of RPSs is limited. Thus, a proper controlling mechanism is essential for efficient power allocation. In addition,

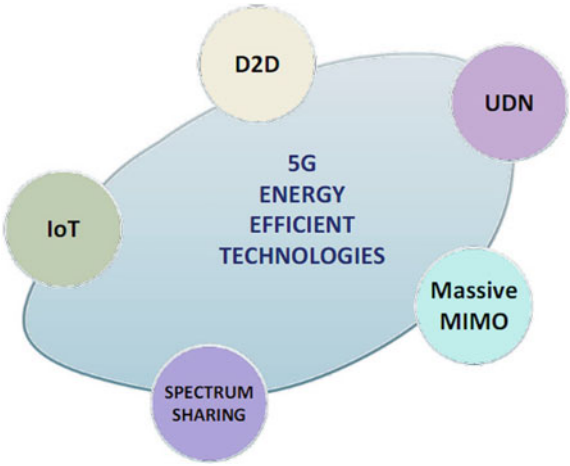

Fig. 1.2 Energy-efficient technologies for green wireless communications [19]

minimizing the cost function of both supply cost of RPSs and energy reservation cost of BSs is the other main criterion in the system design [23]. This system provides a proportion of the required energy of BSs by employing some RPSs, while UEs especially benefit from short D2D links as a promising technique to design energy-efficient HetNets. Indeed, according to our presented model, BSs are jointly powered via a renewable energy source and the electric grid (EG).

As stated, the factor of EE is critical to obtain the maximum performance of cellular networks, according to power consumption of the whole system. Prior researches have considered various conditions and applied different technologies to get a desirable level for EE. Due to the high power consumption of BSs, [20] presents an online algorithm where a BS is able to switch between on and off states based on traffic load. In order to manage and minimize power consumption of the BS, employing RPSs has been developed and some of the famous operators like Huawei and Ericson have started exploiting this technology to provide energy for the BS via these sources [24]. Some beneficial optimal strategies for BS's transmission were considered to reduce the amount of energy demand while considering the QoS requirements [25]. Due to the time-variant energy demands of a BS, article [5] showed that BSs are able to determine the amount of both used and reserved energies. Considering undeniable cost, the recent research in [26] presented a stochastic programming approach in order to minimize energy cost regarding BS's storage and utilizing RPSs. Ref. [23] proposes a new noncooperative game model to achieve an optimal strategy for decentralized allocating energy and minimize the cost of BS for reservation and RPS for supply based on the interaction between them. Indeed, using an M/M/G make-to-stock queue model, the impact of QoS on the energy supply rate of RPS and energy storage level was discussed. On the other hand, D2D communications in wireless cellular networks have attracted researcher's attention. D2D communication is a promising technique for improving the system performance with respect to reducing power consumption of BSs and increasing the whole network throughput. To get this aim, in [27] D2D communications and HetNets have been presented together for designing a future generation of systems in order to maximize the amount of spectrum reusing. Mobile association, as an important factor in choosing access points (APs) with the aim of balancing load distribution and providing the best performance, has been analyzed in [28]. Some practical strategies have also been investigated to provide energy-efficient resource allocation for D2D-aided networks. In [29], authors introduce a method for managing resources by employing a novel model called coalition game. A resource allocation technique based on the game and matching theory has also emerged to get maximum EE of users [30]. Energy harvesting (EH), as an efficient solution to overcome the limitation problem of battery capacity and lifetime, has been promoted recently which enables users to get the required energy from RPSs [31]. This will reduce the amount of power consumption of BSs. In [21], to perform the joint optimization of power control and resource allocation problem in a D2D-aided network using EH technology, authors provided an energy-efficient stable matching algorithm. In [32], an energy-efficient mobile association has been investigated to maximize the EE of networks by solving a joint optimization problem of AP selection, switching mode, and power control.

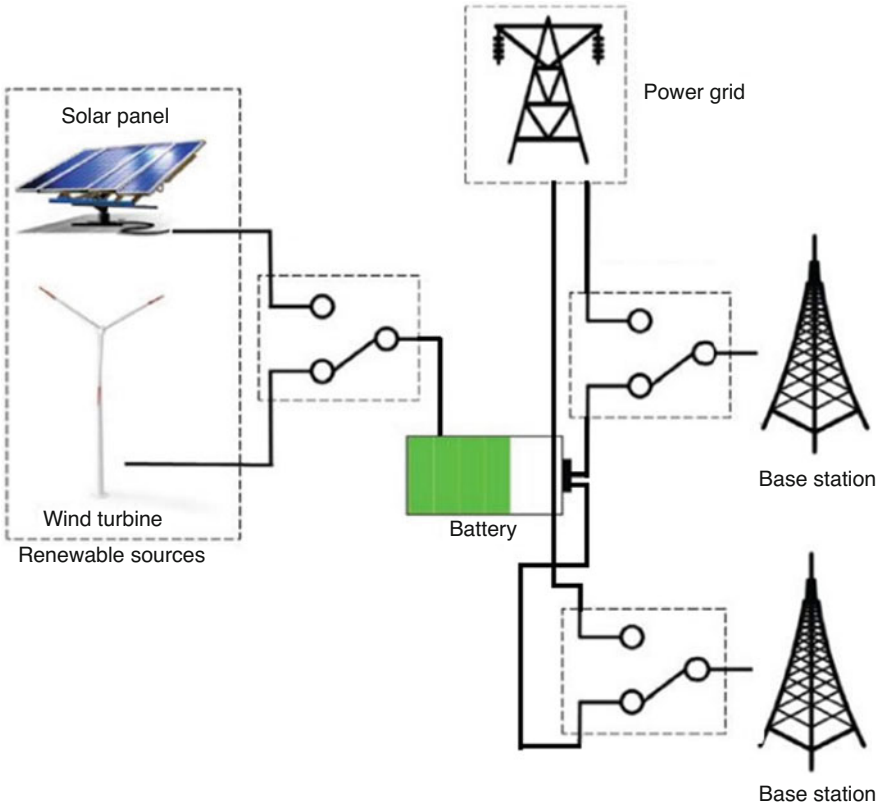

Fig. 1.3 Green-powered communication base stations

Moreover, we provide a green cellular model in which the BSs are jointly powered via RES and EG power sources. Indeed, we present the efficient interaction between the RPS's green power generations and the BSs' dynamic of power consumption via minimization of an energy-based cost function, considering the cache-enabled D2D impacts on efficient utilization of energy and bandwidth. The network performance takes into consideration the downlink (DL) connections as well. In this scenario, the system components are described in detail that refer to the renewable-energy-powered BSs and the power supplier consisting of EG and RPS (Fig. 1.3). The output power of the supplier is considered as random variable with mean η_s^0 (energy per time). Considering the finite capacity of the RPS, η_s is defined as the amount of supply rate of the RPS based on the RPS's production model in the BS's point of view $\left(\eta_s < \eta_s^0\right)$. Indeed, we analyze the power consumption of the BS in a wireless system that involves both static and dynamic parts such that it is related to the type of BS. In addition, estimation of the connection demands over a cell is possible due to the usage history. The connection demand is modeled as a stochastic homogeneous Poisson point process (HPPP) with rate λ_c (the number of connection

demands/unit time). Providing connection demand is due to the order of arrival connections that follows the first-come-first-served model, and E is defined as a unit of consuming energy of a BS in each connection in the DL mode. The energy storage unit of the BS should be charged by the green energy in order to respond to the D2D-aided network demands and provide mobile services. Thus, if the stored energy of the BS is not enough to achieve a desired QoS, the BS will compensate this shortage by requesting and reserving power from the RPS and consequently paying a specific price for each unit energy. The methods of reserving energy from RPS depend on the condition of renewable power production. As a result, the BSs are responsible for paying the cost C_{r} per unit time due to the holding energy in storage unit according to the desired energy level α.

Users in the HetNet can request popular contents from neighboring users through D2D communication, whereas they can also request contents from the BSs by the traditional cellular communication [33, 34]. Users may request files from a set of m files, named "library." We assume the BSs are aware of the stored files and channel state information of the users and control the D2D communications. For example, a user node u establishes a link with a certain BS when the user node u requests a file from the "library" of size m. Then, BS searches the requested file in the certain area where the user is located at the center point. If the file is found, BS allocates a frequency sub-band f_{D2D} for the D2D link between the user u and the user storing the file. Otherwise, user u receives the file through the traditional cellular network. Here, we also assume that users follow PPP with average intensity λ_{U}; that is, the probability that l users exist in the area S is

$$f(l;S) = \frac{(|S|\lambda_{\mathrm{U}})^{l}}{l!}\mathrm{e}^{-|S|\lambda_{\mathrm{U}}} \tag{1.1}$$

where$|S|$ means the area of district S. Denote the probability that a user stores the file i as p_i. Therefore, the file i is distributed with the PPP model with average intensity $\lambda_{UD}p_i$. Also, let r_d be a random variable representing the distance between the reference user requesting file i and the nearest user storing the file i. When $r_d > d$, there exists no user with file i in the area S ($|S| = \pi d^2$). Thus, the probability of the reference user successfully establishing a D2D link to deliver the desired file is

$$Pr(r_d \le d) = 1 - Pr(r_d > d) = 1 - f(0;S) = 1 - \mathrm{e}^{-\pi d^2 \lambda_{UD} p_i} \tag{1.2}$$

Obviously, only users without file i try to send the request to get file i. As a result, averagely, there are $\lambda_{\mathrm{U}}\left|\acute{S}\right|(1-p_i)$ users who may request file i in the network. $\left|\acute{S}\right|$ is the area of the cellular system. The probability that users cache the ith ranked file can be expressed as (Zipf distributions) [35]

$$p_i = \frac{(1/i)^{r_c}}{\sum_{j=1}^{m}(1/j)^{r_c}} \quad i = 1, 2, \ldots, m \tag{1.3}$$

where $r_c \geq 0$ is a parameter named skew coefficient and characterizes the distribution by controlling the relative popularity. Let q_i denote the probability that file i is requested by a user; the user request probability also follows the Zipf distribution [35]. Based on the above explanations, the number of activated D2D links for delivering file i is

$$n_i = \lambda_U \left|\acute{S}\right| (1 - p_i) q_i \left(1 - e^{-\pi d^2 \lambda_{UD} p_i}\right) \tag{1.4}$$

and the expected number of active D2D links for all files can be given by

$$N_{D2D} = \sum_{i=1}^{m} \lambda_U \left|\acute{S}\right| (1 - p_i) q_i \left(1 - e^{-\pi d^2 \lambda_{UD} p_i}\right) \tag{1.5}$$

A cellular link with the reference user is set up if establishing a D2D communication link is a failure. It implies that a traditional cellular link has to be established if the reference receiver cannot find the corresponding user who stores the desired file within the maximum transmission range of D2D links (d). Thus, the expected number of cellular links for all files (or the expected number of users who obtain their desired files from the cellular network) is

$$N_{Cellular} = \sum_{i=1}^{m} \lambda_U \left|\acute{S}\right| (1 - p_i) q_i \left(e^{-\pi d^2 \lambda_{UD} p_i}\right) \tag{1.6}$$

1.5 Energy-Cost Analysis

Considering one time unit for each connection with one unit energy consumption, in the presence of a backlogged access where the BS is not able to provide the desired energy level α for the UE's demand, the BS energy storage should be charged to α units via RPS. Thus, the process of reserving energy follows the energy inventory strategy [23] in order to avoid placing energy replenishment by the BS without paying attention to connection arriving. Scheduling the process of a queuing system has impressive effects on improving QoS. In our model, where the backlogged access occurs, the UE has to wait for a while and this leads to QoS deterioration. As a result, a cost δ will be assigned to the system. This cost is divided into two parts and is devoted to the BS and RPS with a fraction $\delta \in [0, 1]$. We define parameter C_b as the average number of backlogged accesses, C_r as the average energy reservation level, and C_η as the operation cost for the RPS which is considered because of load

factor variation of the RPS (i.e., the relation of the service demand rate and the service supply rate as $\rho = \lambda_c/\eta_s < 1$). Indeed, the RPS is able to distribute energy among several BSs. The mean cost per unit time for both the BS and RPS is respectively formulated as

$$C_{BS}(\alpha, \eta_s) = \varepsilon \cdot C_r - \epsilon R_{D2D} + \delta C_b \tag{1.7}$$

and

$$C_{RPS}(\alpha, \eta_s) = (1 - \delta)C_b + \xi C_\eta \tag{1.8}$$

where ε, ϵ, and ξ are the cost coefficients, and R_{D2D} is defined as a saving energy reward for D2D communications over a cell which may lead to data traffic offloading from the BSs. In order to analyze and optimize the cost functions of the RPS and the BS, we will utilize an M/M/G queue to determine C_r and C_b with the help of α and η_s. Thus, we investigate a model based on the noncooperative strategic game [36] with predefined assumptions, in a way that the BS and the RPS are the players of this game with the strategies α and η_s, respectively. A queuing policy will be followed in our model which is based on the BS that is considered as a single-server queue with specified demand rate λ_c and service rate η_s. Here we assume N_c as a continuous random variable that is geometrically distributed with mean $\rho/(1 - \rho)$ or exponentially distributed with parameter $\beta = (1 - \rho)/\rho = (\eta_s - \lambda_c)/\lambda_c$ and shows the stationary number of waiting connections. It is straightforward to express the average cost functions as $C_r = E[\alpha > N_c]$, $C_b = E[\alpha < N_c]$ and also the average D2D reward function as $R_{D2D} = E[N_{D2D} < \alpha < N_c]$.

A wireless network based on a queuing system with heavy traffic condition has a large ρ, meaning that there is a shortage of green energy production. Since there are several entities (i.e., BSs) with rate λ_b which request power from the RPS, the load factor can be defined as $C_\eta = \lambda_b/(\eta_s^0 - \eta_s) - \lambda_b/\eta_s^0 = \lambda_b\eta_s/\eta_s^0(\eta_s^0 - \eta_s)$ that represents the operation cost (the average power supply cost) of the RPS. Recall that η_s^0 is the maximum power generation rate of the RPS and η_s is the provided power for the BS by the RPS. Thus, a Poisson process is introduced with rate $\eta_s^0 - \eta_s$ that defines the rest of the supply capacity of the RPS. Load factor is an important parameter for a queuing system in order to determine the average queue length. When load factor arrives 1, it means that the average queue length will get to infinity and finally leads to loss QoS totally. Here, we attempt to express average cost of the BS and the RPS while they are normalized and investigated in terms of the α and β (normalized energy supply rate). Therefore, the average cost of the BS and the RPS are respectively given as follows:

$$C_{BS}(\alpha, \beta) = \alpha - \frac{1 - e^{-\alpha\beta}}{\beta} - \epsilon R_{D2D} + \delta\frac{e^{-\alpha\beta}}{\beta} \tag{1.9}$$

$$C_{\mathrm{RPS}}(\alpha,\beta) = (1-\delta)\frac{\mathrm{e}^{-\alpha\beta}}{\beta} + \frac{\lambda_{\mathrm{c}}(\beta+1)}{\eta_{\mathrm{s}}^{0} - \lambda_{\mathrm{c}}(\beta+1)} \tag{1.10}$$

The mentioned demand-response system operates over periodic intervals during which network parameters such as the power production capacity and connection demand rate can be estimated. However, smart grid monitoring systems are able to extract the required network characteristics from history record and atmospheric parameters [23]. It should be noted that fixed power prices are assumed in this model. Therefore, no matter whether the RPS has storage or not, it should respond to the power demands from the BS rather than storing the energy. Indeed, the BSs' action to choose a strategy α corresponds to set a power replenish order to the RPS. Therefore, at the start of the game, the BS should have charged its energy storage to an inventory of α energy units through the existing EG or the RPS. Once the game starts, the RPS attempts to supply the energy with the service rate β and the BS serves the users with the renewable energy, thereby striking a balance between the power consumption and maintaining the QoS. Generally, in a distributed game-theoretic formulation, both BS and RPS attempt to select their individual strategies α and β so that their own cost functions are minimized. It means that the BS will opt α to reach a minimum value for $C_{\mathrm{BS}}(\alpha,\beta)$, assuming that the RPS selects β to minimize $C_{\mathrm{RPS}}(\alpha,\beta)$; similarly, the RPS will simultaneously assign a value for β to minimize $C_{\mathrm{RPS}}(\alpha,\beta)$, assuming the BS uses α to minimize $C_{\mathrm{BS}}(\alpha,\beta)$. Thus, a pair of strategies (α^*,β^*) is a Nash equilibrium (NE) if neither the BS nor the RPS can gain from a one-sided deviation from their strategies, i.e.,

$$\alpha^* = arg\min_{\alpha} C_{\mathrm{BS}}(\alpha,\beta^*) \tag{1.11}$$

and

$$\beta^* = arg\min_{\beta} C_{\mathrm{RPS}}(\alpha^*,\beta) \tag{1.12}$$

Since the existence of the NE is guaranteed as [23], the conventional best response dynamics [36, 37] can be exploited to converge to the NE. Therefore, the RPS and the BS can adopt a plan about the strategies at the start of the game. Further, the performance of the demand-response strategies is evaluated for the RPS and BSs over a HetNet with a specific power consumption profile. Indeed, a model based on the noncooperative strategic game is considered with predefined assumptions, in a way that the BS and the RPS are the players of this game with the strategies α and β, respectively. Then, the D2D communication is exploited to reduce the cost values for the RPS and BSs formulated in this section in order to determine the D2D impacts on efficient utilization of energy.

In the first set of results (Figs. 1.4, 1.5, and 1.6) presented here, the power demand and related cost values for the RPS and $N = 20$ BSs are evaluated according to the specific network power-consumption profile. Later (in Fig. 1.7), the D2D impacts on

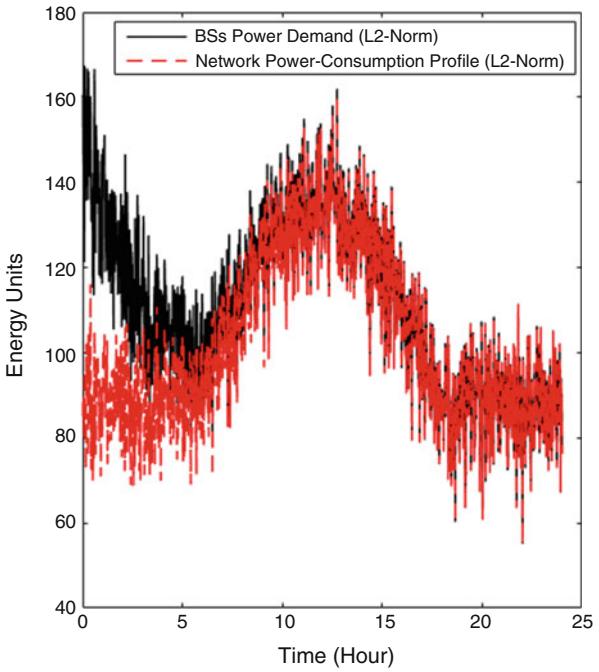

Fig. 1.4 BSs' power demand according to a power-consumption profile

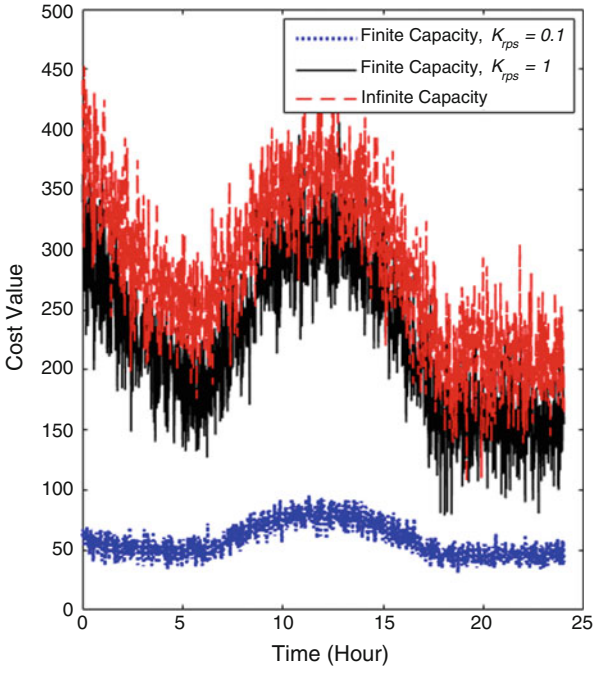

Fig. 1.5 The cost values for the RPS (L2-norm)

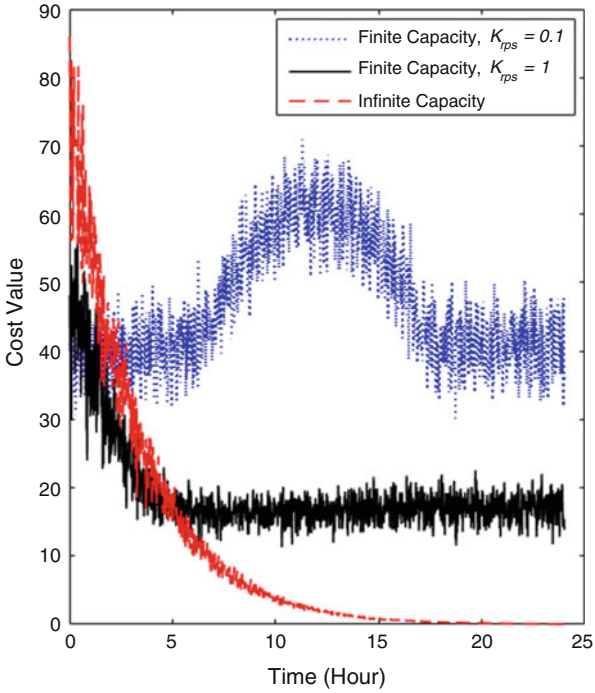

Fig. 1.6 The cost values for the BSs (L2-norm)

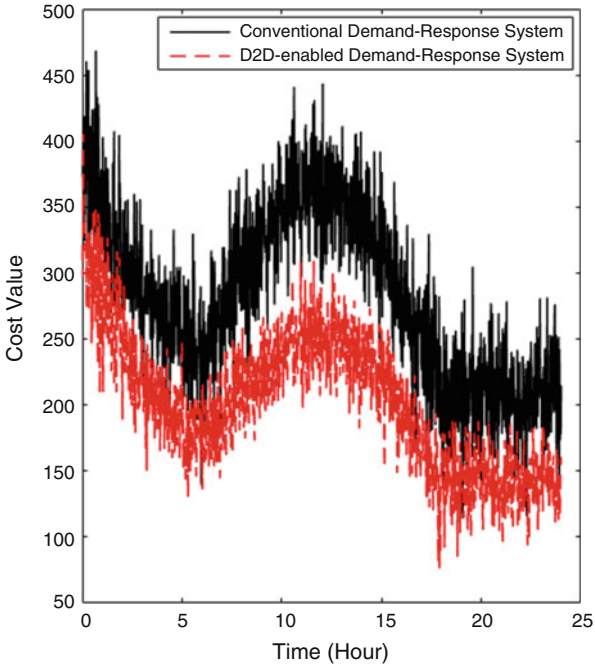

Fig. 1.7 The cost evaluation (L2-norm) for a perfect RPS over the conventional or D2D-enabled demand-response systems

efficient utilization of energy are analyzed. Here, the energy threshold is defined as $k_{\text{rps}} \cdot E_{\text{Req}}$ to indicate the maximum service capacity provided by the RPS. Note that E_{Req} is assumed to be the average energy demand ordered by the BSs. Moreover, k_{rps} is the service coefficient ($0 < k_{\text{rps}} < \infty$). Clearly, lower values for k_{rps} mean that the RPS has finite capacity in response to the received energy demands. Furthermore, in the case of $k_{\text{rps}} \rightarrow \infty$, there is no energy constraint (i.e., infinite capacity); thus maximum cost values can be expected in the RPS side. Indeed, the RPS should acquire the exact energy demand information from the BSs. Meanwhile, the traffic offloading effects of the D2D communication can be observed in Fig. 1.7, where the cost values are reduced for the D2D-enabled network compared to the conventional demand-response system.

1.6 Energy-Optimized Wireless Communications

1.6.1 Wireless Cellular Networks

In the literature—see, e.g., [38–45]—the EE of single-tier (macro-tier) cellular networks has been widely discussed and researched. The authors in [40, 45] suggest using the dynamic BS operation, i.e., adopting a dynamic off/on switching for BSs based on a real network traffic profile. However, both the randomness and the spatial distribution of the network traffic have been ignored. More recently, the cellular network has become multitiered with cells providing overlapping coverage [46, 47]. This is due to the emergence of low-cost small cells. Because of the increased overlapping areas and high fluctuations of traffic demand (both in time and over space) in cellular networks, optimal sleep/wake-up schemes can be designed either for small cells or for the coverage-overlapped macro-BSs (MBSs) [48, 49].

The studies mentioned above consider models such as hexagonal and Manhattan model network [50]. In other words, they only focus on ideal and non-tractable network deployment models. Here, the non-tractability issue is in accordance with signal to interference and noise ratio (SINR) distribution. However, dense and unplanned deployment of small cells over space have called for more tractable models. Using tractable models, key performance metrics can be evaluated quickly without the need to perform complex and time-consuming ray tracing and simulations. A tractable network deployment is modeled by the authors in [51, 52] with the aid of stochastic geometry [53–56]. More specifically, they propose to independently switch off each BS with a fixed probability. However, the HetNet deployment has not been considered in their work. Authors in [35, 57, 58] have studied sleep/wake-up schemes in stochastic geometry-based HetNets. Both dynamic (i.e., traffic load-based) and random sleeping strategies for MBSs have been presented in [35]. To design the optimal sleeping mechanism for MBSs, they consider EE maximization. The authors in [57, 58] also study random sleep/wake-up schemes for BSs. In [57], based on minimizing BS energy consumption, the optimal switch-off probability for

MBSs is determined. Also, in [58], based on maximizing EE with the constraint for coverage probability, the optimal switch-off probability for small cell BSs is derived.

Compared with the dynamic BS sleep/wake-up strategies, the random sleep/wake-up schemes have the advantages of less operational cost and low computational complexity. However, they are not adaptable to the dynamic nature of realistic cellular networks. The basic concepts about dynamic BS operation issues have also been summarized in [42]. They, however, lack the ability to learn the uncertain wireless network environment. Many factors such as intracell and intercell interference, location uncertainty, SINR requirements, and traffic load can be considered for characterizing uncertainty. The use of learning-based mechanisms in wireless networks is not new. For example, in [59–62], in order to optimize range expansion bias, sleep/wake-up scheduling, and transmit power, two learning-based techniques known as regret-based learning and Q-learning have been applied. Another learning-based technique developed in [63] plays a key role for BS energy conservation in cellular radio access networks (RANs). More specifically, they use Markov decision processes with knowledge transferring to formulate and model the BS operations under a variant traffic load. Note that the state of the surrounding environment and available actions to the agents are commonly represented by discrete sets in all lookup-table-based learning-based approaches (such as Q-learning and state-action-reward-state-action [SARSA]). This may lead to inaccuracies and subjectivity in the agent's behavior and consequently the system performance, particularly when the input variables are continuous or the number of state-action pairs is large. To deal with this issue, a fuzzy logic controller is usually combined with Q-learning and SARSA. The combination of the fuzzy logic controller with Q-learning and SARSA is known as fuzzy Q-learning (FQL) and fuzzy SARSA-learning (FSL) [64], respectively. This will help agents (BSs) to better and faster adjust their actions bringing in a considerable benefit in terms of precision and the learning period. Nevertheless, FSL might be somewhat faster than FQL. This is because FQL does not learn the same policy as it follows, i.e., in FQL, the policy is updated dependent on the best possible future scenario, rather than what actually happens after an action is taken (as is the case in FSL) [64, 65]. However, this will lead to a better performance of FQL, while FSL appears to be not flexible enough for uncertain and changing environments and to get stuck in local maxima. Therefore, in general and particularly for uncertain wireless environments, it is believed that the policy learnt by FQL is able not only to satisfy the system constraints, but also to achieve a higher level of system performance in terms of EE.

The unavoidable coverage holes caused by switching some BSs off is one of the key bottlenecks of applying sleep/wake-up mechanisms. Because of this reason, several schemes, such as user association [38, 43, 52] and power control [20, 35, 39, 40, 45], have been suggested to counter the coverage voids. For instance, a fixed power control policy is proposed in [35], where it is assumed that the power of all active BSs is increased equally without considering the channel conditions of the switched off cell users. A perfect power control strategy taking into account power levels at other cells is considered by the authors in [20], which can consequently manage the interference between neighboring cells. Different from these studies, in

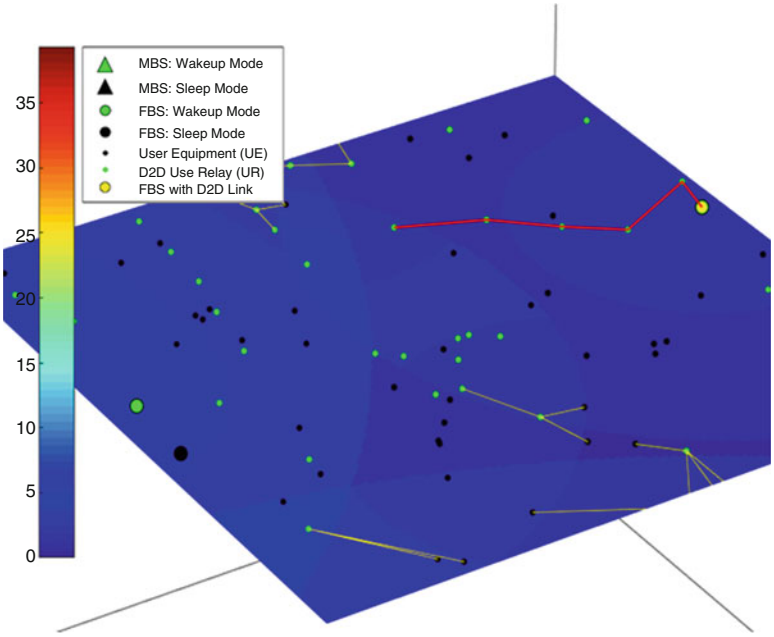

Fig. 1.8 Coverage simulations for learning based on D2D-enabled HetNets (zoomed-in view) [32]

[32], a D2D-enabled FQL scheme is used to fill the coverage holes resulting from switching some BSs off (see Fig. 1.8).

1.6.2 Wireless Sensor Networks

Here, a hierarchical sensor network is considered that means some fusion centers collect reports from the neighboring sensors in the area and send the information to the BS [15, 16, 62]. Indeed, the network is cluster-based in which the cluster heads (CHs) or sinks have a more prominent role than the other sensors. It should be noted that each cluster consists of several nodes and a head node. Generally, the WSN architecture is n-tier ($n > 1$), and WSNs are widely used in a two-tier network format. Thus, we consider a two-tier heterogeneous WSN that includes a number of clusters and several BSs. In this two-tier network, the lower tier consists of nodes of different clusters, while the CHs and the BSs compose the upper tier (see Fig. 1.9).

Sensors, which form the network's lower tier, are responsible for sensing and sending the collected data to the CHs or sinks in their own area. CHs have the ability to collect and transmit the received data to the BS. The BS receives the data from the sinks and, according to its analysis, obtains the full sense of the network. In the defined network model, the cluster can also play the role of the relay and transfer the messages to the BS in multiple hopes. As mentioned before, the energy of BSs is

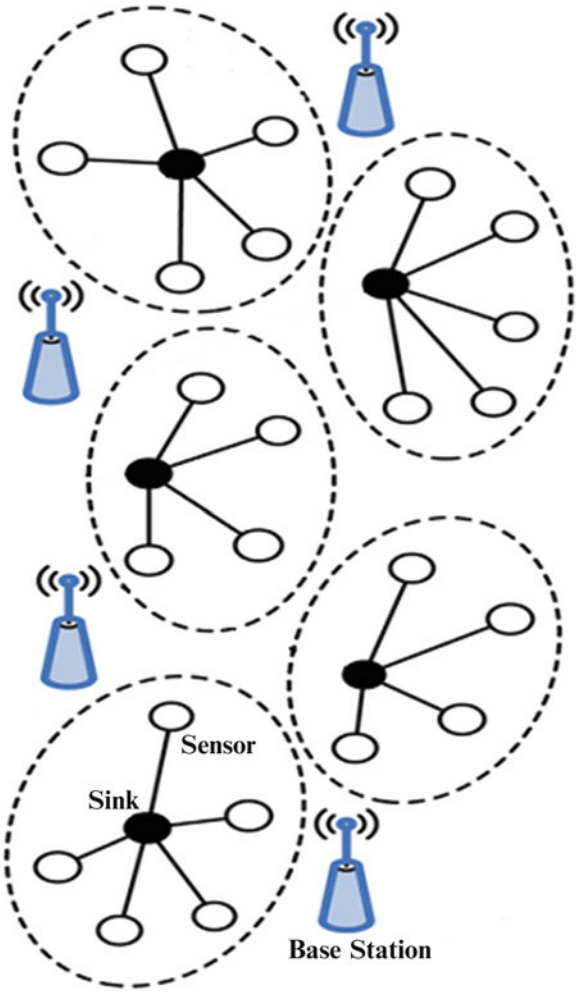

Fig. 1.9 Wireless sensor network with BSs, sinks, and mobile sensors

considered limited. Therefore, the energy consumption of the BSs is our concern and it is clear that in order to decrease power consumption and prolong the lifetime of the two-tier WSN, power management mechanisms should be exploited more precisely. In order to understand the sleep and wake-up mechanisms, it is first necessary to recognize the differences between the different modes of power saving that can be given by a small cell. We describe this concept in terms of "depth." The greater the depth, the higher the power saving, and the deeper the sleep, the more time it takes to

Table 1.1 Different operation modes

Operation mode	Power consumption
On/wake-up	100%
Standby	50%
Sleep	10%
Off	0

wake up. Power consumption is considered as a percentage of total power consumption in each mode. It is assumed that a BS is the most energy consuming when it is turned on. In addition, BS power consumption varies according to different traffic, but we consider the average of the network performance. Therefore, the instantaneous power changes have not been considered for traffic variations in the BS power consumption model. It should be noted that, in this section, sleep/wake-up mechanisms are simply used to control the power consumption of BSs by putting them in different operation modes (see Table 1.1). Indeed, this section addresses the problem of designing of a smart sleep and wake-up mechanism using the genetic algorithm (GA), as a nature-inspired optimization approach, to manage the operation modes of the BSs according to the time-variant profile for the daily traffic load.

In addition, simulation results are presented to analyze the performance of the smart sleep and wake-up mechanism. The impact of network topology and parameters (e.g., density of BSs, CHs, and the related locations) can be investigated according to the comprehensive network simulations (Fig. 1.10). All simulations are performed using Monte Carlo runs. Here, as mentioned before, GA, as a nature-inspired optimization approach, makes the opportunity to design optimal and practical solutions for WSNs. Therefore, the GA-based optimization is performed in the simulations that focuses on a centralized management process to adopt the operation modes of BSs according to the time-variant profile for the daily traffic load. By controlling the operation modes of the densely deployed BSs over the WSN, EE of the network converges to the optimal level as can be observed in Fig. 1.11. Here, L2-norm of the operation modes for the BSs also converges versus iterations that verify the network stability in the steady phase of the GA (Fig. 1.12). In addition, the optimal operation modes for the BSs can be finally considered to form the optimal network configurations as in Fig. 1.13

Indeed, a practical GA-based strategy can also be adopted to obtain the optimal BSs' positions for the two-tiered HetNet. Then, we demonstrate the L2-norm of BSs' positions (Fig. 1.14) and the network EE curve (Fig. 1.15) versus a sufficient number of iterations. We then show the optimal network topology obtained according to the optimal numerical results for the BSs' positions (Fig. 1.16). As mentioned before, the GA-based optimization executes over several generations in order to determine the best set of solutions (i.e., the optimal BS positions) and generally finishes at the best convergence, that is, when the best fit occurs according to the convergence criteria. Results show that convergence can be obtained for the network EE as the number of iterations increase, and this clearly confirms the network stability in the steady phase of the GA.

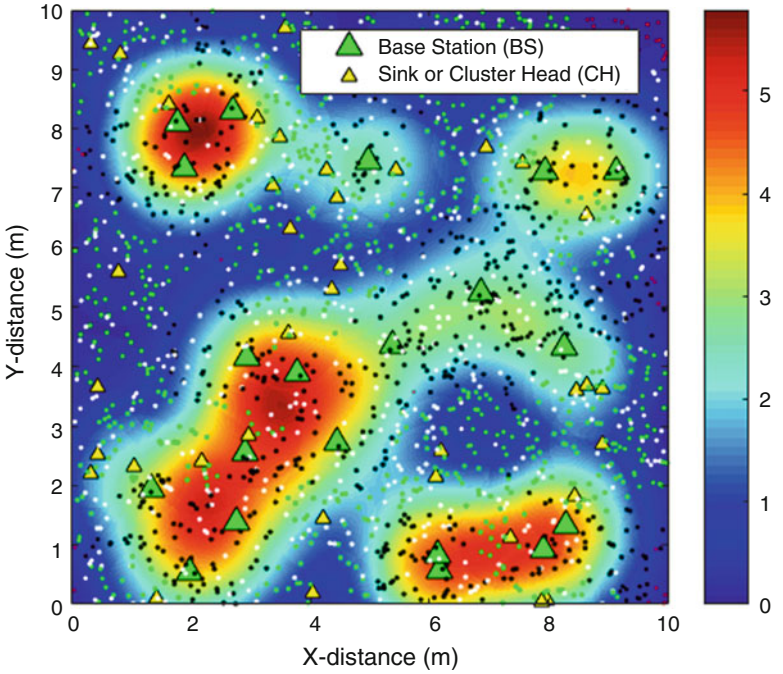

Fig. 1.10 Coverage map for conventional power configurations

Fig. 1.11 Network energy efficiency versus iterations

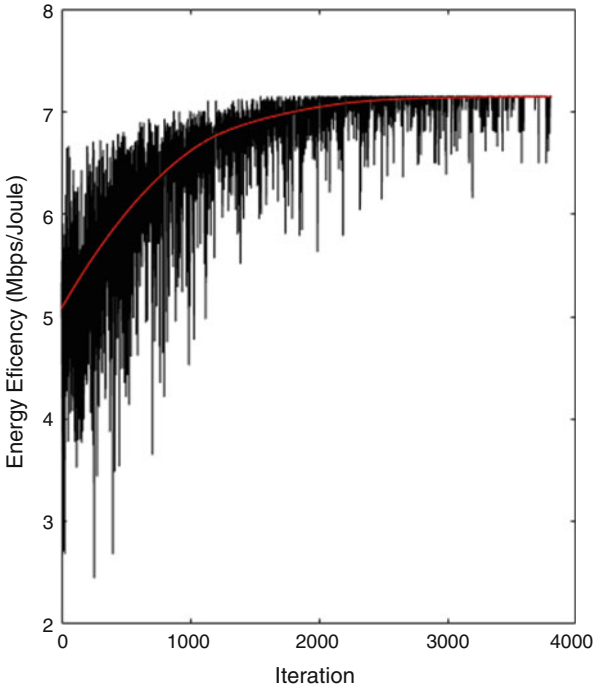

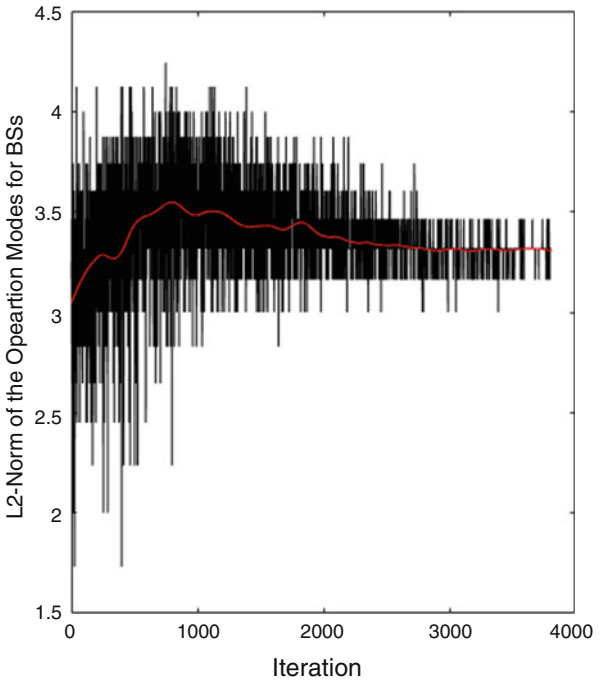

Fig. 1.12 L2-norm of the operation modes for the BSs versus iterations

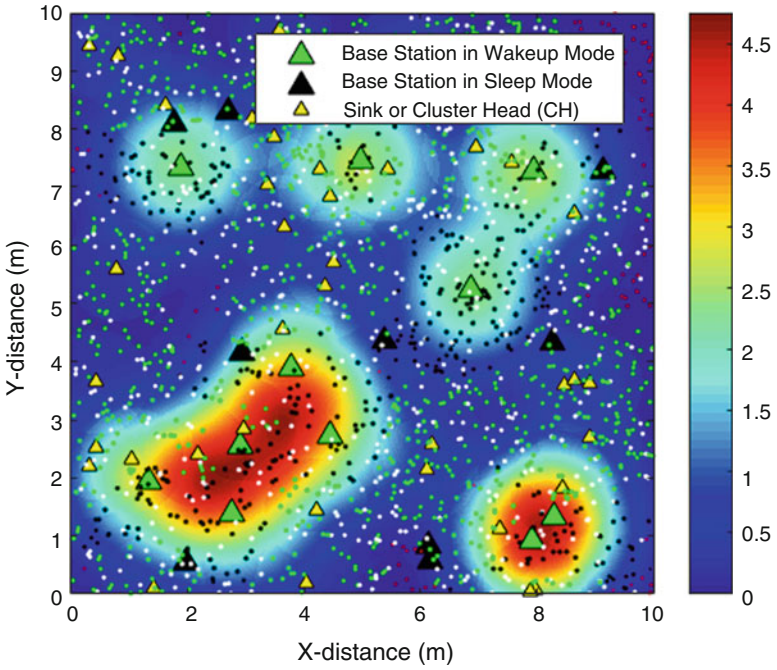

Fig. 1.13 Coverage map for GA-based optimal power configurations

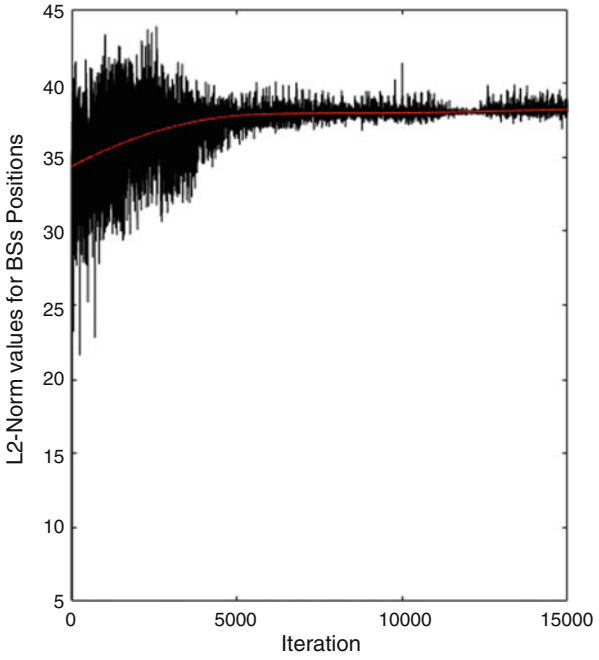

Fig. 1.14 L2-norm of the BSs' positions versus iterations

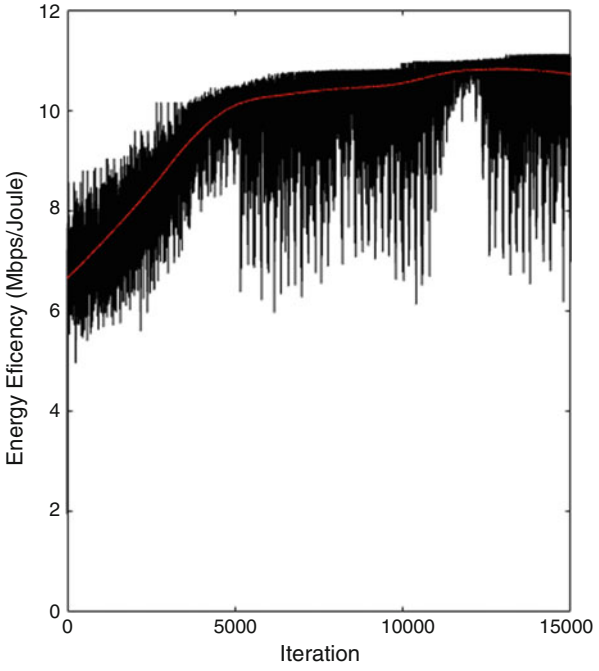

Fig. 1.15 Network energy efficiency versus iterations

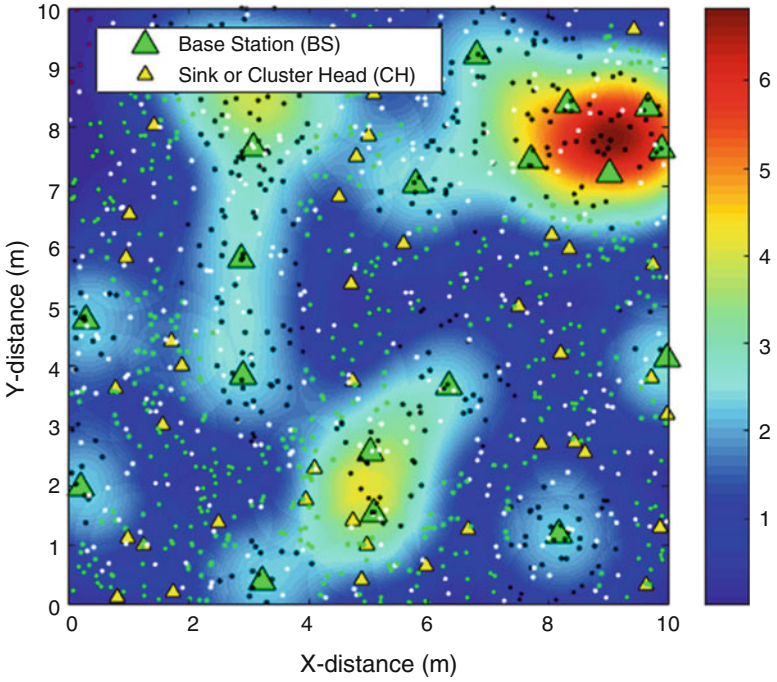

Fig. 1.16 Optimal topology for the wireless sensor network

1.7 Energy Harvesting and Self-Powered Technologies

Generally, the EH has been utilized for quite a long time for bike dynamos or solar panels. Today, it is widely applied to application fields, such as smart cities, automotive vehicles, and security systems. Development inside the areas of big data and IoT and thus the spread of battery-based sensor systems are real power-driving advances in EH and self-powered systems [66, 67]. The most well-known power sources utilized for EH are mechanical and thermal energy and sunlight-based radiations. Recent advances in ultralow-power technologies have accelerated the improvement of self-powered monitoring gadgets for a wide scope of utilizations consisting of SGs, structural health monitoring, and biomedical telemetry [68–71]. A self-powered wireless sensor, which gains surrounding energy for driving its hardware, is among the promising techniques for supporting a maintenance-free sensor network in SGs. The worldwide EH market demonstrates a stunning development: somewhere in the range of 2015 and 2019, it could sum at 21.9% and peak at 28% in 2019 (Fig. 1.17). Governments and public initiatives are the main drivers for EH market development. Public actors utilize EH as a key apparatus for gathering the rising energy request and saving power. The imperative to confront the issue of climate change as a worldwide challenge will fuel the development of the market amid the coming 5 years.

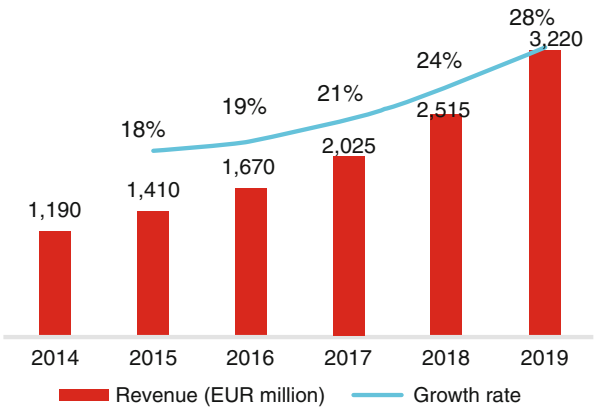

Fig. 1.17 Global energy-harvesting market 2014–2019

In fact, EH supports SGs by powering WSNs that are fundamental to provide connectivity between devices. A huge number of sensors are required to monitor and manage SG processes and the sensors should be powered. Ordinarily, batteries were utilized to enable the sensing nodes but they have a restricted lifetime, and in a network with a huge number of wireless sensors, replacement of the batteries will not be applicable. It should be noted that EH-powered sensors need less maintenance and are easier to arrange than batteries and also more comfortable to manage in mobile sensing strategies. To sum up, development of IoT and energy-efficient communication infrastructures for SGs is driving interest for wireless and battery-less sensors which will be increasingly more powered by EH. Indeed, EH wireless solutions find increasing applications in SGs due to their low-cost installation and maintenance. In addition, EH-based wireless technology is the reliable communication strategy to provide connectivity among thousands of nodes in SGs.

Here, a practical smart scenario for mobile sensors is considered to investigate the power-saving impacts of EH on wireless sensor networks. In addition, to evaluate whether this strategy can help to accelerate the EH process in mobile sensors, we conduct a series of simulations. It should be noted that the simulated environment is configured according to the conventional WSN parameters, and then we present the simulation results corresponding to the conventional EH model (Fig. 1.18a) and a FQL-based EH model (Fig. 1.18b), respectively. After that, a simple definition to evaluate the EH effectiveness over the network is presented. Here, the EH rate (EHR) is formulated as $k_{\mathrm{EH}} \cdot \left(d^0_{\mathrm{EH}}/d^t_{\mathrm{EH}}\right)^2$ to indicate any improvement in acceleration of the charging process for all mobile sensors deployed over the network. Note that d^t_{EH} is assumed to be the mean distance between mobile sensors and power stations (PSs) at the time of t. Moreover, k_{EH} is the EH coefficient ($1 \leq k_{\mathrm{EH}}$). From the results (Fig. 1.19), one can observe the performance degradation in the case of partial PS-state information (where the mobile sensors are moving toward PSs based on partial location information of PSs obtained via M2M communications), for average EHR, as expected. It is assumed that the exact information of PS locations can be accessible for all mobile sensors when the perfect case is performed.

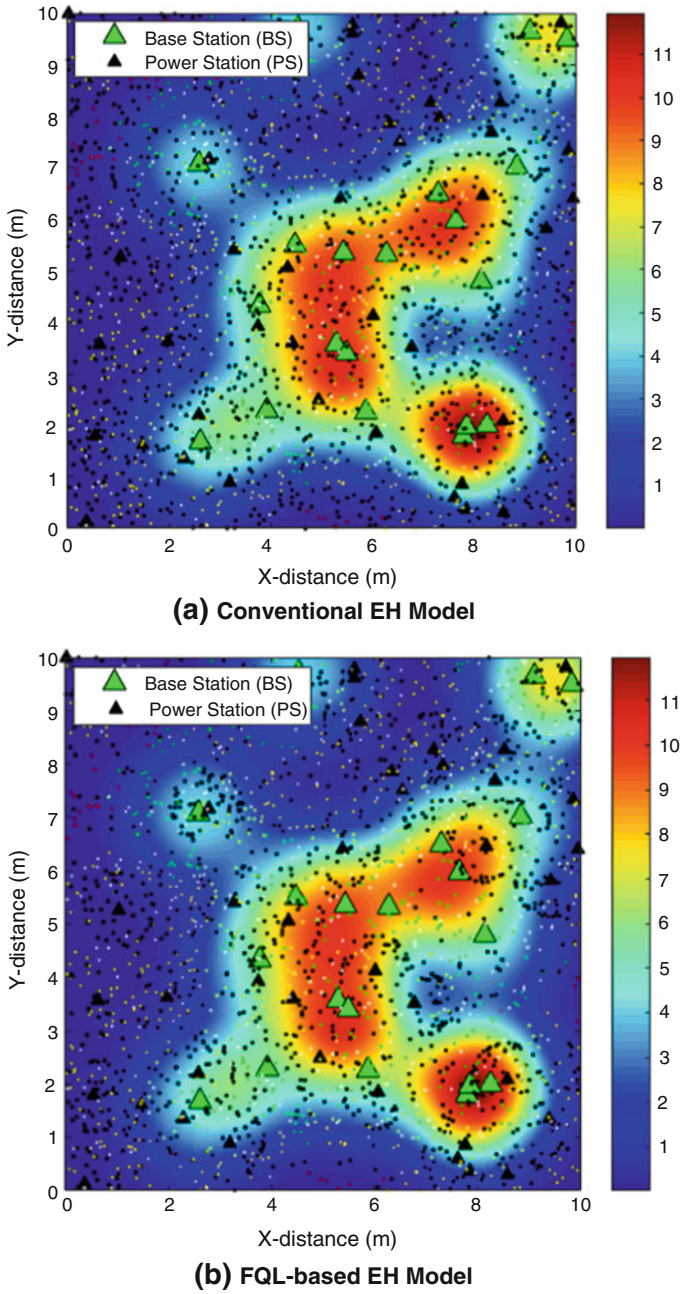

Fig. 1.18 Coverage map for the wireless powered sensor network. (**a**) Conventional EH model. (**b**) FQL-based EH model

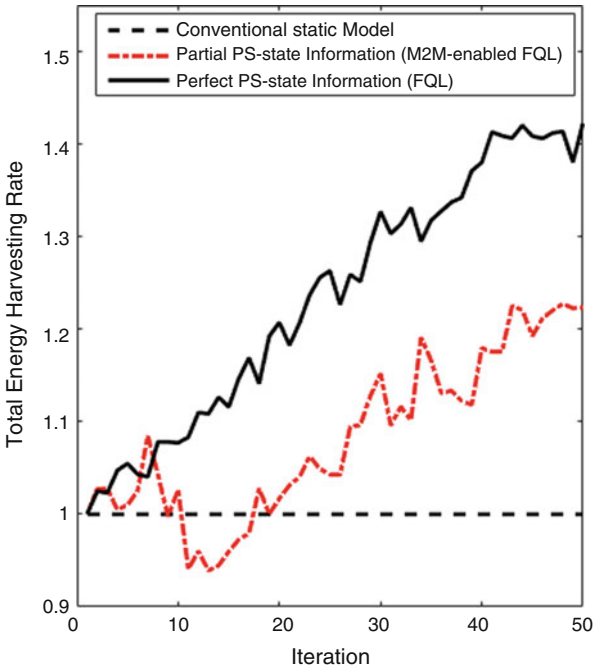

Fig. 1.19 EH rate for static and dynamic sensor scenarios

1.8 Conclusion

The electric power grid is experiencing extraordinary changes that have changed it from a hierarchical system to a distributed, user-based SG. Realizing the vision of the SG is dependent upon energy-efficient communication infrastructures that can empower rapid and reliable data transmission in the grid. Undoubtedly, wireless communication systems play a key role in realizing a lot of the SG features, for example, DR, AMI, electric vehicle, storage units, and microgrid control. Thus, a plenty of strategies for SG communications have been proposed that rely on wireless communications and PLC technologies. The incorporation of ICTs in the grid clearly raises security hazards that must be controlled based on cyber-physical protocols. Indeed, this chapter presented profound contributions in the broad area of SG communications along with various scenarios through computer simulation. Table 1.2 summarizes the general topics to prepare a comprehensive perspective on the recent studies in this area.

Table 1.2 Major topics and the latest research developments on smart grid green communications

Topics	References
Communication architectures for AMI	[72, 73]
Networking methods for realizing new SG capabilities	[74, 75]
Communication-based procedures for DR, demand-side, and power management	[76, 77]
Big data analyses for SGs	[78, 79]
Integrated storage units and electric vehicles in SGs	[80, 81]
Multiple access schemes for SG communications	[82, 83]
PLC challenges in the SG	[84, 85]
Cross-layer design and SG service integration	[86, 87]
Secure and private protocols in the SG	[88, 89]
Resilient communication solutions for SGs	[90, 91]
Cyber-physical models for smart power management	[92, 93]
Nature-inspired optimal algorithms for SGs	[94, 95]
Hybrid wired and wireless architectures for power communications	[96, 97]
Encoding and modulation techniques for PLC and wireless communications in the grid	[98, 99]
Routing and congestion strategies in PLC systems	[100, 101]
Optimal designs for decentralized power sources and microgrids	[102, 103]
Control and communications synergies in the SG	[104, 105]
Green-powered systems for wireless communications	[23, 106]
Device-to-device communications in the SG	[107, 108]
Coexistence of SG communication technologies	[109, 110]
SG-enabled cellular communication networks	[111, 112]
Economic approaches for improving SG communications and energy efficiency	[113, 114]
Optimal positioning for SG communication nodes	[115, 116]
Standard measurements and experimental evaluations for SG communication systems	[117, 118]

References

1. E. Hossain, V.K. Bhargava, G. Fettweis, *Green Radio Communication Networks* (Cambridge Univ. Press, Cambridge, UK, 2012)
2. B. Heile, Smart grids for green communications [industry perspectives]. IEEE Wireless Commun. **17**(3), 3–6 (2010)
3. J. Xu, L. Duan, R. Zhang, Cost-aware green cellular networks with energy and communication cooperation. IEEE Commun. Mag. **53**(5), 257–263 (2015)
4. J. Wu, S. Rangan, H. Zhang, *Green Communications: Theoretical Fundamentals, Algorithms, and Applications* (CRC Press, Boca Raton, 2012)
5. T. Han, N. Ansari, Powering mobile networks with green energy. IEEE Wireless Commun. **21** (1), 90–96 (2014)
6. S. Bu, F.R. Yu, Y. Cai, X.P. Liu, When the smart grid meets energy-efficient communications: green wireless cellular networks powered by the smart grid. IEEE Trans. Wireless Commun. **11**(8), 3014–3024 (2012)
7. M. Erol-Kantarci, H.T. Mouftah, Energy-efficient information and communication infrastructures in the smart grid: a survey on interactions and open issues. IEEE Commun. Surv. Tut. **17** (1), 179–197 (2015)

8. N. Saputro, K. Akkaya, S. Uludag, A survey of routing protocols for smart grid communications. Comput. Networks J. **56**(11), 2742–2771 (2012)
9. G. Miao, N. Himayat, Y. Li, D. Bormann, Energy efficient design in wireless OFDMA, in *IEEE International Conference on Communications* (2008), pp. 3307–3312
10. C.-B. Kim, G.d.V. Chae, R.W. Heath Jr., A cross-layer approach to energy efficiency for adaptive MIMO systems exploiting spare capacity. IEEE Trans. Wireless Commun. **8**(8), 4264–4275 (2009)
11. J. Huang, H. Wang, Y. Qian, C. Wang, Priority-based traffic scheduling and utility optimization for cognitive radio communication infrastructure-based smart grid. IEEE Trans. Smart Grid **4**(1), 78–86 (2013)
12. L. Li, X. Zhou, H. Xu, G.Y. Li, D. Wang, A. Soong, Energy-efficient transmission in cognitive radio networks, in *IEEE Consumer Communications and Networking Conference* (Jan. 2010), pp. 1 and 5
13. M. Erol-Kantarci, J.H. Sarker, H.T. Mouftah, Communication-based plug-in hybrid electrical vehicle load management in the smart grid, in: *IEEE Symposium on Computers and Communications* (June 2011)
14. M.N. Alam, R. Jantti, J. Kneckt, J. Nieminen, Performance analysis of the IEEE 802.11s PSM, J. Comput. Networks Commun. **2012**, 14 p (2012)
15. M. Erol-Kantarci, H.T. Mouftah, Wireless sensor networks for cost-efficient residential energy management in the smart grid. IEEE Trans. Smart Grid **2**(2), 314–325 (2011)
16. L. Li, X. Hu, C. Ke, K. He, The applications of WiFi-based wireless sensor network in internet of things and smart grid, in *IEEE Conference on Industrial Electronics and Applications (ICIEA)* (June 2011), pp. 789–793
17. V. Chandrasekhar, J. Andrews, A. Gatherer, Femtocell networks: a survey. IEEE Commun. Mag. **46**(9), 5967 (2008)
18. F. Richter, A.J. Febske, G.P. Fettweis, Energy efficiency aspects of base station deployment strategies in cellular networks, in *Proceedings of IEEE VTC 09-Fall*, Anchorage, AK (Sept. 2009)
19. P. Gandotra, R.K. Jha, S. Jain, Green communication in next generation cellular networks: a survey. IEEE Access **5**, 11727–11758 (2017)
20. S. Kokkinogenis, G. Koutitas, Dynamic and static base station management schemes for cellular networks, in *IEEE Global Communications Conference (GLOBECOM)* (2012), pp. 3443–3448
21. Z. Zhou, C. Gao, C. Xu, T. Chen, D. Zhang, S. Mumtaz, Energy-efficient stable matching for resource allocation in energy harvesting-based device-to-device communications. IEEE Access **5**, 15184–15196 (2017)
22. S. Shalmashi, E. Björnson, M. Kountouris, K.W. Sung, M. Debbah, Energy efficiency and sum rate tradeoffs for massive MIMO systems with underlaid device-to-device communications. EURASIP J. Wireless Commun. Network. **1**, 175 (2016)
23. D. Li, W. Saad, I. Guvenc, A. Mehbodniya, F. Adachi, Decentralized energy allocation for wireless networks with renewable energy powered base stations. IEEE Trans. Commun. **63**(6), 2126–2142 (2015)
24. J. Gozalvez, Green radio technologies [mobile radio]. IEEE Veh. Technol. Mag. **1**, 9–14 (2010)
25. C.K. Ho, R. Zhang, Optimal energy allocation for wireless communications with energy harvesting constraints. IEEE Trans. Signal Process. **9**, 4808–4818 (2012)
26. D. Niyato, X. Lu, P. Wang, Adaptive power management for wireless base stations in a smart grid environment. IEEE Wireless Commun. **6**, 44–51 (2012)
27. G. Yu, L. Xu, D. Feng, R. Yin, G.Y. Li, Y. Jiang, Joint mode selection and resource allocation for device-to-device communications. IEEE Trans. Commun. **11**, 3814–3824 (2014)
28. Q. Ye, B. Rong, Y. Chen, M. Al-Shalash, C. Caramanis, J.G. Andrews, User association for load balancing in heterogeneous cellular networks. IEEE Trans. Wireless Commun. **6**, 2706–2716 (2013)

29. D. Wu, J. Wang, H. Rose Qingyang, Y. Cai, L. Zhou, Energy-efficient resource sharing for mobile device-to-device multimedia communications. IEEE Trans. Veh. Technol. **5**, 2093–2103 (2014)
30. Z. Zhou, K. Ota, M. Dong, C. Xu, Energy-efficient matching for resource allocation in D2D enabled cellular networks. IEEE Trans. Veh. Technol. **6**, 5256–5268 (2017)
31. U. Saleem, H.K. Qureshi, S. Jangsher, M. Saleem, Transmission power management for throughput maximization in harvesting enabled D2D network, in *2016 IEEE Symposium on Computers and Communication (ISCC)* (2016), pp. 1078–1083
32. S. Xiao, X. Zhou, D. Feng, Y.-W. Yi, G.Y. Li, W. Guo, Energy-efficient mobile association in heterogeneous networks with device-to-device communications. IEEE Trans. Wireless Commun. **8**, 5260–5271 (2016)
33. F.H. Panahi, F.H. Panahi, G. Hattab, T. Ohtsuki, D. Cabric, Green heterogeneous networks via an intelligent sleep/wake-up mechanism and D2D communications. IEEE Trans. Green Commun. Network. **2**(4), 915–931 (2018)
34. F.H. Panahi, F.H. Panahi, G. Hattab, T. Ohtsuki, D. Cabrici, Green heterogeneous networks via an intelligent power control strategy and D2D communications, in *2017 IEEE 28th Annual International Symposium on Personal, Indoor, and Mobile Radio Communications (PIMRC)*, Montreal, QC (2017), pp. 1–8
35. Y.S. Soh, T.Q. Quek, M. Kountouris, H. Shin, Energy efficient heterogeneous cellular networks. IEEE J. Sel. Areas Commun. **31**(5), 840–850 (2013)
36. Z. Han, D. Niyato, W. Saad, T. Başar, A. Hjørungnes, *Game Theory in Wireless and Communication Networks: Theory, Models, and Applications* (Cambridge University Press, Cambridge, 2011)
37. M.J. Osborne, A. Rubinstein, *A Course in Game Theory* (MIT Press, Cambridge, 1994)
38. H. Tabassum, U. Siddique, E. Hossain, M.J. Hossain, Downlink performance of cellular systems with base station sleeping, user association, and scheduling. IEEE Trans. Wireless Commun. **13**(10), 5752–5767 (2014)
39. E. Oh, B. Krishnamachari, Energy savings through dynamic base station switching in cellular wireless access networks, in *2010 IEEE Global Telecommunications Conference GLOBECOM 2010* (Dec 2010), pp. 1–5
40. L. Chiaraviglio, D. Ciullo, M. Meo, M.A. Marsan, Energy-efficient management of umts access networks, in *2009 21st International Teletraffic Congress* (Sept 2009), pp. 1–8
41. A.J. Fehske, F. Richter, G.P. Fettweis, Energy efficiency improvements through micro sites in cellular mobile radio networks, in *2009 IEEE Globecom Workshops* (Nov 2009), pp. 1–5
42. Z. Niu, Y. Wu, J. Gong, Z. Yang, Cell zooming for cost-efficient green cellular networks. IEEE Commun. Mag. **48**(11), 74–79 (2010)
43. K. Son, H. Kim, Y. Yi, B. Krishnamachari, Base station operation and user association mechanisms for energy-delay tradeoffs in green cellular networks. IEEE J. Sel. Areas Commun. **29**(8), 1525–1536 (2011)
44. J. Wu, S. Zhou, Z. Niu, Traffic-aware base station sleeping control and power matching for energy-delay tradeoffs in green cellular networks. IEEE Trans. Wireless Commun. **12**(8), 4196–4209 (2013)
45. M.A. Marsan, L. Chiaraviglio, D. Ciullo, M. Meo, Optimal energy savings in cellular access networks, in *2009 IEEE International Conference on Communications Workshops* (June 2009), pp. 1–5
46. L. Saker, S.E. Elayoubi, R. Combes, T. Chahed, Optimal control of wake up mechanisms of femtocells in heterogeneous networks. IEEE J. Sel. Areas Commun. **30**(3), 664–672 (2012)
47. S.E. Elayoubi, L. Saker, T. Chahed, Optimal control for base station sleep mode in energy efficient radio access networks, in *Proceedings of IEEE INFOCOM 2011* (Apr. 2011), pp. 106–110
48. W.C. Liao, M. Hong, Y.F. Liu, Z.Q. Luo, Base station activation and linear transceiver design for optimal resource management in heterogeneous networks. IEEE Trans. Signal Process. **62** (15), 3939–3952 (2014)

49. M. Oikonomakou, A. Antonopoulos, L. Alonso, C. Verikoukis, Cooperative base station switching off in multi-operator shared heterogeneous network, in *2015 IEEE Global Communications Conference (GLOBECOM)* (Dec 2015), pp. 1–6
50. A.N.F. Iqbal, M. Javed, Interference-aware multipath routing in wireless mesh network. EURASIP J. Wireless Commun. Netw. **140**, 1 (2014)
51. E. Altman, C. Hasan, M.K. Hanawal, S.S. Shitz, J.M. Gorce, R. El-Azouzi, L. Roullet, Stochastic geometric models for green networking. IEEE Access **3**, 2465–2474 (2015)
52. Y.S. Soh, T.Q.S. Quek, M. Kountouris, Dynamic sleep mode strategies in energy efficient cellular networks, in *2013 IEEE International Conference on Communications (ICC)* (June 2013), pp. 3131–3136
53. F.H. Panahi, T. Ohtsuki, Stochastic geometry based analytical modeling of cognitive heterogeneous cellular networks, in *2014 IEEE International Conference on Communications (ICC)* (2014), pp. 5281–5286
54. F.H. Panahi, T. Ohtsuki, Stochastic geometry modeling and analysis of cognitive heterogeneous cellular networks. EURASIP J. Wireless Commun. Network. **2015**(1), 141 (2015)
55. G. Hattab, D. Cabric, Joint resource allocation and user association in multi-antenna heterogeneous networks, in *IEEE GLOBECOM* (Dec. 2016)
56. F.H. Panahi, T. Ohtsuki, Inter-tier interference mitigation in multi-antenna HetNets: a resource blanking approach, in *IEEE GLOBECOM* (Dec. 2016)
57. J. Peng, P. Hong, K. Xue, Stochastic analysis of optimal base station energy saving in cellular networks with sleep mode. IEEE Commun. Lett. **18**(4), 612–615 (2014)
58. C. Liu, B. Natarajan, H. Xia, Small cell base station sleep strategies for energy efficiency. IEEE Trans. Veh. Technol. **65**(3), 1652–1661 (2016)
59. M. Simsek, M. Bennis, I. Guvenc, Enhanced intercell interference coordination in hetnets: single vs. multiflow approach, in *IEEE Globecom Workshops* (Dec 2013), pp. 725–729
60. M. Simsek, M. Bennis, A. Czylwik, Dynamic inter-cell interference coordination in hetnets: a reinforcement learning approach, in *IEEE GLOBECOM* (Dec. 2012)
61. S. Samarakoon, M. Bennis, W. Saad, M. Latva-aho, Opportunistic sleep mode strategies in wireless small cell networks, in *IEEE ICC* (2014), pp. 2707–2712
62. D. Ye, M.Z. Au, A self-adaptive sleep/wake-up scheduling approach for wireless sensor networks. IEEE Trans. Cybern. **48**(3), 979–992 (2018)
63. R. Li, Z. Zhao, X. Chen, J. Palicot, H. Zhang, Tact: a transfer actor-critic learning framework for energy saving in cellular radio access networks. IEEE Trans. Wireless Commun. **13**(4), 2000–2011 (2014)
64. H. Arabnejad, C. Pahl, P. Jamshidi, G. Estrada, A comparison of reinforcement learning techniques for fuzzy cloud auto-scaling, in *Proceedings of the 17th IEEE/ACM International Symposium on Cluster, Cloud and Grid Computing* (IEEE Press, 2017), pp. 64–73
65. S. Chettibi, S. Chikhi, Adaptive maximum-lifetime routing in mobile ad-hoc networks using temporal difference reinforcement learning. Int. J. Evol. Syst. **5**(2), 89–108 (2014)
66. A.S. Adila, A. Husam, G. Husi, Towards the self-powered Internet of Things (IoT) by energy harvesting: trends and technologies for green IoT, in *Second IEEE International Symposium on Small-scale Intelligent Manufacturing Systems (SIMS)* (2018), pp. 1–5
67. P. Kamalinejad et al., Wireless energy harvesting for the internet of things. IEEE Commun. Mag. **53**(6), 102–108 (2015)
68. J. Han, J. Hu, Y. Yang, Z. Wang, S.X. Wang, J. He, A nonintrusive power supply design for self-powered sensor networks in the smart grid by scavenging energy from ac power line. IEEE Trans. Ind. Electron. **62**(7), 4398–4407 (2015)
69. B. Fateh, M. Govindarasu, V. Ajjarapu, Wireless network design for transmission line monitoring in smart grid. IEEE Trans. Smart Grid **4**(2), 1076–1086 (2013)
70. J.L. Wardlaw, I. Karaman, A.I. Karsilayan, Low-power circuits and energy harvesting for structural health monitoring of bridges. IEEE Sensors J **13**(2), 709–722 (2013)

71. S.Y. Tang, S. Chakrabartty, A 5nw quasi-linear cmos hot-electron injector for self-powered monitoring of biomechanical strain variations. IEEE Trans. Biomed. Circuits Syst. **10**(6), 1143–1151 (2016)
72. K. Yu, M. Arifuzzaman, Z. Wen, D. Zhang, T. Sato, A key management scheme for secure communications of information centric advanced metering infrastructure in smart grid. IEEE Trans. Instrum. Measur. **64**(8), 2072–2085 (2015)
73. Qi Wang, A. A. Gebremariam, R. Palacios-Trujillo, F. Granelli, Power saving strategy in advanced metering infrastructure for high-density residential community, in *2015 IEEE 20th International Workshop on Computer Aided Modelling and Design of Communication Links and Networks (CAMAD)*, Guildford (2015), pp. 201–206
74. M. Akerele, I. Al-Anbagi, M. Erol-Kantarci, A fiber-wireless sensor networks QoS mechanism for smart grid applications. IEEE Access **7**, 37601–37610 (2019)
75. S. ivanadBirajdar, M. Mungekar, A centralized microgrid protection using wireless communication network, in *2018 International Conference on Current Trends towards Converging Technologies (ICCTCT)*, Coimbatore (2018), pp. 1–4
76. A. Jindal, G. S. Aujla, N. Kumar, R. Prodan, M. S. Obaidat, DRUMS: demand response management in a smart city using deep learning and SVR, in *2018 IEEE Global Communications Conference (GLOBECOM)*, Abu Dhabi, United Arab Emirates (2018), pp. 1–6
77. D. Bian, D. Shi, M. Pipattanasomporn, M. Kuzlu, S. Rahman, Mitigating the impact of renewable variability with demand-side resources considering communication and cyber security limitations. IEEE Access **7**, 1379–1389 (2019)
78. Y. Simmhan et al., Cloud-based software platform for big data analytics in smart grids. Comput. Sci. Eng. **15**(4), 38–47 (2013)
79. Z. Asad, M.A. Rehman Chaudhry, A two-way street: green big data processing for a greener smart grid. IEEE Syst. J. **11**(2), 784–795 (2017)
80. Y.Q. Xing, J.X. Jin, Y.L. Wang, B.X. Du, S.C. Wang, An electric vehicle charging system using an SMES implanted smart grid. IEEE Trans. Appl. Supercond. **26**(7), 1–4 (2016)
81. V. Calderaro, V. Galdi, G. Graber, G. Graditi, F. Lamberti, Impact assessment of energy storage and electric vehicles on smart grids, in *2014 Electric Power Quality and Supply Reliability Conference (PQ)*, Rakvere (2014), pp. 15–18
82. K.M. Rabie, B. Adebisi, E.H.G. Yousif, H. Gacanin, A.M. Tonello, A comparison between orthogonal and non-orthogonal multiple access in cooperative relaying power line communication systems. IEEE Access **5**, 10118–10129 (2017)
83. R.H.Y. Louie, W. Hardjawana, Y. Li, B. Vucetic, Distributed multiple-access for smart grid home area networks: compressed sensing with multiple antennas. IEEE Trans. Smart Grid **5** (6), 2938–2946 (2014)
84. D. Sharma, A. Dubey, S. Mishra, R.K. Mallik, A frequency control strategy using power line communication in a smart microgrid. IEEE Access **7**, 21712–21721 (2019)
85. G. Artale et al., A new low cost coupling system for power line communication on medium voltage smart grids. IEEE Trans. Smart Grid **9**(4), 3321–3329 (2018)
86. Y. Dong, M.J. Hossain, J. Cheng, V.C.M. Leung, Dynamic cross-layer beamforming in hybrid powered communication systems with harvest-use-trade strategy. IEEE Trans. Wireless Commun. **16**(12), 8011–8025 (2017)
87. G.A. Shah, V.C. Gungor, O.B. Akan, A cross-layer QoS-aware communication framework in cognitive radio sensor networks for smart grid applications. IEEE Trans. Ind. Inform. **9**(3), 1477–1485 (2013)
88. P. Gope, B. Sikdar, An efficient data aggregation scheme for privacy-friendly dynamic pricing-based billing and demand-response management in smart grids. IEEE Internet Things J. **5**(4), 3126–3135 (2018)
89. J. Ni, K. Zhang, X. Lin, X.S. Shen, Balancing security and efficiency for smart metering against misbehaving collectors. IEEE Trans. Smart Grid **10**(2), 1225–1236 (2019)

90. Y. Kim, J. Lee, G. Atkinson, H. Kim, M. Thottan, SeDAX: a scalable, resilient, and secure platform for smart grid communications. IEEE J. Sel. Areas Commun. **30**(6), 1119–1136 (2012)
91. S. Xu, Y. Qian, R. Qingyang Hu, Reliable and resilient access network design for advanced metering infrastructures in smart grid. IET Smart Grid **1**(1), 24–30 (2018)
92. H. Georg, S.C. Müller, C. Rehtanz, C. Wietfeld, Analyzing cyber-physical energy systems: the INSPIRE cosimulation of power and ICT systems using HLA. IEEE Trans. Ind. Inform. **10**(4), 2364–2373 (2014)
93. C. Tham, T. Luo, Sensing-driven energy purchasing in smart grid cyber-physical system. IEEE Trans. Syst. Man Cybern. Syst. **43**(4), 773–784 (2013)
94. M.K. Mishra, S.K. Parida, A game theoretic approach for demand-side management considering generation, storage and the combinatorial nature of load scheduling, in *2018 International Conference and Utility Exhibition on Green Energy for Sustainable Development (ICUE)*, Phuket, Thailand, (2018), pp. 1–8
95. M. Çinar, A. Kaygusuz, Optimization algorithms used for self-healing of smart grids, in *2018 International Conference on Artificial Intelligence and Data Processing (IDAP)*, Malatya, Turkey (2018), pp. 1–5
96. T. Holden, J. Yazdani, Hybrid security for hybrid vehicles exploring smart grid technology, powerline and wireless communication, in *2011 Second IEEE PES International Conference and Exhibition on Innovative Smart Grid Technologies*, Manchester (2011), pp. 1–5
97. F. Salvadori, C.S. Gehrke, A.C. de Oliveira, M. de Campos, P.S. Sausen, Smart grid infrastructure using a hybrid network architecture. IEEE Trans. Smart Grid **4**(3), 1630–1639 (2013)
98. L.T. Berger, A. Schwager, P. Pagani, D.M. Schneider, MIMO power line communications. IEEE Commun. Surv. Tut. **17**(1), 106–124 (2015)
99. M. Sayed, T.A. Tsiftsis, N. Al-Dhahir, On the diversity of hybrid narrowband-PLC/wireless communications for smart grids. IEEE Trans. Wireless Commun. **16**(7), 4344–4360 (2017)
100. C. Vlachou, A. Banchs, P. Salvador, J. Herzen, P. Thiran, Analysis and enhancement of CSMA/CA with deferral in power-line communications. IEEE J. Sel. Areas Commun. **34**(7), 1978–1991 (2016)
101. S. Yoon, D. Kang, S. Bahk, Multichannel CSMA/CA protocol for OFDMA-based broadband power-line communications. IEEE Trans. Power Deliv. **28**(4), 2491–2499 (2013)
102. Y. Han, K. Zhang, H. Li, E.A.A. Coelho, J.M. Guerrero, MAS-based distributed coordinated control and optimization in microgrid and microgrid clusters: a comprehensive overview. IEEE Trans. Power Electron. **33**(8), 6488–6508 (2018)
103. A. Parisio, E. Rikos, L. Glielmo, A model predictive control approach to microgrid operation optimization. IEEE Trans. Control Syst. Technol. **22**(5), 1813–1827 (2014)
104. B. Wang, M. Sechilariu, F. Locment, Intelligent DC microgrid with smart grid communications: control strategy consideration and design. IEEE Trans. Smart Grid **3**(4), 2148–2156 (2012)
105. C. Lo, N. Ansari, Decentralized controls and communications for autonomous distribution networks in smart grid. IEEE Trans. Smart Grid **4**(1), 66–77 (2013)
106. Y. Chia, S. Sun, R. Zhang, Energy cooperation in cellular networks with renewable powered base stations. IEEE Trans. Wireless Commun. **13**(12), 6996–7010 (2014)
107. Z. Fan, R.J. Haines, P. Kulkarni, M2M communications for E-health and smart grid: an industry and standard perspective. IEEE Wireless Commun. **21**(1), 62–69 (2014)
108. W. Chin, Y. Lin, H. Chen, A framework of machine-to-machine authentication in smart grid: a two-layer approach. IEEE Commun. Mag. **54**(12), 102–107 (2016)
109. R. Ma, H. Chen, W. Meng, Dynamic spectrum sharing for the coexistence of smart utility networks and WLANs in smart grid communications. IEEE Network **31**(1), 88–96 (2017)
110. R. Ma, S. Chen, H. Chen, W. Meng, Coexistence of smart utility networks and WLANs in smart grid systems. IEEE Trans. Wireless Commun. **15**(12), 8313–8324 (2016)
111. H. Al Haj Hassan, A. Pelov, L. Nuaymi, Integrating cellular networks, smart grid, and renewable energy: analysis, architecture, and challenges. IEEE Access **3**, 2755–2770 (2015)

112. X. Lu, W. Wang, J. Ma, An empirical study of communication infrastructures towards the smart grid: design, implementation, and evaluation. IEEE Trans. Smart Grid **4**(1), 170–183 (2013)
113. G. Wen, X. Yu, Z. Liu, W. Yu, Adaptive consensus-based robust strategy for economic dispatch of smart grids subject to communication uncertainties. IEEE Trans. Ind. Inform. **14** (6), 2484–2496 (2018)
114. M. Erol-Kantarci, H.T. Mouftah, Energy-efficient information and communication infrastructures in the smart Grid: a survey on interactions and open issues. IEEE Commun. Surv. Tut. **17** (1), 179–197 (2015)
115. B. Appasani, D.K. Mohanta, Optimal placement of synchrophasor sensors for risk hedging in a smart grid. IEEE Sens. J. **17**(23), 7857–7865 (2017)
116. P. Kong, C. Liu, J. Jiang, Cost-efficient placement of communication connections for transmission line monitoring. IEEE Trans. Ind. Electron. **64**(5), 4058–4067 (2017)
117. C. Wiezorek et al., Multi-location virtual smart grid laboratory with testbed for analysis of secure communication and remote co-simulation: concept and application to integration of Berlin, Stockholm, Helsinki. IET Gener. Transm. Distrib. **11**(12), 3134–3143 (2017)
118. W. Song, D. De, S. Tan, S.K. Das, L. Tong, A wireless smart grid testbed in lab. IEEE Wireless Commun. **19**(3), 58–64 (2012)

Chapter 2
Implementation of Demand Response Programs on Unit Commitment Problem

Farkhondeh Jabari, Mousa Mohammadpourfard, and Behnam Mohammadi-Ivatloo

Nomenclature

Sets

t	Operating time interval
i	The thermal generation station
k	The number of the operating zone in the linearized characteristic of the thermal power plants

Variables

P	The electrical power generation of plant i at operating time period t
$FC_{i,\,t}$	The operation cost of the fossil-fuel-based generating unit i at operating time period t
$STC_{i,\,t}$	The start-up cost of the generation station i at operating time period t
$SDC_{i,\,t}$	The shutdown cost of the generation station i at operating time period t
$u_{i,\,t}$	The binary decision variable equals to 1 if the generating unit i is on at hour t, else it is 0.
$P_i^{\max}$, $P_i^{\min}$	The maximum and minimum limits of the power generation of the plant i
$\underline{P}_{i,t}$, $\overline{P}_{i,t}$	The minimum and maximum time-related operating bounds for generation station i

F. Jabari (✉) · B. Mohammadi-Ivatloo
Faculty of Electrical and Computer Engineering, University of Tabriz, Tabriz, Iran
e-mail: f.jabari@tabrizu.ac.ir; bmohammadi@tabrizu.ac.ir

M. Mohammadpourfard
Faculty of Chemical and Petroleum Engineering, University of Tabriz, Tabriz, Iran
e-mail: Mohammadpour@tabrizu.ac.ir

S. Nojavan, K. Zare (eds.), *Demand Response Application in Smart Grids*,
https://doi.org/10.1007/978-3-030-32104-8_2

UT_i	The minimum uptime for the power plant i
DT_i	The minimum downtime for the power plant i
$y_{i,\,t}$, $z_{i,\,t}$	The start-up and shutdown modes for the power plant i at timeframe t
a_i, b_i, c_i	The fuel cost indices for the power plant i
$C^k_{i,\mathrm{ini}}$	The initial operating point of the unit i in the linearized zone k
$C^k_{i,\mathrm{fin}}$	The final operating point of the unit i in the linearized zone k
ΔP^k_i	The deviation of the power generation of power plant i in zone k
n	Number of linear zones
s^k_i	The slope of the fuel cost characteristic of power plant i in zone k
SU_i, SD_i	The boundaries of the start-up and shutdown ramp rates of the power plant i
L^0_t	Base load at hour t without applying the DSM program
Lt	Energy demand at time t
DSM_t	Percentage of load decrease at time t
inc_t	Percentage of demand increase at hour t

2.1 Introduction

The consumption of electrical energy is increasing as a result of global population growth. In developing countries such as Iran, the limited reconfiguration of the interconnected power systems and the higher energy utilization cause a considerable imbalance between load and generation, which usually arises in the summer [1]. Hence, implementation of demand-side management (DSM) strategies for peak load reduction can reduce daily operation cost of thermal power plants [2].

Recently, different approaches have been proposed by scholars to solve a unit commitment (UC) problem, minimize daily fuel cost of power producers, and determine their optimum generation schedules for satisfying demand [3, 4]. If maximization of profit achieved from selling energy in the electricity market is the main objective, hourly variations of market prices are considered in mixed-integer nonlinear programming problem (MINLP) and called a profit-based UC problem [1, 5, 6]. Multiobjective optimization techniques are also presented for simultaneous minimization of fuel cost and emissions associated with coal- and gas-fired power plants [7, 8]. According to Refs. [9, 10], minimization of greenhouse gas footprints is considered in optimization problem to find the Pareto optimal solutions. Weighting method can be applied on economic-emission dispatch problem to change a multiobjective framework to a single objective mixed-integer program [11–13]. Unlike the weighting approaches, the evolutionary algorithm proposed in [14] requires only one run to reach the Pareto optimal frontiers. A modified particle swarm optimization algorithm is introduced in [15, 16], which is able to find better generation schedules than the weighting method and evolutionary algorithm. Authors of [17] presented a bilevel unit commitment model to model the availability of the wind product and find a robust operating point of the generation units against

the wind shortages. In [18], cuckoo search algorithm is exerted on optimal operation of photovoltaic-hydrothermal units. Uncertainties associated with solar irradiations could also be models under clear and cloudy sky conditions. In [19], the information gap decision theory (IGDT) is applied on unit commitment problem to clear the joint reserve and energy market and make robust and opportunistic decisions against the uncertain prices. The IGDT approach is also integrated with load-level control strategies in the UC optimization problem [20]. In [21], minimization of transmission lines overloading probability is incorporated in the UC problem using the dynamic branch loading index. In [22], the fluctuations in the wind power are compensated in the probabilistic UC problem using optimal scheduling of the pumped hydroelectric energy storage and participation of flexible customers in demand response programs. In [23], cooperation of thermal power plants with aggregated pure electric vehicles and advanced adiabatic compressed air energy storage is optimized. Reference [24] combined lexicographic optimization method and augmented-weighted ε-constraint algorithm to reach better solutions than particle swarm optimization and evolutionary algorithm. A fuzzy logic-based security constrained UC problem is solved in [24], which is able to assess the impact of the natural gas availability on generation capability of the thermal power stations. In this research, the genetic algorithm is used for solving the load flow problem in the gas network.

A high investment should be made on large-scale power systems, transmission lines, and distribution grids to procure a maximum electrical demand, which occurs at some hours of hot days [25–27]. To solve this issue, DSM programs are implemented on different district levels. They are defined as follows [28, 29]: changes in energy consumption pattern of industrial/residential/commercial/agricultural end users in response to fluctuations of electricity tariffs aiming to reduce a part of electricity usage when system reliability is at risk or at hours with high energy rates. In other words, the DSM approach applies to power systems faced with contingencies to prevent blackouts. In a general category, there are two types of load management Schemes [30, 31]: incentive-based models and price-based ones. Incentive-based DSM programs consist of direct load control, load curtailment, demand bidding, and emergency load reduction methods [32]. In direct load control, each registered customer or participant receives incentive to allow the system operator to shut its appliances down when system reliability is decreased or events [33, 34]. In load curtailment programs, each registered end user is informed to reduce or curtail its electricity usage by regional distribution companies [35]. If he or she does not fulfill its commitments, he will be penalized. In a demand bidding program, a consumer with more than 1-MW demand can bid to curtail a percentage of its load under a certain rate [36, 37]. The price-based demand response programs consist of time of use, critical peak pricing, and real-time pricing procedures. In the time of use method, consumers are encouraged to shift a part of their consumption from peak hours to mid-peak and off-peak periods and reduce their bill [38–40]. Critical peak pricing is only used for annual peak clipping in the summer [41]. The electricity tariffs in critical peak shifting scheme is higher than the time of use prices [42, 43]. Real-time pricing method is similar to the time of use approach. But hourly electricity prices are considered instead of three-level rates [44].

Although there are many researches on the UC problem, it has not been solved in the presence of load management programs. As known, if the value of the electrical demand is higher than the sum of the generation capacity of thermal units, the UC problem will fail and not be solved. Therefore, the use of the demand response programs can reduce the peak load and shift this value to other mid-peak and low-demand hours. Hence, the load variation curve will be smoother. Therefore, the current chapter proposes the DSM-based UC strategy for reducing the start-up, shutdown, and fuel cost of the power plants as low as possible. A standard system with 10 units is tested without and with consideration of the DSM program in the UC problem. The optimal solutions of two cases are compared and the cost saving is determined.

The rest of the current chapter is presented as follows: In Sect. 2.2, integration of the unit commitment problem with demand response programs (DRPs) is mathematically formulated. Afterward, case study and result analyses are described in Sect. 2.3. Conclusion is presented in Sect. 2.4.

2.2 Problem Formulation

A comprehensive problem formulation section is presented for modeling the day-ahead unit commitment problem. The daily cost of the power procurement process is selected as the objective function and minimized by solving the mixed integer nonlinear programming problem (MINLP). The start-up cost, shutdown cost, and fuel cost of the power plants are incorporated in the objective function. The ramp down and up rates, minimum uptime, minimum downtime, power production capacity, and calculation of the fuel cost of the thermal generating units are completely presented in the optimization model. Firstly, the base unit commitment problem is developed under the general algebraic mathematical modeling system taking into account the mentioned constraints. The power generation schedules of the thermal units are obtained as the main decision variables. Then, the second case study is implemented on the same test system in the presence of a DSM program. The output electrical power of the thermal units and the economic saving achieved from applying the DSM on the unit commitment problem is investigated and compared with the first one. In the DSM strategy, a part of the electrical demand is shifted from on-peak hours to low-demand periods. Therefore, Sect. 2.2.1 presents a cost-based unit commitment problem. Then, the time-value-based DSM approach is formulated in Sect. 2.2.2.

2.2.1 Unit Commitment Problem

Figure 2.1 shows how the fuel cost of the unit i changes with respect to its output power.

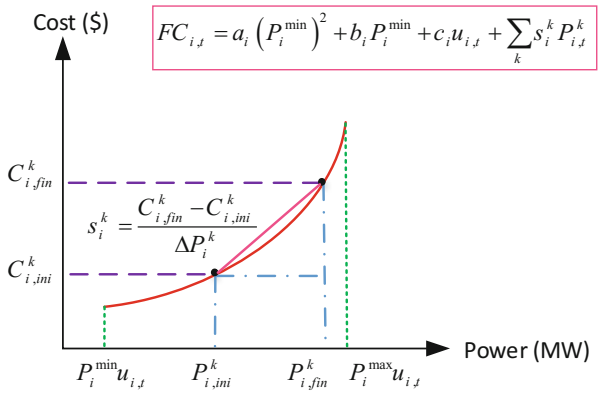

Fig. 2.1 The schematic presentation of the fuel cost calculation for the thermal unit i

In the base UC problem, the sum of the start-up cost, shutdown cost, and fuel cost of generation units is minimized as in Eq. (2.1) subjecting to (2.2)–(2.24).

$$\text{Cost} = Min \sum_{i,t} (\text{FC}_{i,t} + \text{STC}_{i,t} + \text{SDC}_{i,t}) \tag{2.1}$$

According to (2.2), it is assumed that the distance between the lower and the upper bounds of the power generation of unit i is divided into n sections. Moreover, a maximum value of power change within each subinterval k is equal to ΔP_i^k, which is modeled as (2.3).

$$\Delta P_i^k = \frac{P_i^{\max} - P_i^{\min}}{n} \tag{2.2}$$

$$0 \le P_{i,t}^k \le \Delta P_i^k u_{i,t}, \quad \forall k = 1:n \tag{2.3}$$

The initial and final levels of the power for unit i in section k of the linearized cost-power model are calculated based on power changes in this subinterval, ΔP_i^k, and the minimum generation capacity of power plant i,$P_i^{\min}$.

$$P_{i,\text{ini}}^k = (k-1)\Delta P_i^k + P_i^{\min} \tag{2.4}$$

$$P_{i,\text{fin}}^k = \Delta P_i^k + P_{i,\text{ini}}^k \tag{2.5}$$

As expressed by (2.6), the power output of the thermal unit i is equal to the sum of its minimum capacity and power production schedules of this unit in k sections of the linearized model.

$$P_{i,t} = P_i^{\min} u_{i,t} + \sum_k P_{i,t}^k \tag{2.6}$$

The fuel cost of the thermal unit i for generating the initial and final values of power in section k is obtained as (2.7) and (2.8), respectively. These costs depend on constant factors a_i, b_i, and c_i and decision variables $P_{i,\text{ini}}^k$ and $P_{i,\text{fin}}^k$.

$$C_{i,\text{ini}}^k = a_i \left(P_{i,\text{ini}}^k\right)^2 + b_i P_{i,\text{ini}}^k + c_i \tag{2.7}$$

$$C_{i,\text{fin}}^k = a_i \left(P_{i,\text{fin}}^k\right)^2 + b_i P_{i,\text{fin}}^k + c_i \tag{2.8}$$

The slope of the fuel cost-power curve in section k of the linearized model, s_i^k, is calculated from (2.9) and used for finding its fuel cost at hour t. It is obvious from Fig. 2.1 that s_i^k is obtained in terms of \$/MWh. By inserting it in (2.10), $s_i^k P_{i,t}^k$ will be achieved in \$.

$$s_i^k = \frac{C_{i,\text{fin}}^k - C_{i,\text{ini}}^k}{\Delta P_i^k} \tag{2.9}$$

$$\text{FC}_{i,t} = a_i \left(P_i^{\min}\right)^2 + b_i P_i^{\min} + c_i u_{i,t} + \sum_k s_i^k P_{i,t}^k \tag{2.10}$$

The power generation of the thermal unit i at each operating time period t is limited by maximum and minimum values as inequality constraint (2.11).

$$\underline{P}_{i,t} \le P_{i,t} \le \overline{P}_{i,t} \tag{2.11}$$

If the thermal unit i shuts down at time period $t + 1$, its shutdown ramp rate and status will be modeled as $\overline{P}_{i,t} \le \text{SD}_i z_{i,t+1}$, as stated by (2.12) and (2.13). If the generation station i is off at hour $t - 1$ and $P_{i,\,t-1} = 0$, its shutdown ramp rate should be considered to limit the power generation at hour t as $P_{i,\,t} \le \text{SD}_i$. If the power plant i is on at hour $t - 1$ ($u_{i,\,t-1} = 1$) and will be on at the next hour, its power generation, $P_{i,\,t}$, can be increased up to RU_i and $\overline{P}_{i,t} \le P_{i,t-1} + \text{RU}_i u_{i,t-1}$. If the thermal unit i is off at period $t - 1$ ($u_{i,\,t-1} = 0$) and should be on at the next hour ($y_{i,\,t} = 1$), its maximum power generation at hour t, $\overline{P}_{i,t}$, will be smaller than SU_i and $\overline{P}_{i,t} \le \text{SU}_i y_{i,t}$.

$$\overline{P}_{i,t} \le P_i^{\max}[u_{i,t} - z_{i,t+1}] + \text{SD}_i z_{i,t+1} \tag{2.12}$$

$$\overline{P}_{i,t} \le P_{i,t-1} + \text{RU}_i u_{i,t-1} + \text{SU}_i y_{i,t} \tag{2.13}$$

According to constraints (2.14) and (2.15), if the producer i is on at time interval t, its output will be more than the minimum generation value $P_i^{\min} u_{i,t}$. If the unit i is on for the time periods $t - 1$ and t, its electrical power generation at hour t will be higher

than $P_{i,\,t\,-\,1} - \mathrm{RD}_i u_{i,\,t}$. If the generator i is on at time period $t-1$ and off at hour t, the electrical power generated by this unit at hour $t-1$ will be smaller than the value $\mathrm{SD}_i z_{i,\,t}$.

$$\underline{P}_{i,t} \geq P_i^{\min} u_{i,t} \tag{2.14}$$

$$\underline{P}_{i,t} \geq P_{i,t-1} - \mathrm{RD}_i u_{i,t} - \mathrm{SD}_i z_{i,t} \tag{2.15}$$

Based on (2.16) and (2.17), the shutdown and the start-up conditions of the generation station i at hour t are shown with auxiliary binary decision variables $y_{i,\,t}$ and $z_{i,\,t}$, respectively.

$$y_{i,t} - z_{i,t} = u_{i,t} - u_{i,t-1} \tag{2.16}$$

$$y_{i,t} + z_{i,t} \leq 1 \tag{2.17}$$

The minimum uptime (UT_i) of the unit i is modeled as (2.18)–(2.20). If the unit i has been on at $t=0$, for fewer hours than UT_i, constraint (2.18) is considered when modeling the minimum uptime limit of the power plant i. This criterion is imposed on all time subintervals with UT_i hours, as stated by (2.19). According to (2.20), during the last $\mathrm{UT}_i - 1$ hours, the unit i will be committed until the last hour if it is started at each hour of this set.

$$\sum_{t=1}^{\zeta_i} 1 - u_{i,t} = 0; \text{ where } \quad \zeta_i = \min\left\{T, \left(\mathrm{UT}_i - U_i^0\right) u_{i,t=0}\right\} \tag{2.18}$$

$$\sum_{t=k}^{k+\mathrm{UT}_i-1} u_{i,t} \geq \mathrm{UT}_i\, y_{i,k} \quad \forall k = \zeta_i + 1, \ldots, T - \mathrm{UT}_i + 1 \tag{2.19}$$

$$\sum_{t=k}^{T} u_{i,t} - y_{i,t} \geq 0 \quad \forall k = T - \mathrm{UT}_i + 2, \ldots, T \tag{2.20}$$

Similarly, the minimum downtime (DT_i) of unit i is formulated by (2.21)–(2.23). If the generating unit i has been off at $t=0$, for fewer hours than DT_i, Eq. (2.21) will be incorporated into the UC problem to model its minimum downtime constraint. This constraint is used for all time sets with DT_i hours, as expressed in (2.22). Based on (2.23), during the last $\mathrm{DT}_i - 1$ hours, the unit i will be decommitted until the last hour if it is off at each hour of this set.

$$\sum_{t=1}^{\xi_i} u_{i,t} = 0; \text{ where } \xi_i = \min\left\{T, \left(\mathrm{DT}_i - S_i^0\right)[1 - u_{i,t=0}]\right\} \tag{2.21}$$

$$\sum_{t=k}^{k+\mathrm{DT}_i-1} 1-u_{i,t} \geq \mathrm{DT}_i z_{i,k} \quad \forall k = \xi_i + 1, \ldots, T - \mathrm{DT}_i + 1 \tag{2.22}$$

$$\sum_{t=k}^{T} 1-u_{i,t} - z_{i,t} \geq 0 \quad \forall k = T - DT_i + 2, \ldots, T \tag{2.23}$$

The start-up cost ($\mathrm{STC}_{i,t}$) and the shutdown cost ($\mathrm{SDC}_{i,t}$) of the unit i at hour t are assumed as $st_i \times y_{i,t}$ and $sd_i \times z_{i,t}$, respectively. At each hour t, the total electrical power generated by the thermal units should be equal to demand, as given by (2.24).

$$\sum_i P_{i,t} = L_t \tag{2.24}$$

2.2.2 Demand Response Programs

Figure 2.2 demonstrates the concept of the demand-side management approach. It is assumed that the initial value of the electrical demand at time t is described as L_t^0. The percentage of the load decrease and increase at each hour is selected as the decision variables $\mathrm{DSM}_t$and inc_t, respectively.

According to balance equation (2.25), if the DSM program is not considered in the optimization problem, the values of the demand increase $\mathrm{inc}_t \times L_t^0$ and decrease $\mathrm{DSM}_t \times L_t^0$ will be equal to zero. Hence, $L_t = L_t^0$. In the case of application of the DSM strategy in the unit commitment problem, if $0 < \mathrm{DSM}_t < 0.25$, the value of the energy consumption at hour t will decrease to $L_t^0(1 - \mathrm{DSM_t})$. Similarly, if $0 < \mathrm{inc}_t < 0.25$, the demand will increase as $L_t^0 \times \mathrm{inc}_t$.

$$L_t = L_t^0(1 - \mathrm{DSM}_t) + \mathrm{inc}_t \times L_t^0 \tag{2.25}$$

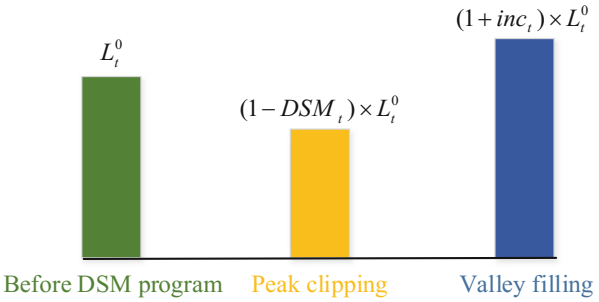

Fig. 2.2 The load value before and after implementation of the DSM program

To shift the demand from 1 h to other times, the value of the load reductions at a 24-h time interval is considered to be equal to the total demand increase at the same period, as stated by (2.26).

$$\sum_{t=1}^{T} \left(\text{inc}_t \times L_t^0\right) = \sum_{t=1}^{T} \left(\text{DSM}_t \times L_t^0\right) \tag{2.26}$$

As mentioned in (2.27) and (2.28), the maximum value of the demand increase and decrease is limited to 25% of the base load and $\text{DSM}_{\max} = \text{inc}_{\max} = 0.25$.

$$0 \leq \text{DSM}_t \leq \text{DSM}_{\max} \tag{2.27}$$

$$0 \leq \text{inc}_t \leq \text{inc}_{\max} \tag{2.28}$$

2.3 Illustrative Example and Discussions

In order to show that time-value-based demand shifting strategy is a cost-effective tool in the unit commitment problem, a real case study has been selected for simulations. The standard power system is composed of 10 thermal power plants [45]. The constant factors related to the generating units are listed in Table 2.1. At the first case study, the value of the coefficients $\text{DSM}_{\max}$ and $\text{inc}_{\max}$ is considered to be equal to zero. Hence, the value of the demand increase and decrease will be equal to zero. In case 1, the demand response program has not been implemented on the unit commitment problem (2.1)–(2.24). In the second case study, it is supposed that $\text{DSM}_{\max} = \text{inc}_{\max} = 0.25$. Hence, a maximum of 25% demand can reduce at peak hours. Moreover, t1maximum value of load increase at hour t is equal to 25% of the base demand L_t^0. The MINLP is solved under the generalized algebraic mathematical modeling system (GAMS) [46] using the standard branch-and-bound (SBB) solver [47]. The hourly variations of the electrical demand over the 24-h study horizon is illustrated in Fig. 2.3.

The optimum generation schedules of the thermal units 2, 4, and 6 in two cases "case 1: without demand response programs" and "case 2: with demand response programs" are depicted in Figs. 2.4, 2.5, and 2.6, respectively. In addition, the on and off status of all units before and after implementation of the load shifting program is reported in Table 2.2. For instance, it is obvious from Fig. 2.4 that unit 2 is off at hours 1 and 2 in two cases. But it turns on at hour 3 and remains on until $t = 24$. Moreover, the output electrical power of this unit at peak demand period and case 1 increases to satisfy a higher electricity load. After implementation of the DSM program, it is economic to reduce its power production to 140 MW at peak time interval (from $t = 8$ to $t = 20$) and increase it up to 140 MW at mid- and off-peak hours (from $t = 3$ to $t = 7$ and $t = 21$ to $t = 24$).

Table 2.1 The specifications of the generating units [45]

i	a_i	b_i	c_i	sd_i	st_i	RU_i	RD_i	UT_i	DT_i	SD_i	SU_i	$P_i^{\min}$	$P_i^{\max}$	U_0	U_{ini}	S_0
1	0.014	12.1	82	42.6	42.6	40	40	3	2	90	110	80	200	1	0	1
2	0.028	12.6	49	50.6	50.6	64	64	4	2	130	140	120	320	2	0	0
3	0.013	13.2	100	57.1	57.1	30	30	3	2	70	80	50	150	3	0	3
4	0.012	13.9	105	47.1	47.9	104	104	5	3	240	250	250	250	1	1	0
5	0.026	13.5	72	56.6	56.9	56	56	4	2	110	130	80	280	1	1	0
6	0.021	15.4	29	141.5	141.5	30	30	3	2	60	80	50	150	0	0	0
7	0.038	14	32	113.5	113.5	24	24	3	2	50	60	30	120	0	1	0
8	0.039	13.5	40	42.6	42.6	22	22	3	2	45	55	30	110	0	0	0
9	0.039	15	25	50.6	50.6	16	16	0	0	35	45	20	80	0	0	0
10	0.051	14.3	15	57.1	57.1	12	12	0	0	30	40	20	60	0	0	0

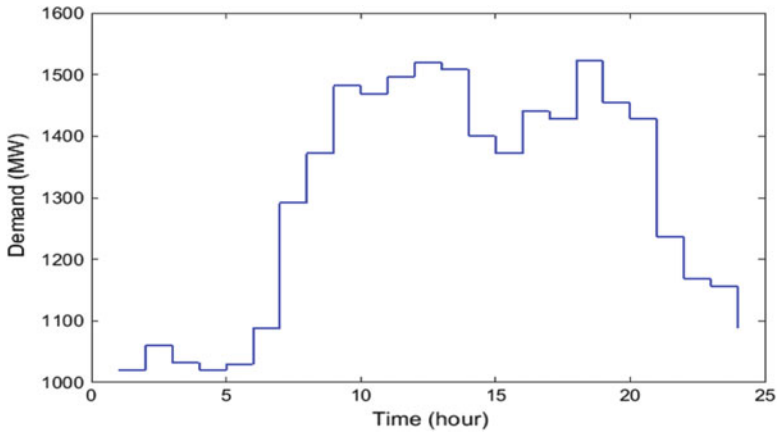

Fig. 2.3 The daily profile of the electrical load

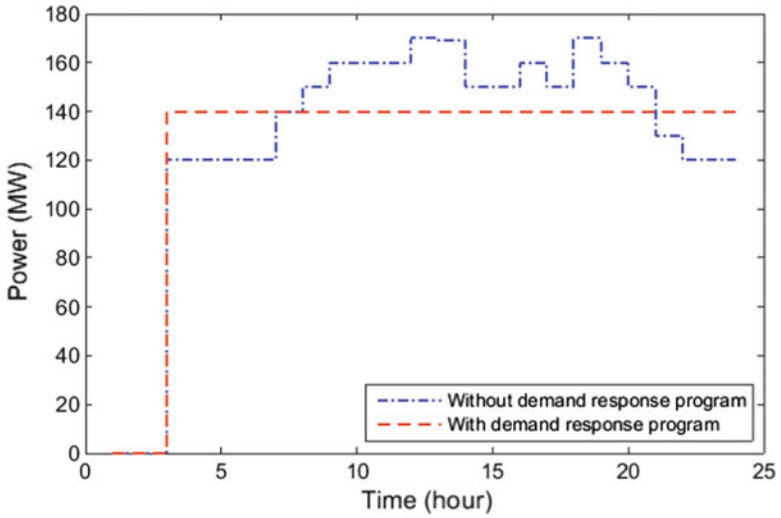

Fig. 2.4 Optimum generation schedule of thermal unit 2 before and after application of demand response program

According to Fig. 2.5, it is found that when the load management program is not applied on a multiperiod UC problem, the hourly production pattern of the thermal power plant 4 changes severely. But it has been flattening by applying the time-value-based demand response program, as shown in red. Moreover, not only does this generation station decrease its power at high-demand hours (from $t = 8$ to $t = 21$), but also the application of the DSM strategy results in a significant reduction of its power generation from 412 and 371 MW to 277 MW at hours 1 and 2, respectively. From $t = 8$ to $t = 20$, the value of the electrical demand decreases in the case

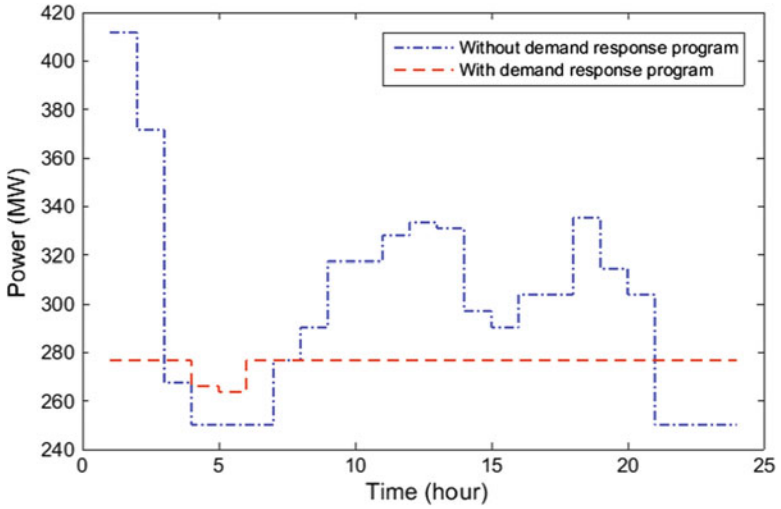

Fig. 2.5 Economic operating point of thermal unit 4 without and with implementation of DSM scheme

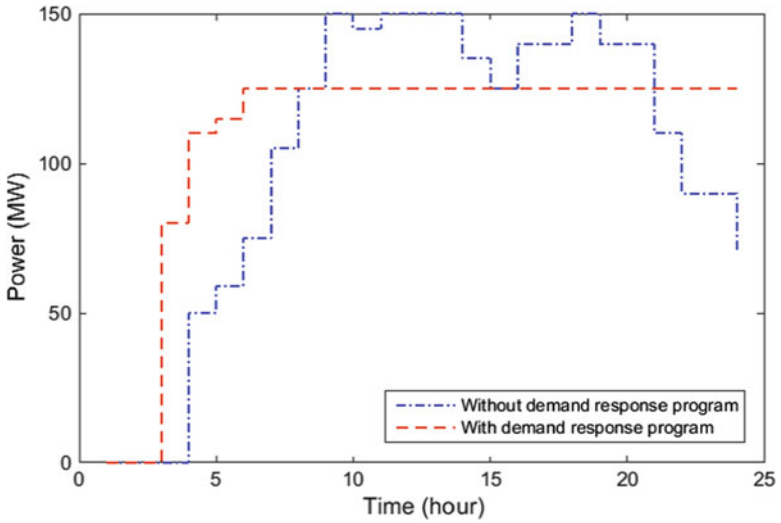

Fig. 2.6 Output power of generating unit 6 in two cases: "without demand response program" and "with demand response program"

of the "with demand response program" case. It is expected from constraint (2.28) that the reduced demand is satisfied at mid−/off-peak load periods. Therefore, the thermal unit 4 should provide the higher electricity from $t = 3$ to $t = 7$ and $t = 21$ to $t = 24$. This leads to flattening of the daily power generation pattern.

Table 2.2 On and off status of thermal units before and after the demand response approach

Hours	Units									
	1	2	3	4	5	6	7	8	9	10
1	0	0	1	1	1	0	1	0	1	1
2	1	0	1	1	1	0	1	0	1	1
3	1	1	1	1	1	0	1	1	1	1
4	1	1	1	1	1	1	1	1	1	1
5	1	1	1	1	1	1	1	1	1	1
6	1	1	1	1	1	1	1	1	1	1
7	1	1	1	1	1	1	1	1	1	1
8	1	1	1	1	1	1	1	1	1	1
9	1	1	1	1	1	1	1	1	1	1
10	1	1	1	1	1	1	1	1	1	1
11	1	1	1	1	1	1	1	1	1	1
12	1	1	1	1	1	1	1	1	1	1
13	1	1	1	1	1	1	1	1	1	1
14	1	1	1	1	1	1	1	1	1	1
15	1	1	1	1	1	1	1	1	1	1
16	1	1	1	1	1	1	1	1	1	1
17	1	1	1	1	1	1	1	1	1	1
18	1	1	1	1	1	1	1	1	1	1
19	1	1	1	1	1	1	1	1	1	1
20	1	1	1	1	1	1	1	1	1	1
21	1	1	1	1	1	1	1	1	1	1
22	1	1	1	1	1	1	1	1	1	1
23	1	1	1	1	1	1	1	1	1	1
24	1	1	1	1	1	1	1	1	1	1

Figures 2.3 and 2.6 demonstrate that the output power of the generating unit 6 before implementation of load curve smoothing approach increases at time interval $t = 8$ to $t = 20$ with large-value power consumption. But if the peak-clipping and valley filling scheme is considered in the optimal scheduling of the committed units, it will be reduced to 125 MW. From $t = 3$ to $t = 7$ and $t = 21$ to $t = 24$, the value of the electrical demand will be increased to supply the shifted power load. In Figs. 2.4, 2.5, and 2.6, the blue curves represent the optimal operating point of the thermal generating units 2, 4, and 6 before using DSM policies. The red one shows the same decision variables for the "with demand response program" case. For all power generating units, the decision variable $P_{i,\,t}$ is reduced when the electrical demand is high and increased at off-peak time interval. This leads to the smooth generation pattern of power plants. Therefore, their fuel costs are reduced after applying the DSM program on the UC problem.

Moreover, the load profile before and after application of the demand response program is compared in Fig. 2.7. The numerical values of the load increase and decrease are reported in Table 2.3. As obvious from Fig. 2.3, the on-peak electrical demand occurs from $t = 8$ to $t = 20$. In addition, the off-peak load occurs at other

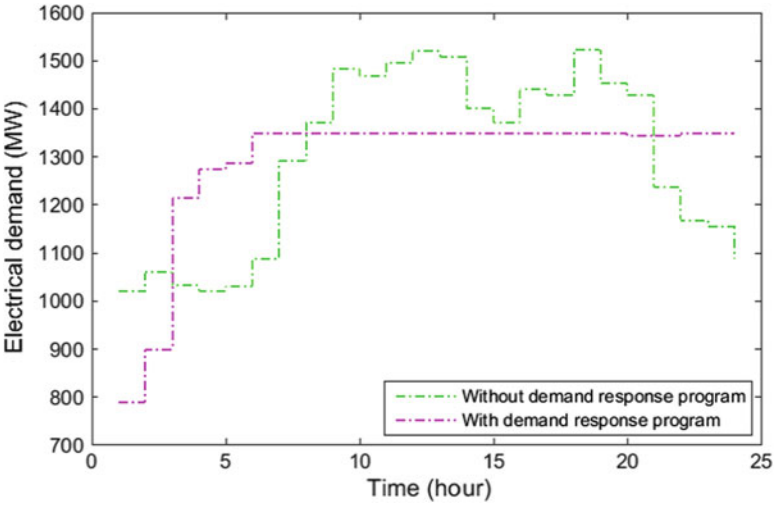

Fig. 2.7 The electrical load profile before and after participation of customers in the DSM scheme

Table 2.3 The values of the load increase and decrease in the demand-side management approach

Time (h)	Load increase or decrease (MW)
1	−230.5
2	−160.5
3	182.5
4	255
5	257.5
6	260.5
7	56.5
8	−23.5
9	−133.5
10	−119.5
11	−147.5
12	−171.5
13	−159.5
14	−51.5
15	−23.5
16	−91.5
17	−79.5
18	−173.5
19	−105.5
20	−83
21	108.5
22	180.5
23	192.5
24	260.5

Table 2.4 The values of the load increase and decrease in the demand-side management approach

Case study	Start-up cost ($)	Shutdown cost ($)	Fuel cost ($)	Objective function ($)	Cost saving ($)
1	420	0	533,978	534,420	3190
2	0	0	531,230	531,230	

time intervals. By solving the optimization problem (2.1)–(2.28), the value of the load increase or decrease at each hour is found in Table 2.3. It is demonstrated that the on-peak demand is shifted to the low-demand hours. In Table 2.3, the negative sign refers to the load decrease and the positive one represents the load increase. It is obvious that from $t = 8$ to $t = 20$, the value of the load change is negative and a part of the electrical demand is shifted to other time intervals. During $t = 3$ to $t = 7$ and $t = 21$ to $t = 24$, the off-peak electrical demand has been increased after implementation of the demand response program, as obvious from Table 2.3 and shown in Fig. 2.7.

According to Table 2.4, the start-up cost of thermal units after implementation of demand response programs is decreased from $442 to 0. By implementing the peak-clipping and valley filling strategy in the electricity consumption pattern, the optimum operating point of the generation units changes in a way that the total fuel cost reduces from $533,978 to $531,230. Therefore, the objective function is reduced from $534,420 to $531,230 using the demand response programs. In fact, when the peak electrical demand is shifted to off-peak load periods, the value of the power generation of the thermal units is reduced at peak time intervals and increased at other hours, as seen from Figs. 2.4, 2.5, and 2.6. This leads to a significant reduction in their fuel costs as well as their optimal generation curves being flattened. In summary, $3190 cost saving results from incorporation of demand response programs in the cost-based unit commitment problem.

2.4 Conclusion

In this chapter, a cost-based unit commitment problem was comprehensively presented to determine the best operating schedule of the conventional generation stations. The start-up cost, shutdown cost, and fuel cost of the fossil-fuel-based power plants were introduced as a single objective function and minimized in two case studies: “without demand response program” and “with demand response program.” It was found that the optimal generation curve of each thermal unit was flattened by shifting a part of the peak electrical demand to off-peak load periods. Therefore, the daily fuel cost and start-up cost of thermal power plants were decreased, considerably. But shutdown cost in two cases was obtained to be equal to zero, which reveals the capability of the generalized mathematical algebraic modeling system software in finding the least operation cost. In future trends, the value of the incentives, which should be paid to participants in demand-side

management strategies, will be considered in the load procurement process. In addition, the uncertainties of electrical load and renewable energy resources in the cost-based unit commitment problem can be modeled using the risk-constrained short-term scheduling methods such as information gap decision theory, game theory, and robust optimization approach.

References

1. H. Anand, N. Narang, J.S. Dhillon, Profit based unit commitment using hybrid optimization technique. Energy **148**, 701–715 (2018)
2. B. Lokeshgupta, S. Sivasubramani, Multi-objective dynamic economic and emission dispatch with demand side management. Int. J. Electr. Power Energy Syst. **97**, 334–343 (2018)
3. V.K. Tumuluru, D.H. Tsang, A two-stage approach for network constrained unit commitment problem with demand response. IEEE Trans. Smart Grid **9**(2), 1175–1183 (2018)
4. L.K. Panwar et al., Binary grey wolf optimizer for large scale unit commitment problem. Swarm Evol. Comput. **38**, 251–266 (2018)
5. K.S. Reddy et al., Binary whale optimization algorithm: a new metaheuristic approach for profit-based unit commitment problems in competitive electricity markets. Eng. Optim., 1–21 (2018)
6. K.S. Reddy et al., A new binary variant of sine–cosine algorithm: development and application to solve profit-based unit commitment problem. Arab. J. Sci. Eng. **43**(8), 4041–4056 (2018)
7. H. Liang et al., A multiobjective hybrid bat algorithm for combined economic/emission dispatch. Int. J. Electr. Power Energy Syst. **101**, 103–115 (2018)
8. F. Chen et al., A nonlinear fractional programming approach for environmental–economic power dispatch. Int. J. Electr. Power Energy Syst. **78**, 463–469 (2016)
9. K. Le et al., Potential impacts of clean air regulations on system operations. IEEE Trans. Power Syst. **10**(2), 647–656 (1995)
10. F.P. Mahdi et al., A holistic review on optimization strategies for combined economic emission dispatch problem. Renew. Sustain. Energy Rev. **81**, 3006–3020 (2018)
11. S. Kuloor, G. Hope, O. Malik, Environmentally constrained unit commitment, in *IEE Proceedings C-Generation, Transmission and Distribution* (IET, 1992)
12. F. Jabari, M. Shamizadeh, B. Mohammadi-Ivatloo, Risk-constrained day-ahead economic and environmental dispatch of thermal units using information gap decision theory. Int. Trans. Electr. Energy Syst. **29**, e2704 (2018)
13. S. Bath, J. Dhillon, D. Kothari, Fuzzy satisfying stochastic multi-objective generation scheduling by weightage pattern search methods. Electr. Power Syst. Res. **69**(2–3), 311–320 (2004)
14. M.A. Abido, Environmental/economic power dispatch using multiobjective evolutionary algorithms. IEEE Trans. Power Syst. **18**(4), 1529–1537 (2003)
15. L. Wang, C. Singh, Environmental/economic power dispatch using a fuzzified multi-objective particle swarm optimization algorithm. Electr. Power Syst. Res. **77**(12), 1654–1664 (2007)
16. L. Wang, C. Singh, Stochastic economic emission load dispatch through a modified particle swarm optimization algorithm. Electr. Power Syst. Res. **78**(8), 1466–1476 (2008)
17. G. Morales-España, Á. Lorca, M.M. de Weerdt, Robust unit commitment with dispatchable wind power. Electr. Power Syst. Res. **155**, 58–66 (2018)
18. B. Ming et al., Robust hydroelectric unit commitment considering integration of large-scale photovoltaic power: a case study in China. Appl. Energy **228**, 1341–1352 (2018)
19. K. Ghahary et al., Optimal reserve market clearing considering uncertain demand response using information gap decision theory. Int. J. Electr. Power Energy Syst. **101**, 213–222 (2018)
20. A. Soroudi, A. Rabiee, A. Keane, Information gap decision theory approach to deal with wind power uncertainty in unit commitment. Electr. Power Syst. Res. **145**, 137–148 (2017)

21. H. Park, Y.G. Jin, J.-K. Park, Stochastic security-constrained unit commitment with wind power generation based on dynamic line rating. Int. J. Electr. Power Energy Syst. **102**, 211–222 (2018)
22. B. Durga Hari Kiran, M. Sailaja Kumari, Demand response and pumped hydro storage scheduling for balancing wind power uncertainties: a probabilistic unit commitment approach. Int. J. Electr. Power Energy Syst. **81**, 114–122 (2016)
23. Z. Soltani et al., Integration of smart grid technologies in stochastic multi-objective unit commitment: an economic emission analysis. Int. J. Electr. Power Energy Syst. **100**, 565–590 (2018)
24. S. Badakhshan, M. Kazemi, M. Ehsan, Security constrained unit commitment with flexibility in natural gas transmission delivery. J. Nat. Gas Sci. Eng. **27**, 632–640 (2015)
25. P. Siano, Demand response and smart grids—a survey. Renew. Sustain. Energy Rev. **30**, 461–478 (2014)
26. M.H. Albadi, E.F. El-Saadany, A summary of demand response in electricity markets. Electr. Power Syst. Res. **78**(11), 1989–1996 (2008)
27. M. Vahid-Ghavidel, N. Mahmoudi, B. Mohammadi-Ivatloo, Self-scheduling of demand response aggregators in short-term markets based on information gap decision theory. IEEE Trans. Smart Grid **10**(2), 2115–2126 (2019)
28. A.R. Jordehi, Optimisation of demand response in electric power systems, a review. Renew. Sustain. Energy Rev. **103**, 308–319 (2019)
29. A. Rabiee et al., Corrective voltage control scheme considering demand response and stochastic wind power. IEEE Trans. Power Syst. **29**(6), 2965–2973 (2014)
30. M. Rahmani-andebili, Modeling nonlinear incentive-based and price-based demand response programs and implementing on real power markets. Electr. Power Syst. Res. **132**, 115–124 (2016)
31. M. Vahid-Pakdel et al., Stochastic optimization of energy hub operation with consideration of thermal energy market and demand response. Energy Convers. Manage. **145**, 117–128 (2017)
32. J. Vuelvas, F. Ruiz, G. Gruosso, Limiting gaming opportunities on incentive-based demand response programs. Appl. Energy **225**, 668–681 (2018)
33. N. Ruiz, I. Cobelo, J. Oyarzabal, A direct load control model for virtual power plant management. IEEE Trans. Power Syst. **24**(2), 959–966 (2009)
34. A. Dorri, et al. A Secure and Efficient Direct Power Load Control Framework Based on Blockchain. arXiv preprint arXiv:1812.08497 (2018)
35. H. Aalami, M.P. Moghaddam, G. Yousefi, Demand response modeling considering interruptible/curtailable loads and capacity market programs. Appl. Energy **87**(1), 243–250 (2010)
36. L. Yao, W.H. Lim, Optimal purchase strategy for demand bidding. IEEE Trans. Power Syst. **33** (3), 2754–2762 (2018)
37. J. Iria, F. Soares, M. Matos, Optimal supply and demand bidding strategy for an aggregator of small prosumers. Appl. Energy **213**, 658–669 (2018)
38. P. Yang, G. Tang, A. Nehorai, A game-theoretic approach for optimal time-of-use electricity pricing. IEEE Trans. Power Syst. **28**(2), 884–892 (2013)
39. E. Celebi, J.D. Fuller, Time-of-use pricing in electricity markets under different market structures. IEEE Trans. Power Syst. **27**(3), 1170–1181 (2012)
40. S. Nojavan, K. Zare, B. Mohammadi-Ivatloo, Optimal stochastic energy management of retailer based on selling price determination under smart grid environment in the presence of demand response program. Appl. Energy **187**, 449–464 (2017)
41. D. Jang et al., Demand responses of Korean commercial and industrial businesses to critical peak pricing of electricity. J. Cleaner Prod. **90**, 275–290 (2015)
42. D. Jang et al., Variability of electricity load patterns and its effect on demand response: a critical peak pricing experiment on Korean commercial and industrial customers. Energy Policy **88**, 11–26 (2016)
43. M. Kazemi, B. Mohammadi-Ivatloo, M. Ehsan, Risk-based bidding of large electric utilities using information gap decision theory considering demand response. Electr. Power Syst. Res. **114**, 86–92 (2014)

44. A.J. Conejo, J.M. Morales, L. Baringo, Real-time demand response model. IEEE Trans. Smart Grid **1**(3), 236–242 (2010)
45. A. Soroudi, *Power System Optimization Modeling in GAMS* (Springer, 2017)
46. https://www.gams.com/
47. https://www.gams.com/latest/docs/S_SBB/

Chapter 3
Hourly Price-Based Demand Response for Optimal Scheduling of Integrated Gas and Power Networks Considering Compressed Air Energy Storage

Mohammad Amin Mirzaei, Morteza Nazari-Heris, Behnam Mohammadi-Ivatloo, Kazem Zare, Mousa Marzband, and Amjad Anvari-Moghaddam

Nomenclature

Index

b, b'	Power system buses
i	Power plants
j	Power demand index
l	Gas demand index
L	Power lines
m, n	Gas system nodes
pl	Gas pipeline

M. A. Mirzaei · B. Mohammadi-Ivatloo · K. Zare
Faculty of Electrical and Computer Engineering, University of Tabriz, Tabriz, Iran
e-mail: mm.mirzaei@tabrizu.ac.ir; bmohammadi@tabrizu.ac.ir; kazem.zare@tabrizu.ac.ir

M. Nazari-Heris (✉)
Faculty of Electrical and Computer Engineering, University of Tabriz, Tabriz, Iran

Department of Architectural Engineering, Pennsylvania State University, Pennsylvania, USA
e-mail: mnazari@tabrizu.ac.ir

M. Marzband
Department of Mathematics, Physics and Electrical Engineering, Northumbria University, Newcastle, England
e-mail: mousa.marzband@northumbria.ac.uk

A. Anvari-Moghaddam
Department of Energy Technology, Aalborg University, Aalborg, Denmark
e-mail: aam@et.aau.dk

S. Nojavan, K. Zare (eds.), *Demand Response Application in Smart Grids*,
https://doi.org/10.1007/978-3-030-32104-8_3

s	Scenario index
sp	Gas provider
t	Time interval

Constants

α_k^{ing}	Conversion factor of the electric power to the stored air
α_k^{w}	Conversion factor of the released air to the electric power
$\alpha_i, \beta_i, \gamma_i$	Fuel consumption coefficients of the power plant i
$\pi_m^{\max}, \pi_m^{\min}$	Max/min pressure
$A_k^{\max}/A_k^{\min}$	Max/min air storage in the CAES
$B_{n,\,j,\,t}$	Marginal benefit of price-responsive shiftable consumer n at time t
$C_{m,\,n}$	Constant of pipeline
$\text{CBL}_{j,\,t,\,s}$	Base value of demand j at time t in scenario s
$\text{DR}_{j,\,t,\,s}$	Adjustable load j at time t in scenario s
$\text{D}_{j,\,t,\,s}$	Power demand
NB	Number of buses
NGL	Sum of gas demands
NGS	Sum of gas suppliers
NS	Number of scenarios
NT	Sum of time intervals
NU	Sum of power plants
P_s	Probability of scenario s
$P_i^{\max}, P_i^{\min}$	Max/min capacity of power plant i
$\text{PF}_L^{\max}$	Capacity of line L
$R_i^{\text{up}}, R_i^{\text{dn}}$	Ramp up/down of power plant i
$T_i^{\text{On}}, T_i^{\text{Off}}$	Minimum up-/downtime of power plant i
$U_{\text{sp}}^{\max}, U_{\text{sp}}^{\min}$	Max/min natural gas injection
x_L	Reactance of line L

Variables

$\delta_{b,\,t}$	Voltage angle of power system buses
$\pi_{m,\,t,\,s}$	Pressure of gas node m at time t in scenario s
$A_{k,\,t,\,s}$	The stored air in CAES at time t in scenario s
$F_{i,t}^{\text{C}}$	Operation cost of power plant i at time t
$F_{i,t,s}^{\text{gasunit}}$	Fuel function of plant i at time t in scenario s
$F_{\text{pl},\,t,\,s}$	Gas flow of pipeline pl at time t in scenario s
$I_{i,\,t,\,s}$	Binary on/off indicator of power plant i at time t in scenario s
$I_{k,t,s}^{\text{DIS}}/I_{k,t,s}^{\text{CH}}$	Generation/storage mode of CAES
$L_{l,\,t,\,s}$	Gas demand l at time t in scenario s
$P_{i,\,t,\,s}$	Power supply of plant i at time t in scenario s

$P^{\mathrm{CH}}_{k,t,s}$	The amount of stored power by the CAES
$P^{\mathrm{DIS}}_{k,t,s}$	The amount of generated power by the CAES
$\mathrm{PF}_{L,\ t}$	Power flow at line L at time t
$\mathrm{SUC}_{i,\ t,\ s}/\mathrm{SDC}_{i,\ t,\ s}$	Start-up and shutdown cost of power plant i
$U_{\mathrm{sp},\ t,\ s}$	Gas supply of provider sp at time t in scenario s
$V^{\mathrm{W}}_{k,t,s}/V^{\mathrm{ING}}_{k,t,s}$	Release/store of compressed air in CAES at time t in scenario s
$X^{\mathrm{on}}_{i,t-1,s}, X^{\mathrm{off}}_{i,t-1,s}$	On/off time of power plant i at time t in scenario s

3.1 Introduction

The annual gas consumption for supplying electrical energy has been rapidly increased since 2007 [1]. Emission regulation and power system reliability improvements show great importance in such research area. One fundamental approach for reliability improvement is to increase the flexibility in system operation. To enhance this flexibility in power networks, different approaches have been proposed such as the use of demand response programs [2], integration of energy storage system (ESS) in the model [3, 4], and the use of flexible gas turbine power plants such as combined heat and power plants [5, 6]. Gas-fired units are more flexible compared to other types of plants with fast starting time (i.e., less than 1 h) and ramp rate ability of more than 50 MW/min, while coal-fueled and nuclear type have 4 up to 8 h starting time and ramp rate of 1 MW/min [7, 8]. From the environmental perspective, gas turbine power plants produce 50–60% CO_2 lesser than coal-fired plants and insignificant SO_2 [9]. Natural gas consumption makes gas-fired power generation plants more dependent on the natural gas network, where the shortage of pressure in a gas transmission line or increase of prices of natural gas can increase power system operation cost.

Recently, according to some considerable improvements in the power industry, new options have appeared to be employed for energy management purposes. One of these options is demand-side management service which itself includes various programs, i.e., time-of-use program according to which some of the load is shifted from peak time intervals into off-peak ones to make the operating system performance the most optimal [10]. Demand response (DR) program is defined as an efficient method to overcome the issues created in the electrical systems during on-peak hours. Recently, significant efforts have been made to apply DR programs in energy systems. In [11, 12], demand response services have been proposed for electrical consumers in multienergy systems in which various energy couplings have been provided to make the system performance more flexible. Higher flexibilities of these energy systems can ease the electricity consumer's participation in such proposed demand response services. In [4], the authors have considered DR programs in providing optimal energy management of micro-grids, where the time-of-use (TOU) program is employed to shift the power load demand from on-peak hours to off-peak hours. The profit of the hydrogen storage system and demand response program (DR) on system operation cost in the SCUC problem has been evaluated in

[13]. The authors have proposed a novel electricity market model based on an agent-based DR program in [14] for managing air-conditioning loads, where machine learning approach is employed. Demand response services can also enhance energy system performances from the viewpoint of various criteria such as reliability. As an example, in [15], demand response services have been proposed for energy consumers in the distribution network to make the system performance more economic and enhance the reliability of the system through reduction of the loss of load index. In [16], a day-ahead scheduling problem is proposed for price-based DR with hydrogen energy storage.

Compressed air energy storage (CAES) plant with compressing air via a compressor and storing it in an underground storage cavern at low load hours is one possible solution for achieving higher system flexibility. Releasing the high-pressure (i.e., over 100 psi) air at peak load hours enables power production utilizing less fuel. Two types of these plants are located in Huntorf, Germany, with 290-MW facility in 1978 and McIntosh, Alabama, with 110-MW capacity in 1991 [17, 18]. An in-hand CAES project with 317-MW capacity in Texas, USA, would be ready to operate in 2019 [19]. In [20, 21], stochastic security-constrained unit commitment (SCUC) problems have been solved with the penetration of wind farms and CAES plants, while in [22], the authors have studied the influence of CAES on operation cost with the integration of wind farms. The authors have proposed a look-ahead operation model for CAES systems considering DR programs in [23]. In [24], the capability of producing both power and heat from CAES systems has been studied for increasing the efficiency of storing energy. In this reference, the optimal operation of the studied advanced adiabatic CAES system is examined in energy and reserve markets. The participation of CAES systems in real-time markets has been investigated in [25] considering fast ramping and fast response abilities of CAES. In [26], a robust bidding strategy problem has been solved for the participation of CAES in the day-ahead market. This literature has modeled the uncertainty of power price under a robust approach. In [27], a stochastic unit commitment problem with CAES and DR program has been proposed. In this literature, the constraints related to natural gas networks have been ignored. A conditional value at risk (CVaR)-based stochastic method for maximizing profit of a company consisting of thermal plants and CAES has been expressed in [28]. An economic assessment of the merit of employing a CAES system to a renewable-based network as well as a financial analysis of the system has been accomplished in [29]. In [30], a non-dominated sorting genetic algorithm has been applied for solving a multiobjective problem in operation of CAES systems considering two conflicting objectives including round-trip efficiency and annual total cost saving.

Recently, several research studies have concentrated on integrated gas and electricity networks. In [31, 32], the dependency of power network on natural gas is analyzed. A day-ahead scheduling scheme using the stochastic model is proposed in [6], where the authors solved the SCUC problem considering natural gas transmission limits. The stochastic model includes network load prediction error, line outage, and generation outage contingencies. The impact of hourly electricity demand responses on dependency reduction of the electric system to gas has been studied in the stochastic day-ahead management of coordinated electricity and gas

networks [2]. In [33], stochastic scheduling of coordinated electricity and gas systems has been performed to firm the variability of wind. The effect of the uncertainty of a natural gas supplier and price changes is studied by solving a two-stage stochastic scheduling problem in [34]. Robust day-ahead management for coordinated gas and electricity system has been performed to facilitate volatile renewable generation via power to gas (P2G) [35]. In [36], the influence of distributed natural gas storage system on the robust operation of an integrated electricity-natural gas system has been studied. In [37], a two-stage stochastic network constrained UC has been proposed for multicarrier energy systems.

This study introduces a SCUC problem for integrated electricity and gas systems with the integration of CAES system and price-based DR program. The main features of the paper are as follows:

- CAES is utilized to reduce dependency of power system operation cost to constraints of the gas system.
- Influence of DR programs on operation cost of the integrated energy networks as well as load profile is investigated.
- Constraints of a natural gas network have been included in day-ahead security-constrained scheduling of the power system.
- The influence of gas system limits is studied on the hourly participants of gas-fired plants in the market and power system operation cost.

The rest of this chapter is organized as follows: the problem formulation and the corresponding concept are provided in Sect. 3.2. Section 3.2.1 provides a full description of the modified six-bus system and the numerical results. The conclusions are provided in Sect. 3.2.2.

3.2 Problem Formulation

The main objective of a SCUC problem is providing an optimal scheduling of plants to maximize the social welfare. The proposed objective function considering a CAES plant is given as (3.1). The first term in (3.1) corresponds to the benefit of DR providers (DRPs). The second three terms include the fuel cost of generation plants, start-up and shutdown costs, respectively. The last term corresponds to the fuel cost of CAES plant in generation mode.

$$\max \sum_{s=1}^{\mathrm{NS}} P_s \left[\begin{array}{l} \sum_{n=1}^{\mathrm{NP}} \sum_{t=1}^{\mathrm{NT}} \sum_{j=1}^{\mathrm{NJ}} B_{n,j,t} d_{n,j,t,s} \\ -\sum_{t=1}^{\mathrm{NT}} \sum_{i=1}^{\mathrm{NU}} \left[F_{i,t}^{\mathrm{C}}(P_{i,t,s}) + \mathrm{SUC}_{i,t,s} + \mathrm{SDC}_{i,t,s} \right] \\ -\sum_{t=1}^{\mathrm{NT}} \sum_{k=1}^{\mathrm{NK}} F_{k,t}^{\mathrm{C}}\left(P_{k,t,s}^{\mathrm{DIS}} \right) \end{array} \right] \tag{3.1}$$

This maximization process is subjected to the following constraints.

3.2.1 Electric Network Constraints

Power generation limits of power plants are as given in (3.2).

$$P_i^{\min} I_{i,t,s} \leq P_{i,t,s} \leq P_i^{\max} I_{i,t,s} \tag{3.2}$$

Increase or decrement in power production of a plant at consecutive periods depends on the up and down ramp rate of the plant, which is shown in (3.3) and (3.4).

$$P_{i,t,s} - P_{i,t-1,s} \leq R_i^{\text{up}} \tag{3.3}$$

$$P_{i,t-1,s} - P_{i,t,s} \leq R_i^{\text{dn}} \tag{3.4}$$

Minimum up-/downtime limits of plants are defined in (3.5) and (3.6).

$$\left(X_{i,t-1,s}^{\text{on}} - T_i^{\text{on}}\right)\left(I_{i,t-1,s} - I_{i,t,s}\right) \geq 0 \tag{3.5}$$

$$\left(X_{i,t-1,s}^{\text{off}} - T_i^{\text{off}}\right)\left(I_{i,t,s} - I_{i,t-1,s}\right) \geq 0 \tag{3.6}$$

Constraints corresponding to start-up and shutdown cost of a plant i are expressed as (3.7) and (3.8).

$$\text{SUC}_{i,t,s} \geq \text{SU}_i \left(I_{i,t,s} - I_{i,t-1,s}\right) \tag{3.7}$$

$$\text{SDC}_{i,t,s} \geq \text{SD}_i \left(I_{i,t-1,s} - I_{i,t,s}\right) \tag{3.8}$$

Conversion of compressed air to electric power and vice versa in CAES system is mentioned by (3.9) and (3.10).

$$P_{k,t,s}^{\text{DIS}} = \alpha_k^{\text{w}} V_{k,t,s}^{W} \tag{3.9}$$

$$P_{k,t,s}^{\text{CH}} = \alpha_k^{\text{ing}} V_{k,t,s}^{\text{ING}} \tag{3.10}$$

The amount of injected air or released air from a storage system depends on gate size and pressure limitations that are modeled as (3.11) and (3.12).

$$V_{k,\min}^{\text{W}} I_{k,t,s}^{\text{DIS}} \leq V_{k,t,s}^{\text{W}} \leq V_{k,\max}^{\text{W}} I_{k,t,s}^{\text{DIS}} \tag{3.11}$$

$$V_{k,\min}^{\text{ING}} I_{k,t,s}^{\text{CH}} \leq V_{k,t,s}^{\text{ING}} \leq V_{k,\max}^{\text{ING}} I_{k,t,s}^{\text{CH}} \tag{3.12}$$

CAES at each time can only operate in one of the three modes of generation, storage and no-load states, which is defined in (3.13).

$$I_{k,t,s}^{\text{DIS}} + I_{k,t,s}^{\text{CH}} \leq 1 \tag{3.13}$$

The following relations (3.14)–(3.16) model the capacity of CAES system. Equation (3.14) is related to the quantity of air stored in CAES system at time t and scenario s, which is limited to its maximum and minimum quantities as defined in (3.15). At each time period, CAES system has a specific initial capacity at time $t = 0$ and final capacity at time $t = 24$ should be the same as given by (3.16).

$$A_{k,t,s} = A_{k,t-1,s} + V^{\mathrm{ING}}_{k,t,s} - V^{\mathrm{W}}_{k,t,s} \tag{3.14}$$

$$A^{\min}_{k} \le A_{k,t,s} \le A^{\max}_{k} \tag{3.15}$$

$$A_{k,0,s} = A_{k,\mathrm{in},s} = A_{k,24,s} \tag{3.16}$$

Equation (3.17) shows the power balance in each bus. Power flow from bus b to b' is determined by (3.18) while constrained by (3.19).

$$\sum_{i=1}^{\mathrm{NU}_b} P_{i,t,s} + \sum_{k=1}^{\mathrm{NK}_b} P^{\mathrm{DIS}}_{k,t,s} - \sum_{k=1}^{\mathrm{NK}_b} P^{\mathrm{CH}}_{k,t,s} - \sum_{j=1}^{\mathrm{NJ}_b} d_{j,t,s} = \sum_{l=1}^{\mathrm{NL}_b} \mathrm{PF}_{L,t,s} \tag{3.17}$$

$$\mathrm{PF}_{L,t,s} = \frac{\delta_{b,t,s} - \delta_{b',t,s}}{x_L} \tag{3.18}$$

$$-\mathrm{PF}^{\max}_{L} \le \mathrm{PF}_{L,t,s} \le \mathrm{PF}^{\max}_{L} \tag{3.19}$$

The constraints related to the DR program are defined by (3.20)–(3.23). Equation (3.20) indicates the relation between blocks of DR demand and total load of the system. Moreover, the limitations of blocks of DR demand are defined by (3.21). The limitation of adjustable load demand is defined by (3.22), and (3.23) indicates that the total curtailed load is shifted to another time interval [16]:

$$\sum_{n=1}^{\mathrm{NP}} d_{n,j,t,s} = D_{j,t,s} - \mathrm{DR}_{j,t,s} - \mathrm{CBL}_{j,t,s} \tag{3.20}$$

$$0 \le d_{n,j,t,s} \le d^{\max}_{n,j,t,s} \tag{3.21}$$

$$\left|\mathrm{DR}_{j,t,s}\right| \le \mathrm{DR}^{\max}_{j,t,s} \tag{3.22}$$

$$\sum_{t=1}^{\mathrm{NT}} \mathrm{DR}_{j,t,s} = 0 \tag{3.23}$$

where the number of levels of DR demand and the associated demand are defined by n and d. Moreover, DR and CBL indicate the adjustable load and base value. It is noticeable that base loads do not participate in the DR program.

3.2.2 Gas Network Constraints

Natural gas transmission network is responsible for transmitting gas from suppliers to consumers. Any gas network includes several gas wells, gas storage systems, gas loads, pipelines, compressor, and other devices such as control taps and regulators. Gas flow within the pipeline is a quadratic function of the end node pressure and is defined by (3.24) and (3.25). The gas flow direction through the pipeline $F_{\mathrm{pl},\,t,\,s}$ is determined by ± 1, which is positive when gas pressure at node m is greater than the pressure at node n and vice versa.

$$F_{\mathrm{pl},t,s} = \mathrm{sgn}\left(\pi_{m,t,s}, \pi_{n,t,s}\right)\ C_{m,n}\sqrt{\left|\pi_{m,t,s}^2 - \pi_{n,t,s}^2\right|} \tag{3.24}$$

$$\mathrm{sgn}\left(\pi_{m,t,s}, \pi_{n,t,s}\right) = \begin{cases} 1 & \pi_{m,t,s} \geq \pi_{n,t,s} \\ -1 & \pi_{m,t,s} \leq \pi_{n,t,s} \end{cases} \tag{3.25}$$

where $F_{\mathrm{pl},\,t,\,s}$ is natural gas flow through the pipeline pl at time t and scenario s and $\pi_{m,\,t,\,s}$ and $\pi_{n,\,t,\,s}$ are natural gas pressure at nodes m and n. Also, $C_{m,\,n}$ determines the pipeline constant in which it's value depends on temperature, and the diameter of the pipeline, fraction and gas composites, natural gas pressure of each node, like the bus voltage limits in an electric network, varies between the upper limit and lower limit as given in (3.26).

$$\pi_m^{\min} \leq \pi_{m,t,s} \leq \pi_m^{\max} \tag{3.26}$$

The delivered natural gas to corresponding nodes by suppliers is limited to maximum and minimum values as (3.27).

$$U_{\mathrm{sp}}^{\min} \leq U_{\mathrm{sp},t,s} \leq U_{\mathrm{sp}}^{\max} \tag{3.27}$$

In each node of gas network, the amount of injected gas should be equal to consumed gas which is modeled as (3.28).

$$\sum_{\mathrm{sp}=1}^{\mathrm{NGS}_m} U_{\mathrm{sp},t,s} - \sum_{l=1}^{\mathrm{NGL}_m} L_{l,t,s} = \sum_{\mathrm{pl}=1}^{\mathrm{NPL}_m} F_{\mathrm{pl},t,s} \tag{3.28}$$

Gas-fired plants and CAES system are the large consumers of gas which are connected to a natural gas network considering (3.29) and (3.30). Amounts of gas fuel used by gas-fired power and CAES plants are indicated by (3.31) and (3.32).

$$L_{l,t,s} = F_{i,t,s}^{\text{gasunit}} \tag{3.29}$$

$$L_{l,t,s} = F_{k,t,s}^{\text{CAES}} \tag{3.30}$$

$$F_{i,t,s}^{\text{gasunit}} = \alpha_i + \beta_i P_{i,t,s} + \gamma_i P_{i,t,s}^2 \tag{3.31}$$

$$F_{k,t,s}^{\text{CAES}} = \text{HR}_k P_{k,t,s}^{\text{DIS}} \tag{3.32}$$

where α_i, β_i, andγ_i are gas-fueled plant coefficients, and HR_k declares the heat rate of the CAES system.

3.3 Simulation Results

For studying the performance of the introduced model, it is applied and tested on a six-bus power system [38] integration with a six-node gas network. A day-ahead stochastic-based SCUC model is performed on the test system taking into account gas system constraints and CAES plant. A six-bus network consists of three gas-fired plants, one CAES plant and two loads of different types. The characteristics of the gas network are also given in [9]. Data for the generation plants, the transmission lines of the power system, the pipelines of the gas system and gas load table, characteristics of the nodes in gas pipelines, characteristics of the gas pipelines, and hourly residential gas load have been reported in Tables 3.1, 3.2, 3.3, 3.4, 3.5, and 3.6. The SCUC problem is solved in four different cases.

Table 3.1 Characteristics of the generation plants

Unit	α (MBtu/h)	β (MBtu/MWh)	c (MBtu/MWh)	Pmax	Pmin	Initial status (h)	Min down (h)	Min up (h)	Ramp (MW/h)
G1	176.95	13.51	0.0004	220	100	4	4	4	55
G2	129.97	32.63	0.001	100	10	−3	3	2	50
G3	137.41	17.7	0.005	20	10	−1	1	1	20

Table 3.2 Characteristics of the transmission lines of power system

Branch	From bus	To bus	X (p.u.)	Flow limit (MW)
Line 1	1	2	0.17	200
Line 2	1	4	0.258	100
Line 3	2	3	0.197	100
Line 4	2	4	0.140	100
Line 5	3	6	0.037	100
Line 6	4	5	0.037	100
Line 7	5	6	0.018	100

Table 3.3 Characteristics of the pipelines of gas system and gas load

Index	From node	To node	*C* (kcf/Psig)	Load no.	Node no.	Load type
Pipe 1	1	2	50.6	1	1	G1
Pipe 2	2	4	50.1	2	1	Residential gas load
Pipe 3	2	5	37.5	3	3	G3
Pipe 4	3	5	43.5	4	3	Residential gas load
Pipe 5	5	6	45.3	5	2	G2

Table 3.4 Characteristics of the nodes in gas pipelines

Node no.	Min pressure (Psig)	Max pressure (Psig)
1	105	120
2	120	135
3	125	140
4	130	155
5	140	155
6	150	175

Table 3.5 Characteristics of the gas pipelines

Supplier no.	Node no.	Min outpout (kcf/h)	Max outpout (kcf/h)
1	4	1500	5000
2	6	2000	6000

Table 3.6 Hourly residential gas load

Time (h)	Residenatial gas load	Time (h)	Residenatial gas load (kcf)	Time (h)	Residenatial gas load (kcf)	Time (h)	Residenatial gas load (kcf)
1	2439.196	7	2607.496	13	2803.68	19	3055.97
2	2298.944	8	2831.73	14	2663.43	20	3168
3	2186.746	9	2887.83	15	2691.48	21	3112.07
4	2214.96	10	2962.576	16	2747.58	22	3055.97
5	1915.814	11	2859.78	17	2831.73	23	2831.73
6	2635.05	12	2859.78	18	2915.88	24	2579.446

3.3.1 Solving Deterministic SCUC (Case 1)

Figure 3.1 shows hourly production dispatch of three gas-fueled plants. The cheapest plant G1 is committed at the whole scheduling item, while the expensive plant G2 is committed between $t = 11$ and $t = 22$. Also, plant G3, as the second expensive plant, is dispatched during hours $t = 10$ to $t = 22$. Total operation cost in case 1 is equal to \$83,242.6.

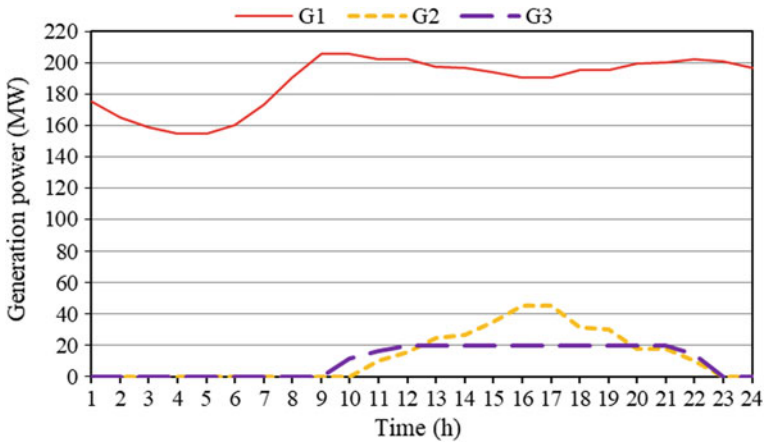

Fig. 3.1 Hourly generation dispatch of gas-fueled power plants

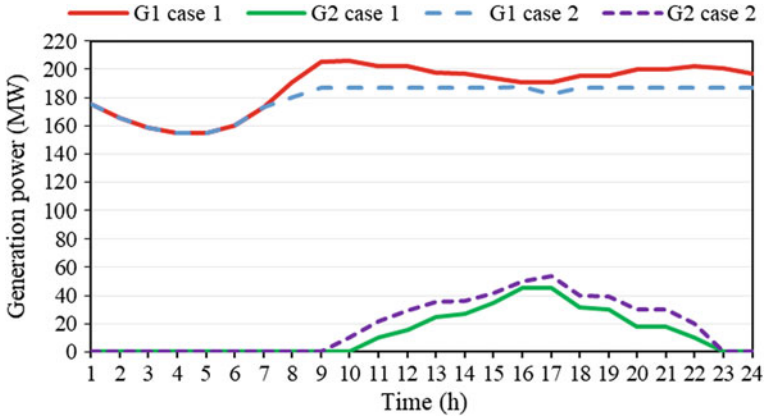

Fig. 3.2 Comparison of hourly generation dispatch of gas-fired power plants in case 1 and 2

3.3.2 SCUC Considering Gas System Constraints (Case 2)

The comparison of the hourly dispatch of plants G1 and G2 with case 1 is demonstrated in Fig. 3.2. As shown in this figure, the limited capacity of gas transmission lines enforces some limitations on gas consumption of generation plant G1 which results in a reduction in its power generation. Consequently, the power generation of plants G2 and G3 is increased. The total operation cost, in this case, is equal to $86,644.5, which shows $3401.9 increase in cost.

3.3.3 Case 2 with CAES (Case 3)

In this case, a CAES with a 30-MW capacity is located at bus 5. Table 3.7 shows the characteristics of the CAES system. Based on [19], coefficients α_k^{w} and α_k^{ing} are assigned as 0.9. The initial capacity of CAES is assumed as 50% of its maximum capacity. It is obvious from Figs. 3.3 and 3.4 that the CAES system is in generation mode during off-peak time periods. In these periods, plant G1 produces more power than case 2, but at other periods specifically at peak hours (i.e., $t = 15$, 16, and 17),

Table 3.7 Characteristics of CAES system

$A_{k,t}^{max}$	$A_{k,t}^{min}$	$V_{k,max}^{W}$	$V_{k,min}^{W}$	$V_{k,max}^{ING}$	$V_{k,min}^{ING}$
180	40	30	5	30	5

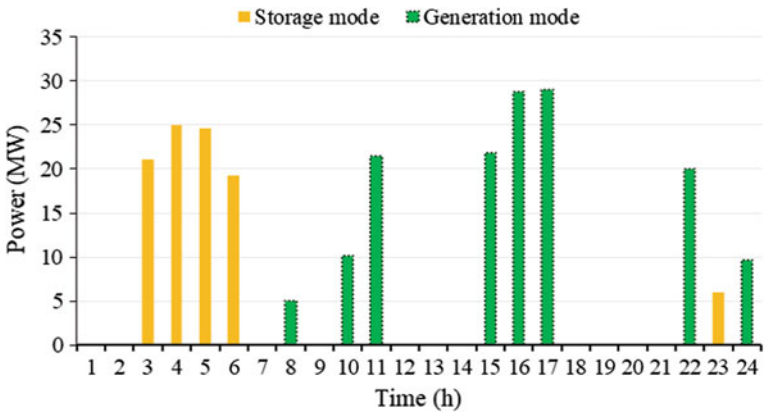

Fig. 3.3 Generated and stored power by CAES system

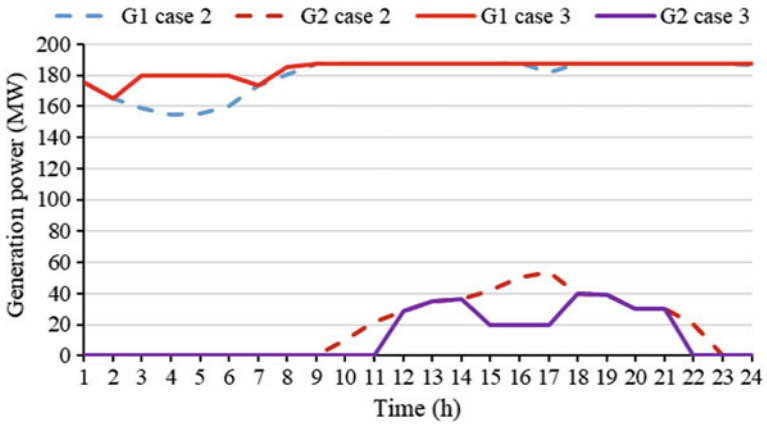

Fig. 3.4 Comparison of hourly generation dispatch of gas-fueled power plants in case 2 and 3

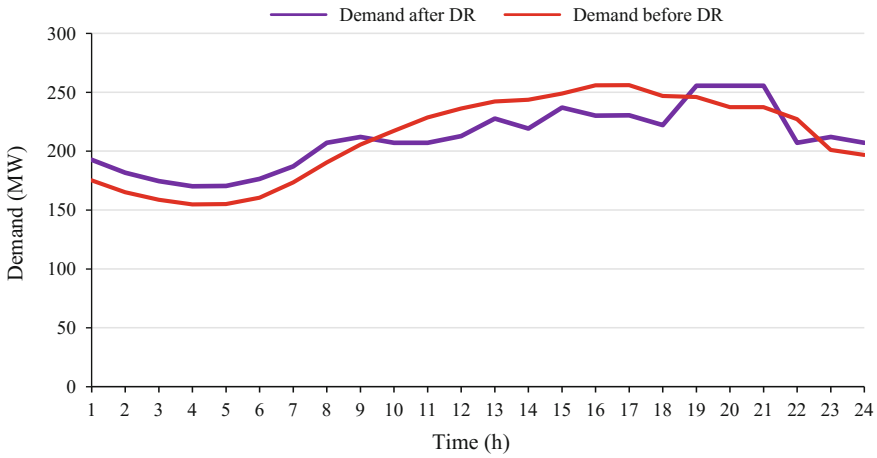

Fig. 3.5 The role of DR on load demand profile of the system

power injection by CAES to the network causes some reduction in power generation of plant G2 with respect to case 2. This results in daily generation cost reduction. In this case, the total system operation cost is reduced to $83,276.4.

3.3.4 Case 3 with DR Program (Case 4)

In this case, the effect of DR as well as the CAES is investigated on the operation cost of the network. The DR includes a demand block with a marginal profit of 45 $/MWh. It is assumed that 10% of the load participate in price-based DR program. Figure 3.5 demonstrates the load profile after application of the DR program. As it is seen in this figure, the load has been shifted from peak hours to off-peak hours, which reduces the participation of expensive power plants. The cost of the system in this case is $79,153.52, which is reduced with respect to case 3.

3.3.5 Solving Stochastic SCUC (Case 5)

In this case, network electric load uncertainty is modeled utilizing Monte Carlo simulation approach. The load prediction error follows a normal distribution function with a mean value that is equal to the load prediction and a standard deviation of 5% of the mean value. The initial scenario set generated by Monte Carlo (which represents 1000 loading conditions) is then decreased to five suitable scenarios utilizing the SCENRED. Such tool includes two reduction methods: the backward approach and forward approach. The first one takes advantage of the best-expected

response time-based performance. Additionally, the obtained results of the forward approach are more accurate than the backward approach; however, the forward approach requires higher computation time. SCENRED has the capability of selecting a desired number of preserved scenarios, which is called *Red_num_leaves.* In addition, *red_percentage* is an option of SCENRED, which works based on the relative distance between the initial and reduced scenarios. This chapter has used fast backward reduction approach according to the running time and performance accuracy with *red_num_leaves* factor of 5.

The power generation of power plants G1–G3 for different scenarios has been reported in Tables 3.8, 3.9, and 3.10. In addition, Tables 3.11 and 3.12 report the optimal charge/discharge of the CAES system in different scenarios. Daily operation cost in different scenarios is shown in Table 3.13. As shown in Table 3.13, scenarios 2 and 3 result more operation cost with respect to deterministic case (i.e., case 4). Total operation cost is equal to $79076.3, which is less than case 4.

3.4 Conclusions

This paper solved a stochastic-based SCUC with CAES plant. Moreover, gas delivery to gas-fueled power plants and CAES plant is modeled. Considering the gas system model could result in dispatch of more expensive plants in the energy provision process and therefore imposes higher daily operation costs. The impact of CAES plant as a flexible source with high ramp rate on electric network dependency to natural gas fuel reduction has been studied. Also, it's impact on the reduction of expensive unit commitment and power system operation cost has been investigated. In addition, the role of the DR program in optimal scheduling of integrated energy networks is studied, and the effect of such programs is investigated on the operation cost of the system, which shows reduction in such index. Moreover, the influence of DR on the load demand profile shows that such programs are effective in shifting demand from on-peak hours to off-peak hours. The numerical results proved the effectiveness of the introduced concept.

Table 3.8 Daily power generation of G1 in different scenarios

Time	S_1	S_2	S_3	S_4	S_5	Time	S_1	S_2	S_3	S_4	S_5
1	187.091	187.091	187.091	187.091	187.091	13	188.921	188.921	188.921	188.921	188.921
2	176.745	169.317	174.65	175.412	173.27	14	188.921	188.921	188.921	188.921	188.921
3	176.745	169.317	174.65	175.412	173.27	15	188.921	188.921	188.921	188.921	188.921
4	176.745	169.317	174.65	175.412	173.27	16	188.921	188.921	188.921	188.921	188.921
5	176.745	169.317	174.65	175.412	173.27	17	188.921	188.921	188.921	188.921	188.921
6	176.745	169.317	174.65	175.412	173.27	18	188.921	188.921	188.921	188.921	188.921
7	176.745	169.317	174.65	175.412	173.27	19	188.921	188.921	188.921	188.921	188.921
8	188.921	185.45	188.921	188.921	188.921	20	188.921	188.921	188.921	188.921	188.921
9	188.921	188.921	188.921	188.921	188.921	21	188.921	188.921	188.921	188.921	188.921
10	188.921	188.921	188.921	188.921	188.921	22	188.921	188.921	188.921	188.921	188.921
11	188.921	188.921	188.921	188.921	188.921	23	188.921	188.921	188.921	188.921	188.921
12	188.921	188.921	188.921	188.921	188.921	24	188.921	188.921	188.921	188.921	188.921

Table 3.9 Daily power generation of G2 in different scenarios

Time	S_1	S_2	S_3	S_4	S_5	Time	S_1	S_2	S_3	S_4	S_5
1	0	0	0	0	0	13	25.254	15.699	22.559	23.539	20.869
2	0	0	0	0	0	14	25.254	15.699	22.559	23.539	20.869
3	0	0	0	0	0	15	25.254	15.699	22.559	23.539	20.869
4	0	0	0	0	0	16	25.254	15.699	22.559	23.539	20.869
5	0	0	0	0	0	17	25.254	15.699	22.559	23.539	20.869
6	0	0	0	0	0	18	25.254	15.699	22.559	23.539	20.869
7	0	0	0	0	0	19	25.254	15.699	22.559	23.539	20.869
8	0	0	0	0	0	20	25.254	15.699	22.559	23.539	20.869
9	0	0	0	0	0	21	25.254	15.699	22.559	23.539	20.869
10	10	10	10	10	10	22	21.172	12.313	18.673	19.582	17.106
11	22.661	13.745	20.146	21.061	18.569	23	188.921	188.921	188.921	188.921	188.921
12	25.254	15.699	22.559	23.539	20.869	24	188.921	188.921	188.921	188.921	188.921

Table 3.10 Daily power generation of G3 in different scenarios

Time	S_1	S_2	S_3	S_4	S_5	Time	S_1	S_2	S_3	S_4	S_5
1	0	0	0	0	0	13	20	20	20	20	20
2	0	0	0	0	0	14	20	20	20	20	20
3	0	0	0	0	0	15	20	20	20	20	20
4	0	0	0	0	0	16	20	20	20	20	20
5	0	0	0	0	0	17	20	20	20	20	20
6	0	0	0	0	0	18	20	20	20	20	20
7	0	0	0	0	0	19	20	20	20	20	20
8	0	0	0	0	0	20	20	20	20	20	20
9	0	0	0	0	0	21	20	20	20	20	20
10	20	20	20	20	20	22	20	20	20	20	20
11	20	20	20	20	20	23	14.743	16.902	12.531	13.335	11.144
12	20	20	20	20	20	24	12.387	14.713	10.422	11.009	10.865

Table 3.11 Daily power charge of CAES in different scenarios

Time	S_1	S_2	S_3	S_4	S_5	Time	S_1	S_2	S_3	S_4	S_5
1	9.624	16.456	11.551	10.85	12.76	13	0	0	0	0	0
2	9.448	8.461	9.17	9.271	8.929	14	0	0	0	0	0
3	15.976	14.738	15.627	15.754	15.341	15	0	0	0	0	0
4	20.004	18.61	19.611	19.753	19.696	16	0	0	0	0	0
5	19.669	18.289	19.28	19.421	18.969	17	0	0	0	0	0
6	14.179	13.01	13.849	13.969	13.576	18	0	0	0	0	0
7	0	0	0	0	0	19	0	0	0	0	0
8	0	0	0	0	0	20	0	0	0	0	0
9	0	0	0	0	0	21	0	0	0	0	0
10	0	0	0	0	0	22	0	0	0	0	0
11	0	0	0	0	0	23	0	0	0	0	0
12	0	0	0	0	0	24	0	0	0	0	0

Table 3.12 Daily power discharge of CAES in different scenarios

Time	S_1	S_2	S_3	S_4	S_5	Time	S_1	S_2	S_3	S_4	S_5
1	0	0	0	0	0	13	11.153	11.263	11.184	11.173	11.204
2	0	0	0	0	0	14	12.592	12.646	12.607	12.602	12.617
3	0	0	0	0	0	15	17.92	17.769	17.878	17.893	17.851
4	0	0	0	0	0	16	24.94	24.519	24.822	24.865	24.747
5	0	0	0	0	0	17	25.153	24.724	25.032	25.076	24.956
6	0	0	0	0	0	18	15.773	15.704	15.753	15.76	15.741
7	0	0	0	0	0	19	14.993	14.955	14.982	14.986	14.975
8	0	0	0	0	0	20	6.261	6.559	6.345	6.314	6.397
9	0	0	0	0	0	21	6.22	6.52	6.305	6.274	6.358
10	0	0	0	0	0	22	0	0	0	0	0
11	0	0	0	0	0	23	0	0	0	0	0
12	5.994	5.341	5.092	5.057	5.154	24	0	0	0	0	0

Table 3.13 Daily operation cost in different scenarios

Scenario	S_1	S_2	S_3	S_4	S_5
Daily operation cost ($)	75780.3	82708.4	81620.9	76209.9	78865.1

References

1. Annual Energy Review, Washington, DC, USA (2011) [Online]. http://www.eia.doe.gov/emeu/aer/
2. H. Wu, M. Shahidehpour, M.E. Khodayar, Hourly demand response in day-ahead scheduling considering generating unit ramping cost. IEEE Trans. Power Syst. **28**, 2446–2454 (2013)
3. M. Korpaas, A.T. Holen, R. Hildrum, Operation and sizing of energy storage for wind power plants in a market system. Int. J. Electr. Power Energy Syst. **25**, 599–606 (2003)
4. M. Nazari-Heris, S. Abapour, B. Mohammadi-Ivatloo, Optimal economic dispatch of FC-CHP based heat and power micro-grids. Appl. Therm. Eng. **114**, 756–769 (2017)
5. M. Nazari-Heris, B. Mohammadi-Ivatloo, G.B. Gharehpetian, M. Shahidehpour, Robust short-term scheduling of integrated heat and power microgrids. IEEE Syst. J. **99**, 1–9 (2018)
6. M. Nazari-Heris, B. Mohammadi-Ivatloo, G.B. Gharehpetian, A comprehensive review of heuristic optimization algorithms for optimal combined heat and power dispatch from economic and environmental perspectives. Renew. Sust. Energ. Rev. **81**, 2128–2143 (2018)
7. M. Henderson, Energy system flexibility: the importance of being nimble [from the editor]. IEEE Power Energy Mag. **15**, 4–6 (2017)
8. J. Klimstra, M. Hotakainen, *Smart Power Generation* (Avain Publishers, Helsinki, 2011)
9. A. Alabdulwahab, A. Abusorrah, X. Zhang, M. Shahidehpour, Stochastic security-constrained scheduling of coordinated electricity and natural gas infrastructures. IEEE Syst. J. **11, 2015**(3), 1674–1683
10. M. Majidi, S. Nojavan, K. Zare, A cost-emission framework for hub energy system under demand response program. Energy **134**, 157–166 (2017)
11. M. Majidi, B. Mohammadi-Ivatloo, A. Anvari-Moghaddam, Optimal robust operation of combined heat and power systems with demand response programs. Appl. Therm. Eng. **149**, 1359–1369 (2019)
12. M. Majidi, K. Zare, Integration of smart energy hubs in distribution networks under uncertainties and demand response concept. IEEE Trans. Power Syst. **34**, 566–574 (2019)
13. M.A. Mirzaei, A.S. Yazdankhah, B. Mohammadi-Ivatloo, Integration of demand response and hydrogen storage system in security constrained unit commitment with high penetration of wind energy, in *Iranian Conference Electrical Engineering (ICEE)* (2018), pp. 1203–1208
14. K. Dehghanpour, M.H. Nehrir, J.W. Sheppard, N.C. Kelly, Agent-based modeling of retail electrical energy markets with demand response. IEEE Trans. Smart Grid. **9**, 3465–3475 (2018)
15. S. Nojavan, M. Majidi, N. Nourani Esfetanaj, An efficient cost-reliability optimization model for optimal siting and sizing of energy storage system in a microgrid in the presence of responsible load management. Energy **139**, 89–97 (2017)
16. M.A. Mirzaei, A. Sadeghi Yazdankhah, B. Mohammadi-Ivatloo, Stochastic security-constrained operation of wind and hydrogen energy storage systems integrated with price-based demand response. Int. J. Hydrog. Energy **44, 2019**(27), 14217–14227
17. V. Biasi, 110 MW McIntosh CAES plant over 90% availability and 95% reliability. Gas Turbine World **28**, 26–28 (1998)
18. O. Weber, Air-storage gas-turbine power-station at HUNTORF. Brown Boveri Rev. **62**, 332–337 (1975)
19. S. Shafiee, H. Zareipour, A.M. Knight, N. Amjady, B. Mohammadi-Ivatloo, Risk-constrained bidding and offering strategy for a merchant compressed air energy storage plant. IEEE Trans. Power Syst. **32**, 946–957 (2017)

20. H. Daneshi, A. Daneshi, N. Tabari, A.N. Jahromi, Security-constrained unit commitment in a system with wind generation and compressed air energy storage, in *6th International Conference on the European Energy Market, 2009, EEM 2009* (2009), pp. 1–6
21. H. Daneshi, A. Srivastava, Security-constrained unit commitment with wind generation and compressed air energy storage. IET Gener Transm Distrib **6**, 167–175 (2012)
22. M. Abbaspour, M. Satkin, B. Mohammadi-Ivatloo, F.H. Lotfi, Y. Noorollahi, Optimal operation scheduling of wind power integrated with compressed air energy storage (CAES). Renew. Energy **51**, 53–59 (2013)
23. P. Aliasghari, M. Zamani-Gargari, B. Mohammadi-Ivatloo, Look-ahead risk-constrained scheduling of wind power integrated system with compressed air energy storage (CAES) plant. Energy **160**, 668–677 (2018)
24. Y. Li, S. Miao, S. Zhang, B. Yin, X. Luo, M. Dooner, J. Wang, A reserve capacity model of AA-CAES for power system optimal joint energy and reserve scheduling. Int. J. Electr. Power Energy Syst. **104**, 279–290 (2019 Jan 1)
25. Y. Li, S. Miao, B. Yin, W. Yang, S. Zhang, X. Luo, J. Wang, A real-time dispatch model of CAES with considering the part-load characteristics and the power regulation uncertainty. Int. J. Electr. Power Energy Syst. **105**, 179–190 (2019)
26. S. Nojavan, A. Najafi-Ghalelou, M. Majidi, K. Zare, Optimal bidding and offering strategies of merchant compressed air energy storage in deregulated electricity market using robust optimization approach. Energy **142**, 250–257 (2018)
27. A.N. Ghalelou, A.P. Fakhri, S. Nojavan, M. Majidi, H. Hatami, A stochastic self-scheduling program for compressed air energy storage (CAES) of renewable energy sources (RESs) based on a demand response mechanism. Energy Convers. Manag. **120**, 388–396 (2016)
28. E. Akbari, R.A. Hooshmand, M. Gholipour, M. Parastegari, Stochastic programming-based optimal bidding of compressed air energy storage with wind and thermal generation units in energy and reserve markets. Energy **171**, 535–546 (2019)
29. O. Ramadan, S. Omer, Y. Ding, H. Jarimi, X. Chen, S. Riffat, Economic evaluation of installation of standalone wind farm and wind+ CAES system for the new regulating tariffs for renewables in Egypt. Therm Sci Eng Prog **7**, 311–325 (2018)
30. R. Jiang, H. Yin, K. Peng, Y. Xu, Multi-objective optimization, design and performance analysis of an advanced trigenerative micro compressed air energy storage system. Energy Convers. Manag. **186**, 323–333 (2019)
31. T. Li, M. Eremia, M. Shahidehpour, Interdependency of natural gas network and power system security. IEEE Trans. Power Syst. **23**, 1817–1824 (2008)
32. C. Liu, M. Shahidehpour, Y. Fu, Z. Li, Security-constrained unit commitment with natural gas transmission constraints. IEEE Trans. Power Syst. **24**, 1523–1536 (2009)
33. A. Alabdulwahab, A. Abusorrah, X. Zhang, M. Shahidehpour, Coordination of interdependent natural gas and electricity infrastructures for firming the variability of wind energy in stochastic day-ahead scheduling. IEEE Trans. Sustain. Energy **6**, 606–615 (2015)
34. B. Zhao, A.J. Conejo, R. Sioshansi, Unit commitment under gas-supply uncertainty and gas-price variability. IEEE Trans. Power Syst. **32**, 2394–2405 (2017)
35. H. Chuan, L. Tianqi, W. Lei, M. Shahidehpour, Robust coordination of interdependent electricity and natural gas systems in day-ahead scheduling for facilitating volatile renewable generations via power-to-gas technology. J. Mod. Power Syst. Clean Energy **5**, 375–388 (2017)
36. Y. He, M. Shahidehpour, Z. Li, C. Guo, B. Zhu, Robust constrained operation of integrated electricity-natural gas system considering distributed natural gas storage. IEEE Trans. Sustain. Energy **9, 2017**(3), 1061–1071
37. M.A. Mirzaei, A.S. Yazdankhah, B. Mohammadi-Ivatloo, M. Marzband, M. Shafie-khah, J.P. Catalão, Stochastic network-constrained co-optimization of energy and reserve products in renewable energy integrated power and gas networks with energy storage systems. J. Clean. Prod. **223**, 747 (2019)
38. X. Zhang, M. Shahidehpour, A. Alabdulwahab, A. Abusorrah, Hourly electricity demand response in the stochastic day-ahead scheduling of coordinated electricity and natural gas networks. IEEE Trans. Power Syst. **31**, 592–601 (2016)

Chapter 4
Energy Management of Hybrid AC-DC Microgrid Under Demand Response Programs: Real-Time Pricing Versus Time-of-Use Pricing

Ramin Nourollahi, Kazem Zare, and Sayyad Nojavan

Nomenclature

Index

n Index of PHEV
t Index of time

Parameter

α_{dcharge}	The coefficient of PHEVs' discharging (P.U.)
$\eta_{\text{AC-DC}}$	Rectifier efficiency (P.U.)
$\eta_{\text{DC-AC}}$	Inverter efficiency (P.U.)
η_{DG}	Efficiency of DG unit (P.U.)
$C_{\text{O \& M}}$	The cost of maintenance and operation of DG ($)
DRmax	Maximum participant load in DRP (%)
HR	Heat rate of natural gas (kWh/m^3)
Incmax	Maximum load that can be increased (kW)
load_t^0	Initial load (kW)
$\text{Load}_{\text{AC}}(t)$	AC load at time t (kW)
$\text{Load}_{\text{DC}}(t)$	DC load at time t (kW)
$\text{Load}_{\text{Total}}(t)$	Load at time t (kW)

R. Nourollahi (✉) · K. Zare
Faculty of Electrical and Computer Engineering, University of Tabriz, Tabriz, Iran
e-mail: ramin.nourollahi96@ms.tabrizu.ac.ir; kazem.zare@tabrizu.ac.ir

S. Nojavan
Department of Electrical Engineering, University of Bonab, Bonab, Iran
e-mail: sayyad.nojavan@bonabu.ac.ir

S. Nojavan, K. Zare (eds.), *Demand Response Application in Smart Grids*,
https://doi.org/10.1007/978-3-030-32104-8_4

P_{av}	Average electricity demand
P_{conv}	Converter nominal power (kW)
$P_{DG,\ max}$	Maximum power of DG unit (kW)
$P_{PV}(t)$	Generated power in PV panels at time t (kW)
$P_{WT}(t)$	Generated power in wind turbine at time t (kW)
PR_{fuel}	The fuel price ($)
PR_{sell}	Selling price to the external grid ($/kWh)
$PR_{TOU}(t)$	TOU prices at time t ($/kWh)
$PEV^{n}_{charge,\ max}$	Maximum charged power of PHEV (kW)
$PEV^{n}_{dcharge,\ max}$	Maximum discharged power of PHEV (kW)
PG_{max}	Maximum exchange power through external grid (kW)
QEV^{n}	Capacity of PHEV (kWh)
RR	Ramp rate of DG unit (kW/h)
SOC^{n}_{min}	Minimum state of charge of PHEV (kWh)
$SOC^{n}\left(t^{n}_{arr}\right)$	PHEV SOC at the time of arrival (kWh)
$SOC^{n}\left(t^{n}_{dep}\right)$	PHEV SOC at the time of departure (kWh)
SOC^{n}_{in}	Input state of charge of PHEV (kWh)
SOC^{n}_{out}	PHEV state-of-charge output (kWh)

Binary Variables

X^{n}_{charge}	Binary variable for PHEV's charging at time t
$X^{n}_{dcharge}$	Binary variable for PHEV's discharging at t
$X_{AC\text{-}DC}(t)$	Binary variable for AC to DC converted power at time t
$X_{DC\text{-}AC}(t)$	Binary variable for DC to AC converted power at time t
$XG_{in}(t)$	Binary variable for external grid purchased power at time t
$XG_{out}(t)$	Binary variable for sold power to external grid at time t

Variables

DR_t	Potential of DRP execution (%)
$F(t)$	Gas consumption at time t (m^3)
inc_t	Amount of increasing load in DRP (kW)
ldr_t	Shiftable load at time t (kW)
$load^{inc}_{t}$	Load increased in DRP (kW)
$load^{t}_{RTP}$	Load demand considering real-time pricing of DRP
$load^{t}_{TOU}$	Load demand considering time-of-use pricing of DRP (kW)
$P_{DG}(t)$	Power generation by DG units at time t (kW)
$P_{AC\text{-}DC}(t)$	AC to DC converted power at time t (kW)
$P_{DC\text{-}AC}(t)$	DC to AC converted power at time t (kW)
$PEV^{n}_{charge}(t)$	Charging power of PHEV at time t (kW)

$PEV^{n}_{dcharge}(t)$	Discharging power of PHEV at time t (kW)
$PG_{in}(t)$	Purchased power from external grid at time t (kW)
$PG_{out}(t)$	Sold power to external grid at time t (kW)
$SOC^{n}(t)$	State of charge of PHEV at time t (P.U.)

4.1 Introduction

Microgrid (MG) is a distributed system with various distributed generators such as renewable generation units, storage system, microturbine, and controllable loads which can be operated in two modes connected to the upstream grid or isolated [1, 2]. The new design of microgrids, which is called H-AC-DC-MG, has recently become popular in power systems, because the H-AC-DC-MG can feed AC and DC loads individually and also have fewer losses than the C-AC-MGs. In addition, H-AC-DC-MG does not need a separate converter to feed DC loads. So, H-AC-DC-MG can be a serious competitor for C-AC-MGs.

4.1.1 Literature Review

The microgrid can be categorized into two types of AC and DC based on the type of supply voltage. The use of AC microgrid is more common because of its prevalence [3]. However, the main advantage of DC microgrid is that it supports better DC power output of DC units such as photovoltaic system and PHEVs. In addition, DC loads can be fed with lower losses [4]. Recently, a new type of microgrid has been introduced that has one or more AC and DC microgrids. In addition, all the benefits mentioned above are combined. References [5, 6] describe the common topology of H-AC-DC-MG and compare them to conventional networks.

Distributed resources such as generators and storage systems depending on their type of voltages are jointed to the corresponding bus. AC-DC converters enable power exchange among the AC and DC buses. In [7, 8], planning of a H-AC-DC-MG has been performed. Planning problems consist of minimum generation, cost of distributed energy resources (DER), determining the feeder type (i.e., AC or DC), and the optimal location of each DERs. In [9], the problem of optimal microgrid performance is solved by implementation of renewable energy resources, storage systems, and exchanged power between the AC and DC grid. Also, maintaining the state of charge (SOC) in batteries is the right strategy for optimal operation of the mentioned problem. Power management strategies for a hybrid AC/DC microgrid system are proposed in [10]. In [11], a new operation model is introduced for the H-AC-DC-MG which consisted of system-based and device-level H-AC-DC-MG. In [12], robust optimal power management of the system is proposed for a H-AC-DC-MG in which the power flow in the microgrid is controlled by solving the optimization problem.

The penetration of renewable energy sources, especially the photovoltaic system, has led to the prevalence use of the AC-DC microgrid. The economic and environmental analysis of renewable energy sources has been done in [13–15]. In addition, the penetration of storage systems, including battery storages and PHEVs, has increased in microgrid in recent years. In [16], a novel method for energy management for PHEV has been introduced. Also, impacts of PHEV on the cost and pollution have been evaluated in [17].

The existence of flexible loads in microgrid has led to many advantages, in which one of the advantages is the use of DRP. Demand response program (DRP) can be an option to reduce costs in the H-AC-DC-MG. Reference [18] shows the positive effect of DRP on the economic performance of microgrid in the presence of flexible loads. Therefore, multiple types are presented in literature for DRP such as time-of-use (TOU) and real-time pricing (RTP). In [19], the effects of DRP on the total cost of the smart grid are analyzed and their formulation has been introduced. In [20], a time-based type and incentive-based type of DRP are used in a smart grid to reduce total cost.

According to the reviewed literature, it can be concluded that the work done for the H-AC-DC-MG is very low. As far as we know, in few articles, the optimal operation issue of H-AC-DC-MG has been addressed. Also, any article does not focus on RTP of DRPs in H-AC-DC-MGs.

4.1.2 Novelty and Contribution

The DC network along with the AC network is intended to increase the efficiency of the storage and photovoltaic system. The DC voltage generated by the photovoltaic system is transmitted by the DC network and stored directly in the storage system. In addition, according to loss reduction, the operation cost reduction is the main advantage of this plan that will be proven in this chapter. Also, TOU and RTP of DRPs can be used as useful options to reduce cost. Therefore, this novelty and contributions section is summarized as follows:

1. DC link is used to increase efficiency of microgrid operation.
2. PHEVs are used for flexible use of renewable resources in the microgrid.
3. Time-of-use pricing of DRP is proposed to manage peak load in order to reduce the operation cost of the microgrid.
4. In order to reduce the MG operation cost, real-time DR has been proposed.

4.1.3 Chapter Organization

The rest of this chapter is categorized as follows: Introduction of hybrid AC-AC microgrid and C-AC-MG topologies is proposed in Sect. 4.2. The problem formulation of both microgrids, which consist of operation, cost minimization, and

relevant constraints, is introduced in Sect. 4.3. In Sect. 4.4, both types of DRP formulation including RTP and TOU modeling are proposed in Section 4.5. The case study section which includes obtained results and input data will be presented in Sect. 4.6. Finally, the conclusions will be provided in Sect. 4.6.

4.2 Topology Introduction of Hybrid AC-AC Microgrid

Two topologies for supplying demand are presented in this chapter. These two topologies include the convention AC microgrid and H-AC-DC-MG. The structure of these two topologies is described as follows:

4.2.1 Conventional AC-MG

This topology is an AC network wherein power is generated by AC generators, as well as by renewable energy resources (wind turbine and photovoltaic system), which is transmitted by the use of AC bus and DC loads as well as charging PHEVs. In addition, the external grid is used to maintain power balance in the AC network. The schematic of this topology is shown in Fig. 4.1.

4.2.2 Hybrid-AC-DC-MG

H-AC-DC-MG has provided many benefits to distribution networks. Power loss reduction and easy provision of DC loads are the main benefits of this topology. DC resources such as a photovoltaic system which uses DC bus provide the DC loads and required energy of PHEVs. Also, AC resources such as the wind turbine and AC generators, using AC bus, provide the AC loads. Between the AC and DC buses, there is a converter for the electrical connection between the two buses. In addition, the external grid is used to maintain power balance in the AC network. The schematic of this topology is shown in Fig. 4.2.

4.3 Problem Formulation

In this section, the formulation of the C-AC-MG and H-AC-DC-MG will be provided. By solving the scheduling problem, the power generated by DG units and charge/discharge rate of PHEVs, as well as the power purchased from the external network in the considered time horizon, will be determined.

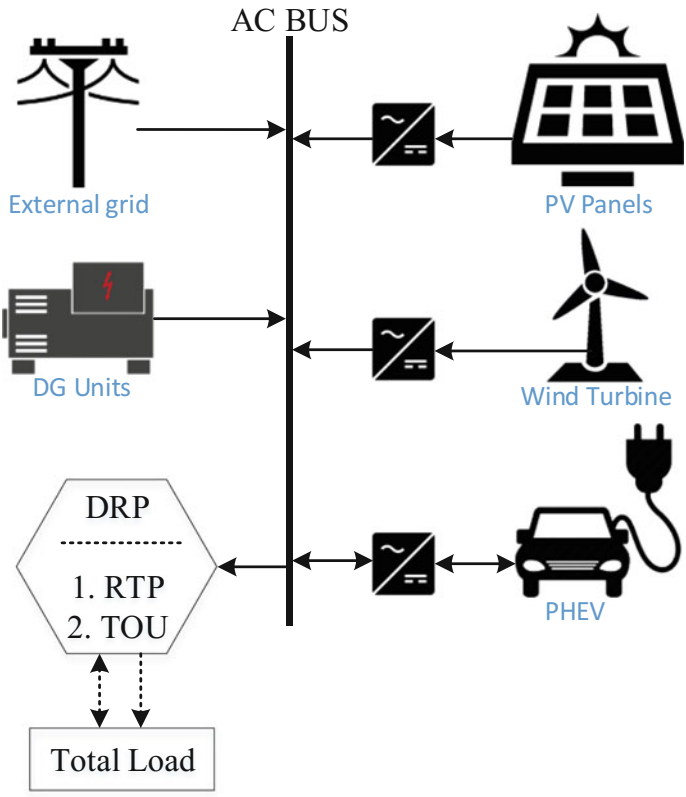

Fig. 4.1 The structure of C-AC-MG

4.3.1 Objective Function

In this chapter, minimizing the overall operation cost is the objective function of the microgrid in both topologies. The mathematical model for objective function is presented in Eq. (4.1)

$$\mathrm{OC} = \sum_{t=1}^{24} \begin{bmatrix} \mathrm{PG_{in}}(t) \times \mathrm{PR_{TOU}}(t) \\ -\mathrm{PG_{out}}(t) \times \mathrm{PR_{sell}} \\ +(F(t) \times \mathrm{PR_{Fuel}} + C_{\mathrm{O\&M}}) \\ \sum_{n=1}^{10} \left(\begin{matrix} \left(\mathrm{PEV}^{n}_{\mathrm{dcharge}}(t) \times \mathrm{PR_{TOU}}(t) \times \alpha_{\mathrm{dcharge}}\right) \\ -\mathrm{PEV}^{n}_{\mathrm{charge}}(t) \times \mathrm{PR_{TOU}}(t) \end{matrix} \right) \end{bmatrix} \tag{4.1}$$

The first term of Eq. (4.1) represents the cost of power purchased from the external grid. In addition, the second term of Eq. (4.1) shows the revenue from the surplus

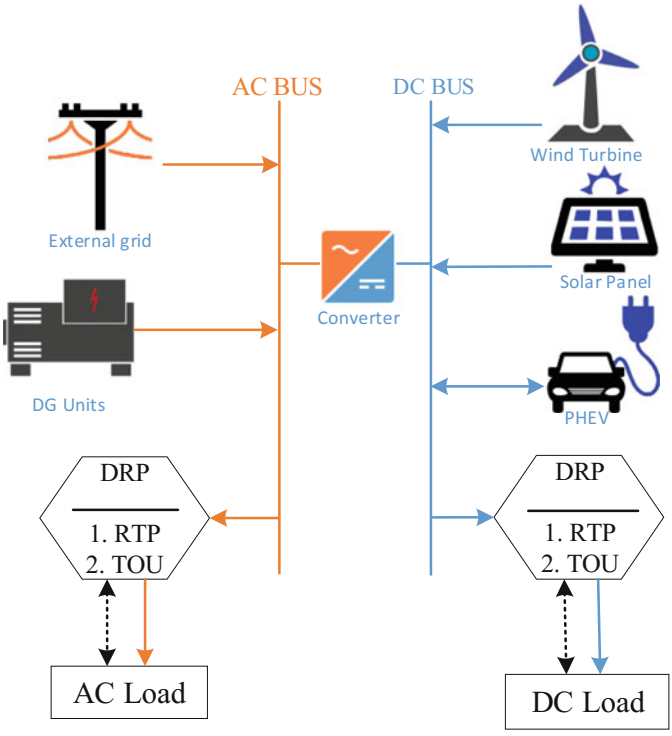

Fig. 4.2 The structure of H-AC-DC-MG

power which is sold to the external network. The third part shows the operation cost of DGs, which includes the cost of fuel and the maintenance cost of the microturbines. The fourth term also shows the cost of the discharge of PHEV and obtained revenues from charging them.

Problem constraints can be categorized as follows:

4.3.2 C-AC-MG Constraint

The C-AC-MG constraints, which include the power balance equation and AC unit constraints, are presented in this section.

4.3.2.1 Power Balance Constraint

Equation (4.2) presents the power balance constraint for C-AC-MG.

$$\eta_{\text{DC-AC}}\left[P_{\text{WT}}(t)+P_{\text{PV}}(t)+\sum_{n=1}^{N}\text{PEV}^{n}_{\text{dcharge}}(t)\right]+P_{\text{DG}}(t)+\text{PG}_{\text{in}}(t)= \text{Load}_{\text{Total}}(t)+\sum_{n=1}^{N}\text{PEV}^{n}_{\text{charge}}(t)+\text{PG}_{\text{out}}(t) \tag{4.2}$$

where

$$\text{Load}_{\text{Total}}(t)=\text{Load}_{\text{AC}}(t)+\frac{\text{Load}_{\text{DC}}(t)}{\eta_{\text{AC-DC}}} \tag{4.3}$$

In Eq. (4.3), due to the connection of the DC load to the AC bus, the rectifier losses are considered in the second term of the right side of Eq. (4.3).

4.3.2.2 DG Unit Constraint

DG units are AC generators that use fossil fuels, convert them to electricity, and have various mechanical and electrical constraints. These constraints can be expressed as follows:

$$0\le P_{\text{DG}}(t)\le P_{\text{DG, max}} \tag{4.4}$$

$$0\le P_{\text{DG}}(t+1)-P_{\text{DG}}(t)\le \text{RR} \tag{4.5}$$

$$P_{\text{DG}}(t)=F(t)\times \text{HR}\times\eta_{\text{DG}} \tag{4.6}$$

Equation (4.4) expresses the maximum and minimum power generation of the DG units. Equations (4.5) and (4.6) indicate the ramp-up and ramp-down constraints of DG units, respectively. Equation (4.7) expressed the output power delivered to the AC bus.

4.3.2.3 PHEV Constraint

The constraints of PHEV can be expressed as follows:

$$0\le \text{PEV}^{n}_{\text{charge}}(t)\le X^{n}_{\text{charge}}(t)\times \text{PEV}^{n}_{\text{charge, max}}(t) \tag{4.7}$$

$$0\le \text{PEV}^{n}_{\text{dcharge}}(t)\le X^{n}_{\text{dcharge}}(t)\times \text{PEV}^{n}_{\text{dcharge, max}}(t) \tag{4.8}$$

Equations (4.7) and (4.8) expressed the charge/discharge limits of the PHEVs.

$$\begin{cases} X^n_{\text{charge}}(t) + X^n_{\text{dcharge}}(t) \le 1, & t^n_{\text{arr}} \le t \le t^n_{\text{dep}} \\ X^n_{\text{charge}}(t) = X^n_{\text{dcharge}}(t) = 0, & \text{otherwise} \end{cases} \tag{4.9}$$

Equation (4.9) defined that the battery can only be charged/discharged at any moment in the parking. Also, Eq. (4.9) states that the battery cannot charge/discharge when PHEV is not parked.

The SOC of PHEV's battery constraints can be formulated as follows:

$$\text{SOC}^n_{\min} \le \text{SOC}^n(t) \le 1 \tag{4.10}$$

$$\text{SOC}^n(t+1) = \text{SOC}^n(t) + \frac{\text{PEV}^n_{\text{charge}}(t) - \text{PEV}^n_{\text{charge}}(t)}{\text{QEV}^n} \tag{4.11}$$

$$\text{SOC}^n\left(t^n_{\text{arr}}\right) = \text{SOC}^n_{\text{in}} \tag{4.12}$$

$$\text{SOC}^n\left(t^n_{\text{dep}}\right) = \text{SOC}^n_{\text{dep}} \tag{4.13}$$

SOC range is limited according Eq. (4.10). In addition, SOC of batteries at time t can be calculated from Eq. (4.11). PHEV's SOC at each time is the different amounts determined at arrival and departure time from the parking, according to Eqs. (4.12) and (4.13).

4.3.2.4 Constraint of Traded Power with the Grid

Microgrid can buy power from the upstream grid and also sell its surplus power to the upstream grid. Constraints of buy and sell power came as follows:

$$0 \le \text{PG}_{\text{in}}(t) \le X_{\text{in}}(t) \times \text{PG}_{\max} \tag{4.14}$$

$$0 \le \text{PG}_{\text{out}}(t) \le X_{\text{out}}(t) \times \text{PG}_{\max} \tag{4.15}$$

$$X_{\text{in}}(t) + X_{\text{out}}(t) \le 1 \tag{4.16}$$

Equations (4.14) and (4.15) are the constraints of buy and sell powers from and to the grid. Also, Eq. (4.16) shows that buying and selling power cannot happen at the same time.

4.3.3 H-AC-DC-MG Constraint

The H-AC-DC-MG has two power balance constraints, which are defined for AC bus and DC bus. In the following the H-AC-DC-MG constraints will be provided.

4.3.3.1 AC Bus Power Balance Constraint

$$\begin{aligned} &P_{\mathrm{DG}}(t) + \mathrm{PG}_{\mathrm{in}}(t) + (P_{\text{DC-AC}}(t) \times \eta_{\text{DC-AC}}) \\ &= \mathrm{Load}_{\mathrm{AC}}(t) + \mathrm{PG}_{\mathrm{out}}(t) + P_{\text{AC-DC}}(t) \end{aligned} \tag{4.17}$$

According to Eq. (4.17), input power to AC bus which includes power generated in DG units, input power from the external grid, and converted power from the DC bus should be equal to output power from the AC bus which includes AC load, power sold to the external grid, and rectified power to the DC bus.

4.3.3.2 DC Bus Power Balance Constraint

$$\begin{aligned} &P_{\mathrm{WT}}(t) + P_{\mathrm{PV}}(t) + \sum_{n=1}^{N} \mathrm{PEV}^{n}_{\mathrm{dcharge}}(t) + (P_{\text{AC-DC}}(t) \times \eta_{\text{AC-DC}}) \\ &= \mathrm{Load}_{\mathrm{DC}}(t) + \sum_{n=1}^{N} \mathrm{PEV}^{n}_{\mathrm{charge}}(t) + P_{\text{DC-AC}}(t) \end{aligned} \tag{4.18}$$

According to Eq. (4.18), input power to the DC bus, which includes power generated in wind turbine and PV panels, discharged power from PHEV's battery, and rectified power from AC bus, should be equal to output power from the AC bus which includes DC load, charged power to PHEV's battery, and converted power to the AC bus.

4.3.4 Converter Constraint

The converter is installed between the AC and DC bus, which enables the power exchange between the two buses. Equations (4.19)–(4.21) present the constraint of the converter.

$$P_{\text{AC-DC}}(t) \le X_{\text{AC-DC}}(t) \times P_{\mathrm{conv}} \tag{4.19}$$

$$P_{\text{DC-AC}}(t) \le X_{\text{DC-AC}}(t) \times P_{\mathrm{conv}} \tag{4.20}$$

$$X_{\text{AC-DC}}(t) + X_{\text{DC-AC}}(t) \le 1 \tag{4.21}$$

Equations (4.19) and (4.20) define the maximum power exchanged in each mode of converter (AC/DC of DC/AC modes). Also, Eq. (4.21) shows that the converter can be charged or discharged at any time.

4.3.4.1 Other Constraints of H-AC-DC-MG

Constraints (4.4)–(4.16) of C-AC-MG can also be considered for H-AC-DC-MG.

4.4 DRP Modeling

DRPs are used in order to reduce operation costs of MG. In this chapter, two types of DRP are used, which include TOU and RTP. The description and formulation of these DRPs are presented in the following subsections.

4.4.1 TOU of Demand Response Program

The TOU program is a time-based DRP which changes prices at different times. In addition, in TOU DRP incentives may be provided to consumers to shift their loads from peak times to off-peak times. It should be noted that the shifted load is limited, in which in this chapter 15% of base load are considered (DRmax = 15%). This type of DRP is modeled in Fig. 4.3.

According to Fig. 4.3, at any peak time, some of the load can be shifted, which is called *ldr*. The mathematical model of this figure is presented in (4.22) and (4.23).

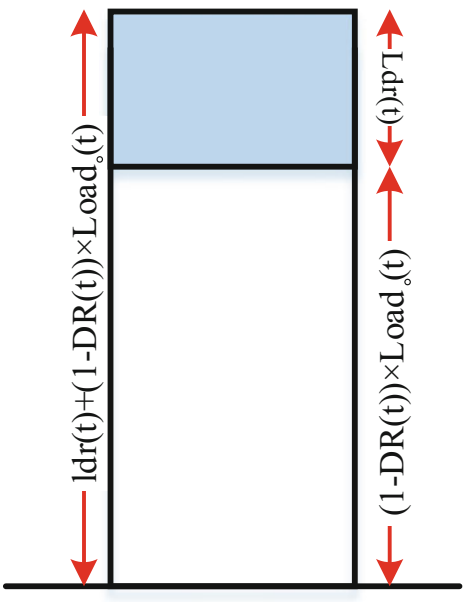

Fig. 4.3 Load model considering TOR DRP

$$\text{load}_{\text{TOU}}^{t} = (1 - \text{DR}_t) \cdot \text{load}_t^0 + \text{ldr}_t \tag{4.22}$$

$$\text{load}_t^0 - \text{load}_{\text{TOU}}^{t} = \text{DR}_t \cdot \text{load}_t^0 - \text{ldr}_t \tag{4.23}$$

In Eqs. (4.22) and (4.23), load_t^0 shows the base load in the considered time horizon, and $\text{load}_{\text{TOU}}^{t}$ is the amount of load after shifting load operation. DR_t is the percentage of DR at each time t. Also, the other constraints are presented as follows:

$$\sum_{t=1}^{T} \text{ldr}_t = \sum_{t=1}^{T} \text{DR}_t \cdot \text{load}_t^0 \tag{4.24}$$

$$\text{load}_t^{\text{inc}} \leq \text{inc}_t \cdot \text{load}_t^0 \tag{4.25}$$

$$\text{DR}_t \leq \text{DRmax} \tag{4.26}$$

$$\text{inc}_t \leq \text{inc max} \tag{4.27}$$

Equation (4.24) expresses that the shifted load in the time horizon is equal to the total load increased in the time horizon. Also, Eq. (4.25) shows that the load increase at any time is lower from the total load increase. Equations (4.26) and (4.27) show the maximum amount of reduction and increase in load at any time.

4.4.2 RTP of Demand Response Program

RTP like TOU is a pricing method for changing the consumption time of consumers. In this type of pricing (RTP), the price is proportional to the price of the wholesale market. Economists believe that RTP is the most suitable DRP for the competitive electricity market. The formulation of this DRP type is expressed as follows [19]:

$$W_{\text{d}} = \sum_{t=1}^{24} \text{load}_t^0 \tag{4.28}$$

$$P_{\text{av}} = \frac{W_{\text{d}}}{24} \tag{4.29}$$

$$\gamma^t = \frac{\text{load}_t^0}{P_{\text{av}}} \tag{4.30}$$

Equation (4.28) shows that the W_{d} is equal to the total load in the considered time horizon (one day). Equation (4.29) shows the average electricity demand and Eq. (4.30) expresses the float factor of real-time pricing (RTP).

The RTP is expressed in Eq. (4.31). Also, the maximum and minimum bound of this price are shown in Eq. (4.32).

$$\mathrm{PR}^{t}_{\mathrm{RTP}} = \gamma^{t} \cdot \mathrm{PR}^{t}_{\mathrm{TOU}} \tag{4.31}$$

$$\mathrm{PR}^{\min}_{\mathrm{RTP}} \leq \mathrm{PR}^{t}_{\mathrm{RTP}} \leq \mathrm{PR}^{\max}_{\mathrm{RTP}} \tag{4.32}$$

The load demand formulation for RTP can be shown as follows using Refs. [21, 22].

$$\mathrm{load}^{t}_{\mathrm{RTP}} = \mathrm{load}^{0}_{t} + E \cdot \mathrm{load}^{0}_{t} \left(\frac{\mathrm{PR}^{t}_{\mathrm{RTP}} - \mathrm{PR}^{t}_{\mathrm{TOU}}}{\mathrm{PR}^{t}_{\mathrm{TOU}}} \right) \tag{4.33}$$

Considering Eq. (4.33), E is the elasticity of demand price in the RTP type of DR, which is considered -0.5. load^{0}_{t} is the primary demand, $\mathrm{PR}^{t}_{\mathrm{TOU}}$ is the TOU prices, and $\mathrm{PR}^{t}_{\mathrm{RTP}}$ is the RTP prices of electricity.

4.5 Case Study

To study the effects of the proposed topology, a four-story university building [23] is considered. This building has an air-conditioning system, lighting, computer, and laboratory supplies. Figure 4.4 shows both the AC and DC loads in this university building. The existing power resources include the DG units, wind turbines, and PV arrays, with a capacity of 40 kW, 25 kW, and 25 kW, respectively. Ten electric vehicles are trafficking to the parking which include specifications like arrival/departure time and related SOCs, as presented in Table 4.1. Also, this microgrid can be used as an upstream grid to supply their power shortages and sell excess power. Other information of DGs, PHEVs, and converters is proposed in Table 4.2. In addition, natural gas is used to generate power in DGs purchased in the price of 0.328 USD/m^3 [24]. Also, Fig. 4.5 shows the sale price to the external grid and time-of-use rate.

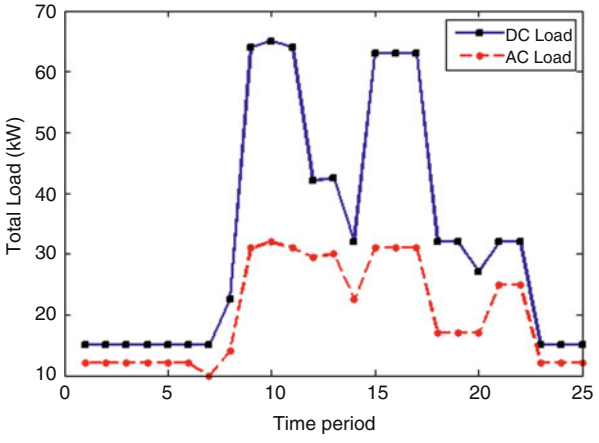

Fig. 4.4 Total AC and DC load curve

Table 4.1 Required traffic data of PHEV

PHEV no.	t_{arr}(h)	t_{dep}(h)	SOC_{in}	SOC_{out}
1	7	20	0.8	0.8
2	8	18	0.2	1
3	8	17	0.5	0.9
4	9	14	0.8	0.3
5	9	17	0.4	1
6	9	17	0.35	0.9
7	9	18	0.5	0.9
8	10	18	0.7	0.7
9	10	19	0.85	0.3
10	11	20	0.4	0.9

Table 4.2 More required data

DG unit		PHEV's battery		Converter	
η_{DG}	0.35	QEV^n	5(kWh)	P_{conv}	40 (kW)
RR	20 (kW/h)	$PEV^n_{charge,\,max}$	1.1(kW)		
$C_{O\ \&\ M}$	0.03 (USD/h)	$PEV^n_{dcharge,\,max}$	2.45(kW)	$\eta_{AC\text{-}DC}$	0.9
HR	10.78 (kWh/m^3)	SOC^n_{min}	0.2	$\eta_{DC\text{-}AC}$	0.85

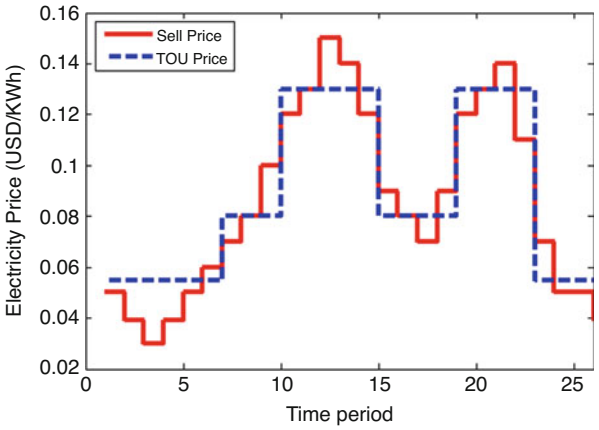

Fig. 4.5 Sell price and TOU price curve

Here, the obtained results from solving the problem are presented in Table 4.3 in two types of microgrids (H-AC-DC-MG and C-AC-MG) which show the importance of H-AC-DC-MGs. According to Table 4.3, it can be concluded that the cost reduction due to the use of H-AC-DC-MG is more than the C-AC-MG in the presence of various DRPs. Cost reduction in H-AC-DC-MG compared to the C-AC-MG is 15.7% in the no DRP mode and 17.17% and 25.18 % for the use of TOU and RTP, respectively. In addition, according to Table 4.3, it can be seen that the total

Table 4.3 Comparison results of operation cost of microgrids

Parameters	C-AC-MG			H-AC-DC-MG		
	No DRP	TOU	RTP	No DRP	TOU	RTP
Total cost	85.206$	79.551$	59.923$	73.432	67.892	47.866
Cost reduction versus no DRP	0	7.1%	42.1%	0	8.1%	53.89%
Cost reduction versus C-AC-MG	0	0	0	15.7%	17.17%	25.18%

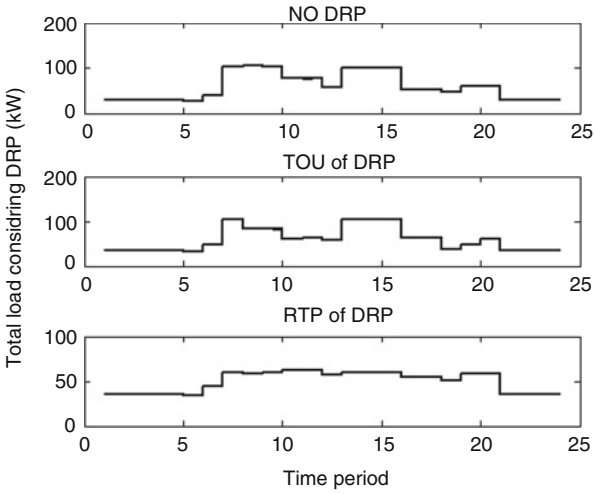

Fig. 4.6 Total load considering of DRP

operation cost of C-AC-MG has been reduced to 7.1% and 42.1% due to the use of TOU and RTP, respectively. Also, in H-AC-DC-MG, operation cost reduction is 8.1% and 53.89%, due to the use of TOU and RTP, respectively.

According to Fig. 4.6, the effect of DRP on the C-AC-MG is obtained. It should be noted that due to the comparison of the university load curve with the residential load curve, the effects of both RTP and TOU on the university load curve will be significant. In Fig. 4.6, it can be seen that the DRP has a great effect on the total load curve of the university. It is also seen that the impact of RTP is more than the TOU.

In Fig. 4.7, the microgrid load is separated in terms of the AC and DC loads of H-AC-DC-MG. According to Fig. 4.7, the effects of RTP on AC and DC loads are significant and make the AC and DC load curve more smoother. In addition, the effects of TOU and RTP on the AC and DC loads are observable and have an equal effect on both loads.

One of the positive effects of DRP in the H-AC-DC-MG is less use of the converter to convert AC to DC and DC to AC. Figure 4.8 shows the converted power in the converter. As shown in Fig. 4.8, the conversion power from DC to AC is zero which is due to the use of DRP. Also, the power converted from AC to DC is reduced due to the use of DC, in which reduction in the conversion power using RTP is greater than the TOU.

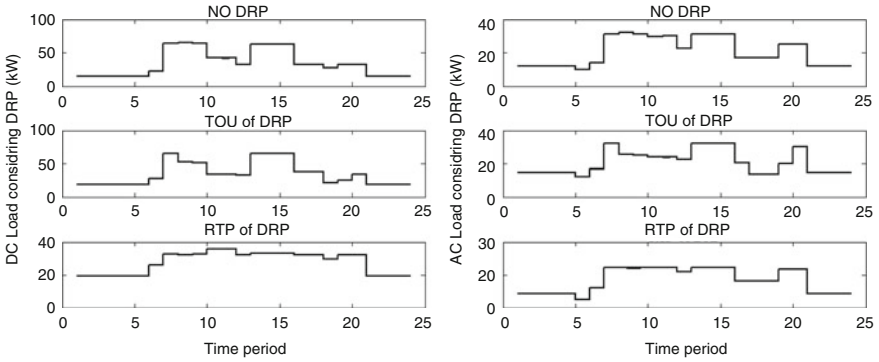

Fig. 4.7 DC and AC load consideration of DRP

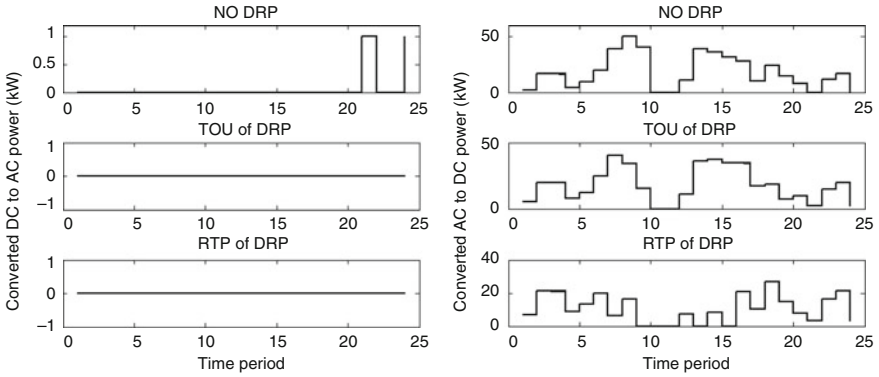

Fig. 4.8 AC to DC and DC to AC converted power

The battery status of hybrid vehicles is also shown in Fig. 4.9 at various times. According to Fig. 4.9, the DC loads in the H-AC-DC-MG cause a change in the performance of the hybrid vehicles. In addition, use of DRP reduces hybrid vehicle charging at the market price at peak periods. It can be seen that even the time of charging and discharging the battery in the hybrid microgrid is different from that of the conventional microgrid. It can be also seen that the effect of RTP is greater than the TOU. According to Fig. 4.9, the hybrid vehicles are charged at the off-peak periods of DC loads and discharged at the DC load peak periods.

Fuel consumption and power generated by the DG units are also shown in Fig. 4.10. According to this figure, the use of DRP, fuel consumption, and power generated by the DG units are reduced, in which fuel consumption and power-generated reduction using RTP are greater than the TOU and no DRP mode. Also, in the three modes (no DRP, TOU, and RTP), fuel consumption in conventional MG is more than the H-AC-DC-MG.

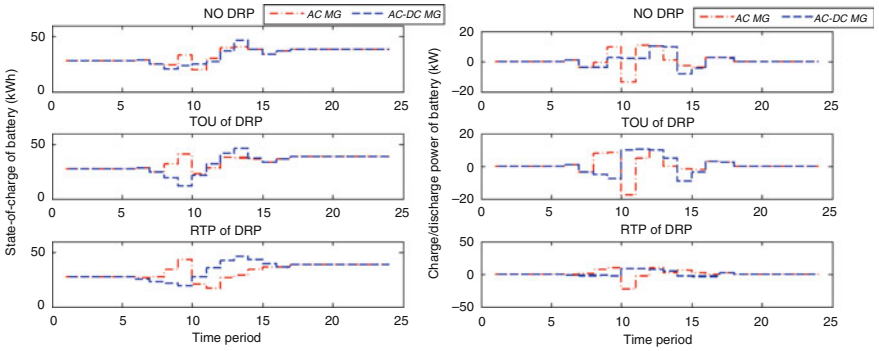

Fig. 4.9 State-of-charge and charge and discharge power of PHEVs

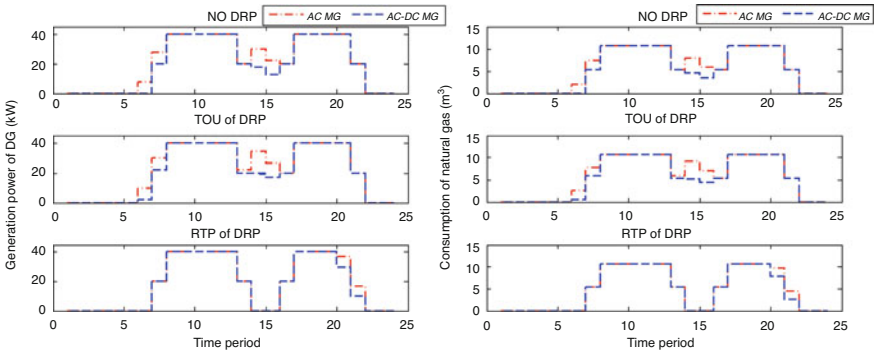

Fig. 4.10 Generated power and fuel consumption of MT

One of the DRP advantages in the H-AC-DC-MG is reducing the power to trade upstream grid, as indicated in Fig. 4.11. According to this figure, in the university, peak period power is purchased from the external grid, and at the pool market, peak time power is sold to the external grid. Also, it can be seen that the power exchange to the external grid by the use of RTP is less than the TOU and no DRP and use of TOU is less than the no DRP.

4.6 Conclusion

H-AC-DC-MG is a new design of microgrid, which is introduced in the electricity network to reduce power procurement cost. In this chapter, a H-AC-DC-MG is introduced and then compared to C-AC-MGs. In addition, two famous types of DRP are used to reduce the cost of H-AC-DC-MG. These DRPs are RTP and TOU. According to the obtained results, total operation cost of H-AC-DC-MG has been reduced to 8.1% and 53.89% and to 7.1% and 42.1% in C-AC-MG, due to the use of

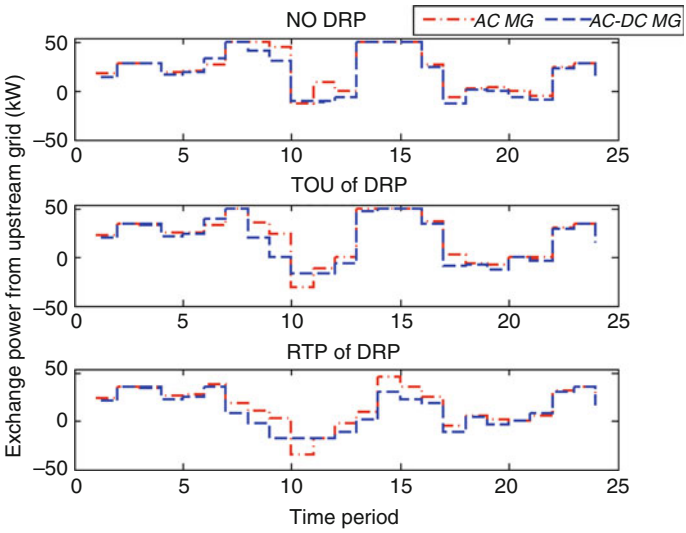

Fig. 4.11 Exchange power from upstream grid

TOU and RTP, respectively. In addition, the amount of cost reduction in the H-AC-DC-MG is greater than the C-AC-MG. In addition, the percentage of cost reduction in H-AC-DC-MG than the C-AC-MG is equal to 5.1%, 17.17%, and 25.81% due to the effect of no DRP, TOU, and RTP modes, respectively. Also, power converted losses in the H-AC-DC-MG are less than the C-AC-MG. In addition, fuel consumption of DG units and exchange power with external grid in the H-AC-DC-MG are less than the C-AC-MG. So it can be computed that the use of H-AC-DC-MG is cost-efficient with lower loss than the C-AC-MG. Therefore, H-AC-DC-MG can be replace with the C-AC-MG.

References

1. S. Singh, S. Jagota, M. Singh, Energy management and voltage stabilization in an islanded microgrid through an electric vehicle charging station. Sustain. Cities Soc. **41**, 679–694 (2018)
2. Y. Zhang, F. Meng, R. Wang, W. Zhu, X.J. Zeng, A stochastic MPC based approach to integrated energy management in microgrids. Sustain. Cities Soc. **41**, 349–362 (2018)
3. A. Alfergani, A. Khalil, Z. Rajab, Networked control of AC microgrid. Sustain. Cities Soc. **37**, 371–387 (2018)
4. T. Dragičević, X. Lu, J.C. Vasquez, J.M. Guerrero, DC microgrids—Part II: a review of power architectures, applications, and standardization issues. IEEE Trans. Power Electron. **31**(5), 3528–3549 (2016 May)
5. E. Unamuno, J.A. Barrena, Hybrid ac/dc microgrids—Part I: review and classification of topologies. Renew. Sust. Energ. Rev. **52**, 1251–1259 (2015)
6. E. Unamuno, J.A. Barrena, Hybrid ac/dc microgrids—Part II: review and classification of control strategies. Renew. Sust. Energ. Rev. **52**, 1123–1134 (2015)

7. H. Lotfi, A. Khodaei, Static hybrid AC/DC microgrid planning, in *Innovative Smart Grid Technologies Conference (ISGT), 2016 IEEE Power & Energy Society* (IEEE, 2016), pp. 1–5
8. H. Lotfi, A. Khodaei, Hybrid AC/DC microgrid planning. Energy **118**, 37–46 (2017)
9. V. Indragandhi, R. Logesh, V. Subramaniyaswamy, V. Vijayakumar, P. Siarry, L. Uden, Multi-objective optimization and energy management in renewable based AC/DC microgrid. Comput. Electr. Eng. **70**, 179–198 (2018)
10. F. Nejabatkhah, Y.W. Li, Overview of power management strategies of hybrid AC/DC microgrid. IEEE Trans. Power Electron. **30**(12), 7072–7089 (2015)
11. P.T. Baboli, M. Shahparasti, M.P. Moghaddam, M.R. Haghifam, M. Mohamadian, Energy management and operation modelling of hybrid AC–DC microgrid. IET Gener. Transm. Distrib. **8**(10), 1700–1711 (2014)
12. M. Hosseinzadeh, F.R. Salmasi, Robust optimal power management system for a hybrid AC/DC microgrid. IEEE Trans. Sustain. Energy **6**(3), 675–687 (2015)
13. I. Komušanac, B. Ćosić, N. Duić, Impact of high penetration of wind and solar PV generation on the country power system load: the case study of Croatia. Appl. Energy **184**, 1470–1482 (2016)
14. S. Pereira, P. Ferreira, A.I. Vaz, Generation expansion planning with high share of renewables of variable output. Appl. Energy **190**, 1275–1288 (2017)
15. P. Sreedharan, J. Farbes, E. Cutter, C.K. Woo, J. Wang, Microgrid and renewable generation integration: University of California, San Diego. Appl. Energy **169**, 709–720 (2016)
16. Z. Chen, B. Xia, C. You, C.C. Mi, A novel energy management method for series plug-in hybrid electric vehicles. Appl. Energy **145**, 172–179 (2015)
17. G. Razeghi, S. Samuelsen, Impacts of plug-in electric vehicles in a balancing area. Appl. Energy **183**, 1142–1156 (2016)
18. M. Jin, W. Feng, P. Liu, C. Marnay, C. Spanos, MOD-DR: microgrid optimal dispatch with demand response. Appl. Energy **187**, 758–776 (2017)
19. S. Nojavan, K. Zare, B. Mohammadi-Ivatloo, Optimal stochastic energy management of retailer based on selling price determination under smart grid environment in the presence of demand response program. Appl. Energy **187**, 449–464 (2017)
20. M.M. Eissa, First time real time incentive demand response program in smart grid with "i-Energy" management system with different resources. Appl. Energy **212**, 607–621 (2018)
21. S. Nojavan, M. Majidi, N.N. Esfetanaj, An efficient cost-reliability optimization model for optimal siting and sizing of energy storage system in a microgrid in the presence of responsible load management. Energy **139**, 89–97 (2017)
22. S. Nojavan, M. Majidi, A. Najafi-Ghalelou, M. Ghahramani, K. Zare, A cost-emission model for fuel cell/PV/battery hybrid energy system in the presence of demand response program: ε-constraint method and fuzzy satisfying approach. Energy Convers. Manag. **138**, 383–392 (2017)
23. S. Nojavan, H. Ghesmati, K. Zare, Robust optimal offering strategy of large consumer using IGDT considering demand response programs. Electr. Power Syst. Res. **130**, 46–58 (2016)
24. M.S. Ngan, C.W. Tan, Assessment of economic viability for PV/wind/diesel hybrid energy system in southern Peninsular Malaysia. Renew. Sust. Energ. Rev. **16**(1), 634–647 (2012)

Chapter 5
Distribution Feeder Reconfiguration Considering Price-Based Demand Response Program

Ehsan Hooshmand and Abbas Rabiee

Nomenclature

Sets and Indices

b, b'	Index for network buses
l	Index for network feeders
S_b	Set of all network nodes
S_{dr}	Set of nodes participating in demand response
S_{l}	Set of lines in distribution network
S_t	Set of time periods
t	Index for operation intervals

Variables

$\vartheta_{b,\,t}$	Demand response decision variable of bus b at time period t
$\mathrm{Bi}_b^{\mathrm{dr}}$	Binary decision variable indicating whether bus b participates in DR or not
$\mathrm{Bi}_b^{\mathrm{pv}}$	Binary decision variable for installation of PV at bus b
Bi_l^{r}	Binary decision variable to model the on/off status of feeder l
$\mathrm{Bi}_b^{\mathrm{w}}$	Binary decision variable for installation of WT at bus b
CENS	Cost of energy not supplied ($)
ENS_t	Energy not supplied at time period t ($/h)
$I_{l,\,t}$	Current flowing through the line l at time t (pu)

E. Hooshmand · A. Rabiee (✉)
Electrical Engineering Department, University of Zanjan, Zanjan, Iran
e-mail: e.hooshmand@znu.ac.ir; rabiee@znu.ac.ir

S. Nojavan, K. Zare (eds.), *Demand Response Application in Smart Grids*,
https://doi.org/10.1007/978-3-030-32104-8_5

$(P/Q)_{b,t}^{\mathrm{D}}$ Active/reactive demand of bus b at time period t with demand response (pu)
$(P/Q)_{b,t}^{\mathrm{G}}$ Active/reactive power generation in bus b at time period t (pu)
$(P/Q)_{b,t}^{\mathrm{net}}$ Net active/reactive power injection to bus b at time period t with demand response (pu)
$(P/Q)_{b,t}^{\mathrm{pv}}$ Active/reactive power injection of bus b at time period t with PV (pu)
$(P/Q)_{b,t}^{\mathrm{w}}$ Active/reactive power injection of bus b at time period t with WT (pu)
TOC Total operation cost ($)
$V_{b,\,t}$ Voltage magnitude at bus b at time t (pu)

Parameters

β_b^+, β_b^- Coefficients for modeling the lower/upper limits of wind turbine reactive power output
λ_l Failure rate of branch l [failures/year]
$\Gamma^{\mathrm{w/pv}}$ Rated active power of WT and PV connected to bus b (pu)
$\Phi_{\mathrm{t}}^{\mathrm{w/pv}}$ Forecasted output of WT and PV at time period t(%)
$\vartheta_b^{\max\,/\,\min}$ Maximum/minimum demand flexibility at bus b(%)
$I_l^{\max}$ Maximum feeder of l capacity
$\aleph_t^{\mathrm{dr}}$ Energy rate of DR at time t in day-ahead market ($/MWh)
$\aleph_t^{\mathrm{pv}}$ Energy rate of PV at time t in day-ahead market ($/MWh)
$\aleph_t^{\mathrm{ups}}$ Pool market price at time t in day-ahead market ($/MWh)
$\aleph_t^{\mathrm{w}}$ Energy rate of WT at time t in day-ahead market ($/MWh)
N^{dr} Maximum number of nodes allowed to participate in demand response
N^{pv} Maximum number of nodes allowed to install the PV
N^{w} Maximum number of nodes allowed to install the wind plant
$(P/Q)_{b,t}^{\mathrm{D0}}$ Initial active/reactive demand of bus b at time period t without demand response (pu)
R_l Resistance of line l
U_l Average repair time of branch l [h]
$V^{\min/\max}$ Maximum/minimum voltage magnitude
VOLL_t Value of lost load at time t ($/MWh)
X_l Reactance of line l

Abbreviations

CENS Cost of energy not supplied
DFR Distribution feeder reconfiguration
DERs Distributed energy resources
DG Distributed generation
DR Demand response
DS Distribution system

DSO	Distribution system operator
MISOCP	Mixed-integer second-order cone programming
PV	Photovoltaic
RESs	Renewable energy sources
TOC	Total operation cost
WT	Wind turbine

5.1 Introduction

5.1.1 Background and Motivations

Due to the rapid increase in the demand for electricity, as well as the need for higher reliability, better power quality, voltage profile enhancement, and total cost minimization in distribution systems (D**S**s), more attention is paid to distributed energy resources (DERs). On the other hand, RESs such as photovoltaic (PV) cells and wind turbine (WT) generators are expected to play an important role in the future electricity sector and low cost/emission energy systems. The principal aim of any energy supply system is to procure sustainable and reliable energy for the customers [1]. Usually DSs are relatively less expensive than a transmission system and the outages in a typical DS have localized effects [2]. However, the DS is the main source of energy supply interruption to the end users, and more attention should be paid to its reliability enhancement [3]. Some methods and tools are used to improve reliability, mainly including DS automation, well-designed and coordinated protection schemes, proper reclosing and switching, fault prediction approaches, and well-organized and fast repair teams [4]. Besides, by optimal allocation of DERs such as WTs, PVs, and DR as well as distribution feeder reconfiguration (DFR), more flexibility in DS operation could be attained.

5.1.2 Literature Survey

Many researchers focused on DFR impacts on DS operation over the last several decades [5–7]. It is shown that DFR is an effective tool to power loss reduction [8], load balancing [9], etc. Consideration of reliability as an objective for DS operator (DSO) has been explored in several researches. In [3, 4, 10], the DFR is introduced as a promising operational strategy to be considered together with the aforementioned aims, taking into account the enhancement of reliability. DFR has a key role in improvement of network flexibility. On the other hand, efficiency of DFR depends on the ability of DSO to control the sectionalizer switches. In planning studies, sectionalizers in DFR are mostly manual switches [11]. But in operation studies, by using remotely controlled sectionalizers, the topology of the grid could be changed

in a short time period by DSO. The DFR method proposed in [12] is used for operation and coordination of a protective device in DS. In [13], the total operation cost of a microgrid is minimized by performing the jointly optimal generation scheduling and optimal DFR on a day-ahead market. The energy storage system (ESS) planning proposed in [14] is used to minimize the operation cost of DS with regard to the hourly topology change of the grid, by using the hourly DFR. Also the operation and planning indices are evaluated in [15] with regard to the presence or absence of DFR, RESs, and DR.

Optimal WT, PV, and DR placement and scheduling have been proposed in different literatures under different loading conditions by considering different objectives. For example, in [16, 17] a robust model is proposed for optimal allocation of renewable energy sources, energy storage systems, and demand response in DSs via uncertainty management techniques. The optimal placement of these tools by considering the aims such as load margins as well as voltage stability improvement of network is analyzed [18]. Also, [19] determines the optimal size and location of wind farms (WFs) using a sensitivity analysis to enhance voltage stability. It is evidently observed from the above literature review that some traditional objective functions such as active/reactive power losses, voltage deviation, and total cost are the main goals.

Recently, DR or load flexibility has been offered by electricity utilities to encourage consumers to participate in the demand-side management program that is advantageous from system and customer viewpoints [20]. Various techniques of DR programs are on-peak cutting, off-peak filling, and load shifting [20, 21]. In the on-peak cutting mechanism, the load increase is prevented from predetermined level during the on-peak period by removing load. Also off-peak filling is a technique to increase the demand by using energy storage devices (such as ESS and electric vehicles) in the off-peak period. Finally, in the load shifting mechanism, in order to change the energy consumption times to the desired interval for DSO, the load is shifted from on-peak to off-peak period, without any elimination in the total load demand of the customer within the considered interval. The relevant researches have shown that instead of expanding the generation systems, DR programs can be implemented to improve the reliability of the power system [22], by providing dependable reserve capacity. Also in [23], the impact of DR on voltage profile improvement during peak periods as well as loss reduction in DSs is studied. The capability of DR to optimize the energy dispatch by minimizing the operation costs and peak demand of isolated microgrids is investigated in [24]. However, most previous works have not considered the impact of DR on DFR. In this chapter, the load shifting mechanism is utilized in a price-based DR program [25].

AC power flow models are important for planning problems of power systems as well as in determining the optimal operation of existing systems [26]. The principal information obtained from the AC power flow is the magnitude and phase angle of voltage at each bus and the real and reactive power flowing through each line. Despite its capability to accurately model the real power system behavior, an optimization problem based on AC power flow model is nonconvex and nonlinear [3–5, 9, 10, 16, 17, 19, 26–28]. Besides, the computational burden of AC optimal

power flow (OPF) models is heavy and only local optimal solutions could be attained, whereas in a constrained optimization problem, a convex feasible area can more easily be assured such that an infeasible solution cannot be generated when searching for an optimal solution. If there are several feasible solutions, any solution within the line segment connecting them is also feasible. In the case of the convex objective function, the convex feasible area ensures that all of the locally optimal solutions are the global optimal solution. On the other hand, when acquiring an acceptable optimal solution, there will be no better optimal solution in its neighborhood. However, in a nonconvex optimization problem, when looking for optimal solutions, it is possible to find a local optimal solution (i.e., a suboptimal solution). As an alternative AC model, the line flow-based (LFB) model has been proposed in [29]. The LFB model directly uses bus voltage magnitudes and line power flows as independent variables and thus the power loss and voltage can be effectively considered. The LFB model has also a good convergence characteristic and computational efficiency, which make it favorable for large-scale nonlinear and mixed-integer models related to operation and planning of DSs [15]. Based on this model, in [14] a convex model for active distribution network planning is proposed by integration of ESSs. In [30], a second-order conic programming (SOCP) model is proposed based on information gap decision theory to maximize load pickup considering the uncertainty of load. Recently, several methods have been proposed to convexify the OPF in distribution systems [15, 31, 32].

5.1.3 Contributions

This chapter presents a reliability-/economy-oriented energy management model for DSs, via a multiobjective optimization framework. The cost of energy not supplied (CENS) and total operation cost (TOC) are considered as the competitive aims of DSO. DFR, WTs, PVs, and DR are considered as the energy management tools in the network for a given operation horizon. The proposed model for DS's energy management (DSEM) is formulated as a mixed-integer second-order cone programming (MISOCP) problem, which is convex and returns global optimal solutions.

5.2 Description of the Proposed DSEM Model

5.2.1 Basic Description of the Proposed Model

The proposed DSEM framework provides a convex optimization model with a global optimal solution. The developed DSEM model enables the DSO to adequately schedule the energy supply sources, with a variety of options such as RESs and consumer participation via the DR program. The proposed DSEM model is illustrated conceptually in Fig. 5.1. Given that the DSO aims to schedule

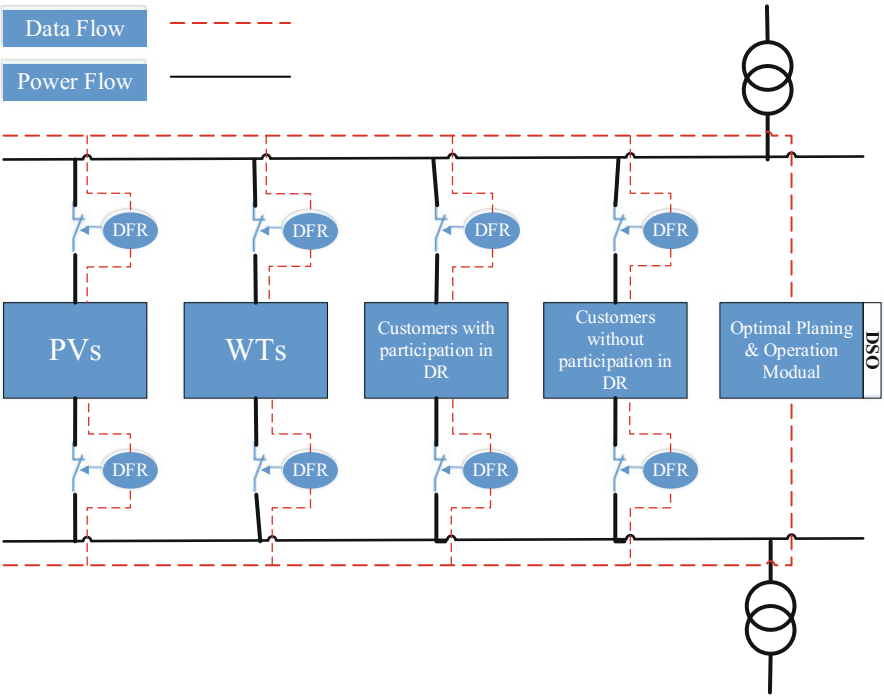

Fig. 5.1 Simplified structure of the proposed DSEM model

for a 24-h horizon, according to Fig. 5.1, the inputs are the forecasted values of DGs' available capacity and hourly load demand. Based on the input values of load forecast data [16] and the forecast data of PV/WT available capacity [27, 33], the outputs of the proposed DSEM model are the optimal placement and schedule of RESs, DR participants, and optimal DFR.

5.2.2 Problem Formulation

In order to express the proposed DSEM problem considering the DFR option from both economic and reliability viewpoints, a bi-objective optimization model is developed in this chapter.

Since the proposed DSEM model consists of AC power flow constraints as well as placement variables which are inherently binary variables, we are faced with a mixed-integer nonlinear problem (MINLP) optimization model. By applying proper relaxations, it is possible to convert the complicating constraints to some proper convex constraints. In this chapter, by utilizing a proper relaxation technique, the proposed DSEM model is relaxed to a second-order cone programming (SOCP) model. The mathematical formulation is presented in the following.

5.2.2.1 Objective Functions

Total Operation Cost (TOC)

It is assumed that the DSO is responsible for energy procurement from the day-ahead electricity market. The TOC to be minimized in (5.1) is composed of several individual costs, which are presented through Eqs. (5.2)–(5.5). The TOC consists of the cost of energy purchase from the upstream network (i.e., C^{ups}), PV (i.e., C^{pv}), DR action (i.e., C^{dr}), and WT (i.e., C^{w}) in the day-ahead market. The TOC of the system is expressed as follows.

$$\text{TOC} = C^{\text{Ups}} + C^{\text{pv}} + C^{\text{dr}} + C^{\text{w}} \tag{5.1}$$

$$C^{\text{Ups}} = \sum_{t \in S_t} \sum_{b \in S_s} \left[P_{t,b}^{\text{Ups}} \times \aleph_t^{\text{ups}} \right] \tag{5.2}$$

$$C^{\text{pv}} = \sum_{t \in S_t} \sum_{b \in S_{\text{pv}}} \left[P_{b,t}^{\text{pv}} \times \aleph_t^{\text{pv}} \right] \tag{5.3}$$

$$C^{\text{dr}} = \sum_{t \in S_t} \sum_{b \in S_{\text{dr}}} \left[\left(P_{b,t}^{\text{D}} - P_{b,t}^{\text{D0}} \right) \times \aleph_t^{\text{dr}} \right] \tag{5.4}$$

$$C^{\text{w}} = \sum_{t \in S_t} \sum_{b \in S_{\text{w}}} \left[P_{b,t}^{\text{w}} \times \aleph_t^{\text{w}} \right] \tag{5.5}$$

where $\aleph_t^{\text{ups}}$, $\aleph_t^{\text{pv}}$, $\aleph_t^{\text{dr}}$, and $\aleph_t^{\text{w}}$ are the electricity price of upstream network, PVs, DRs, and WT at time slot t, respectively. It is obvious that the proper location and scheduling of the energy management options (i.e., WTs, PVs, and DR) can decrease the TOC in the system.

Cost of Energy Not Supplied (CENS)

The DFR and optimal allocation of DERs are aimed to maximize the reliability of the DS. One of the main system-oriented reliability indices used for power systems is to minimize the cost of energy not served due to the component outage. This index is called cost of energy not supplied (CENS). In this chapter, the CENS is considered as an objective function, in addition to TOC. In DSs, CENS is mainly related to the failure rate of branches. The DSO aims to reduce CENS as much as possible, since the interruption of customer loads forces the DSO to pay value of lost load (VOLL) to the affected customers. In order to define the CENS, firstly the ENS should be calculated using the failure rate, interrupted load, and outage duration, as follows:

$$\mathrm{ENS} = \sum_{i} \mathrm{FOR}_i \times D_i \quad i \in \text{set of Failures} \tag{5.6}$$

$$\mathrm{FOR}_i = \frac{\lambda_i \times U_i}{8760} \quad i \in \text{set of Failures} \tag{5.7}$$

where D_i and FOR_i are the total active power of load not supplied and the forced outage rate during failure i, respectively. Also, λ_i and U_i are respectively the failure rate (in failure/year) and repair time (in hours) of a branch which leads to the ith failure.

In order to calculate CENS, the ENS should be expressed as a function of absolute power flowing through the lth branch at time t, as follows.

$$\mathrm{ENS}_t = \sum_{l \in S_l} \mathrm{FOR}_l \, |P_{l,t}| \tag{5.8}$$

where FOR_l is the FOR of the lth branch. The above equation contains absolute value of power flowing through the lth branch, which is a nonlinear term. In the following a simple linearization technique is proposed for this aim. Suppose the absolute value of variable x is required. By introducing two positive variables x^+ and x^-, the constraints (5.9)–(5.14) give the absolute value of x, as follows.

$$|x| = x^+ + x^- \tag{5.9}$$

$$x = x^+ - x^- \tag{5.10}$$

$$0 \le x^+ \le M \times \mathrm{Bi}^+ \tag{5.11}$$

$$0 \le x^- \le M \times \mathrm{Bi}^- \tag{5.12}$$

$$\mathrm{Bi}^+ + \mathrm{Bi}^- = 1 \tag{5.13}$$

$$\mathrm{Bi}^+, \mathrm{Bi}^- \in \{0, 1\}. \tag{5.14}$$

where M in (5.11) and (5.12) is a sufficiently big positive constant (big-M). Also, $\mathrm{Bi}^{+/-}$are binary variables. Now, using the above linearization for $|P_{l,\,t}|$, the CENS is calculated as follows.

$$\mathrm{CENS} = \sum_{t \in S_t} \mathrm{ENS}_t \times \mathrm{VOLL}_t \tag{5.15}$$

where VOLL_t is the value of lost load at time t.

5.2.2.2 Problem Constraints

Network Reconfiguration Constraints

The DSs are usually radial feeders with a tree structure and without any loops. The total number of lines equals the number of buses minus one [29]. Equations (5.16)–(5.18) guarantees the tree structure for the DS.

$$\sum_{l\in S_l} \mathrm{Bi}_l^r = S_b - S_s \tag{5.16}$$

$$\mathrm{Bi}_{bb'}^r + \mathrm{Bi}_{b'b}^r = \mathrm{Bi}_l^r, \quad l \text{ is between } b, b' \tag{5.17}$$

$$\sum_{b'\in S_b} \mathrm{Bi}_{bb'}^r = 1 \quad \forall b \in S_\mathrm{b}/S_\mathrm{s} \tag{5.18}$$

where S_s is the set of substation buses and S_b is the number of system buses. When $\mathrm{Bi}_l^r = 1$, the line switch is closed, and $\mathrm{Bi}_l^r = 0$ means that the line switch is open. $\mathrm{Bi}_{bb'}^r$ is an auxiliary binary variable, which equals to 1 if bus b' is the parent bus of b and 0 otherwise. The constraints ensure that each node only has one parent; thus the network topology is a spanning tree.

Power Flow Equations

As it is aforementioned, in order to develop a convex optimization model for the proposed model, the LFB model is used to characterize AC power flow equations as follows [29].

$$\forall b \in S_b, \ \ \forall t \in S_t, \ \ \forall l \in S_l :$$

$$\sum_{l\in S_l} A_{lb}\, P_{l,t}^{\mathrm{net}} = P_{b,t}^{\mathrm{G}} + P_{b,t}^{\mathrm{w}} + P_{b,t}^{\mathrm{pv}} - P_{b,t}^{\mathrm{D}} - \sum_{l\in S_l} B_{lb}\, R_l\, J_{l,t} \tag{5.19}$$

$$\sum_{l\in S_l} A_{lb}\, Q_{l,t}^{\mathrm{net}} = Q_{b,t}^{\mathrm{G}} + Q_{b,t}^{\mathrm{w}} - Q_{b,t}^{\mathrm{D}} - \sum_{l\in S_l} B_{lb}\, X_l\, J_{l,t} \tag{5.20}$$

$$-\left(1-\mathrm{Bi}_l^r\right)M \le U_{b',t} - 2\sum_{l\in S_l} B_{lb'}\left(R_l\, P_{l,t}^{\mathrm{net}} + X_l\, Q_{l,t}^{\mathrm{net}}\right) - U_{b,t} + \left(R_l^2 + X_l^2\right) J_{l,t} \le \left(1-\mathrm{Bi}_l^r\right)M \tag{5.21}$$

$$\left(P_{l,t}^{\mathrm{net}}\right)^2 + \left(Q_{l,t}^{\mathrm{net}}\right)^2 = J_{l,t}\, U_{b,t} \quad \forall A_{lb} > 0 \tag{5.22}$$

$$\left(V^{\min}\right)^2 \le U_{b,t} \le \left(V^{\max}\right)^2 \tag{5.23}$$

$$0 \le J_{l,t} \le \mathrm{Bi}_l^r \left(I_l^{\max}\right)^2 \tag{5.24}$$

where, $U_{b,t} = V_{b,t}^2$ and $J_{l,t} = I_{l,t}^2$.

In addition, since only the connection to the upstream network is possible via the substation, the following constraint should be considered:

$$P_{b,t}^{\mathrm{G}} = \begin{cases} P_{t,b}^{\mathrm{Ups}} & b \in S_{\mathrm{s}} \\ 0 & \text{otherwise} \end{cases} \tag{5.25}$$

$$Q_{b,t}^{\mathrm{G}} = \begin{cases} Q_{t,b}^{\mathrm{Ups}} & b \in S_{\mathrm{s}} \\ 0 & \text{otherwise} \end{cases} \tag{5.26}$$

$P_{l,t}^{\mathrm{net}}, Q_{l,t}^{\mathrm{net}}$ in (5.19) and (5.20) are active/reactive power flow of line l at time t, respectively. Also, (5.21) models the voltage drop across the branch which is quadratically related to the active/reactive power, voltage, and line conductance. Equation (5.22) models the nodal relationship between power, voltage, and current. Also, (5.23) and (5.24) show the lower/upper limits of quadratic bus voltage ($U_{b,\ t}$) and line current ($J_{l,\ t}$) at time t. In addition, A_{lb} is ljth element of the bus line incidence matrix, which is equal to 1, if bus b is the sending bus of line l, -1 if bus b is the receiving bus of line l, and 0 otherwise. Also, B_{lb} is the modified A_{lb} with all `+1′ set to 0. In this chapter the big-M concept is used to model the DFR constraints. When the line is open, $\mathrm{Bi}_l^r = 0$, then (5.21) will be relaxed. If $\mathrm{Bi}_l^r = 1$, then the voltage drop constraint must be satisfied.

Besides, $(P, Q)_{b,t}^{\mathrm{G}}$ and $(P, Q)_{b,t}^{\mathrm{w}}$ in (5.19) and (5.20) are the active and reactive power injected to the network by the upstream grid and WTs. It is obvious that $(P, Q)_{b,t}^{\mathrm{G}}$ are only nonzero in the nodes connected to the upstream grid. Besides, $P_{b,t}^{\mathrm{pv}}$ is the power injected by PVs. S_b, S_l are the set of system nodes and branches, respectively.

It is evidently observed that all power flow constraints are linearized or convexified, except (5.22), which still remained as a nonconvex constraint. To convexify it, the conic relaxation technique [34] is utilized by relaxation to the following inequality constraint.

$$\left(P_{l,t}^{\mathrm{net}}\right)^2 + \left(Q_{l,t}^{\mathrm{net}}\right)^2 \leq J_{l,t}\, U_{b,t} \quad \forall A_{lb} > 0 \tag{5.27}$$

According to this relaxation, the proposed DSEM model became a convex MISOCP optimization problem. This convex model could be easily solved by common commercial solvers such as CPLEX, GUROBI, and MOSEK [35], and its global optimal solution is attained.

Finally, using the linearization technique presented by (5.9)–(5.14) the absolute value of active power flowing through a branch could be calculated as follows:

$$\forall t \in S_t;\ \forall l \in S_l$$

$$\left|P_{l,t}^{\text{net}}\right| = \left(P_{l,t}^{\text{net}}\right)^{+} + \left(P_{l,t}^{\text{net}}\right)^{-} \tag{5.28}$$

$$P_{l,t}^{\text{net}} = \left(P_{l,t}^{\text{net}}\right)^{+} + \left(P_{l,t}^{\text{net}}\right)^{-} \tag{5.29}$$

$$0 \le \left(P_{l,t}^{\text{net}}\right)^{+} \le M\ \text{Bi}^{+} \tag{5.30}$$

$$0 \le \left(P_{l,t}^{\text{net}}\right)^{-} \le M\ \text{Bi}^{-} \tag{5.31}$$

$$\text{Bi}_{l,t}^{+} + \text{Bi}_{l,t}^{-} = \text{Bi}_{l}^{r} \tag{5.32}$$

WT and PV Constraints

The WT and PV placement and scheduling constraints could be expressed as follows:

$$0 \le P_{b,t}^{\text{w}} \le \Phi_{t}^{\text{w}} \times \Gamma_{b}^{\text{w}} \times \text{Bi}_{b}^{\text{w}};\quad \forall b \in S_{\text{w}},\ \forall t \in S_{t},\ \forall l \in S_{l} \tag{5.33}$$

$$\beta_{b}^{-} \times P_{b,t}^{\text{w}} \le Q_{b,t}^{\text{w}} \le \beta_{b}^{+} \times P_{b,t}^{\text{w}};\quad \forall b \in S_{w},\ \forall t \in S_{t},\ \forall l \in S_{l} \tag{5.34}$$

$$0 \le P_{b,t}^{\text{pv}} \le \Phi_{t}^{\text{pv}} \times \Gamma_{b}^{\text{pv}} \times Bi_{b}^{\text{pv}};\quad \forall b \in S_{\text{pv}},\ \forall t \in S_{t},\ \forall l \in S_{l} \tag{5.35}$$

$$\sum_{b \in S_{w}} \text{Bi}_{b}^{\text{w}} \le N^{\text{w}} \tag{5.36}$$

$$\sum_{b \in S_{\text{pv}}} \text{Bi}_{b}^{\text{pv}} \le N^{\text{pv}} \tag{5.37}$$

Equations (5.33) and (5.34) are the active and reactive power generation limits of the WT connected to bus i in time t, respectively. Also, (5.35) is the PV active power generation limit. Bi_{b}^{w} and $\text{Bi}_{b}^{\text{pv}}$ in (5.36) and (5.37) are the binary variables that specify the presence (if equal 1) or absence (if equal 0) of WT and PV connected to bus i, respectively. Equations (5.36) and (5.37) model the maximum number of WTs and PVs that could be installed in the network.

DR Constraints

Demand response constraints are expressed as follows ($\forall b \in S_{\text{dr}}$ and $\forall t \in S_{t}$).

$$P_{b,t}^{\text{D}} = P_{b,t}^{\text{D0}} \times \vartheta_{b,t} \tag{5.38}$$

$$Q_{b,t}^{\text{D}} = Q_{b,t}^{\text{D0}} \times \vartheta_{b,t} \tag{5.39}$$

$$\sum_{t\in S_t} P_{b,t}^{\mathrm{D}} = \sum_{t\in S_t} P_{b,t}^{\mathrm{D0}} \tag{5.40}$$

$$\sum_{t\in S_t} Q_{b,t}^{\mathrm{D}} = \sum_{t\in S_t} Q_{b,t}^{\mathrm{D0}} \tag{5.41}$$

$$\left(1 - \vartheta_b^{\min} \mathrm{Bi}_b^{\mathrm{dr}}\right) \le \vartheta_{b,t} \le \left(1 + \vartheta_b^{\max}\, \mathrm{Bi}_b^{\mathrm{dr}}\right) \tag{5.42}$$

$$\sum_{b\in S_{\mathrm{dr}}} \mathrm{Bi}_b^{\mathrm{dr}} \le N^{\mathrm{dr}} \tag{5.43}$$

The set of demands participating in the DR program is represented by S_{dr}. $(P/Q)_{b,t}^{\mathrm{D0}}$ and $(P/Q)_{b,t}^{\mathrm{D}}$ in (5.38) and (5.39) specify the initial/modified demand pattern without/with DR activation. $\vartheta_{b,\,t}$ denotes the decision variable for changing the demand pattern. Besides, (5.40) and (5.41) ensure the energy of load before and after the DR program remains constant (i.e., DR is activated via the load shifting mechanism). Also, (5.42) is the flexibility degree of demands. $\vartheta_b^{\min\,/\,\max}$ specifies the maximum possible increase and decrease of demand in node b. $\mathrm{Bi}_b^{\mathrm{dr}}$ is a binary variable. If $\mathrm{Bi}_b^{\mathrm{dr}} = 0$, then the load at node b does not participate in a DR program, and, contrarily, if $\mathrm{Bi}_b^{\mathrm{dr}} = 1$, it means that the load at bus b participates in the DR program. The total number of nodes which can participate in the DR program are limited by (5.43).

5.2.2.3 Decision Variables

The decision variables (DV), parameters (Y), and sets are as follows:

$$\mathrm{DV} = \left\{ \begin{array}{c} U_{b,t}, J_{l,t}, (P/Q)_{b,t}^{\mathrm{G/D}}, (P/Q)_{b,t}^{\mathrm{w}}, P_{b,t}^{\mathrm{pv}}, \mathrm{CEP}, \mathrm{ENS}_t, \mathrm{TOC} \\ \mathrm{CENS}, \vartheta_{b,t}, \mathrm{Bi}_b^{\mathrm{w}}, \mathrm{Bi}_b^{\mathrm{pv}}, \mathrm{Bi}_b^{\mathrm{dr}}, \mathrm{Bi}_b^{r}, \mathrm{Bi}_{l,t}^{+}, \mathrm{Bi}_{l,t}^{-} \end{array} \right\} \tag{5.44}$$

$$Y = \left\{ \begin{array}{c} V^{\min\,/\,\max}, I^{\max},\ \ R_l,\ \ X_l,\ \ (P/Q)_{b,t}^{\mathrm{D0}},\ \ \Phi_t^{\mathrm{w}},\ \ \Phi_t^{\mathrm{pv}}, \Gamma^{\mathrm{w}},\ \ \Gamma^{\mathrm{pv}} \\ A_{lb},\ \ B_{lb},\ \ \mathrm{FOR}_l, \aleph_t,\ \ N^{\mathrm{dr}}, N^{\mathrm{pv}}, N^{\mathrm{w}} \end{array} \right\} \tag{5.45}$$

$$\mathrm{Sets} = \left\{ S_{\mathrm{dr}}, S_t, S_b, S_l, S_{\mathrm{w}}, S_{\mathrm{pv}} \right\} \tag{5.46}$$

5.3 Simulation Results

5.3.1 Data

The aim of this study is to show how DERs and DFR can participate in the day-ahead DSEM. The proposed optimization model is implemented in GAMS environment

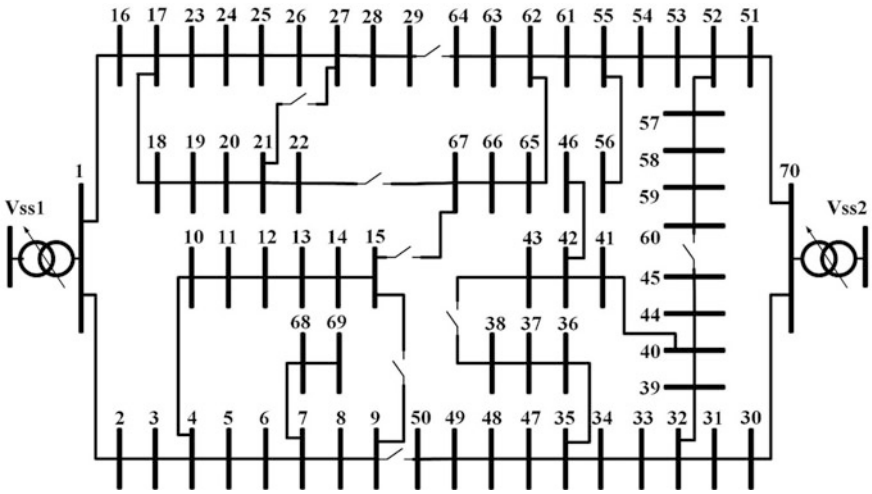

Fig. 5.2 Single-line diagram of the 70-node distribution network [38]

[36] and solved by the GUROBI solver [37], on Intel Xeon CPU 3.2 GHz and 8 GB RAM. The proposed model is applied to a 70-bus distribution network [38] shown in Fig. 5.2. The voltage at the substations is fixed to 1 pu, with a base voltage of 11 kV. The peak demand values used in this study are higher than what is reported in [38] in order to increase the stress on the network. The total peak load of the system is 7 MW. The load demand of this system, along with the WTs' and PVs' forecasted power outputs, is shown in Table 5.1 for a typical 24-hour horizon. The forecasted power outputs of WT and PV are adopted from [27, 33], respectively. It is worth to note that these values for demand and WTs' and PVs' power generations are respected to the corresponding peak values; for example, at hour 18, the total load of the system is $1.000 \times 7\ \text{MW} = 7\,\text{MW}$. All nodes are considered as the candidate locations for WTs, PVs, and DR. The upper and lower voltage limits on the nodes are 1.10 pu and 0.90 pu, respectively. And the current limit on all feeders is 0.06 pu. The hourly price of energy procurement from RESs and DR participants (i.e., $\aleph_t^{\text{w}}$, $\aleph_t^{\text{pv}}$ and $\aleph_t^{\text{dr}}$) are assumed to be 80% of the market prices (i.e., $\aleph_t^{\text{ups}}$), given in Table 5.1.

As it is also shown in Fig. 5.2, there are 69 normally closed lines and 8 normally open lines in the studied system. Also, the rated capacity of each WT and PV is considered 1.00 MW. The coefficients for modeling lower/upper limits of WT reactive power outputs (i.e., $\beta^{+/-}$) are −0.80 and +0.80, respectively. Without loss of generality, it is assumed that the DSO aims to optimally allocate three WT, PV, and DR participants (i.e., $N^{\text{dr}} = N^{\text{w}} = N^{\text{pv}} = 3$) in the network for the given load and energy price. It is assumed that the DR flexibility degree is 0.7 (i.e., $\vartheta_{b,t}^{\max/\min} = 0.7$).

It is also assumed that the line with the highest impedance has a failure rate of 0.4 f/year and the line with the least impedance has a failure rate of 0.1 f/year.

Table 5.1 Forecasted hourly demand (%), output power of WTs and PVs (%), and energy prices ($/MWh)

Time	Demand [16]	Φ_t^w [33]	Φ_t^{pv} [27]	$\aleph_t$ [17]	Time	Demand [16]	Φ_t^w [33]	Φ_t^{pv} [27]	$\aleph_t$ [17]
1	0.719	0.119	0	28	13	0.875	0.261	0.956	42
2	0.674	0.119	0	24	14	0.868	0.158	0.842	43
3	0.624	0.119	0	22	15	0.851	0.119	0.315	46
4	0.588	0.119	0	22.5	16	0.875	0.087	0.169	47.5
5	0.582	0.119	0	23.5	17	0.951	0.119	0.022	48.5
6	0.588	0.061	0	25	18	1	0.119	0	48.5
7	0.6	0.119	0	27.5	19	0.981	0.0868	0	50
8	0.633	0.087	0.008	31.5	20	0.948	0.119	0	44.5
9	0.644	0.119	0.15	37.5	21	0.9	0.0867	0	43
10	0.73	0.206	0.301	44	22	0.875	0.0867	0	41
11	0.793	0.585	0.418	42.5	23	0.801	0.061	0	39
12	0.844	0.694	0.478	40	24	0.722	0.041	0	38

Consequently, the failure rate of other lines can be evaluated according to these two values, proportionally. The repair time of each line is assumed to be 2 h [3]. Also, the VOLL is assumed to be 20 $/kWh [28].

5.3.2 Results

The simulations are carried out in four cases. In Study 1, the base case operation point of the system is given. The initial configuration of the system which is considered in Study 1 is shown in Fig. 5.2. Also in this study, no energy generation/management tools such as WTs, PV, and DR are utilized. In Study 2, the DSEM model is solved with the aim of minimizing the CENS. Minimization of TOC is performed in Study 3, and finally the compromise solution, which is a trade-off between the CENS and TOC, is given in Study 4. In Studies 2–4 the DFR, RESs, and DR are utilized as the energy management tools. The overall obtained results in all studies are summarized in Table 5.2, for the sake of comparison.

5.3.2.1 Study 1: Base Case Condition

In Study 1, the network demand is provided only via the upstream network (i.e., buses 1 and 70 in Fig. 5.2). In this case, the CENS is $ 781.89 and TOC is $ 5428.04, for the configuration shown in Fig. 5.2. The voltage profile of the system during the peak load condition (i.e., hour 18:00) is shown in Fig. 5.3. According to this figure, in Study 1 the minimum and maximum voltage of buses are 0.878 pu (at bus 67) and 1.000 pu (at buses 1 and 70) at the peak load condition.

Table 5.2 Summary of the obtained results in all studies

Study no.	Study 1	Study 2	Study 3	Study 4
DFR (open lines)	(29–64), (21–27), (9–50), (22–67), (15–67), (9–15), (38–43), (45–60)	(8–9), (14–15), (44–45) (61–62), (67–15), (21–27), (29–64), (43–38)	(8–9, (14–15), (42–43) (44–45), (61–62), (67–15), (21–27), (29–64)	(8–9), (14–15), (42–43) (49–50), (61–62), (21–27), (29–64), (59–60)
WT location (bus no.)	–	26, 50, 66	26, 50, 66	26, 35, 66
PV location (bus no.)	–	7, 41, 63	7, 41, 61	7, 20, 41
DR location (bus no.)	–	26, 62, 66	4, 62, 66	26, 62, 66
TOC ($)	5428.04	4788.72	4633.14	4673.79
CENS ($)	781.89	422.83	471.94	443.04
TOC reduction (%)	–	11.77	14.64	13.89
CENS reduction (%)	–	45.92	39.64	43.33

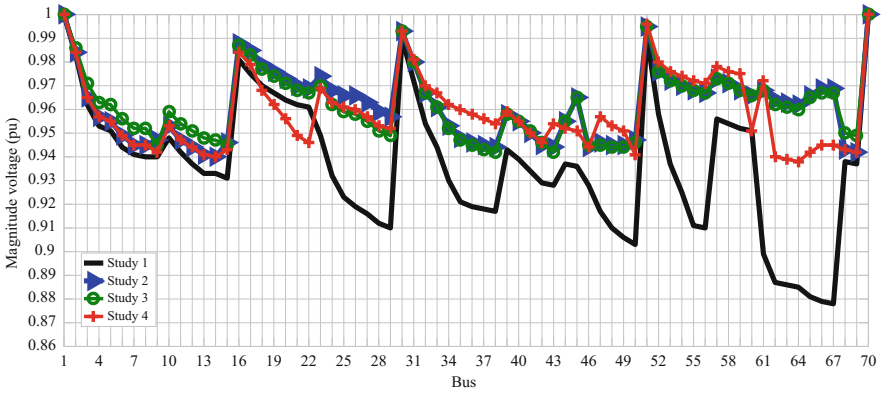

Fig. 5.3 Voltage profile in different studies at the peak load (hour 18:00)

5.3.2.2 Study 2: DSEM to Maximize Reliability

The aim of this study is to show how the proposed DSEM model can improve the reliability of DS via minimization of CENS. The optimal locations of WTs, PVs, and DRs in this study are given in Table 5.2. The optimal CENS in this case is $ 422.83

and TOC is $ 4788.72, which means a 45.92% and 11.77% reduction with respect to Study 1 for CENS and TOC, respectively.

Three WTs are installed at nodes 26, 50, and 66, while the optimal allocation of PVs is the nodes 7, 41, and 63. For this case, the optimal schedule of RESs as well as the energy purchased from WTs and PVs are shown in Table 5.3. According to this table, it can be seen at the interval [1:00, 16:00]. Due to the high available power generation by RESs, less energy is received from the upstream network. On the other hand, in the interval [17:00, 24:00], since the power output of RESs decreased, the power procured from the upstream network is increased. The voltage profile of the system in peak load condition is also shown in Fig. 5.3. As it is observed from this figure, the voltage profile of the system is improved considerably by optimal allocation of WTs, PVs, DRs, and DFR.

As given in Table 5.2, in this study the optimal locations of DR participants are nodes 26, 62, and 66. Figure 5.4a shows the modified demand pattern of these buses at the presence of DR. It can be seen from Fig. 5.4a that the consumers shift their demand from on-peak hours (i.e., [16:00, 24:00]) to the off-peak hours (i.e., [1:00,

Table 5.3 Optimal power dispatch in Study 2

	WTs (MW)			PVs (MW)			Upstream network (MW)	
Time	Bus 26	Bus 50	Bus 66	Bus 7	Bus 41	Bus 63	Bus 1	Bus 70
1	0.815	0.809	0.815	0.000	0.000	0.000	1.077	1.769
2	0.844	0.840	0.880	0.000	0.000	0.000	0.996	1.656
3	0.787	0.795	0.886	0.000	0.000	0.000	0.920	1.531
4	0.745	0.761	0.844	0.000	0.000	0.000	0.865	1.441
5	0.738	0.754	0.836	0.000	0.000	0.000	0.856	1.426
6	0.745	0.761	0.844	0.000	0.000	0.000	0.865	1.441
7	0.759	0.779	0.863	0.000	0.000	0.000	0.883	1.471
8	0.797	0.814	0.901	0.008	0.008	0.008	0.925	1.545
9	0.810	0.824	0.841	0.150	0.150	0.150	0.794	1.426
10	0.909	0.901	0.813	0.301	0.301	0.301	0.769	1.486
11	0.982	0.963	0.791	0.418	0.418	0.415	0.747	1.524
12	0.979	0.971	0.838	0.478	0.478	0.442	0.763	1.591
13	0.945	0.942	0.743	0.766	0.707	0.458	0.585	1.439
14	0.776	0.776	0.670	0.760	0.701	0.455	0.644	1.552
15	0.673	0.673	0.673	0.315	0.315	0.315	1.064	1.989
16	0.591	0.591	0.591	0.169	0.169	0.169	1.354	2.314
17	0.487	0.487	0.487	0.022	0.022	0.022	2.047	2.864
18	0.466	0.466	0.466	0.000	0.000	0.000	2.306	3.095
19	0.373	0.373	0.373	0.000	0.000	0.000	2.444	3.130
20	0.339	0.339	0.339	0.000	0.000	0.000	2.405	3.045
21	0.339	0.339	0.339	0.000	0.000	0.000	2.239	2.864
22	0.372	0.372	0.372	0.000	0.000	0.000	2.082	2.733
23	0.393	0.393	0.393	0.000	0.000	0.000	1.787	2.435
24	0.339	0.339	0.339	0.000	0.000	0.000	1.637	2.204

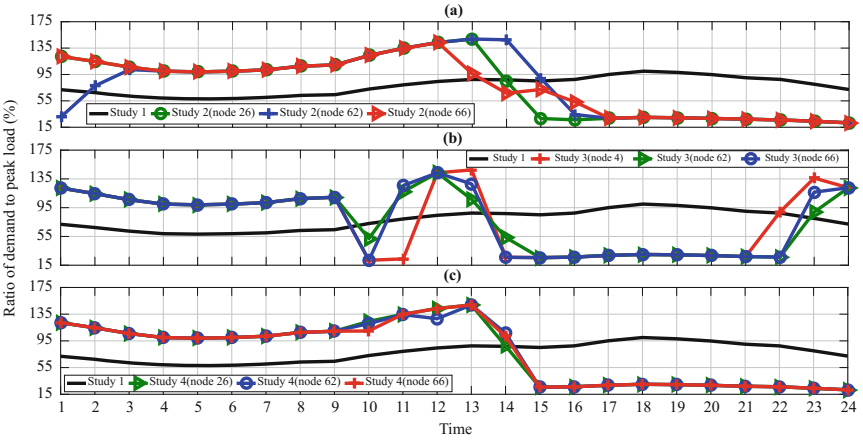

Fig. 5.4 The hourly demand pattern in different studies: (**a**) Study 2, (**b**) Study 3, (**c**) Study 4

14:00]). According to Table 5.1, the forecasted outputs of RESs have the highest level in the period from [1:00, 14:00]. Since the energy production near to consumers decreases the ENS, load shifting via the DR program in these buses is carried out from on-peak period to this interval. Also, since the generation of PVs in the interval [10:00, 16:00] is considerable, the DR program increases the demand of nodes 62 that is near bus 63 (the location of a PV generation). For the remaining hours, the demand is reduced.

5.3.2.3 Study 3: DSEM to Minimize TOC

The objective function of the DSO in this study is minimization of TOC. The minimum value of TOC is $ 4633.14, which means a 14.64% reduction in TOC compared to Study 1. On the other hand, the CENS is $ 471.94. Hence the CENS is decreased by 39.64%, in comparison with Study 1.

For this study, the optimal location of WTs, PVs, and DRs as well as the optimal DFR is shown in Table 5.2. The optimal location of DR in this study is buses 4, 62, and 66, respectively. Figure 5.4b shows the optimal load shifting in these buses. Since the objective function in this study is to minimize the TOC, the new demand pattern of consumers participating in the DR program will be according to hourly price of energy in the day-ahead market. According Fig. 5.4b, the demand is shifted to off-peak period, especially to the intervals [1:00, 3:00] and [21:00, 24:00]. On the other hand, due to the high rate of energy price in the interval [10:00, 11:00] and [14:00, 15:00], demand of consumers is decreased. Also, since the optimal locations of PVs are close to the DR buses and the maximum production of PVs occurs in the interval [12:00, 13:00], the customers' demand at buses 4, 6, and 66 increases via DR activation.

Table 5.4 Optimal power dispatch in Study 3

	WTs (MW)			PVs (MW)			Upstream network (MW)	
Time	Bus 26	Bus 50	Bus 66	Bus 7	Bus 41	Bus 61	Bus 1	Bus 70
1	0.815	0.815	0.815	0.000	0.000	0.000	1.348	1.700
2	0.880	0.880	0.880	0.000	0.000	0.000	1.026	1.476
3	0.886	0.886	0.886	0.000	0.000	0.000	0.806	1.294
4	0.880	0.880	0.880	0.000	0.000	0.000	0.668	1.173
5	0.881	0.881	0.881	0.000	0.000	0.000	0.641	1.151
6	0.881	0.881	0.881	0.000	0.000	0.000	0.666	1.172
7	0.953	0.953	0.953	0.000	0.000	0.000	0.576	1.145
8	0.987	0.987	0.987	0.008	0.008	0.008	0.637	1.212
9	0.985	0.985	0.985	0.150	0.150	0.083	0.570	1.029
10	0.962	0.962	0.962	0.301	0.301	0.301	0.126	0.978
11	1.000	1.000	1.000	0.418	0.418	0.418	0.509	0.927
12	0.979	0.979	0.979	0.478	0.478	0.478	1.046	1.006
13	0.945	0.945	0.945	0.956	0.956	0.956	0.610	0.210
14	0.776	0.776	0.776	0.842	0.842	0.842	0.376	0.572
15	0.673	0.673	0.673	0.315	0.315	0.315	0.990	1.666
16	0.591	0.591	0.591	0.169	0.169	0.169	1.385	2.139
17	0.487	0.487	0.487	0.022	0.022	0.022	2.010	2.841
18	0.466	0.462	0.462	0.000	0.000	0.000	2.244	3.100
19	0.373	0.373	0.373	0.000	0.000	0.000	2.385	3.131
20	0.339	0.339	0.339	0.000	0.000	0.000	2.349	3.045
21	0.339	0.339	0.339	0.000	0.000	0.000	2.186	2.864
22	0.372	0.372	0.372	0.000	0.000	0.000	2.190	2.733
23	0.393	0.393	0.393	0.000	0.000	0.000	2.437	2.435
24	0.339	0.339	0.339	0.000	0.000	0.000	2.387	2.204

As shown in Table 5.2, the optimal locations of WTs are the buses 26, 50, and 66. Also, the optimal locations of PVs are buses 7, 41, and 61. For this study, the optimal energy dispatch of different sources is shown in Table 5.4. Since the price of energy produced by RESs is lower than that of the upstream network, it is observed from Table 5.4 that whole available power generated by RESs is purchased by DSO. The voltage profile of the system for the peak loading hour is also depicted in Fig. 5.3.

5.3.2.4 Study 4: DSEM to Make a Compromise Between TOC and CENS

In this study, the TOC and CENS are minimized in a multiobjective optimization model. The proposed multiobjective model is solved via weighted sum approach [39]. According to Fig. 5.5, the TOC and CENS are conflicting objectives, and the

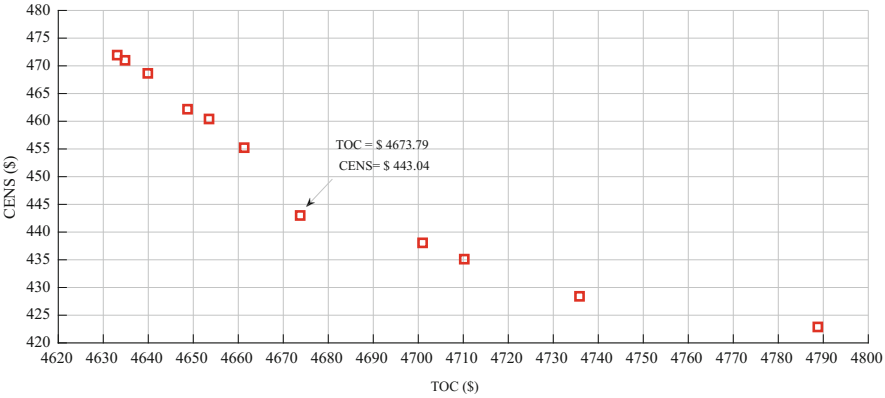

Fig. 5.5 Pareto optimal front of TOC versus CENS in Study 3

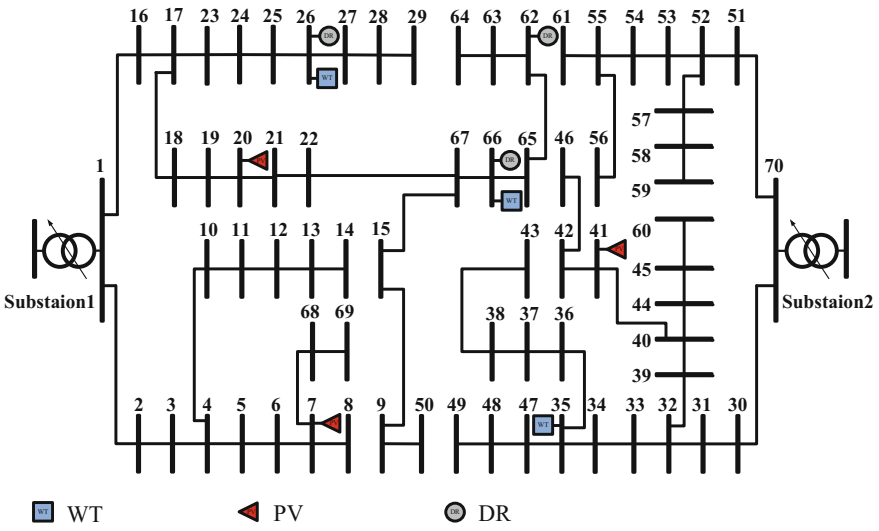

Fig. 5.6 Optimal configuration of the system along with optimal allocation of WTs, PVs, and DRs in Study 4

corresponding Pareto optimal solutions are obtained by the weighted sum approach. In such nondominated Pareto optimal solutions, the decision maker (here the DSO) aims to find a compromise solution which is a trade-off between the TOC and CENS. In this paper, the compromise solution is obtained by fuzzy satisfying criterion [17]. This solution is also shown on Fig. 5.5. Figure 5.6 shows the results obtained for this solution. Also, the optimal DFR and locations of WTs, PVs, and DRs are given in Table 5.2.

Table 5.5 Optimal power dispatch for the compromise solution in Study 4

	WTs (MW)			PVs (MW)			Upstream network (MW)	
Time	Bus 26	Bus 35	Bus 66	Bus 7	Bus 20	Bus 41	Bus 1	Bus 70
1	0.815	0.815	0.815	0.000	0.000	0.000	1.531	1.468
2	0.836	0.880	0.880	0.000	0.000	0.000	1.236	1.257
3	0.718	0.886	0.886	0.000	0.000	0.000	1.123	1.091
4	0.676	0.880	0.880	0.000	0.000	0.000	1.010	0.982
5	0.669	0.881	0.881	0.000	0.000	0.000	0.989	0.962
6	0.774	0.881	0.881	0.000	0.000	0.000	0.912	0.981
7	0.847	0.953	0.953	0.000	0.000	0.000	0.820	0.948
8	0.905	0.987	0.987	0.008	0.008	0.008	0.858	1.011
9	0.857	0.985	0.985	0.150	0.150	0.150	0.665	0.903
10	0.956	0.962	0.962	0.301	0.301	0.301	0.621	1.047
11	1.000	1.000	1.000	0.418	0.418	0.418	0.623	1.092
12	0.979	0.979	0.979	0.478	0.478	0.478	0.736	1.215
13	0.945	0.909	0.945	0.956	0.889	0.956	0.100	0.908
14	0.776	0.776	0.776	0.842	0.842	0.842	0.263	1.130
15	0.673	0.673	0.673	0.315	0.315	0.315	0.991	1.714
16	0.591	0.591	0.591	0.169	0.169	0.169	1.547	2.031
17	0.487	0.487	0.487	0.022	0.022	0.022	2.363	2.553
18	0.466	0.466	0.466	0.000	0.000	0.000	2.644	2.766
19	0.373	0.373	0.373	0.000	0.000	0.000	2.782	2.804
20	0.339	0.339	0.339	0.000	0.000	0.000	2.732	2.730
21	0.339	0.339	0.339	0.000	0.000	0.000	2.547	2.567
22	0.372	0.372	0.372	0.000	0.000	0.000	2.377	2.446
23	0.393	0.393	0.393	0.000	0.000	0.000	2.051	2.176
24	0.339	0.339	0.339	0.000	0.000	0.000	1.873	1.971

It can be seen from Fig. 5.5 that at the best compromise solution, the TOC and CENS are $ 4673.79 and $ 443.04, respectively. With regard to Table 5.2, this strategy can reduce the TOC and CENS up to 13.89% and 43.33%, respectively, in comparison with Study 1. In this study the optimal locations of DR are buses 26, 62, and 66. The new demand patterns of these buses are depicted in Fig. 5.4c. These new patterns of demand depend on the locations of WTs, as well as the hourly electricity price. It can be seen from Fig. 5.4c that since the energy price at the interval [1:00, 9:00] is relatively low, the demand is shifted to these hours. In addition, due to the high energy price at the interval [14:00, 20:00], the load demand reduced in these hours. Also, the demand of nodes 26 and 66 are more sensitive to the power generation of WTs, such that in the interval [1:00, 13:00] by increase of generation of WTs installed in these nodes, the demand of these buses increased at this time. The optimal power dispatch for the compromise solution in this study is presented in Table 5.5.

5.4 Conclusions

In this chapter an approach has been proposed for DSEM. Optimal DFR and allocation of the WTs, PVs, and DR are the main tools that DSO can utilize for DSEM. The purpose of the proposed DSEM model is to enhance the reliability as well as to minimize the energy procurement cost. In this regard, two objective functions, namely, CENS and TOC, are introduced and the proposed DSEM model is formulated as a multiobjective optimization model. The proposed optimization model is formulated as a MISOCP model, which is convex and returns a global optimal solution. In order to efficiently solve the proposed multiobjective optimization model with the objectives of TOC and CENS, the weighted sum approach is utilized to handle these conflicting objectives and to obtain Pareto optimal solutions. Also, fuzzy satisfying criterion is utilized to select the best compromise solution. The proposed methodology has been tested on a 70-bus DS with radial configuration. The simulation results substantiate the effectiveness of the proposed approach for the optimal energy management of DSs. As a future work, uncertainty modeling of input parameters (such as the WTs and PVs forecasted power outputs as well as hourly energy price) can be considered.

References

1. Y. Liu, Y. Su, Y. Xiang, J. Liu, L. Wang, W. Xu, Operational reliability assessment for gas-electric integrated distribution feeders. IEEE Trans. Smart Grid **10**, 1091–1100 (2019)
2. R.N. Allan, *Reliability Evaluation of Power Systems* (Springer Science & Business Media, New York, 2013)
3. N.G. Paterakis, A. Mazza, S.F. Santos, O. Erdinç, G. Chicco, A.G. Bakirtzis, et al., Multi-objective reconfiguration of radial distribution systems using reliability indices. IEEE Trans. Power Syst. **31**, 1048–1062 (2016)
4. A. Kavousi-Fard, T. Niknam, Optimal distribution feeder reconfiguration for reliability improvement considering uncertainty. IEEE Trans. Power Deliv. **29**, 1344–1353 (2014)
5. M.E. Baran, F.F. Wu, Network reconfiguration in distribution systems for loss reduction and load balancing. IEEE Trans. Power Deliv. **4**, 1401–1407 (1989)
6. S.K. Goswami, S.K. Basu, A new algorithm for the reconfiguration of distribution feeders for loss minimization. IEEE Trans. Power Deliv. **7**, 1484–1491 (1992)
7. Y.-J. Jeon, J.-C. Kim, J.-O. Kim, J.-R. Shin, K.Y. Lee, An efficient simulated annealing algorithm for network reconfiguration in large-scale distribution systems. IEEE Trans. Power Deliv. **17**, 1070–1078 (2002)
8. R. Pegado, Z. Ñaupari, Y. Molina, C. Castillo, Radial distribution network reconfiguration for power losses reduction based on improved selective BPSO. Electr. Power Syst. Res. **169**, 206–213 (2019)
9. P. Prasad, S. Sivanagaraju, N. Sreenivasulu, Network reconfiguration for load balancing in radial distribution systems using genetic algorithm. Electr. Power Compon. Syst. **36**, 63–72 (2007)
10. B. Amanulla, S. Chakrabarti, S. Singh, Reconfiguration of power distribution systems considering reliability and power loss. IEEE Trans. Power Deliv. **27**, 918–926 (2012)

11. J. Liu, Y. Yu, C. Qin, Unified two-stage reconfiguration method for resilience enhancement of distribution systems. IET Gener. Transm. Distrib. **13**, 1734 (2019)
12. B. Khorshid-Ghazani, H. Seyedi, B. Mohammadi-ivatloo, K. Zare, S. Shargh, Reconfiguration of distribution networks considering coordination of the protective devices. IET Gener. Transm. Distrib. **11**, 82–92 (2017)
13. M. Sedighizadeh, G. Shaghaghi-shahr, M. Esmaili, M.R. Aghamohammadi, Optimal distribution feeder reconfiguration and generation scheduling for microgrid day-ahead operation in the presence of electric vehicles considering uncertainties. J. Energy Storage **21**, 58–71 (2019)
14. L. Bai, T. Jiang, F. Li, H. Chen, X. Li, Distributed energy storage planning in soft open point based active distribution networks incorporating network reconfiguration and DG reactive power capability. Appl. Energy **210**, 1082–1091 (2018)
15. E. Hooshmand, A. Rabiee, Energy management in distribution systems, considering the impact of reconfiguration, RESs, ESSs and DR: A trade-off between cost and reliability. Renew. Energy **139**, 346 (2019)
16. A. Soroudi, P. Siano, A. Keane, Optimal DR and ESS scheduling for distribution losses payments minimization under electricity price uncertainty. IEEE Trans. Smart Grid **7**, 261–272 (2016)
17. E. Hooshmand, A. Rabiee, Robust model for optimal allocation of renewable energy sources, energy storage systems and demand response in distribution systems via information gap decision theory. IET Gener. Transm. Distrib. **13**(4), 511–520 (2018)
18. A. Rabiee, S. Nikkhah, A. Soroudi, E. Hooshmand, Information gap decision theory for voltage stability constrained OPF considering the uncertainty of multiple wind farms. IET Renew. Power Gener. **11**, 585–592 (2016)
19. R. Al Abri, E.F. El-Saadany, Y.M. Atwa, Optimal placement and sizing method to improve the voltage stability margin in a distribution system using distributed generation. IEEE Trans. Power Syst. **28**, 326–334 (2013)
20. C.W. Gellings, Evolving practice of demand-side management. J. Mod. Power Syst. Clean Energy **5**, 1–9 (2017)
21. R. Deng, Z. Yang, M.-Y. Chow, J. Chen, A survey on demand response in smart grids: mathematical models and approaches. IEEE Trans. Ind. Inf. **11**, 570–582 (2015)
22. J. Teh, C. Ooi, Y.-H. Cheng, M. Atiqi Mohd Zainuri, C.-M. Lai, Composite reliability evaluation of load demand side management and dynamic thermal rating Systems. Energies **11**, 466 (2018)
23. N. Venkatesan, J. Solanki, S.K. Solanki, Residential demand response model and impact on voltage profile and losses of an electric distribution network. Appl. Energy **96**, 84–91 (2012)
24. D. Neves, A. Pina, C.A. Silva, Assessment of the potential use of demand response in DHW systems on isolated microgrids. Renew. Energy **115**, 989–998 (2018)
25. J.S. Vardakas, N. Zorba, C.V. Verikoukis, A survey on demand response programs in smart grids: pricing methods and optimization algorithms. IEEE Commun. Surveys Tuts. **17**, 152–178 (2015)
26. M. Rider, A. Garcia, R. Romero, Power system transmission network expansion planning using AC model. IET Gener. Transm. Distrib. **1**, 731–742 (2007)
27. A.A. Moghaddam, A. Seifi, T. Niknam, M.R.A. Pahlavani, Multi-objective operation management of a renewable MG (micro-grid) with back-up micro-turbine/fuel cell/battery hybrid power source. Energy **36**, 6490–6507 (2011)
28. A. Ameli, S. Bahrami, F. Khazaeli, M.-R. Haghifam, A multiobjective particle swarm optimization for sizing and placement of DGs from DG owner's and distribution company's viewpoints. IEEE Trans. Power Del. **29**, 1831–1840 (2014)
29. P. Yan, A. Sekar, Analysis of radial distribution systems with embedded series FACTS devices using a fast line flow-based algorithm. IEEE Trans. Power Syst. **20**, 1775–1782 (2005)
30. Y. Xie, X. Chen, Q. Wu, Q. Zhou, Second-order conic programming model for load restoration considering uncertainty of load increment based on information gap decision theory. Int. J. Electr. Power Energy Syst. **105**, 151–158 (2019)

31. S. Huang, Q. Wu, J. Wang, H. Zhao, A sufficient condition on convex relaxation of AC optimal power flow in distribution networks. IEEE Trans. Power Syst. **32**, 1359–1368 (2017)
32. Q. Li, R. Ayyanar, V. Vittal, Convex optimization for DES planning and operation in radial distribution systems with high penetration of photovoltaic resources. IEEE Trans. Sustain. Energy **7**, 985–995 (2016)
33. A. Soroudi, A. Rabiee, A. Keane, Information gap decision theory approach to deal with wind power uncertainty in unit commitment. Electr. Power Syst. Res. **145**, 137–148 (2017)
34. S. Drewes, S. Ulbrich, *Mixed Integer Second Order Cone Programming* (Verlag Dr. Hut, Germany, 2009)
35. I. Frontline Systems, Linear Programming and Quadratic Programming. http://www.solver.com, Online; Accessed 14 May 2018
36. A. Brooke, D. Kendrick, A. Meeraus, R. Raman, *GAMS, A User's Guide* (GAMS Dev Corp., Washington, DC, 1998)
37. Gurobi Optimization, Inc., Gurobi optimizer reference manual, 2015. http://www.gurobi.com (2014)
38. M. Nick, R. Cherkaoui, M. Paolone, Optimal planning of distributed energy storage systems in active distribution networks embedding grid reconfiguration. IEEE Trans. Power Syst. **33**, 1577–1590 (2018)
39. A. Rabiee, M. Parniani, Voltage security constrained multi-period optimal reactive power flow using benders and optimality condition decompositions. IEEE Trans. Power Syst. **28**, 696–708 (2013)

Chapter 6
Risk-Constrained Intelligent Reconfiguration of Multi-Microgrid-Based Distribution Systems under Demand Response Exchange

Ata Ajoulabadi, Farhad Samadi Gazijahani, and Sajad Najafi Ravadanegh

Nomenclature

Abbreviations

CHP	Combined heat and power
DG	Distributed generation
DNO	Distribution network operator
DR	Demand response
FC	Fuel cell
NMG	Networked microgrid
MG	Microgrid
MT	Microturbine
PV	Photovoltaic
WT	Wind turbine

Sets and Indices

b_r	Index for branches
CHPi	Index for CHP
FCi	Index for FC
k	Index for components
MTi	Index for MT
MGi	Index for MG
n	Index for buses
N_{bus}	Set of buses
N_{br}	Set of branches

A. Ajoulabadi · F. S. Gazijahani (✉) · S. Najafi Ravadanegh
Department of Electrical Engineering, Azarbaijan Shahid Madani University, Tabriz, Iran
e-mail: f.samadi@azaruniv.ac.ir

S. Nojavan, K. Zare (eds.), *Demand Response Application in Smart Grids*,
https://doi.org/10.1007/978-3-030-32104-8_6

N_{CHP}	Set of CHP
N_{FC}	Set of FC
N_{mg}	Set of MGs
N_{MT}	Set of MT
N_{PV}	Set of PV
N_{WT}	Set of WT
PVi	Index for PV
t	Time period index
WTi	Index for WT

Parameters

α, β, φ	Coefficients of Weibull PDF
α_r	Confidence level
β_r	Risk aversion parameter
η_r	Auxiliary coefficient
μ	Mean value of normal PDF
π_{sc}	Probability of scenarios
π_{sc}^{lo}	Probability of load demand at scenario *sc*
π_{sc}^{pv}	Probability of PV generation at scenario *sc*
π_{sc}^{wt}	Probability of WT generation at scenario *sc*
ρ_0	Initial electricity price
$\rho(i)^{max}$	Electricity maximum price
$\rho(i)^{min}$	Electricity minimum price
θ_{max}	Maximum voltage angle
θ_{min}	Minimum voltage angle
σ	Standard deviation of normal PDF
a, b	Linear load model coefficients
$a_{CHP}, b_{CHP}, c_{CHP}$	Operation cost coefficient of CHP
a_{MT}, b_{MT}, c_{MT}	Operation cost coefficient of MT
B_0	Customer's income when demand is P_{d0}
B_{br}	Susceptance of branch b_r
B^{sh}	Total line susceptance
c_{FC}	Operation cost of FC
c_{PV}	Operation cost of PV
c_{Wind}	Operation cost of WT
$E(i,i)$	Self-elasticity of demand
$E(i,j)$	Cross-elasticity of demand
G_{ING}	Incident irradiance
G_{nm}	Conductance of branch b_r
G_{STC}	Irradiance at standard test condition
k	Maximum power correction for air temperature
P_d	Power demand
P_{d0}	Initial demand

P_{CHPmax}	Maximum power generation of CHP
P_{CHPmin}	Minimum power generation of CHP
P_{FCmax}	Maximum power generation of FC
P_{FCmin}	Minimum power generation of FC
P_{MTmax}	Maximum power generation of MT
P_{MTmin}	Minimum power generation of MT
P_{PVmax}	Maximum power generation of PV
P_{PVmin}	Minimum power generation of PV
P_{rate}	Rated power of WT units
P_{STC}	Rated power of PV unit
P_{WTmax}	Maximum power generation of WT
P_{WTmin}	Minimum power generation of WT
$\Delta P_{\mathrm{d}}(i)^{\max}$	Maximum load (demand) variation
$\Delta P_{\mathrm{d}}(i)^{\min}$	Minimum load (demand) variation
Q_{CHPmin}	Minimum power generation of CHP
Q_{MTmax}	Maximum power generation of MT
Q_{MTmin}	Minimum power generation of MT
R	Branch resistance
$S_{\max}$	Power flow limits
T_{c}	PV cell temperature
T_{r}	Reference temperature
v	Wind speed
$V_{\text{cut-in}}$	Cut-in speed of WT units
$V_{\text{cut-out}}$	Cut-out speed of WT units
V_r	Rated wind speed
$\lvert V\rvert_{\max}$	Maximum voltage magnitude
$\lvert V\rvert_{\min}$	Minimum voltage magnitude
X	Branch reactance

Variables

ρ	Electricity price
θ_n	Voltage angle of bus n
θ_{nm}	Admittance angle of branch b_r
B	Customer's income
P_{br}	Active power flow in branch b_r
P_{CHP}	Power generation of CHP
P_{FC}	Power generation of FC
P_{MT}	Power generations of MT
P_n	Active load of bus n
P_{PV}	Power generation of PV
P_{WT}	Power generation of WT
Q_{br}	Reactive power flow in branch b_r
Q_{CHP}	Reactive power generation of CHP

Q_{MT}	Reactive power generation of MT
Q_n	Reactive load of bus n
S	Customer's benefit
St_t	Switch state at hour t
$\|V_n\|$	Voltage magnitude of bus n

Functions

$Cost_{CHP}$	CHP operation cost function
$Cost_{MT}$	MT operation cost function
$Cost_{FC}$	FC operation cost function
$Cost_{Wind}$	WT operation cost function
$Cost_{PV}$	PV operation cost function
$CVaR_{\alpha}$	Conditional VaR in the confidence level α
Opcost	Total operation cost function
$opcost_{expected}$	Expected operation cost
$opcost_{risk}$	Operation cost considering risk index
$opcost_{sc}$	Operation cost in maximum at scenario sc
$opcost_{worstsc}$	Operation cost at worst scenario
VaR_{α}	Value at risk in the confidence level α

6.1 Introduction

Owing to the increasing need for energy as well as concerns about climate changes, the interest in using renewable resources is substantially increased [1]. Regardless of their benefits, these clean resources add a lot of uncertainties to the power system and make the system operation more complex [2]. Several solutions have already been proposed to cope with their uncertainties aimed at increasing system reliability and improving energy management. One of the important solutions to solve these issues is to decentralize the control of distribution systems into a set of small-scale zones so called microgrid (MG) [3]. For a distribution network, the MG concept is introduced to synthesize the small-scale resources into the power sector [4]. The U.S. Department of Energy Microgrid Exchange Group has defined MG as follows: "a group of interconnected loads and distributed energy resources within clearly defined electrical boundaries that acts as a single controllable entity with respect to the grid. A MG can connect/disconnect to/from the grid for enabling it to operate in both grid-connected or island mode" [5]. A lot of researches have been done in various fields of MGs such as controlling, protecting, planning, operating, scheduling, and energy management [2–5].

In the MG planning optimization problem, various goals like optimization of distributed energy resources and optimization of size and type of MGs can be considered [6]. Resilient network design against natural disasters, based on MG

operation scheduling [7], could be considered as another motivation for designing a MG-based distribution network. Due to the possibility of connected and islanded operating modes in the MGs, their controlling and protecting is one of the interesting and important fields. A new strategy for voltage control at smart MG is proposed in [8] to stabilize voltage fluctuations. In [9], a novel design algorithm is designed for frequency and voltage control in diverse operating modes of MGs. A protecting strategy is also resented in reference [10], which enables the MGs' islanding feature during fault onset. By increasing the use of renewable resources in distribution networks, severe fluctuations of renewable generations impose considerable challenges into distribution network operation and planning. Distributed renewable energy resources and different load behaviors make the network operation and management more complicated. One of the most important features of MGs is their exchangeable operation modes, which can help the operator to operate the network in normal and emergency situations. By merging MGs into the distribution networks, the operators will have various options to optimize operation actions [10].

Nowadays, one of the main operational and management strategies in the smart distribution network is to change the configuration and the connections of MGs in an economically efficient manner. A lot of researches have been devoted to the conventional and active distribution network reconfiguration topic. The network reconfiguration problem may have many goals like minimizing the network losses, optimizing network operational cost, maximizing system reliability, and improving voltage profile. Minimizing network losses is one of the significant aims in distribution network reconfiguration problem [11]. A networked MG-based structure has been suggested in [12] to implement the reconfiguration problem for reducing power losses and enhancing reliability. Various reconfiguration methods with different objectives are also presented in [13]. Active distribution network scheduling using various 24-h load profiles, such as industrial, commercial, and residential, is proposed in [14]. It should be emphasized that because of switching transients, the number of switching is an important parameter in the reconfiguration problem. Reducing this parameter can be considered as an objective for operators. To this end, minimizing power losses and number of switching was presented in [15]. Because of the capabilities and advantages of MGs, more MGs will be created at the conventional distribution networks and the structure of distribution networks will change as a cluster of MGs, resulting in multiple MGs (MMGs). The transition state of smart grids was MMG systems [16]. For example, three linked MGs with various distribution generation units as a MMG system can be illustrated in Fig. 6.1.

In MG-based distribution systems, the connection between MGs and the main network as well as between neighbor MGs is the first thing that comes to mind. Reconfiguration in MMG is a strategy used by the system operator that can optimize the system performance by changing the MG arrangements. For minimizing losses in a MMG network, an islanded MG reconfiguration is proposed [17]. Moreover, topology control of MMG is shown in [18] and MMG reconfiguration for reducing power losses considering various constrains is investigated in [19]. Optimal and smart energy management system is outlined in [20] for a standalone MG. From a MG energy management point of view, reconfiguration and probabilistic unit

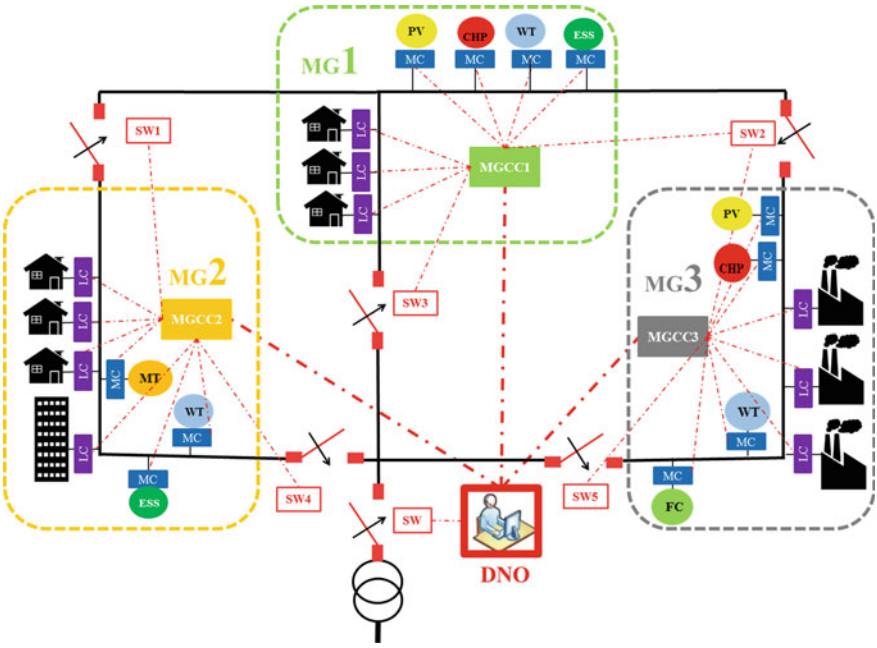

Fig. 6.1 MMG network configuration

commitment are traditionally used as a stochastic model [21]. Coordinated operation for autonomous networked MG is examined in [22] to create a fair trade-off among different stockholders. A centralized control model is executed in reference [23] to manage linked MGs and new control characteristics are developed in [24]. Besides, references [25–27] have addressed deterministic and probabilistic power flow dispatching in MMG networks.

Development of information and communications technologies and widespread use of advanced control and metering devices have caused the system operators to establish a two-way communication with subscribers to maximize energy efficiency [28]. Demand-side management (DSM) system is one the most important strategies in energy management of MGs that provides a flexible option to control consumption of MGs. The DSM is defined by the Electric Power Research Institute (EPRI) as "DSM is the planning, implementation and monitoring of those utility activities designed to influence customer use of electricity in ways that will produce desired changes in the utility's load shape, i.e. time pattern and magnitude of a utility's load. Utility programs falling under the umbrella of DSM include load management, new uses, strategic conservation, electrification, customer generation and adjustments in market share." As shown in Fig. 6.2, DSM has four sections: load management, self-production, energy savings, and energy efficiency [28]. Among these actions, the load management and demand response (DR) programs are noticeable. Under this condition, the Federal Energy Regulatory Commission (FERC) has defined DR [29] as "Changes in electric usage by demand-side resources from their normal consumption patterns in response to changes in the price of electricity over time, or to

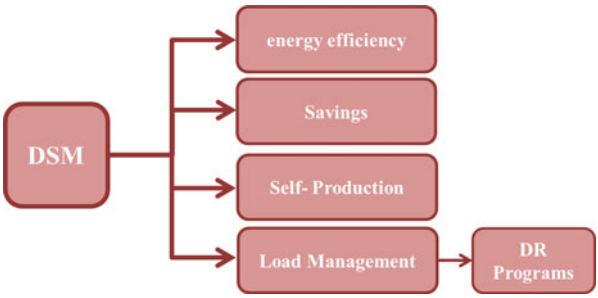

Fig. 6.2 DSM sections from operation standpoint

incentive payments designed to induce lower electricity use at times of high wholesale market prices or when system reliability is jeopardized." With the help of DR programs, different load shapes can change and energy management can be done easily. For example, price-based DR programs can be utilized for residential loads [30]. Historically, the MG owners have used DR programs to increase their profits [31]. A new energy management strategy, for instance, is presented in [32] for price-sensitive loads by implementing DR programs.

Generally, the major contribution of this chapter is to focus on time-based DR programs such as real-time pricing (RTP) and time-of-use (TOU) programs in such a way as to influence the topology control of renewable-based MMG systems. The main contributions of this chapter can be summarized as follows:

1. Executing a dynamic reconfiguration model for MMG-based distribution networks through determining the best switch states between MGs and main grid for a 24-h period.
2. Both RTP and TOU programs have been taken into account for distinct consumers to investigate how they can affect the switching number and MMG network reconfiguration problem.
3. An effective risk-constrained scenario-based framework has been extended to curb the intermittencies of variable generations.

This chapter is organized as follows: Sect. 6.2 describes DR program classification and description and the mathematical model of responsive loads. MMG reconfiguration is formulated in Sect. 6.3. In Sect. 6.4, a MMG reconfiguration optimization problem aimed at minimizing power loss and operation cost is represented. Uncertainty management and risk analysis are demonstrated in Sect. 6.4. Section 6.5 shows simulation results and finally Sect. 6.6 contains discussion and conclusions of the proposed problem.

6.2 Taxonomy of DR Programs

DR programs are divided into two main categories, namely, incentive-based and time-based programs. This classification is graphically shown in Fig. 6.3 which is explained in the following:

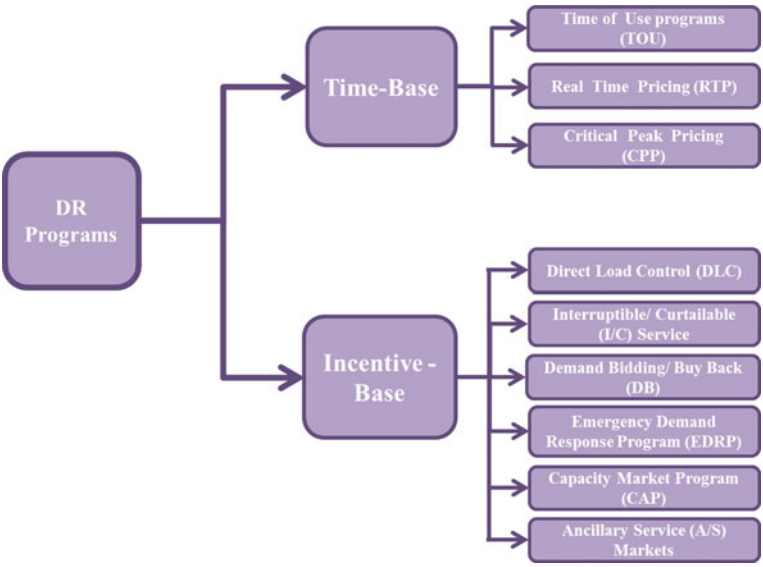

Fig. 6.3 DR program classification

6.2.1 Incentive-Based Programs

Incentive-based programs are divided into six main groups [33].

6.2.1.1 Direct Load Control (DLC)

In this type of DR program, the system operator can remotely control and change the consumption of clients [34].

6.2.1.2 Interruptible Curtailable (I/C) Service

In this program the customer is guaranteed to reduce its consumption during power system contingencies; otherwise, the customer will be penalized [34].

6.2.1.3 Emergency Demand Response (EDRP)

In this type of DR program, the system operator provides payments to consumers for decreasing their usage during power system emergency conditions or when the electricity price at the power market is relatively high [34].

6.2.1.4 Demand Bidding (DB)

In this program, consumers like generation companies can participate in power markets to earn economic benefit [34].

6.2.1.5 Capacity Market (CAP)

In this program, the customer is guaranteed to reduce their predetermined loads; otherwise, they will be penalized [34].

6.2.1.6 Ancillary Service (A/S) Market

In this type of DR program, consumers notify the reduction of their consumption to the operator. Then, they can participate as a reserve option in the ancillary service market [34].

6.2.2 Time-Based Programs

Time-based programs are divided into three sections: TOU, RTP, and critical peak pricing (CPP) [33].

6.2.2.1 TOU Program

In this type, energy prices change according to load consumption. Energy consumption is assumed in about three parts: high energy price in the peak load periods, average energy price in the off-peak time periods, and low energy price in the valley time periods [34]. Energy price changing in the TOU program is shown in Fig. 6.4.

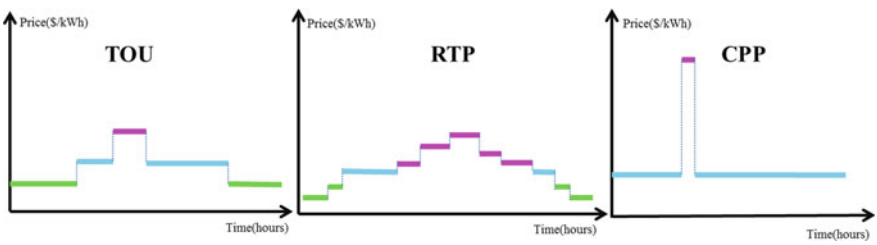

Fig. 6.4 Time-based DR program pricing schemes

6.2.2.2 RTP Program

As shown in Fig. 6.4, this type is similar to TOU programs, but the main difference is that in the RTP programs, price variety is numerous. This program is suitable for those loads that can easily and rapidly change their consumption [34].

6.2.2.3 CPP Program

This type is generally used in critical situations. These types of programs are applicable at times of system's excessive load peak [34]. Energy price changing in these types of programs is shown in Fig. 6.4.

6.3 Mathematical Modeling

The responsive load is necessary for implementing DR programs. Loads that are sensitive to changes in energy prices are called price-responsive demand. Responsive loads are divided into two groups: single-period loads and multiperiod loads [34]. For a responsive demand, the elasticity concept is necessary to define.

6.3.1 Elasticity

Elasticity is defined as a load sensitivity considering the energy price. The elasticity mathematical model is given in Eq. (6.1) [34].

$$E = \frac{\rho_0}{P_{\mathrm{d0}}} \frac{\partial P_{\mathrm{d}}}{\partial \rho} \tag{6.1}$$

Elasticity can be divided in two main sections: self-elasticity ($E(i,i)$) and cross-elasticity ($E(i,j)$). Changing the amount of load at a specified time interval (ith) because of the electricity price changing at same time interval (ith) is defined as self-elasticity; this parameter is positive. Changing the amount of load at a specified time interval (ith) because of the electricity price changing in another time interval (jth) is defined as cross-elasticity, and this parameter is negative. Self-elasticity and cross-elasticity are given in Eqs. (6.2) and (6.3), respectively [31].

$$E(i,i) = \frac{\rho_0(i)}{P_{\mathrm{d0}}(i)} \frac{\partial P_{\mathrm{d}}(i)}{\partial \rho(i)} \tag{6.2}$$

$$E(i,j) = \frac{\rho_0(j)}{P_{\mathrm{d0}}(i)} \frac{\partial P_{\mathrm{d}}(i)}{\partial \rho(j)} \quad i \neq j \tag{6.3}$$

Suppose that the load mathematical model is a linear function (6.4); therefore, the elasticity for a linear load is shown in Eq. (6.5) [34].

$$P_{\mathrm{d}} = a + b \cdot \rho \tag{6.4}$$

$$E = b \cdot \frac{\rho_0}{P_{\mathrm{d0}}} \tag{6.5}$$

According to the elasticity definition, Eq. (6.6) can be written. For network scheduling in a day (24 h), self- and cross-elasticity can be constructed as a 24 × 24 matrix (6.7). In the elasticity matrix, the diagonal elements denote self-elasticity and the other elements are cross-elasticity [34].

$$\Delta P_{\mathrm{d}} = E \cdot \Delta \rho \tag{6.6}$$

$$\begin{bmatrix} \Delta P_{\mathrm{d}}(i) \\ \vdots \\ \Delta P_{\mathrm{d}}(j) \end{bmatrix} = \begin{bmatrix} E(1,1) & \cdots & E(1,24) \\ \vdots & E(i,j) & \vdots \\ E(24,1) & \cdots & E(24,24) \end{bmatrix} \times \begin{bmatrix} \Delta \rho(i) \\ \vdots \\ \Delta \rho(j) \end{bmatrix} \tag{6.7}$$

6.3.2 *Single-Period Load Model*

For a specified time interval (*i*th), Eqs. (6.8) and (6.9) refer to consumer demand changing and consumer benefit, respectively.

$$\Delta P_{\mathrm{d}}(i) = P_{\mathrm{d}}(i) - P_{\mathrm{d0}}(i) \tag{6.8}$$

$$S(P_{\mathrm{d}}(i)) = B(P_{\mathrm{d}}(i)) - P_{\mathrm{d}}(i) \cdot \rho(i) \tag{6.9}$$

Single-period loads are not shiftable in time intervals. To achieve the single-period load model, the customer's profit must be maximized, where equation $\frac{\partial S(P_{\mathrm{d}}(i))}{\partial P_{\mathrm{d}}(i)} = 0$ must be calculated, resulting in (6.10).

$$P_{\mathrm{d}}(i) = P_{\mathrm{d0}}(i)\left\{1 + \frac{E(i,i)[\rho(i) - \rho_0(i)]}{\rho_0(i)}\right\} \tag{6.10}$$

6.3.3 Multiperiod Load Model

The multiperiod load is shiftable in time intervals. Similar to single-period loads, the multiperiod load model can be calculated. So, the multiperiod model can be displayed by Eq. (6.11).

$$P_{\mathrm{d}}(i) = P_{\mathrm{d0}}(i) + \sum_{\substack{j=1 \\ j \neq i}}^{24} E(i,j) \frac{P_{\mathrm{d0}}(i)}{\rho_0(j)} [\rho(j) - \rho_0(j)] \tag{6.11}$$

According to Eqs. (6.10) and (6.11), single-period and multiperiod load models are related to self-elasticity and cross-elasticity, respectively.

6.3.4 Final Responsive Load Model

The final model of responsive loads can be calculated by combining Eqs. (6.10) and (6.11). As a result, Eq. (6.12) denotes the final model of responsive loads.

$$P_{\mathrm{d}}(i) = P_{\mathrm{d0}}(i) \left\{ 1 + \frac{E(i,i)[\rho(i) - \rho_0(i)]}{\rho_0(i)} + \sum_{\substack{j=1 \\ j \neq i}}^{24} E(i,j) \frac{[\rho(j) - \rho_0(j)]}{\rho_0(j)} \right\} \tag{6.12}$$

6.4 Reconfiguration of MMGs

Reconfiguration is one of the significant strategies that operators can use to manage and optimize the network topology aimed at achieving desired targets. Network reconfiguration as an optimization problem could have various objectives like maximizing distribution network reliability, improving system voltage profile, minimizing operation cost, and minimizing network losses. Among the goals mentioned above, operation cost and loss minimizing are important for the distribution network operator (DNO). In this chapter, these objective functions are taken into account and will be formulated in the next section.

It is worth noting that one of the limiting factors in network reconfiguration problem is switching number. Switching number in a distribution network can be obtained from Eq. (6.13) [35]. In conventional distribution networks, the network's radial topology is an important constraint in the reconfiguration problem. In the

hypothesized MG-based distribution network, the constraint (6.14) is considered to guarantee the radiality of the network during reconfiguration process.

$$N_S^{\mathrm{SW}} = \sum_{t=1}^{24} |\mathrm{St}_t - \mathrm{St}_{t-1}| \tag{6.13}$$

$$N_l = N_{\mathrm{br}} - N_{\mathrm{bus}} + 1 \tag{6.14}$$

It should be stated that due to the penetration of various resources in the MGs, reconfiguration of MMG will be quietly different with traditional reconfiguration of distribution network. Actually, in the MMG-based distribution networks, there are some remotely controlled switches available between MGs to exchange energy among themselves. Our purpose to execute the reconfiguration in this structure is to determine how the MGs can be connected to each other to transact the power.

6.5 Problem Formulation

6.5.1 Objective Function

From the DNO viewpoint, two basic objectives are considered. Minimizing operation cost and power loss are two objectives that will separately be reviewed and incorporated into the problem.

6.5.2 First Objective

In each MG, it is assumed that various dispatchable and non-dispatchable DGs are installed. High penetration of renewable energy resources such as photovoltaic (PV) and wind turbine (WT) in each MG is considered. In addition, because of MG's islanding mode, at least one dispatchable generation unit such as combined heat and power (CHP) or microturbine (MT) is needed.

In this chapter, the first objective is network operation cost, which depends on each DG's operation cost in each MG. Because of dispatchable output of nonrenewable DGs, the operating cost function of this resource depends on its output power. To model these types of DGs, a quadratic function is considered [36]. Equations (6.15) and (6.16) show CHP and MT cost functions, respectively. For fuel cell (FC), PV, and WT, a constant cost function is considered. Furthermore, Eqs. (6.17)–(6.19) express their operating cost functions, respectively [37]. The MG-based distribution network operating cost is obtained from Eq. (6.20) that should be minimized (6.21).

$$\text{Cost}_{\text{CHP},t} = a_{\text{CHP}} P^2_{t,\text{mg,CHP}} + b_{\text{CHP}} P_{t,\text{mg,CHP}} + c_{\text{CHP}} \tag{6.15}$$

$$\text{Cost}_{\text{MT},t} = a_{\text{MT}} P^2_{t,mg,\text{MT}} + b_{\text{MT}} P_{t,mg,\text{MT}} + c_{\text{MT}} \tag{6.16}$$

$$\text{Cost}_{\text{FC},t} = c_{\text{FC}} \cdot P_{\text{FC}} \tag{6.17}$$

$$\text{Cost}_{\text{PV},t} = c_{\text{PV}} \cdot P_{\text{PV}} \tag{6.18}$$

$$\text{Cost}_{\text{WT},t} = c_{\text{WT}} \cdot P_{\text{WT}} \tag{6.19}$$

$$\text{opcost}_t = \sum_{\text{mg}i=1}^{N_{\text{mg}}} \left(\sum_{\text{CHP}i=1}^{N_{\text{CHP}}} \text{Cost}_{\text{CHP}i,\text{mg},t} + \sum_{\text{MT}i=1}^{N_{\text{MT}}} \text{Cost}_{\text{MT}i,\text{mg},t} + \sum_{\text{FC}i=1}^{N_{\text{FC}}} \text{Cost}_{\text{FC}i,\text{mg},t} + \sum_{\text{PV}i=1}^{N_{\text{PV}}} \text{Cost}_{\text{PV}i,\text{mg},t} + \sum_{\text{WT}i=1}^{N_{\text{WT}}} \text{Cost}_{\text{WT}i,\text{mg},t} \right) \tag{6.20}$$

$$\text{mincost} = \min \left[\text{opcost}_t \right] \tag{6.21}$$

6.5.3 Second Objective

Equation (6.22) displays the mathematical formulation of power losses in distribution systems [38]. In the proposed problem, the second goal of DNO is to minimize the network loss (6.23).

$$\text{loss}_t = \sum_{\text{mg}i=1}^{N_{\text{mg}i}} \sum_{\text{br}=1}^{N_{\text{br}}} \text{Real} \left(\frac{\left| V_{n,\text{mg}i,t} - V_{m,\text{mg}i,t} \right|^2}{R_{\text{br,mg}i} - jX_{\text{br,mg}i}} \right) \tag{6.22}$$

$$\text{minloss} = \min \left[\text{loss}_t \right] \tag{6.23}$$

6.5.4 Constraints

The proposed objective functions have the following constraints. Active and reactive power flow equations are given in (6.24) and (6.25), respectively. Before and after implementing DR programs, active and reactive power balance constraints are maintained by Eqs. (6.26)–(6.28) respectively. In (6.27), all DG active power generation is considered; while in (6.28) CHP and MT are assumed to have ability to generate reactive power. The thermal limit of branches is restricted by Eq. (6.29). Equation (6.30) illustrates all bus voltage limits; the voltage of slack bus should be set as 1 per unit as (6.31) and also voltage angle constraint is given in Eq. (6.32). Active power generation constraints for all types of DGs can be imposed by (6.33) to

(6.37), respectively. For dispatchable DGs, reactive power generation constraints are performed by (6.38) and (6.39).

$$P_{t,\mathrm{mg}i,\mathrm{nm}} = \left|V_{t,\mathrm{mg}i,n}\right|^2 G_{\mathrm{nm}} - \left|V_{t,\mathrm{mg}i,n}\right|\left|V_{t,\mathrm{mg}i,m}\right| \left(G_{\mathrm{nm}}\cos\theta_{t,\mathrm{mg}i,\mathrm{nm}} + B_{\mathrm{nm}}\sin\theta_{t,\mathrm{mg}i,\mathrm{nm}}\right) \tag{6.24}$$

$$Q_{t,\mathrm{mg},\mathrm{nm}} = -\left|V_{t,\mathrm{mg}i,n}\right|^2\left(B_{\mathrm{nm}} + B_{\mathrm{nm}}^{\mathrm{sh}}\right) - \left|V_{t,\mathrm{mg}i,n}\right|\left|V_{t,\mathrm{mg}i,m}\right| \left(G_{\mathrm{nm}}\sin\theta_{t,\mathrm{mg}i,\mathrm{nm}} - B_{\mathrm{nm}}\cos\theta_{t,\mathrm{mg}i,\mathrm{nm}}\right) \tag{6.25}$$

$$P_{t,\mathrm{mg}i,\mathrm{CHP}i} + P_{t,\mathrm{mg}i,\mathrm{MT}i} + P_{t,\mathrm{mg}i,\mathrm{FC}i} + P_{t,\mathrm{mg}i,\mathrm{PV}i} + P_{t,\mathrm{mg}i,\mathrm{WT}i} - P_{t,\mathrm{mg}i,\mathrm{dn}} = \sum_{m\in\Omega_b} P_{t,\mathrm{mg}i,\mathrm{nm}} \tag{6.26}$$

$$P_{t,\mathrm{mg}i,\mathrm{CHP}i} + P_{t,\mathrm{mg}i,\mathrm{MT}i} + P_{t,\mathrm{mg}i,\mathrm{FC}i} + P_{t,\mathrm{mg}i,\mathrm{PV}i} + P_{t,\mathrm{mg}i,\mathrm{WT}i} - \left[P_{\mathrm{d0}}(i)\left\{1 + \frac{E(i,i)[\rho(i)-\rho_0(i)]}{\rho_0(i)} + \sum_{\substack{j=1\\ j\neq i}}^{24} E(i,j)\frac{[\rho(j)-\rho_0(j)]}{\rho_0(j)}\right\}\right] = \sum_{m\in\Omega_b} P_{t,\mathrm{mg}i,\mathrm{nm}} \tag{6.27}$$

$$Q_{t,\mathrm{mg}i,\mathrm{CHP}i} + Q_{t,\mathrm{mg}i,\mathrm{MT}i} - Q_{t,\mathrm{mg}i,\mathrm{dn}} = \sum_{m\in\Omega_b} Q_{t,\mathrm{mg}i,\mathrm{nm}} \tag{6.28}$$

$$\sqrt{\left[\left(P_{t,\mathrm{mg}i,\mathrm{nm}}\right)^2 + \left(Q_{t,\mathrm{mg}i,\mathrm{nm}}\right)^2\right]} \le S_{\mathrm{max},t,\mathrm{mg}i,\mathrm{nm}} \tag{6.29}$$

$$|V|_{\mathrm{min}} \le |V|_{t,\mathrm{mg}i,n} \le |V|_{\mathrm{max}} \tag{6.30}$$

$$|V|_{t,\mathrm{mg}i,n} = 1 \quad n \in n_{\mathrm{ref}} \tag{6.31}$$

$$\theta_{\mathrm{min}} \le \theta_{t,n} \le \theta_{\mathrm{max}} \quad n \in n_{\mathrm{ref}} \tag{6.32}$$

$$P_{\mathrm{CHPmin}} \le P_{t,\mathrm{mg}i,\mathrm{CHP}i} \le P_{\mathrm{CHPmax}} \tag{6.33}$$

$$P_{\mathrm{MT,\,min}} \le P_{t,\mathrm{mg}i,\mathrm{MT}i} \le P_{\mathrm{MT,\,max}} \tag{6.34}$$

$$P_{\mathrm{FC,\,min}} \le P_{t,\mathrm{mg}i,\mathrm{FC}i} \le P_{\mathrm{FCmax}} \tag{6.35}$$

$$P_{\mathrm{PVmin}} \le P_{t,\mathrm{mg}i,\mathrm{PV}i} \le P_{\mathrm{PVmax}} \tag{6.36}$$

$$P_{\mathrm{WTmin}} \le P_{t,\mathrm{mg}i,\mathrm{WT}i} \le P_{\mathrm{WTmax}} \tag{6.37}$$

$$Q_{\mathrm{CHPmin}} \le Q_{t,\mathrm{mg}i,\mathrm{CHP}i} \le Q_{\mathrm{CHPmax}} \quad n \in n_{\mathrm{ref}} \tag{6.38}$$

$$Q_{\mathrm{MTmin}} \le Q_{t,\mathrm{mg}i,\mathrm{MT}i} \le Q_{\mathrm{MTmax}} \quad n \in n_{\mathrm{ref}} \tag{6.39}$$

6.5.5 PV and WT Generation Modeling

6.5.5.1 PV Model

The power generation of PV depends on air temperature and solar radiation; therefore, its output power will change hourly. The normal distribution function is used in this chapter to model PV generation (6.40). The generated power by PV is exhibited in (6.41) [39].

$$f_n\left(P_{\mathrm{pv}}\right) = \frac{1}{\sqrt{2\pi\sigma^2}} \quad \exp\left(\frac{-\left(P_{\mathrm{pv}} - \mu\right)^2}{2 \times \sigma^2}\right) \tag{6.40}$$

$$P_{\mathrm{pv}} = P_{\mathrm{STC}} \times \frac{G_{\mathrm{ING}}}{G_{\mathrm{STC}}} \times \left(1 + k\left(T_{\mathrm{C}} - T_{\mathrm{r}}\right)\right) \tag{6.41}$$

6.5.5.2 WT Model

The power generated by WT depends on wind speed, so its output power will be extremely variable. To this end, the Weibull distribution (6.42) is applied to show the distribution of wind speed. The power generated by WT can be depicted as (6.43) [39].

$$f_v(v) = \begin{Bmatrix} \frac{\beta}{\alpha} \times \left(\frac{v}{\beta}\right)^{\varphi-1} \times \mathrm{e}^{\left(\frac{v}{\alpha}\right)\beta} & v \geq 0 \\ 0 & \text{otherwise} \end{Bmatrix} \tag{6.42}$$

$$P_{\mathrm{WT}} = \begin{Bmatrix} \frac{\nu_{\text{cut-out}}^n - \nu^n}{\nu_{\text{cut-in}}^n - \nu_r^n} \times P_{\mathrm{rate}} & \nu_{\text{cut-in}} \leq \nu \leq \nu_r \\ P_{\mathrm{rate}} & \nu_r \leq \nu \leq \nu_{\text{cut-out}} \\ 0 & \text{otherwise} \end{Bmatrix} \tag{6.43}$$

6.5.6 Uncertainty Modeling

Due to the increasing share of renewable resources in the power sector, uncertainty makes the distribution network operation a more complicated problem. Uncertain parameters in power systems are divided into two major sections: technical parameters and economic parameters. Uncertainty in the power system operation is part of the technical parameter section [40]. Among the methods developed to handle the system uncertainty, in this chapter an effective scenario-based programming has

been selected. In this modeling, scenarios are initially produced, and then because of excessive number of scenarios that imposes significant implementation challenges, these scenarios can be reduced by using scenario reduction techniques.

6.5.6.1 Scenario Generation

One of the most beneficial ways to generate scenarios is the Monte Carlo method (MCS) [41]. Equation (6.44) depicts the probability of scenarios generated from multiple uncertain parameters. Given Eq. (6.45), the sum of the probabilities of the scenarios generated by MCS must be equal to one.

$$\pi_{\mathrm{sc}}^{\mathrm{t}} = \pi_{\mathrm{sc}}^{\mathrm{lo}} \times \pi_{\mathrm{sc}}^{\mathrm{pv}} \times \pi_{\mathrm{sc}}^{\mathrm{wt}} \tag{6.44}$$

$$\sum_{\mathrm{sc}=1}^{N_{\mathrm{s}}} \pi_{\mathrm{sc}}^{\mathrm{lo}} \times \pi_{\mathrm{sc}}^{\mathrm{pv}} \times \pi_{\mathrm{sc}}^{\mathrm{wt}} = 1 \tag{6.45}$$

6.5.6.2 Scenario Reduction

Due to the creation of a large number of scenarios and also regarding the fact that most of their occurrence probabilities are very low, scenario reduction techniques should be used. One of these techniques is the Kantorovich scenario reduction technique that specifies a probability measure to select a subset of scenarios from initial scenarios. Equation (6.46) represents the mathematical form of this approach [42]. Simulation time is reduced by scenario reduction techniques effectively.

$$H_{\mathrm{t}} = \sqrt{\sum_{\mathrm{sc}=1}^{N_{\mathrm{sc}}} \left(\pi_{\mathrm{sc}}^{i} - \pi_{\mathrm{sc}}^{j}\right)^2}, \quad N_{\mathrm{S}} = \left\{N_{\mathrm{sc}}^{\mathrm{lo}} \times N_{\mathrm{sc}}^{\mathrm{pv}} \times N_{\mathrm{sc}}^{\mathrm{wt}}\right\} \tag{6.46}$$

6.5.7 Risk Measure

The uncertainty of renewable resources and demand will pose a considerable risk for DNO. As mentioned in literature, an appropriate method for measuring and controlling risk in scenario-based modeling is the conditional value at risk (CVaR) index. In this method, first, the expected objective function should be calculated by Eq. (6.47) and then value at risk (VaR) is calculated by Eq. (6.48) which is the difference between the values of the objective function in the worst scenario in the most probable scenario. β_{r} is a risk factor and is between 0 and 1. When β is equal to 0, the DNO is risk-neutral, and if β is equal to 1, the system operator is risk aversion.

In this research, risk factor is considered to be 0.9. On the other hand, α_r denotes the confidence level where its parameter is assumed to be 0.95. Moreover, η_r is considered as an auxiliary variable which is defined in Eq. (6.49). Finally, with respect to (6.50) and (6.51), CVaR and the expected objective function are combined together taking into account the specific risk level [43].

$$\text{opcost}_{\text{expected}} = \sum_{\text{sc}=1}^{N_{\text{sc}}} (\text{scper}) \cdot (\text{opcost}_{\text{sc}}) \tag{6.47}$$

$$\text{VaR} = (\text{opcost}_{\text{worstsc}}) - (\text{opcost}_{\text{maxsc}}) \tag{6.48}$$

$$\eta = \left\{ \begin{matrix} \text{VaR} - \text{opcost}_{\text{expected}} & \text{VaR} < \text{opcost}_{\text{maxsc}} \\ 0 & \text{others} \end{matrix} \right\} \tag{6.49}$$

$$\text{CVaR} = \text{VaR} - \left(\frac{1}{1 - \alpha_r} \right) \cdot \text{scper} \cdot \eta_r \tag{6.50}$$

$$\text{opcost}_{\text{risk}} = \text{opcost}_{\text{expected}} + \beta_r \cdot \text{CVaR} \tag{6.51}$$

6.6 Simulation Results

6.6.1 Data and Case Study

The modified IEEE 85-bus distribution network [44] has been chosen to implement the proposed problem. Six MGs in 85-bus radial network are supposed. Different real 24-h load profiles are taken into account from an electric distribution company. Residential, industrial, commercial, and academia are 24-h load profiles which are considered in this work [45]. Each load point within the MGs is multiplied by its specific 24-h coefficient.

To identify the boundaries between the MGs and main grid, eight tie switches are assumed to be installed. The main goal of tie switches is to change the MG configuration. The proposed MMG topology is shown in Fig. 6.5. As can be seen, comprehensive MG connections are considered; in particular, MG1, MG2, MG3, and MG5 are connected to the main grid directly, MG4 and MG6 are connected to other MGs, MG6 is connected to two MGs, and MG2, MG3, and MG5 are also connected to both main grid and other MGs. The load profiles of the main network, MG1, MG4, and MG5, are considered as residential load profiles, the load profile of MG3 is considered as commercial, the load profile of MG6 is known as industrial, and also MG2 is assumed to have a 24-hour academia load profile.

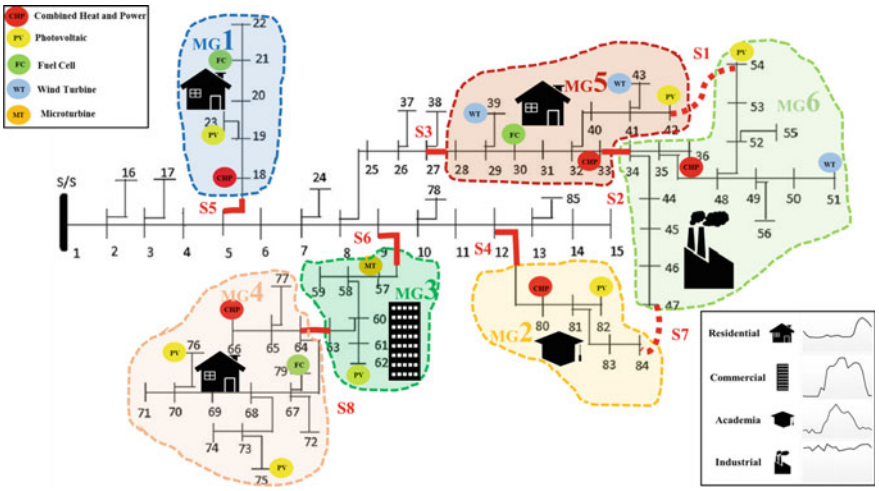

Fig. 6.5 Outline of proposed MMG topology

Table 6.1 Self- and cross-elasticity

	Peak	Off-peak	Valley
Peak	−0.1	0.016	0.012
Off-peak	0.016	−0. 1	0.01
Valley	0.012	0.01	−0. 1

6.6.2 DR Parameters

Since all consumers are unlikely to participate in the proposed DR programs, the number of consumers wishing to participate in the DR programs must be determined before the DR execution. For this reason, in this work the participating factor is assumed to be 10%. For all industrial loads, cross-elasticity and self-elasticity are considered 0.01 and −0.2, respectively. In addition, for all residential loads, the price elasticity of loads is presented in Table 6.1 [34].

Industrial loads can easily follow the prices but other loads cannot follow the hourly changes of electricity prices. For this reason, in this research, RTP is used for industrial loads and TOU is utilized for commercial, residential, and academia loads. Because of different peak time periods in residental loads and other loads, energy pricing in the TOU program will be different for each type of demands. Elasticity prices for TOU and for RTP have been demonstrated in Table 6.2 [34]. TOU and RTP pricing chart for residential, commercial, and industrial 24-hour load profiles is also illustrated in Fig. 6.6.

Table 6.2 Different time period electricity prices

Load type	Program	Electricity price (R/kWh)	Time (h)
Residential	TOU	40 at valley, 160 at off-peak, and 400 at peak	Valley period: 4:00 to 7:00 and 14:00 to 16:00 Off-peak time period: 1:00 to 3:00, 8:00 to 13:00 and 17:00 to18:00 Peak period: 19:00 to 24:00
Commercial	TOU	40 at valley, 160 at off-peak, and 400 at peak	Valley period: 1:00 to 6:00 and 23:00 to 24:00 Off-peak period: 7:00 to 8:00 Peak period: 9:00 to 22:00
Academia	TOU	40 at valley, 160 at off-peak, and 400 at peak	Valley period: 1:00 to 6:00 and 23:00 to 24:00 Off-peak period: 7:00 to 8:00 Peak period: 9:00 to 22:00
Industrial	RTP	160,160,160 20 40,500 40 20,500,200,160,200 20 20 40 40 40,160,160,200,200,500,500,200	–

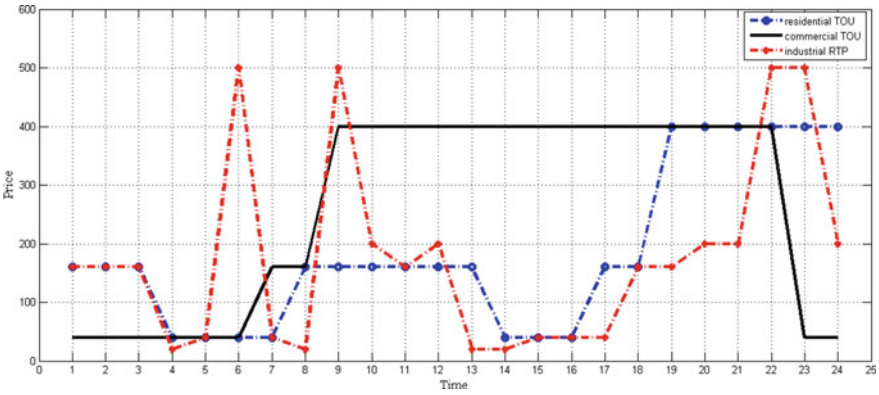

Fig. 6.6 TOU and RTP pricing chart for residential, commercial, and industrial 24-h load profiles

6.6.3 DG Parameters

The operation cost of the system depends on so many components such as types of DGs. According to the proposed model, the operating cost must be specified based on the levelized cost of energy for various energy resources. These coefficients are presented in Table 6.3 [37].

Table 6.3 DER operation cost coefficient

DG type	Location	*a*	*b*	*c*
CHP	MG 1,2, and 6	0.02	0.01	0.02
CHP	MG 4,5	0.0005	0.0495	0.001
MT	MG3	0.02	0.01	0.02
FC	MG 1, 4, and 5	–	–	0.1976
WT	MG5 and 6	–	–	0.002
PV	MG 1, 2, 3, 4, 5, and 6	–	–	0.0011

6.6.4 Numerical Results

In this research, two different operation strategies are proposed to operate MG-based distribution networks: hourly reconfiguration and DR programs. Both the proposed scheduling strategies are implemented in MATLAB environment. To carry out the aforementioned schedules, the network operator, i.e., DNO, must solve an AC optimal power flow (ACOPF) problem, which is a nonlinear and nonconvex optimization problem. In order to solve this complex issue, open-source MATPOWER package including its own primal-dual interior point solver (MIPS) has been employed. In this research, MATPOWER 6.0 has successfully been used to solve the ACOPF problem [38]. In the proposed MMG network, to analyze and evaluate the effect of network topology and MG connection on the objective functions, an hourly reconfiguration problem associated with DR programs has been carried out. Effect of TOU program on residential, commercial, and academia and effect of RTP on industrial 24-hour load profile are illustrated in Fig. 6.7. Besides, in Table 6.4, peak load and peak to valley factors are chosen to show the positive effect of time-based DR programs on these factors. To investigate the effectiveness of proposed DR programs on the network configuration and objective functions, the simulation results have been fulfilled once before the DR implementation and once after DR implementation.

6.6.5 Before DR Implementation

Before running of TOU and RTP via DNO, the results are presented for the expected scenario which has the probability of occurrence more than the rest of the scenarios. In minimizing operation cost and power losses, Tables 6.5 and 6.6 are given to express the states of switches in 24 h, respectively. The number of switching for each objective functions is presented in Table 6.7. Before DR program implementation, the network operational cost and power losses at all scenarios are illustrated in Fig. 6.8.

Fig. 6.7 DR program effect in 24 hours and various load shapes

Table 6.4 DR program effect on distribution system factors

Load type	Peak before DR program (MW)	Peak after DR program (MW)	Peak to valley before DR program	Peak to valley after DR program
Residential	0.0353	0.0318	0.0205	0.0162
Commercial	0.0560	0.0505	0.0526	0.0473
Academia	0.0353	0.0319	0.0296	0.0265
Industrial	0.0560	0.0547	0.0101	0.0079
Total load	2.3541	2.1702	1.2287	0.9798

Table 6.5 Open switches before DR implementation for minimizing network operation cost

Hours	Open switches
7, 8, 10, 11, 12, 14, 15, 16, 17, 18	S2, S3
19, 20, 21, 22, 23	S1, S7
1, 2, 4, 9	S1, S3
3, 5, 6	S1, S2
13, 24	S2, S7

Table 6.6 Open switches before DR implementation for minimizing network losses

Hours	Open switches
1, 7, 8, 9, 10, 14, 15, 16, 17, 18	S1, S3
2, 3, 4, 5, 6, 19, 20, 21	S1, S2
22, 23	S1, S4
13, 24	S1, S7
11, 12	S2, S3

Table 6.7 Number of switching before DR implementation

Objective function	Number of switching
Operation cost	22
Losses	18

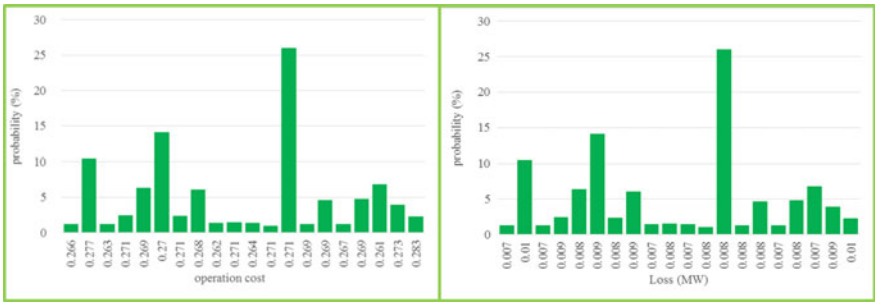

Fig. 6.8 Network operational cost and power losses in terms of scenarios before DR implementation

Table 6.8 Open switches after DR implementation for minimizing network operation cost

Hours	Open switches
1, 2, 3, 4, 5, 6, 7, 9, 10, 15, 16, 17, 18, 19, 23	S1, S3
8, 11, 12, 13, 14	S2, S3
20, 21, 22	S1, S7
24	S2, S7

6.6.6 After DR Implementation

After TOU and RTP implementation, the results are presented at the expected scenario which has the probability of occurrence more than others. The operation cost and power losses are depicted in Tables 6.8 and 6.9, respectively. The switching number for each objective function is presented in Table 6.10. After DR program implementation, network operational cost and power losses at all scenarios are illustrated in Fig. 6.9. Besides, a comparison of the total network operation cost considering risk analysis has been presented in Table 6.11 before and after DR perfomance.

Table 6.9 Open switches after DR implementation for minimizing network losses

Hours	Open switches
1, 2, 7, 8, 9, 10, 11, 12, 13, 14, 15, 16, 17, 18	S1, S3
3, 4, 5, 6, 19, 20, 21	S1, S2
22, 23	S1, S4
24	S1, S7

Table 6.10 Number of switching after DR implementation

Objective function	Number of switching
Operation cost	16
Losses	10

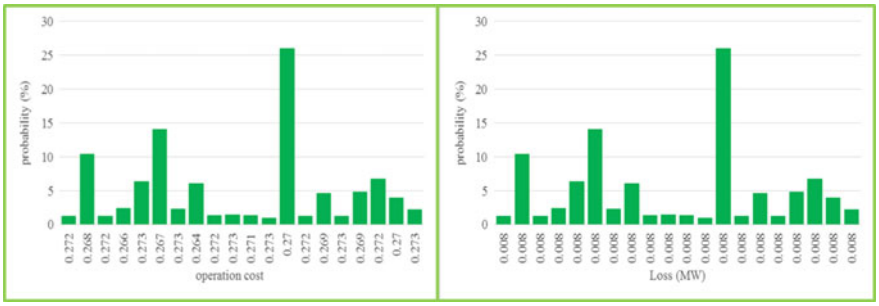

Fig. 6.9 Network operational cost and power losses in terms of scenarios after DR implementation

Table 6.11 Comparison of operating cost function

	Expected operation cost	CVaR	Operation cost
Without DR programs	0.2703	0.0121	0.2812
With DR programs	0.2696	0.0036	0.2729

The results evidenced that applying DR programs can highly restrict the adverse impacts of renewable uncertainties. Moreover, dynamic reconfiguration can optimize the procurement costs of MGs by modifying the connections of networked MGs. The results obtained from simulations justify that the reconfigurable structure for MGs will increase the reliability of the system by exchanging the power between the MGs from different ways. On the other hand, the simulation results have confirmed the feasibility of the proposed risk-based reconfiguration scheduling in conjunction with the CVaR index for minimizing the procurement costs of MGs. It is also found that the proposed DR program leads to a 12.83% and 19.54% reduction in economic costs and power losses, respectively.

6.7 Conclusion

In this research, the main focus was on the daily risk-constrained reconfiguration scheduling of networked MGs. The optimization problem has been solved from a network operator viewpoint. Changing the connection of MGs and implementing time-based DR programs are two strategies that have been used to operate the MGs. In each MG, different renewable and nonrenewable generation units are considered to supply demand of MGs locally. According to operation cost and power losses, the connection between the main network and MGs or between two neighbor MGs was changed and the optimal topology for each hour is presented. For more similarity to the actual distribution network, four different daily load profiles (i.e., residential, commercial, industrial, and academia) are taken into account. By observing the results, it can be deduced that by connecting the MGs to each other, the overall operation costs will be significantly lower than those in which the MGs are operated separately. On the other hand, the results confirm that DR programs lead to reduced energy management cost and mitigate the fluctuations of renewable generations. Moreover, it can be seen that the final optimal network configurations are affected by the time-based DR programs.

References

1. S. Nojavan, B. Mohammadi-Ivatloo, K. Zare, Optimal bidding strategy of electricity retailers using robust optimisation approach considering time-of-use rate demand response programs under market price uncertainties. IET Gener. Transm. Distrib. **9**(4), 328–338 (2015)
2. F.S. Gazijahani, J. Salehi, Reliability constrained two-stage optimization of multiple renewable-based microgrids incorporating critical energy peak pricing demand response program using robust optimization approach. Energy **161**, 999–1015 (2018)
3. M. Shamshirband et al., Decentralized trading of plug-in electric vehicle aggregation agents for optimal energy management of smart renewable penetrated microgrids with the aim of CO_2 emission reduction. J. Clean. Prod. **200**, 622–640 (2018)
4. Y.P. Hirsch, J. Guerrero, Microgrids: a review of technologies, key drivers, and outstanding issues. Renew. Sust. Energ. Rev. **90**, 402–411 (2018)
5. D.T. Ton, M.A. Smith, The US department of energy's microgrid initiative. Electr. J. **25**, 84–94 (2012)
6. F.S. Gazijahani, J. Salehi, Stochastic multi-objective framework for optimal dynamic planning of interconnected microgrids. IET Renew. Power Gener. **11**(14), 1749–1759 (2017)
7. W. Yuan, J. Wang, F. Qiu, C. Chen, C. Kang, B. Zeng, Robust optimization-based resilient distribution network planning against natural disasters. IEEE Trans. Smart Grid **7**, 2817–2826 (2016)
8. P. Wang, C. Yang, Y.W. Ye, Z. Xu, Voltage control strategy for three/single phase hybrid multimicrogrid. IEEE Trans. Energy Conv. **31**, 1498–1509 (2016)
9. R. Zamora, A.K. Srivastava, Multi-layer architecture for voltage and frequency control in networked microgrids. IEEE Trans. Smart Grid **9**, 2076–2085 (2018)
10. A. Arif, Z. Wang, Service restoration in resilient power distribution systems with networked microgrid, in *2016 IEEE Power and Energy Society General Meeting (PESGM)* (2016), pp. 1–5

11. B. Sultana, M.W. Mustafa, U. Sultana, A.R. Bhatti, Review on reliability improvement and power loss reduction in distribution system via network reconfiguration. Renew. Sust. Energ. Rev. **66**, 297–310 (2016)
12. F.S. Gazijahani, J. Salehi, Integrated DR and reconfiguration scheduling for optimal operation of microgrids using Hong's point estimate method. Int. J. Electr. Power Energy Syst. **99**, 481–492 (2018)
13. H. Nafisi, V. Farahani, H.A. Abyaneh, M. Abedi, Optimal daily scheduling of reconfiguration based on minimization of the cost of energy losses and switching operations in microgrids. IET Gener. Transm. Distrib. **9**, 513–522 (2015)
14. M.R. Dorostkar-Ghamsari et al., Value of distribution network reconfiguration in presence of renewable energy resources. IEEE Trans. Power Syst. **31**, 1879–1888 (2016)
15. E. Milani, M. Haghifam, A new probabilistic approach for distribution network reconfiguration: applicability to real networks. Math. Comput. Model. **57**, 169–179 (2013)
16. Z. Xu, P. Yang, C. Zheng, Y. Zhang, J. Peng, Z. Zeng, Analysis on the organization and development of multi-microgrids. Renew. Sust. Energ. Rev. **81**, 2204–2216 (2018)
17. M.H. Hemmatpour, M. Mohammadian, A.A. Gharaveisi, Optimum islanded microgrid reconfiguration based on maximization of system loadability and minimization of power losses. Int. J. Electr. Power Energy Syst. **78**, 343–355 (2016)
18. K. Utkarsh, D. Srinivasan, A. Trivedi, W. Zhang, T. Reindl, Distributed model-predictive real-time optimal operation of a network of smart microgrids. IEEE Trans. Smart Grid **10**, 1–1 (2018)
19. C. Shao, C. Xu, S. He, X. Lin, X. Li, Operation of microgrid reconfiguration based on MAS (multi-agent system), in *2013 IEEE International Conference of IEEE Region 10 (TENCON 2013)* (2013), pp. 1–4
20. S. Chen, T. Duan, B.L. Cai, G. Hu, Smart energy management system for optimal microgrid economic operation. IET Renew. Power Gener. **5**, 258–267 (2011)
21. F.S. Gazijahani, J. Salehi, Optimal bi-level model for stochastic risk-based planning of microgrids under uncertainty. IEEE Trans. Ind. Inform. **14**(7), 3054–3064 (2018)
22. X. Fang, Q. Yang, J. Wang, W. Yan, Coordinated dispatch in multiple cooperative autonomous islanded microgrids. Appl. Energy **162**, 40–48 (2016)
23. A. Ouammi, H. Dagdougui, R. Sacile, Optimal control of power flows and energy local storages in a network of microgrids modeled as a system of systems. IEEE Trans. Control Syst. Technol. **23**, 128–138 (2015)
24. A. Kavousi-Fard, A. Khodaei, Efficient integration of plug-in electric vehicles via reconfigurable microgrids. Energy **111**, 653–663 (2016)
25. S. Nojavan, B. Mohammadi-Ivatloo, K. Zare, Robust optimization based price-taker retailer bidding strategy under pool market price uncertainty. Int. J. Electr. Power Energy Syst. **73**, 955–963 (2015)
26. N. Nikmehr, S. Najafi Ravadanegh, A study on optimal power-sharing in interconnected microgrids under uncertainty. Int. Trans. Electr. Energy Syst. **26**, 208–232 (2016)
27. N. Nikmehr, S. Najafi Ravadanegh, A. Khodaei, Probabilistic optimal scheduling of networked microgrids considering time-based demand response programs under uncertainty. Appl. Energy **198**(15), 267–279 (2017)
28. N.G. Paterakis, O. Erdinç, J.P.S. Catalão, An overview of demand response: key-elements and international experience. Renew. Sustain. Energy Rev. **69**, 871–891 (2017)
29. Staff Report. Assessment of Demand Response and Advanced Metering. http://www.FERC.gov (August 2006)
30. K. McKenna, A. Keane, Residential load modeling of Price-based demand response for network impact studies. IEEE Trans. Smart Grid **7**, 2285–2294 (2016)
31. F.S. Gazijahani, J. Salehi, Game theory based profit maximization model for microgrid aggregators with presence of EDRP using information gap decision theory. IEEE Syst. J. **99**, 1–9 (2018)

32. S. Nojavan, K. Zare, B. Mohammadi-Ivatloo, Optimal stochastic energy management of retailer based on selling price determination under smart grid environment in the presence of demand response program. Appl. Energy **187**, 449–464 (2017)
33. H. Aalami, M. Moghaddam, G. Yousefi, Demand response modeling considering interruptible/curtailable loads and capacity market programs. Appl. Energy **87**, 243–250 (2010)
34. S. Nojavan, H. Aalami, Stochastic energy procurement of large electricity consumer considering photovoltaic, wind-turbine, micro-turbines, energy storage system in the presence of demand response program. Energy Convers. Manag. **103**, 1008–1018 (2015)
35. S. Golshannavaz, S. Afsharnia, F. Aminifar, Smart distribution grid: optimal day-ahead scheduling with reconfigurable topology. IEEE Trans. Smart Grid **5**, 2402–2411 (2014)
36. A. Rabiee, M. Moradi-dalvand, Combined heat and power system operation cost minimization using frog leaping based intelligent search algorithm. J. Energy Manag. Technol. **1**, 28–35 (2017)
37. F.S. Gazijahani, J. Salehi, Robust design of microgrids with reconfigurable topology under severe uncertainty. IEEE Trans. Sustain. Energy **9**(2), 559–569 (2018)
38. R.D. Zimmerman, C.E. Murillo-Sanchez, R.J. Thomas, MATPOWER: steady-state operations, planning, and analysis tools for power systems research and education. IEEE Trans. Power Syst. **26**, 12–19 (2011)
39. N. Nikmehr, S.N. Ravadanegh, Optimal power dispatch of multi-microgrids at future smart distribution grids. IEEE Trans. Smart Grid **6**, 1648–1657 (2015)
40. A. Soroudi, T. Amraee, Decision making under uncertainty in energy systems: state of the art. Renew. Sust. Energ. Rev. **28**, 376–384 (2013)
41. P. Salyani et al., Chance constrained simultaneous optimization of substations, feeders, renewable and non-renewable distributed generations in distribution network. Electr. Power Syst. Res. **158**, 56–69 (2018)
42. N. Growe-Kuska, H. Heitsch, W. Romisch, Scenario reduction and scenario tree construction for power management problems, in *2003 IEEE Bologna Power Tech Conference Proceedings, vol. 3* (2003), pp. 1–7
43. S. Gazijahani, S. Najafi Ravadanegh, J. Salehi, Stochastic multi-objective model for optimal energy exchange optimization of networked microgrids with presence of renewable generation under risk-based strategies. ISA Trans. **73**, 100–111 (2018)
44. A. Abdolahi et al., Probabilistic multi-objective arbitrage of dispersed energy storage systems for optimal congestion management of active distribution networks including solar/wind/CHP hybrid energy system. J. Renew. Sustain. Energy **10**(4), 045502 (2018)
45. M. Shamshirband et al., Look-ahead risk-averse power scheduling of heterogeneous electric vehicles aggregations enabling V2G and G2V systems based on information gap decision theory. Electr. Power Syst. Res. **173**, 56–70 (2019)

Chapter 7
AC Optimal Power Flow Incorporating Demand-Side Management Strategy

Farkhondeh Jabari, Mousa Mohammadpourfard, and Behnam Mohammadi-Ivatloo

Nomenclature

Indices

i, j	Bus
g	Thermal power plant
t	Time

Parameters

α	Maximum percentage of active demand decrease and increase at bus i
a_g, b_g, c_g	Fuel consumption factors
$\mathrm{DSM}_{i,\,t}$	Value of active demand increase/decrease at bus i and time t
$P^{0}_{i,t}$	Base active demand of bus i at hour t
$P^{g,\max}_{i}$	Maximum value of active power generated by unit g at bus i
$P^{g,\min}_{i}$	Minimum value of active power generated by unit g at bus i
$P^{\max}_{ij}$	Active power capacity of transmission line i to j
$Q_{i,\,t}$	Reactive power demand of bus i at time t
r_{ij}	Resistance of transmission line i to j
x_{ij}	Reactance of transmission line i to j

F. Jabari (✉) · B. Mohammadi-Ivatloo
Faculty of Electrical and Computer Engineering, University of Tabriz, Tabriz, Iran
e-mail: f.jabari@tabrizu.ac.ir; bmohammadi@tabrizu.ac.ir

M. Mohammadpourfard
Faculty of Chemical and Petroleum Engineering, University of Tabriz, Tabriz, Iran
e-mail: Mohammadpour@tabrizu.ac.ir

S. Nojavan, K. Zare (eds.), *Demand Response Application in Smart Grids*,
https://doi.org/10.1007/978-3-030-32104-8_7

Decision Variables

$\delta_{i,\,t}$ Bus voltage angle
$I_{ij,\,t}$ Current passes through transmission line i to j
OF Daily cost
$P_{i,\,t}$ Active power demand of bus i at time t
$P^{g}_{i,t}$ Active power generation of gas-fired power plant g
$P^{w}_{i,t}$ Wind power production at bus i and hour t
$Q^{g}_{i,t}$ Reactive power generation of gas-fired power plant g, which is connected to bus i
$S_{ij,\,t}$ Complex power transmitted from bus i to j
$V_{i,\,t}$ Bus voltage magnitude

7.1 Motivation and Literature Review

As a result of population growth and electrical demand increase, interconnected power systems may intentionally or non-optimally be islanded to some regions. In large power systems, load-generation mismatch may cause voltage instability, cascaded outages of transmission lines, and wide area blackouts. There are some solutions to avoid from wide spread outages: (1) use of renewable energy sources for supplying not-supplied demand, (2) generation side management by saving surplus energy at low-demand periods and supplying high-demand at peak hours using storage technologies, and (3) demand-side management strategy by peak loads and shifting them to low-demand times. Many scholars have studied AC optimal power flow (AC-OPF) analysis to find a good solution vector for interconnected power systems [1, 2]. Because, if a fast and cost-efficient approach is not used for solving AC-OPF problem, a simple contingency such as transmission outages may lead to overloading of another lines as well as cascaded failures and a wide spread blackout [3, 4].

AC-OPF problem is usually solved as a mixed integer nonlinear program (MINLP). Meanwhile, penetration level of renewable energies in transmission and distribution power systems and their fluctuations as well as uncertainties of energy demand make this problem more complex [5, 6]. Many researches have not considered these issues [7–9]. Hence, OPF problem may be non-optimal when uncertainties of renewable energy sources and loads are not modeled. Stochastic programming methods can model their variations by generating some scenarios to ensure security under different operating conditions [10–13]. Stochastic OPF algorithms have two drawbacks [14]: (a) higher computational burden and calculation time and (b) required distributional data of uncertain variable, which usually is not available. Interval robust optimization technique overcomes these limitations [15]. In robust DC-OPF problem, voltage magnitude and reactive power are not considered and optimum operating point of system may be insecure and inaccurate [16]. As summarized in Table 7.1, the fuel cost of active and reactive power

Table 7.1 Objectives in OPF problem

Ref.	Generation cost		External suppliers	Losses	CO_2 footprint	Involuntarily load interruptions
	Active	Reactive				
[40]	*			*		*
[41]	*				*	
[42]	*		*			
[43]	*	*				
[44]	*	*	*	*		
[45]	*		*	*		
[46]		*	*	*		*
[47]			*			
[48]	*		*	*		
[49]						*
[50]	*					*
[51]	*		*			*
[52]				*		
[53]				*		
[54]	*			*		
[55]	*					
[56]	*			*		*
[57]	*		*			
[58]	*		*		*	
[59]	*					
[60]	*					
[61]				*		
[62]	*		*			*
[63]	*		*			*
[64]	*		*			
[65]	*		*			
[66]	*					
[67]	*					

generation processes, energy procurement from external energy suppliers, emissions of greenhouse gases, real power losses of transmission system, and involuntarily load interruptions have been considered in OPF problem. According to Table 7.2, real and reactive power generation capacities, voltage magnitude limit, current or power transmission capacity, load shedding limits, and balance criterion are considered as constraints of OPF problem.

Annual peak electrical demand usually occurs in summer [17], because a huge number of air conditioning systems are simultaneously connected to regional power systems, which imposes additional investment costs to distribution and interconnected networks [18, 19]. Meanwhile, DSM strategies are cost-effective and energy-efficient tools to overcome this problem. Their main advantage is to change daily electricity usage curve of consumers in a way that the system reliability

Table 7.2 Constraints of OPF problem

Ref.	Real generation capacity	Reactive power capacity	Voltage security constraint	Voltage angle	Involuntarily load interruptions
[40]	*	*	*	*	*
[41]	*	*	*		
[42]	*	*	*	*	
[43]	*	*	*	*	
[44]	*	*	*	*	
[45]	*	*			
[46]	*			*	*
[47]	*	*			
[48]	*	*	*	*	
[49]			*	*	*
[50]	*	*	*		*
[51]	*	*	*	*	*
[52]	*		*	*	
[53]	*			*	
[54]	*		*	*	
[55]	*				
[56]	*	*	*		*
[57]	*				
[58]	*		*	*	
[59]	*	*	*	*	
[60]	*				
[61]	*	*	*		
[62]	*				*
[63]	*				*
[64]	*				
[65]	*				
[66]	*			*	
[67]	*	*	*	*	

is improved and the load profile is flatten under severe contingencies [20–22]. Based on incentives paid to customers and electricity tariffs, demand response procedures are classified as follows [23, 24]:

- Incentive-based DSM schemes.
  - Direct load control: An end user, who registered in this program, receives incentive allowing the system operator to curtail its power consumption when needed [25, 26].
  - Load curtailment: Regional distribution companies inform participants to reduce their energy consumption under contingencies [27]. If a registered customer does not participate in load curtailment strategy, he will severely be fined.

  - Demand bidding method: Customers with higher demand than 1 MW can participate in bidding plan. They can bid a certain price which mitigate their power consumption by getting it [28, 29].
  - Emergency load control: This is similar to load curtailment program. But, it is implemented on flexible consumers only at annual peak demand periods.
- Price-based load management.
  - Time of use: Each registered consumer decreases a percentage of power consumption during peak time intervals and satisfies it at low-demand hours for reducing his electricity bill [30–33].
  - Critical peak pricing: This program is only performed in hot summer days, when the energy tariffs are significantly more than the real-time prices and the time of use rates [34].
  - Real-time pricing: Instead of three level pricing at low, medium, and peak load hours, hourly energy prices are considered to encourage consumers for participation in peak clipping and valley filling project [35].

As summarized in Tables 7.1 and 7.2, there is no study on demand-side management (DSM) strategy [36, 37] based optimal power flow analysis. Several scholars presented load shedding based power system optimization problems [38, 39]. But, it should be noted that if a part of active power loads of some buses is shifted from peak hours to off-peak and mid-peak times, daily fuel cost of thermal generating units will be reduced, significantly. Moreover, there will be no need to purchase electricity from external power suppliers such as renewable energy resources. Therefore, the capital investment, maintenance, and operation costs of the renewable energy resource-based power generation plants are saved if the electrical consumers are participated in peak shaving programs. The main idea of the DSM policies is to shift the use of the electricity consumption equipment from high-load hours (when the power system is overloaded) to low-demand periods. The electrical demand profile over the study horizon will be flattened by demand shifting strategy. It should be mentioned that only a certain amount of electrical utilization of different customers can be reduced. Because, if this limit is not considered in DSM program, other peak energy demand points may be occurred at other hours. This chapter implements a time-amount-based DSM approach on optimal AC load flow analysis and decrease daily operation cost of a benchmark power system, while considering (a) limits of voltage magnitude and angle, (b) active and reactive power generation capacities, and (c) active and reactive load-generation balance constraint. It is assumed that maximum 20% of base active power demand of each bus can be decreased or increased at hour t. Time and value of active power demand shift are considered as decision variables of optimization problem. Moreover, active and reactive power generation at each bus, transmission flows, bus voltage angle and magnitude, and objective cost function are found in two cases "without DSM" and "with DSM" and compared to prove its cost-effectiveness capability in OPF strategy.

In Sect. 7.2, a DSM-based AC optimal power flow problem is modeled. Then, Section 7.3 proves that implementation of DSM program on AC load flow analysis is a cost-effective tool. Afterward, conclusion is presented in Section 7.4.

7.2 Problem Formulation

The AC optimal power flow problem is applied on the transmission scale level power system. As illustrated in Fig. 7.1, the voltage magnitude of the buses i and j at time t are shown with $V_{i,\,t}$ and $V_{i,\,t}$, respectively. Moreover, $\delta_{i,\,t}$ and $\delta_{j,\,t}$ refer to the bus voltage angle of the nodes i and j. The resistance and reactance of the transmission line between nodes i and j are represented as r_{ij} and x_{ij}, respectively.

The objective function of the optimization problem is the fuel cost of the thermal units over a $T = 24$ h study period, which is minimized as (7.1). The constant coefficients a_g, b_g, and c_g determine the operation cost of the thermal unit g for generating the power $P^g_{i,t}$ at hour t.

$$\mathrm{OF} = \sum_{i,\,t} a_g \left(P^g_{i,t}\right)^2 + b_g P^g_{i,t} + c_g \tag{7.1}$$

The load-generation-transmission balance constraints (7.2) and (7.3) are stated for active and reactive powers. The parameter $P_{i,\,t}$ is the active power consumption at bus i and time t in the presence of DSM program.

$$P^g_{i,t} + P^w_{i,t} - P_{i,t} = \sum_{j \in \Omega^i_l} P_{ij,t} \tag{7.2}$$

$$Q^g_{i,t} - Q_{i,t} = \sum_{j \in \Omega^i_l} Q_{ij,t} \tag{7.3}$$

The current flowing from bus i to node j through the branch i-j is computed as (7.4). The variables $S_{ij,\,t}$, $P_{ij,\,t}$, and $Q_{ij,\,t}$ represent the complex, real, and reactive power flows of the branch i-j and are calculated in Eqs. (7.5)–(7.7) and limited by $S^{\max}_{ij,t}$ as constraint (7.8).

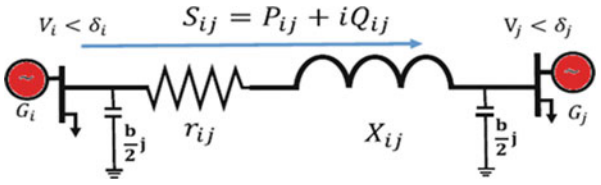

Fig. 7.1 The power system modeling in the AC load flow analysis

$$I_{ij,t} = \frac{V_{i,t}\angle\delta_{i,t} - V_{j,t}\angle\delta_{j,t}}{Z_{ij}\angle\theta_{ij}} + \frac{bV_{i,t}}{2}\angle\left(\delta_{i,t} + \frac{\pi}{2}\right) \tag{7.4}$$

$$S_{ij,t} = I^{*}_{j,t} \times V_{i,t}\angle\delta_{i,t} \tag{7.5}$$

$$P_{ij,t} = \frac{V^2_{i,t}}{Z_{ij}}\cos\left(\theta_{ij}\right) - \frac{V_{i,t}V_{j,t}}{Z_{ij}}\cos\left(\delta_{i,t} - \delta_{j,t} + \theta_{ij}\right) \tag{7.6}$$

$$Q_{ij,t} = \frac{V^2_{i,t}}{Z_{ij}}\sin\left(\theta_{ij}\right) - \frac{V_{i,t}V_{j,t}}{Z_{ij}}\sin\left(\delta_{i,t} - \delta_{j,t} + \theta_{ij}\right) - \frac{bV^2_{i,t}}{2} \tag{7.7}$$

$$-S^{\max}_{ij,t} \le S_{ij,t} \le S^{\max}_{ij,t} \tag{7.8}$$

The output active and reactive power generations of the unit g are limited by the capacity constraints (7.9) and (7.10), respectively. The ramp up and ramp down limits of the power plant g are considered in (7.11) and (7.12). If there is a wind farm at bus i, its power generation can be modeled as $P^{w}_{i,t}$ in balance Eq. (7.2).

$$P^{g,\min}_{i} \le P^{g}_{i,t} \le P^{g,\max}_{i} \tag{7.9}$$

$$Q^{g,\min}_{i} \le Q^{g}_{i,t} \le Q^{g,\max}_{i} \tag{7.10}$$

$$P^{g}_{i,t} - P^{g}_{i,t-1} \le \mathrm{RU}_{g} \tag{7.11}$$

$$P^{g}_{i,t-1} - P^{g}_{i,t} \le \mathrm{RD}_{g} \tag{7.12}$$

7.3 DSM Program

In Fig. 7.2, the grey section represents the initial load level before application of DSM program.

Equation (7.13) calculates the value of the electrical power consumption at bus i and time t in the presence of the demand response scheme. The decision variable $\mathrm{DSM}_{i,\,t}$ is defined to model the increase and decrease of the demand for each bus i. If $\mathrm{DSM}_{i,\,t} = 0$, the demand response programs will not be considered in optimization problem and $P_{i,t} = P^{0}_{i,t}$. If $\mathrm{DSM}_{i,\,t} < 0$, the real power load will be reduced after using DSM strategy. Therefore, $P_{i,t} < P^{0}_{i,t}$, as shown with green bar. At the same manner, if $\mathrm{DSM}_{i,\,t} > 0$, the active power demand of the ith bus will increase at hour t. Hence, $P_{i,t} > P^{0}_{i,t}$, as illustrated in red color.

$$P_{i,t} = P^{0}_{i,t} + \mathrm{DSM}_{i,t}; \quad \forall i \tag{7.13}$$

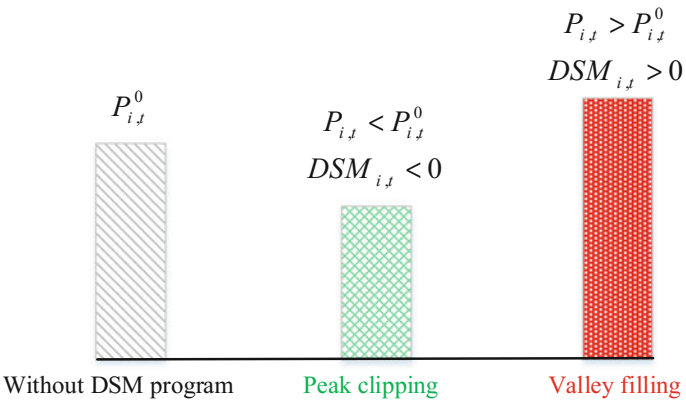

Fig. 7.2 The amount of the active power demand of the bus i at time t without and with impacts of demand response program

Inequality constraint (7.14) is stated to guarantee that although a part of each demand is reduced at some hours, this will be satisfied at other periods. In other words, sum of $DSM_{i,\ t}$ during 24-h time interval should be equal to 0.

$$\sum_{t=1}^{T} \mathrm{DSM}_{i,t} = 0; \quad \forall i \tag{7.14}$$

To avoid from occurring another peak, the value of the shifted demand should be limited as constraint (7.15), in which α represents the maximum percentage of the i^{th} load increase and decrease at hour t. The active power demand increase and decrease are selected as other decision variables. At each scenario, $P_{i,\ t}$ is calculated from (7.13) and inserted in (7.2).

$$-\alpha \times P^0_{i,t} \leq DSM_{i,t} \leq +\alpha \times P^0_{i,t}; \quad \forall i \tag{7.15}$$

7.4 Illustrative Example and Discussions

The validation of the proposed DSM-based AC optimal power flow analysis is carried out using general algebraic mathematical modeling system (GAMS) [68]. The MINLP problem (7.1)–(7.15) is solved under the convex over and under envelopes for nonlinear estimation (COUENNE) [68] tool. The IEEE 24-bus standard system [69] is tested in two cases "before applying DSM strategy" and "after using DSM program." Figure 7.3 depicts the single-line diagram of the test system. As obvious from this figure, three-wind farm with 200, 150, and 100 MW generation capacity are connected to buses 8, 19, and 21, respectively. It is supposed that the

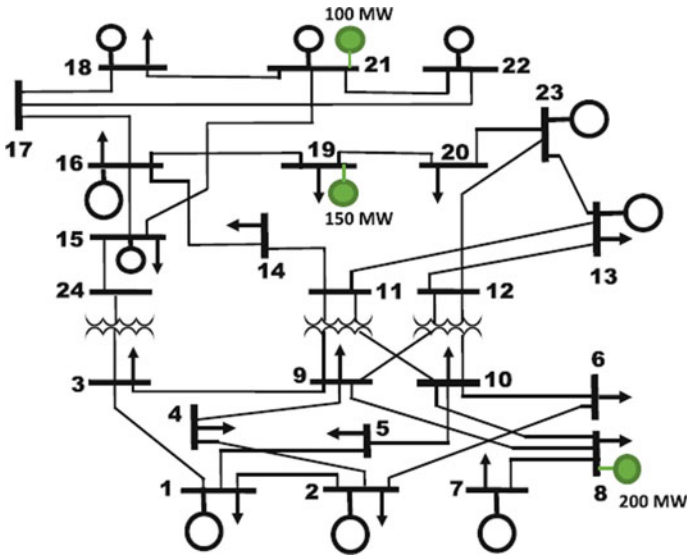

Fig. 7.3 The single-line diagram of the IEEE 24-bus test power system

Table 7.3 The fuel cost factor, ramp up, ramp down, and minimum and maximum limits of active and reactive power generation for each thermal unit g at each bus i [69]

i	b_g	RU_g	RD_g	$P_i^{g,\min}$	$P_i^{g,\max}$	$Q_i^{g,\min}$	$Q_i^{g,\max}$
1	13.32	21	21	30.4	152	−50	192
2	13.32	21	21	30.4	152	−50	192
7	20.7	43	43	75	350	0	300
13	20.93	31	31	206.85	591	0	591
15	21	31	31	66.25	251	−100	215
16	10.52	31	31	54.25	155	−50	155
18	5.47	70	70	100	400	−50	400
21	5.47	70	70	100	400	−50	400
22	0	53	53	0	300	−60	300
23	10.52	31	31	248.5	360	−125	310

maximum percentage of the demand increase and decrease, α, at each bus and hour is equal to 20%. The fuel cost factor, ramp up, ramp down, and minimum and maximum limits of active and reactive power generation for each thermal unit are presented in Table 7.3. The nominal values of the real and reactive loads of each bus i are summarized in Table 7.4. The changes of the wind product and the active and reactive loads in terms of per unit are shown in Fig. 7.4. The resistance and the reactance of the transmission lines are reported in [69]. The lower and upper bounds of the bus voltage limit are equal to 0.9 and 1.1 per unit, respectively. The base power is equal to 100 MVA.

Table 7.4 The nominal values of the real and reactive loads of each bus [69]

i	Active load (MW)	Reactive load (MVAr)
1	108	22
2	97	20
3	180	37
4	74	15
5	71	14
6	136	28
7	125	25
8	171	35
9	175	36
10	195	40
13	265	54
14	194	39
15	317	64
16	100	20
18	333	68
19	181	37
20	128	26

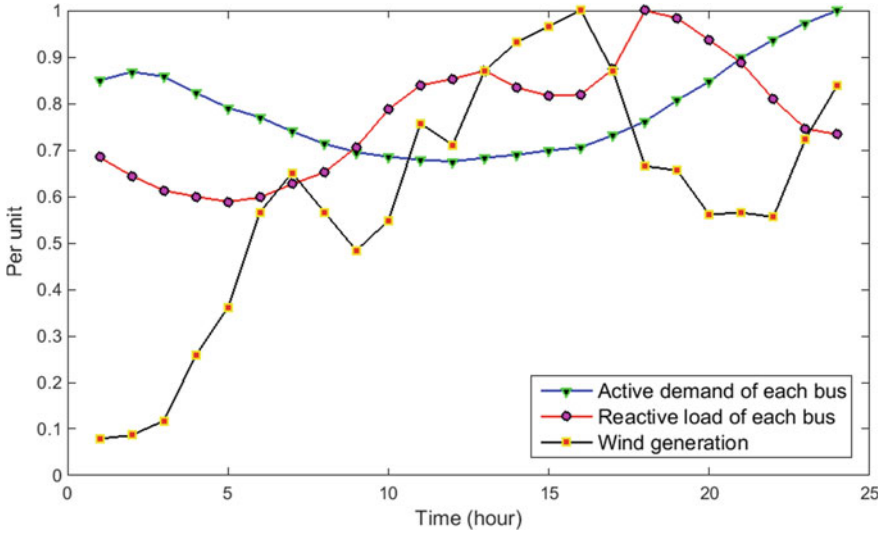

Fig. 7.4 The variable wind power and demands over the sample day

The decision variables of the AC optimal power flow problem are presented as follows: The active and reactive products at nodes 7 and 16 are shown in Figs. 7.5 and 7.6, respectively. It is obvious that the thermal unit 3, which is located at bus 7, generates less active power in case of "after using DSM program" than that of reported for the base case. In addition, the power plant 6, which placed in bus 16, should produce higher real power after implementing DSM strategy, because the

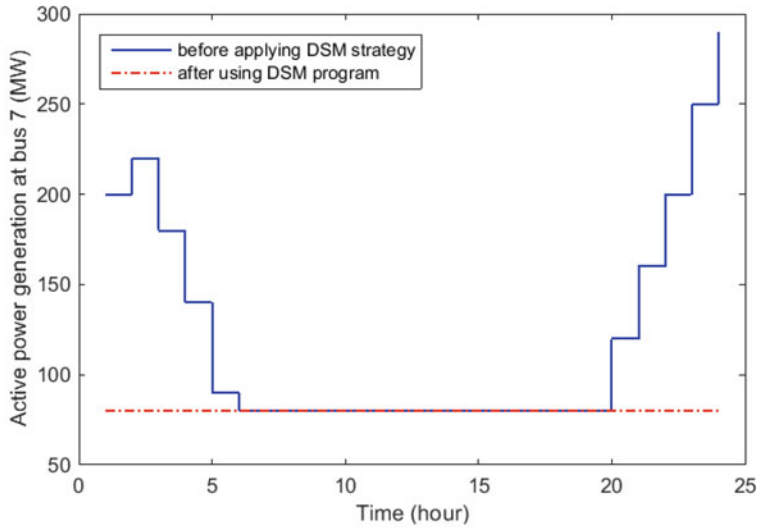

(a)

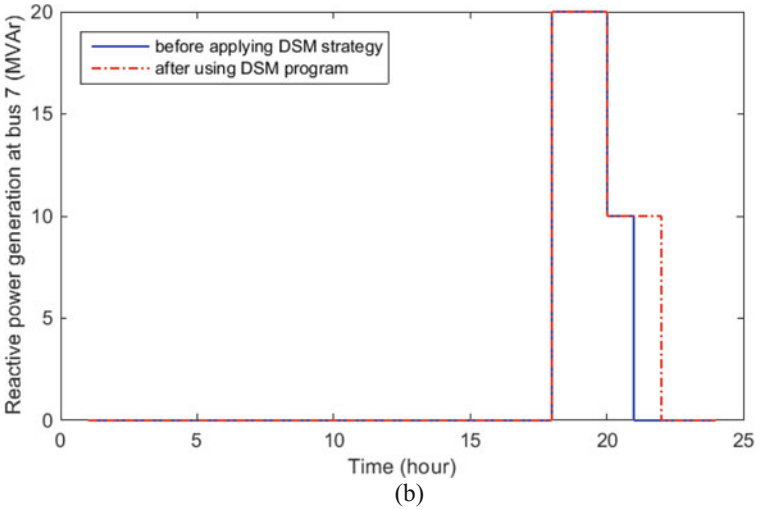

(b)

Fig. 7.5 The active and reactive power generation at bus 7. (**a**) Active power generation. (**b**) Reactive power generation

power generation cost of the unit 3 (20.7 $/MW) is more than the fuel cost factor of the power plant 6 (10.52 $/MW).

For example, the blue line of the Fig. 7.5a shows that without application of real power load management approach, the generated power of the thermal unit 3 is higher than 75 MW at mid and on-peak active power consumption hours (from $t = 1$ to $t = 5$ and $t = 20$ to $t = 24$). But, it is reduced to 75 MW after implementation of

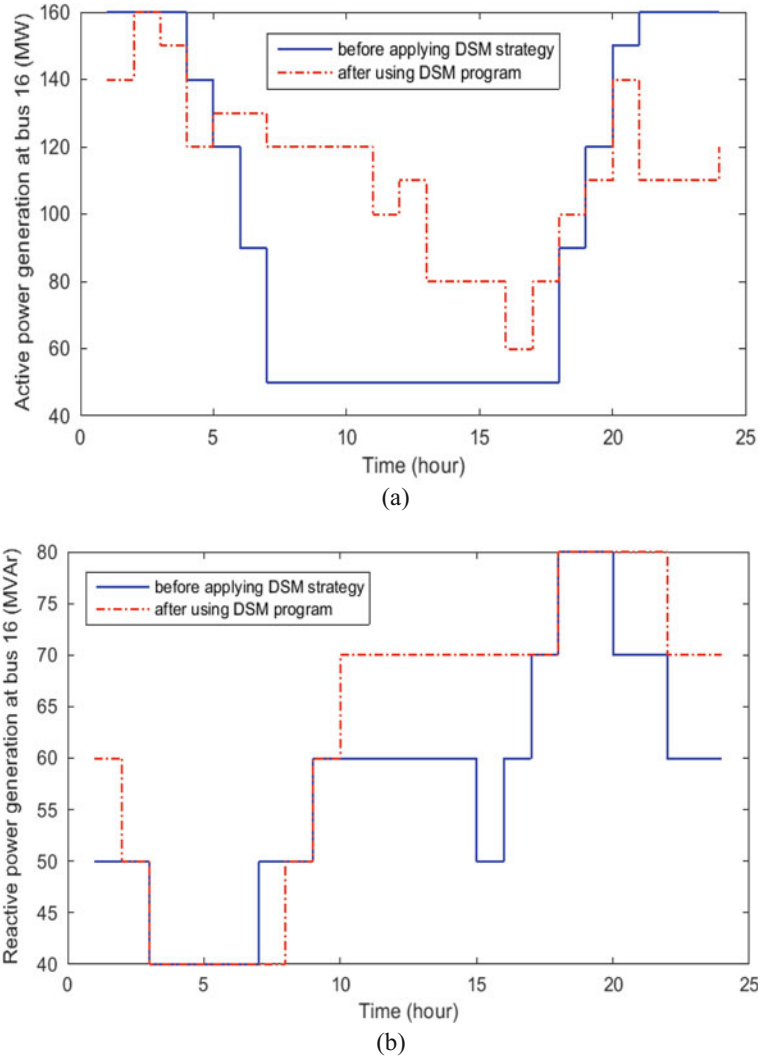

Fig. 7.6 The active and reactive power generation at bus 16. (**a**) Active power generation. (**b**) Reactive power generation

time-amount-based demand response program on AC load flow problem. Additionally, the reactive power production of the generating unit 3 after applying the active demand management polices is similar to that of obtained from solving the base AC optimal power flow problem at all hours except $t = 21$. At this hour, the injected reactive power to the bus 7 increases in the case of "after using DSM program."

Figure 7.6 illustrates the hourly active and reactive power production at bus 16. The blue line represents the power before implementation of DSM strategy. The red one refers the outputs after applying the real power load management scheme. It is

seen that the electrical power produced by the unit 6 during the high-demand hours (from $t = 1$ to $t = 4$ and $t = 19$ to $t = 24$) decreases in the presence of the DSM procedure. In addition, the active power generation of the mentioned unit increases from $t = 5$ to $t = 18$ (off-peak active demand hours). Figure 7.6b proved that by applying the peak shaving and valley filling strategy to the active power consumption, the reactive power injected to the bus 16 will be equal to or higher than that of found in the base AC optimal power flow problem in most hours.

Moreover, it is found that although the DSM program is only applied on the active power demand of the load buses, the reactive power generation pattern of the units is also changed in the presence of this strategy, because as expected from (7.2), if the active power consumption at both or one of buses i and j are changed, the active and reactive power flows in transmission line i to j will vary, as seen in Fig. 7.7. Therefore, their voltage magnitudes will also change as depicted in Figs. 7.8 and 7.9. In Figs. 7.8 and 7.9, the voltage magnitude of two selected buses are compared in two cases. It is proved that the voltage profile at nodes 16 and 21 are improved while applying DSM polices on active loads. As expected from equality constraints (7.2) and (7.3), if the value of the active power consumption is controlled at bus 16, the reactive power produced by the thermal unit 6 and transmitted to node 19 will optimally change in a way that a significant reduction in objective cost function and improvement in bus voltage magnitude are resulted as shown in Figs. 7.8 and 7.9.

The positive and negative variations of the real power demands of the buses 8, 13, and 16 obtained from solving the DSM-based AC optimal power flow problem (7.1)–(7.15) are displayed in Fig. 7.10. The positive side of the load change curve demonstrates the load increase. In the same manner, the negative part represents the load decrease at each hour. If the mentioned changes at real power demands of the loads cause the operation cost of the power generation stations reduces from \$446,701 to \$418,377. In other words, the time-value-based demand response program results in \$28,324 cost saving during the sample day. Figures 7.7 and 7.9 demonstrate that after application of DSM program, the reactive power flowing from bus 16 to node 19 is reduced. But, the value of the reactive power injected from node 16 to bus 21 increases, which results an increase in voltage magnitude of node 21.

7.5 Conclusion and Future Works

In the presented chapter, the demand response program was incorporated in AC power flow problem. The operation cost of the interconnected power system was selected as the objective function and minimized over the 24-h time period. The GAMS software was employed for solving the MINLP to find the active and reactive power productions of the thermal power plants, the bus voltage magnitude and angle, the real and reactive power flows of the transmission lines, the magnitude and phase of the current flowing through the branches, and the hourly changes of the active power demands of the load buses. The ramp up/down rate limits, the

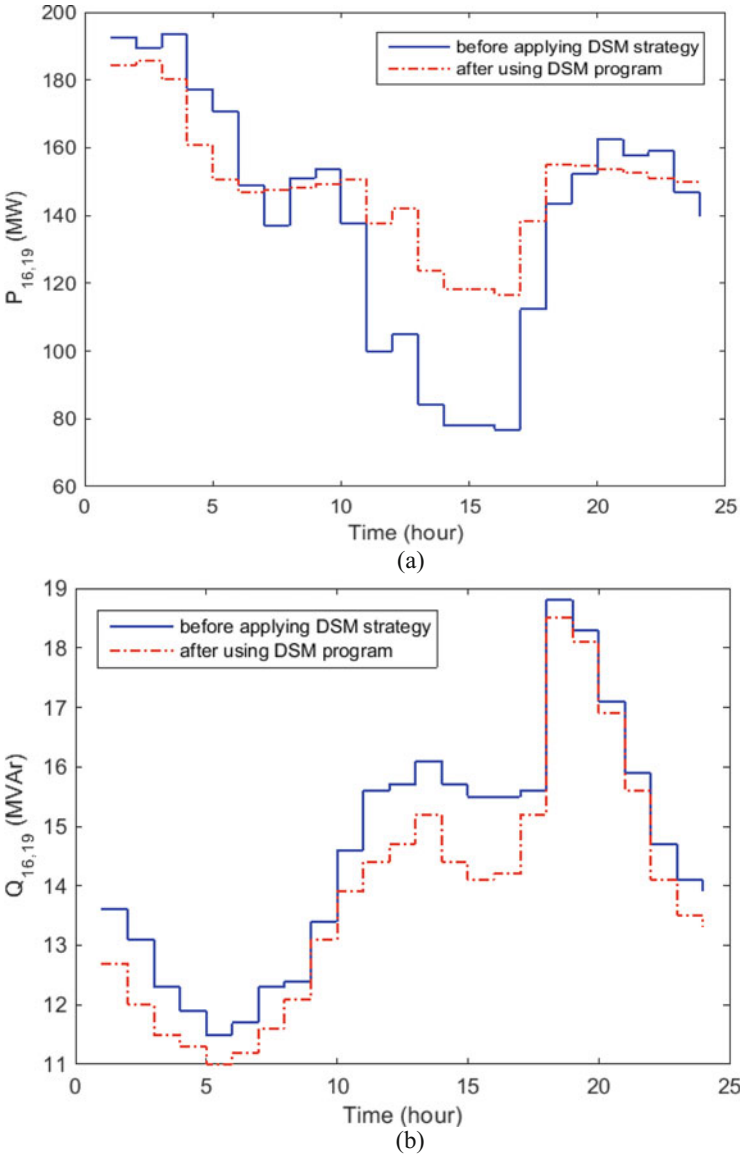

Fig. 7.7 The power flowing through the transmission line between nodes 16 and 19. (**a**) Active power flow in line 16–19. (**b**) Reactive power flow in transmission line 16–19

active/reactive power balance constraint, the transmission power flow calculation and limits, and the bus voltage magnitude bounds were considered in optimal load flow process. It was found that the use of the DSM program results in $28,324 cost saving in 24-h operation interval. The DSM-based optimal power flow problem can be solved in water-energy hub networks and gas-water-power trigeneration systems.

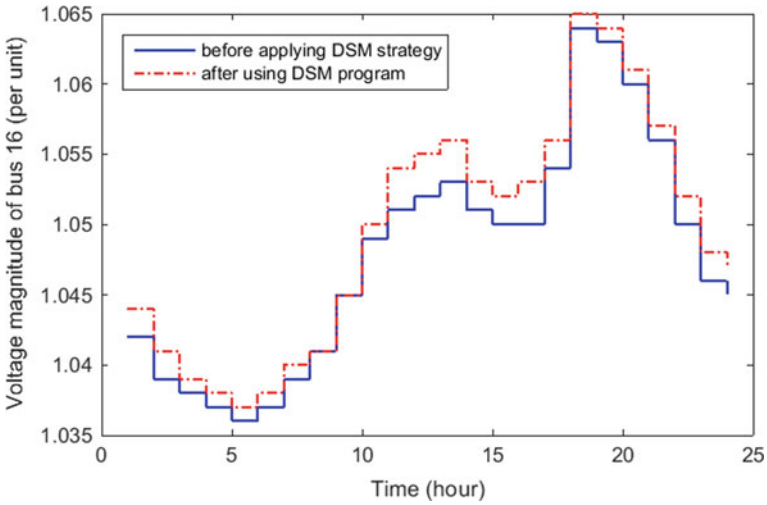

Fig. 7.8 The voltage magnitude of the bus 16

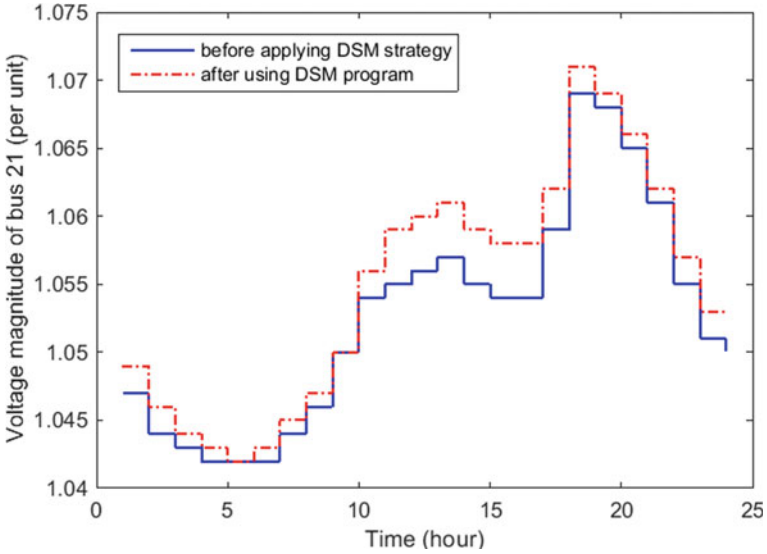

Fig. 7.9 The voltage magnitude of the bus 21

As known, the application of the load shifting strategy changes the best operating points of the combined potable water and power generation units and affects the operation cost of the cogeneration grid. Similarly, the changes in gas demand profile cause the variation of the operation cost of the gas-fired units as well as the gas extraction cost of the gas suppliers.

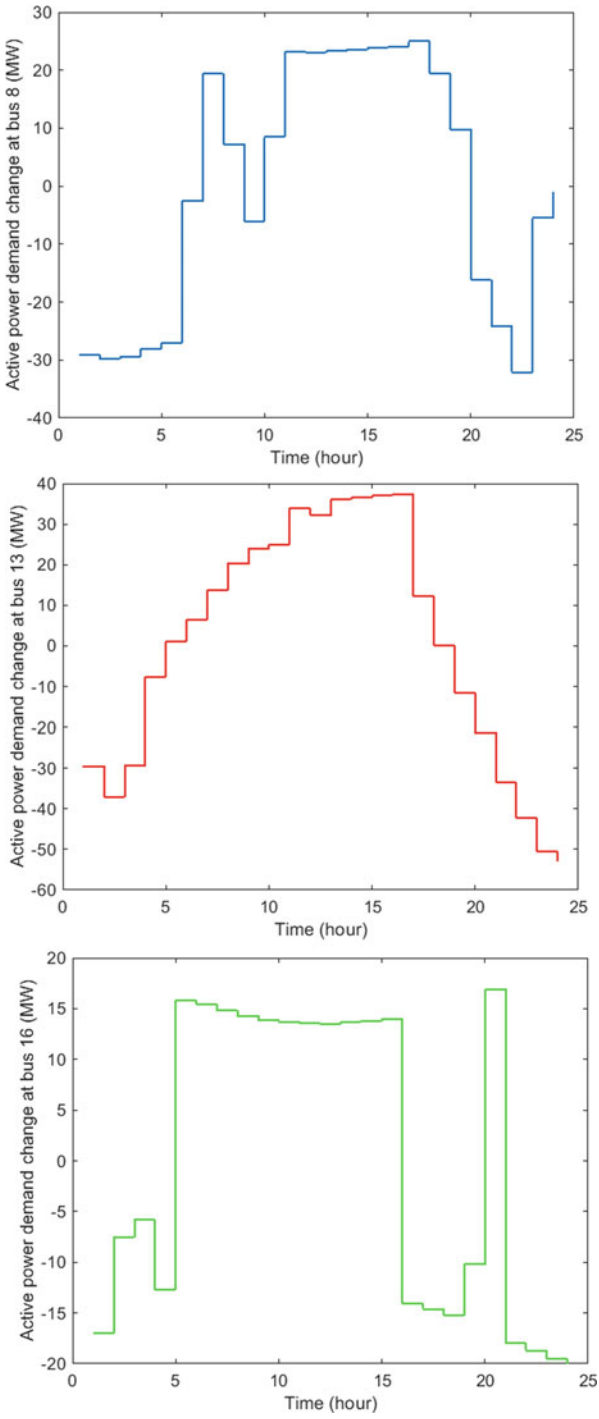

Fig. 7.10 Daily changes of active power demands of buses 8, 13, and 16

References

1. A. Attarha, N. Amjady, A.J. Conejo, Adaptive robust AC optimal power flow considering load and wind power uncertainties. Int. J. Electr. Power Energy Syst. **96**, 132–142 (2018)
2. E. Dall'Anese, A. Simonetto, Optimal power flow pursuit. IEEE Tran. Smart Grid **9**(2), 942–952 (2018)
3. F. Capitanescu, Critical review of recent advances and further developments needed in AC optimal power flow. Electr. Power Syst. Res. **136**, 57–68 (2016)
4. Conforti, D., et al. Optimal load-flow with N-1 steady-state security via high performance computing, in *Electrotechnical Conference,* 1996. *MELECON'96, 8th Mediterranean* (IEEE, 1996)
5. A. Attarha, N. Amjady, Solution of security constrained optimal power flow for large-scale power systems by convex transformation techniques and Taylor series. IET Gener. Transm. Distrib. **10**(4), 889–896 (2016)
6. H. Abdi, S.D. Beigvand, M. La Scala, A review of optimal power flow studies applied to smart grids and microgrids. Renew. Sust. Energ. Rev. **71**, 742–766 (2017)
7. J. Hazra, A. Sinha, A multi-objective optimal power flow using particle swarm optimization. Eur. T. Electr. Power **21**(1), 1028–1045 (2011)
8. N. Amjady, M.R. Ansari, Non-convex security constrained optimal power flow by a new solution method composed of benders decomposition and special ordered sets. Int. Trans. Electr. Energy Syst. **24**(6), 842–857 (2014)
9. P.K. Roy, C. Paul, Optimal power flow using krill herd algorithm. Int. Trans. Electr. Energy Syst. **25**(8), 1397–1419 (2015)
10. H. Sharifzadeh, N. Amjady, Stochastic security-constrained optimal power flow incorporating preventive and corrective actions. Int. Trans. Electr. Energy Syst. **26**(11), 2337–2352 (2016)
11. C. Hamon, M. Perninge, L. Soder, A stochastic optimal power flow problem with stability constraints—Part I: Approximating the stability boundary. IEEE Trans. Power Syst. **28**(2), 1839–1848 (2013)
12. J. Liang et al., Two-level dynamic stochastic optimal power flow control for power systems with intermittent renewable generation. IEEE Trans. Power Syst. **28**(3), 2670–2678 (2013)
13. T. Summers, et al. Stochastic optimal power flow based on convex approximations of chance constraints, in *2014 Power Systems Computation Conference* (IEEE, 2014)
14. T. Yong, R. Lasseter, Stochastic optimal power flow: formulation and solution, in *Power Engineering Society Summer Meeting* (IEEE, 2000)
15. D. Bertsimas et al., Adaptive robust optimization for the security constrained unit commitment problem. IEEE Trans. Power Syst. **28**(1), 52–63 (2013)
16. T. Ding et al., Adjustable robust optimal power flow with the price of robustness for large-scale power systems. IET Gener. Transm. Distrib. **10**(1), 164–174 (2016)
17. F. Jabari et al., Optimal short-term scheduling of a novel tri-generation system in the presence of demand response programs and battery storage system. Energy Convers. Manag. **122**, 95–108 (2016)
18. P. Siano, Demand response and smart grids—a survey. Renew. Sust. Energ. Rev. **30**, 461–478 (2014)
19. M.H. Albadi, E.F. El-Saadany, A summary of demand response in electricity markets. Electr. Power Syst. Res. **78**(11), 1989–1996 (2008)
20. A.R. Jordehi, Optimisation of demand response in electric power systems, a review. Renew. Sust. Energ. Rev. **103**, 308–319 (2019)
21. S. Nojavan, K. Zare, B. Mohammadi-Ivatloo, Selling price determination by electricity retailer in the smart grid under demand side management in the presence of the electrolyser and fuel cell as hydrogen storage system. Int. J. Hydrog. Energy **42**(5), 3294–3308 (2017)
22. P. Aliasghari et al., Optimal scheduling of plug-in electric vehicles and renewable micro-grid in energy and reserve markets considering demand response program. J. Clean. Prod. **186**, 293–303 (2018)

23. M. Rahmani-andebili, Modeling nonlinear incentive-based and price-based demand response programs and implementing on real power markets. Electr. Power Syst. Res. **132**, 115–124 (2016)
24. A. Dolatabadi, B. Mohammadi-Ivatloo, Stochastic risk-constrained scheduling of smart energy hub in the presence of wind power and demand response. Appl. Therm. Eng. **123**, 40–49 (2017)
25. N. Ruiz, I. Cobelo, J. Oyarzabal, A direct load control model for virtual power plant management. IEEE Trans. Power Syst. **24**(2), 959–966 (2009)
26. A. Dorri, et al., *A Secure and Efficient Direct Power Load Control Framework Based on Blockchain,* arXiv preprint arXiv:1812.08497 (2018)
27. H. Aalami, M.P. Moghaddam, G. Yousefi, Demand response modeling considering interruptible/curtailable loads and capacity market programs. Appl. Energy **87**(1), 243–250 (2010)
28. L. Yao, W.H. Lim, Optimal purchase strategy for demand bidding. IEEE Trans. Power Syst. **33** (3), 2754–2762 (2018)
29. J. Iria, F. Soares, M. Matos, Optimal supply and demand bidding strategy for an aggregator of small prosumers. Appl. Energy **213**, 658–669 (2018)
30. P. Yang, G. Tang, A. Nehorai, A game-theoretic approach for optimal time-of-use electricity pricing. IEEE Trans. Power Syst. **28**(2), 884–892 (2013)
31. E. Celebi, J.D. Fuller, Time-of-use pricing in electricity markets under different market structures. IEEE Trans. Power Syst. **27**(3), 1170–1181 (2012)
32. S. Nojavan, B. Mohammadi-Ivatloo, K. Zare, Optimal bidding strategy of electricity retailers using robust optimisation approach considering time-of-use rate demand response programs under market price uncertainties. IET Gener. Transm. Distrib. **9**(4), 328–338 (2015)
33. M. Vahid-Pakdel et al., Stochastic optimization of energy hub operation with consideration of thermal energy market and demand response. Energy Convers. Manag. **145**, 117–128 (2017)
34. S. Nojavan, K. Zare, B. Mohammadi-Ivatloo, Optimal stochastic energy management of retailer based on selling price determination under smart grid environment in the presence of demand response program. Appl. Energy **187**, 449–464 (2017)
35. A.J. Conejo, J.M. Morales, L. Baringo, Real-time demand response model. IEEE Trans. Smart Grid **1**(3), 236–242 (2010)
36. H. Su et al., A systematic data-driven demand side management method for smart natural gas supply systems. Energy Convers. Manag. **185**, 368–383 (2019)
37. R. Kanimozhi, K. Selvi, K.M. Balaji, Multi-objective approach for load shedding based on voltage stability index consideration. Alex. Eng. J. **53**(4), 817–825 (2014)
38. V. Tamilselvan, T. Jayabarathi, A hybrid method for optimal load shedding and improving voltage stability. Ain Shams Eng. J. **7**(1), 223–232 (2016)
39. D. Chattopadhyay, B.B. Chakrabarti, A preventive/corrective model for voltage stability incorporating dynamic load-shedding. Int. J. Electr. Power Energy Syst. **25**(5), 363–376 (2003)
40. S. Chanda, A. De, A multi-objective solution algorithm for optimum utilization of smart grid infrastructure towards social welfare. Int. J. Electr. Power Energy Syst. **58**, 307–318 (2014)
41. S.-Y. Lin, J.-F. Chen, Distributed optimal power flow for smart grid transmission system with renewable energy sources. Energy **56**, 184–192 (2013)
42. T. Erseghe, S. Tomasin, Power flow optimization for smart microgrids by SDP relaxation on linear networks. IEEE Trans. Smart Grid **4**(2), 751–762 (2013)
43. López-Lezama, J., et al. A contingency-based security-constrained optimal power flow model for revealing the marginal cost of a blackout risk-equalizing policy in the colombian electricity market, in *Transmission & Distribution Conference and Exposition: Latin America, 2006. TDC'06* (IEEE/PES, 2006)
44. L.R. de Araujo, D.R.R. Penido, F. de Alcântara Vieira, A multiphase optimal power flow algorithm for unbalanced distribution systems. Int. J. Electr. Power Energy Syst. **53**, 632–642 (2013)
45. Y. Levron, J.M. Guerrero, Y. Beck, Optimal power flow in microgrids with energy storage. IEEE Trans. Power Syst. **28**(3), 3226–3234 (2013)

46. S. Bruno et al., Unbalanced three-phase optimal power flow for smart grids. IEEE Trans. Ind. Electron. **58**(10), 4504–4513 (2011)
47. S. Paudyal, C.A. Cañizares, K. Bhattacharya, Optimal operation of distribution feeders in smart grids. IEEE Trans. Ind. Electron. **58**(10), 4495–4503 (2011)
48. E. Dall'Anese, H. Zhu, G.B. Giannakis, Distributed optimal power flow for smart microgrids. IEEE Trans. Smart Grid **4**(3), 1464–1475 (2013)
49. B. Hayes et al., Optimal power flow for maximizing network benefits from demand-side management. IEEE Trans. Power Syst **29**(4), 1739–1747 (2014)
50. S. Derafshi Beigvand, H. Abdi, Optimal power flow in the smart grid using direct load control program. J. Oper. Autom. Power Eng. **3**(2), 102–115 (2015)
51. T. Sousa et al., A multi-objective optimization of the active and reactive resource scheduling at a distribution level in a smart grid context. Energy **85**, 236–250 (2015)
52. E.R. Sanseverino et al., Optimal power flow in three-phase islanded microgrids with inverter interfaced units. Electr. Power Syst. Res. **123**, 48–56 (2015)
53. E.R. Sanseverino et al., Optimal power flow in islanded microgrids using a simple distributed algorithm. Energies **8**(10), 11493–11514 (2015)
54. M. Hosseinzadeh, F.R. Salmasi, Robust optimal power management system for a hybrid AC/DC micro-grid. IEEE Trans. Sustain. Energy **6**(3), 675–687 (2015)
55. H. Morais et al., Optimal scheduling of a renewable micro-grid in an isolated load area using mixed-integer linear programming. Renew. Energy **35**(1), 151–156 (2010)
56. W. Shi et al., Distributed optimal energy Management in Microgrids. IEEE Trans. Smart Grid **6** (3), 1137–1146 (2015)
57. N. Nikmehr, S.N. Ravadanegh, Optimal power dispatch of multi-microgrids at future smart distribution grids. IEEE Trans. Smart Grid **6**(4), 1648–1657 (2015)
58. S.A. Alavi, A. Ahmadian, M. Aliakbar-Golkar, Optimal probabilistic energy management in a typical micro-grid based-on robust optimization and point estimate method. Energy Convers. Manag. **95**, 314–325 (2015)
59. M.H. Moradi, M. Abedini, S.M. Hosseinian, Optimal operation of autonomous microgrid using HS–GA. Int. J. Electr. Power Energy Syst. **77**, 210–220 (2016)
60. B. Mathiesen et al., The interaction between intermittent renewable energy and the electricity, heating and transport sectors. Energy **48**(2), 2–4 (2012)
61. Z. Ziadi et al., Optimal power scheduling for smart grids considering controllable loads and high penetration of photovoltaic generation. IEEE Trans. Smart Grid **5**(5), 2350–2359 (2014)
62. M. Sechilariu et al., DC microgrid power flow optimization by multi-layer supervision control. Design and experimental validation. Energy Convers. Manage. **82**, 1–10 (2014)
63. M. Sechilariu, B.C. Wang, F. Locment, Supervision control for optimal energy cost management in DC microgrid: design and simulation. Int. J. Electr. Power Energy Syst. **58**, 140–149 (2014)
64. S. Mohammadi, S. Soleymani, B. Mozafari, Scenario-based stochastic operation management of microgrid including wind, photovoltaic, micro-turbine, fuel cell and energy storage devices. Int. J. Electr. Power Energy Syst. **54**, 525–535 (2014)
65. S. Mohammadi, B. Mozafari, S. Solimani, Optimal operation management of microgrids using the point estimate method and firefly algorithm while considering uncertainty. Turkish J. Electr. Eng. Comput. Sci. **22**(3), 735–753 (2014)
66. W.A. Bukhsh, C. Zhang, P. Pinson, An integrated multiperiod OPF model with demand response and renewable generation uncertainty. IEEE Trans. Smart Grid **7**(3), 1495–1503 (2016)
67. S. Magnússon, P.C. Weeraddana, C. Fischione, A distributed approach for the optimal power-flow problem based on ADMM and sequential convex approximations. IEEE Trans. Control Network Syst. **2**(3), 238–253 (2015)
68. https://www.gams.com/latest/docs/S_COUENNE.html
69. A. Soroudi, *Power System Optimization Modeling in GAMS* (Springer, 2017)

Chapter 8
Demand Side Integration in the Operation of LV Smart Grids

Susanna Mocci and Simona Ruggeri

8.1 Introduction

At the end of 2018, the European Commission presented the strategic long-term vision for a prosperous, new, competitive and climate-neutral economy by 2050, with the aim of achieving net-zero greenhouse gas emissions by 2050 through a socially fair transition in a cost-efficient manner [1].

The environmental targets and the 2050 decarbonization roadmap can be reached through an exploitation of renewable energy sources (RES) on a different level (from wind farms to small-scale photovoltaic systems—PV), at the expense of conventional generation (e.g. fossil fuels). Moreover, moving from traditional vehicle which uses fossil fuels and oils to electric-powered vehicles (the so-called e-mobility) could contribute to a reduction in CO_2 emissions. Finally, thanks to the support of communication and measurement systems, also end users could be more actively involved in the integration of renewable energy and in the network operation, modifying their energy demand and providing their flexibility.

For distribution system operators (DSO), this evolution is a challenge, since the planning and operation of distribution networks require significant changes in their approach. Mostly LV networks, usually considered "passive", are not ready for the transition towards the *low-carbon* society. New consumption profiles (e.g. domestic electric vehicles recharge systems, induction cooking systems), characterized by high coincidence factors, and small generation (e.g. photovoltaic, CHP and small wind generators) are undermining the reliability of the system.

Many DSO have begun to investigate on the possibility to "smarten" their networks, in order to identify the necessary costs to achieve a smarter grid. Technology costs are expected to decrease by 2030 with rising levels of R&D

S. Mocci · S. Ruggeri (✉)
Department of Electrical and Electronic Engineering (DIEE),
University of Cagliari, Cagliari, Italy
e-mail: susanna.mocci@unica.it; simona.ruggeri@unica.it

S. Nojavan, K. Zare (eds.), *Demand Response Application in Smart Grids*,
https://doi.org/10.1007/978-3-030-32104-8_8

investments. This trend is expected to continue as technology matures, making low-carbon technologies (LCTs) more affordable and accessible to industries and end customers. Then, further studies of prospective cost data may be helpful to further inform R&D investments.

Smart grid operation could considerably reduce these costs. To limit costly traditional reinforcements, distribution systems need to become more flexible and intelligent so network elements (including storage) and participants (that consume, generate or do both) can be adequately managed.

Although in a nearly past the only answer would be reinforcing and extend the network, such approach could require considerable investment that should be postponed by exploiting the flexibility from the DERs spread in the network. Flexibility can be defined as the change of generated power injection and/or consumption behaviour, in reaction to an external input (e.g. a price signal from the DSO) in order to provide a service to the distribution grid. Particularly, with the aim of exploiting existing LV assets (i.e. secondary substations, transformers and lines/breakers) without reducing the usage of electric energy and the activation of innovative markets open to final consumers, the resort to demand side integration (DSI) policies, with the direct control of customers, is becoming more and more necessary. DSI is recognized as a mean to modify the consumer's load to meet the network constraints. These load profile modifications can spontaneously be implemented by the end users themselves, typically driven by price signals, or be managed by an aggregator, as powerfully recommended in the European Clean Energy Package [1] and in in the European Winter Package [2]. In Literature, several models have been proposed to help the DSO in the management of the network in the presence of a high share of resources. Part of the research focused on the analysis of the single customer and on the analysis of the flexibility that could be reached, examining different behaviours and the load typology, in order to "quantify" their willingness to be adaptable and their flexibility. A part of the research focused its efforts in defining suitable consumption models, through domestic load management systems that considers also the charging/discharging of EV [3–6].

In [3] an energy management strategy is proposed, from the demand side and generation side, in order to meet the electricity demand while minimizing the overall operating and environmental costs. In this methodology, day-ahead and real-time weather forecasting, demand response and model updating are integrated through a receding horizon optimization strategy. In particular, the load demand is properly modelled, considering a residential customer and the appliances installed, supplied by a stand-alone renewable energy generation system, characterized by a wind turbine, a PV generator, a battery and a diesel generator. A DR strategy coupled with a smart charging/discharging strategy of EV and ESS is proposed in [4]. The strategy is developed through a home energy management that performs a mixed integer linear programming (MILP), with the aim of reducing the total daily cost of electricity consumption (i.e. the difference between the energy bought from the network and the energy sold to the system). A smart household operation is proposed also in [5], where the game theory model is applied in order to determine the optimal power and demand bidding of Microgrids (MGs) aggregators that allow achieving

the equilibrium point that can maximize the profit of both aggregators and DSO, which will lead to increase the social welfare of system, taking into account the different objectives in the electricity market.

Since the resources distributed in the network, considered singularly, are often too small to contribute in the system operation, controlled as an aggregation (physically located within a small private network, as a Microgrid, or spread farther on the distribution grid, as a Virtual Power Plant), they can provide the required flexibility for the achievement of the target [7–17]. In the ADDRESS project, the role of the aggregator has been defined [7]. The aggregator is not a new player in the electricity market [8], but in the project its role has been reinforced: it is not only a key mediator between the consumers, the markets and the other power system participants, but also it has a complete overview of its pool of clients. Moreover, the aggregator provides the technical knowledge, including a hardware and software solution, to aggregate individual loads into a larger pool and to offer the energy into the market, monitor the performance of each asset in real time, and control the assets in a way that delivers a reliable product that can be sold into the power market.

In the field of the aggregation of the resources, different techniques and models have been proposed. In [9, 10], the authors propose centralized approach, based on DR programs (incentive-based and critical peak pricing, respectively) with the aim of encouraging the customers to modify their behaviour, when requested by the DSO, in order to flatten the load profile as well as to postpone the investments and reinforcements of network. Moreover, in order to increase the efficiency and the resiliency of linked MGs, the configuration of the network is changed using section switches and tie switches. In [11], a paradigm for energy hubs that combine distributed energy supply/combined cooling heating and power, renewable energy and energy storage is designed with the objective of minimizing prosumer's cost of electricity and natural gas and the cost of GHG emission during different time periods. In [12], in the European projects *Microgrid* and *MoreMicrogrid*, MAS are used for the control of MG. MAS are proposed for LV system's control and for the optimal scheduling EV charging, in order to avoid its negative impact on network's voltage profile [13–17]. In [13], a distributed multi-agent approach is developed for the EV charging control, based on the Nash certainty equivalence principle. The proposed EV management system allows ensuring the efficient operation of the network and satisfying the energy demand of a large number of EVs, taking into account their owner's preferences. In [14], a MAS approach for the optimal schedule of EV charging is presented. The strategy permits to fill the valleys in electric load profiles but does not provide other services to the network. In [15], the authors compare two classes of EV charging coordination (the first based on quadratic programming and the second on market-based MAS) based on power quality analysis. The aim of the strategy is to reduce the peak load and the load variability in a distribution network; however the voltage profile is not optimized by the MAS. A MAS architecture based on MATLAB/JAVA/JADE for smart home energy management is proposed in [16]. The proposed strategy, starting from customers' preferences, is to furnish services to the distribution system. In [17], a hierarchical MAS for the DER management is presented, using a platform developed in

MATLAB and ZEUS. The MAS is characterized by different layers in which different types of agents act (e.g. the decision maker agent, the zone agent responsible of the DER available in its zone, the load agent and the DG agent).

In the chapter, in opposition to the most common energy management systems (EMS) that are centralized, a decentralized control system for LV active distribution network is described. The proposed model exploits the MAS technology for the control of LV networks following specific DSO requests. The agents perform a day-ahead optimization taking into account local targets (e.g. minimize the cost of the EV charging) and global objective (offering service to the network, avoiding voltage contingencies in the network as required by the DSO). The optimization process is based on the Nash Game theory guided by a virtual cost function that avoids the creation of new contingencies in the network.

The chapter is organized as follows. In Sect. 8.2, DERs and the services they could offer, managed by an aggregator, are described. In Sect. 8.3, the strategies and methodologies that could be used to manage DERs are proposed. In particular, the MAS approach developed is described, analysing the optimization process. In Sect. 8.4, the strength of the proposed methodology is validated through some study cases, considering realistic LV distribution networks. Finally, in Sect. 8.5, some concluding remarks are reported.

8.2 Distributed Energy Resources (DERs) and Low-Carbon Technologies (LCT)

DERs comprise a number of different technologies (e.g. generators, loads, energy storage systems), characterized by different operational characteristics that should be properly modelled, dispatched and metered in order to exploit their potential in the power system management. In order to avoid critical situations, determined by an uncontrolled exploitation of DERs, suitable management systems, capable to harness their potential reducing the possible drawbacks, have to be developed.

Low-carbon technologies (LCTs) are equipment and infrastructure that support energy efficiency or renewable energy production and use, leading to a reduction of carbon emissions, directly or indirectly. LCTs refer to distributed generation, such as wind and PV; electro-thermal technologies, such as electric heat pumps and micro combined heat and power units; and transport electrification, such as electric vehicles (EVs). New and innovative LCTs help reduce greenhouse gas emissions and create new employment and growth. These technologies are gradually being deployed around Europe.

LCTs that have been installed so far can be divided into two categories, those that are connected to the transmission systems and to the distribution systems. Big wind farms belong to the first category, PV, and small CHP and mini-micro wind turbines to the second. Transmission systems can accommodate generation without any problem, but this is not true for distribution systems, which have weak networks

and limited hosting capacity. Even if it is not possible to plan where new LCTs will be installed, it should be highly advisable that small generation is connected close to customers and with a size that fosters the local consumption of the energy produced, by avoiding the concentration of generation in areas with small demand and the use of distribution systems as transmission networks, with suitable regulation frameworks.

For instance, DERs, if properly managed, provide services to the distribution network, minimizing the negative impact of a massive installation of distributed generation (DG) in the network. In the following, these resources are described underlining their characteristics but also the potential downsides.

8.2.1 Load Flexibility

Historically, loads have been mainly seen as passive devices that consume energy. However, in the last years, thanks to new technologies that allow the remote control of loads (mostly at domestic level), the introduction of smart meters have increased the interest of the load participation in the network management. Moreover, it is expected in the next years a growth of peak and annual energy demand on the networks, caused by heating sector and transport electrification [18].

Regulation should promote small-scale generation and the flexibility of demand with distributed storage devices that are both fundamental to move from the classical load following towards the generation following paradigm, which is more suited to the carbon-free society. By so doing, LV systems—that have started experiencing the burden of new domestic-scale LCTs (e.g. domestic EV recharge systems), new high efficiency domestic appliances, for example, heat pumps and induction cooking systems) and the impact of small generation can be exploited at maximum level.

This situation is leading to an increased interest of domestic customers and small and medium enterprises (attracted from economic incentives or tariffs) in modifying their consumption in order to reduce electricity costs. It may seem that the load flexibility offers a range of promising advantages, but potential downsides must be considered. Such downsides include added complexity (complex contracts with suppliers and the need for additional hardware), privacy concerns (sensitive information should be protected), high investment required (e.g. installation of new equipment), and potential increase in total consumption immediately following the period of demand reduction, which is an issue that requires careful management.

8.2.1.1 Customers' Classification

The active customer, i.e. the customer who participates to the active demand program, can respond to the DSO/aggregator request with three general actions:

1. The customer accepts the request and reduces his consumption during peak periods, without modifying its consumption profile during other periods, accepting a temporary loss of comfort. This response is achieved, for instance, when heaters' thermostat settings or air conditioners are temporarily varied.
2. The customer responds positively to the request, shifting part of his consumption to off-peak periods (e.g. postponing some household activities like washing machine). In this case, the residential customer will bear no loss and will incur no cost while an industrial customer should take into account rescheduling costs to make up for lost services.
3. The customer with DG (the prosumer) may use onsite generation, experiencing no or very little change in its electricity usage pattern; however, from utility prospective, the load demand will change significantly (demand decrease).

8.2.1.2 Willingness of Customers to Make Change

As stated before, an important issue to be tackled is the energy payback, which should appear when the control actions over consumption are released and the devices, whose consumption decreased, are newly activated, leading to an increase in the demand. Such change could cause unexpected problems (e.g. new peaks, voltage drop) on the DSO network. Figure 8.1 shows two different reactions to the AD request. Let assume that, in order to relieve critical congestions, the DSO (or the aggregator) asks the customers to reduce their consumptions (the scheduled load demand is depicted with blue line) by 50% (yellow dashed line). Customer 1 totally agrees with the AD request (green line fully overlaid to the yellow line), while

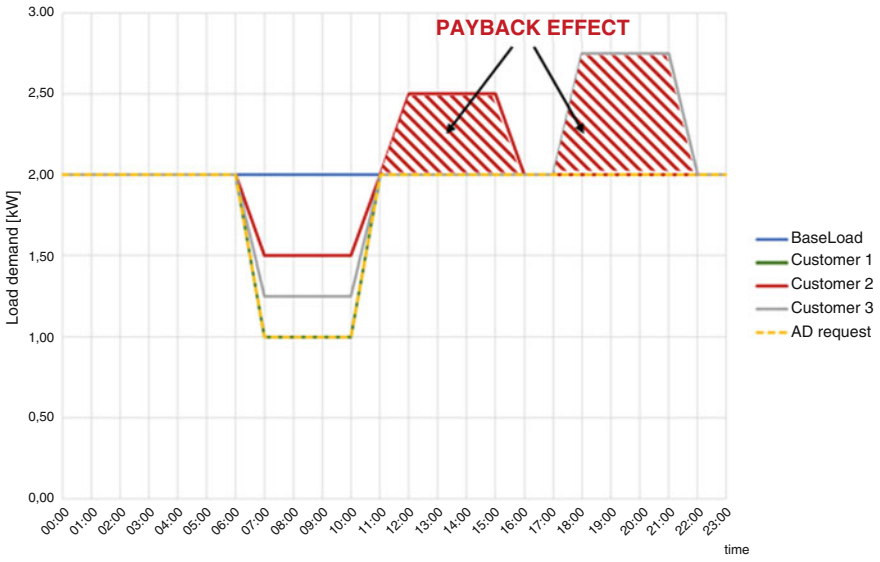

Fig. 8.1 Payback effect

Customer 2 and Customer 3 (respectively, red and grey lines) do not curtail their consumptions of the amount requested and resume part of the demand immediately after the AD measure (Customer 2) or far from it (Customer 3). Such behaviour can be negative for the network, because it could potentially create a new, possibly higher, demand peak and/or introduce imbalances to the electricity market.

Payback Effect Management

For the operation of a distribution system (and for novel planning methodologies), the worth of DSI acceptance cannot be limited to an instantaneous analysis of effects.

For the above-mentioned reasons, it is important to be able to characterize the payback effect, even if it will not probably be possible to remove it.

Depending on the devices that are being controlled, different techniques can be adopted for reducing the payback effect. There are loads whose reconnection can be shifted in time like washing machines, dishwashers, etc. These can be reconnected consecutively in time, in order to reduce the payback peak. Other loads such as those with thermal inertia like heating and cooling can be gradually recovered or even preheating and pre-cooling techniques can be used for reducing the payback effect.

In the ADDRESS project, three alternatives for managing the energy payback effect are proposed, taking into account the role of the aggregator since it knows the behaviour of its portfolio of consumers [7]:

1. If the service is required by the DSO to the aggregator, it could fix at the time of requesting the service the maximum acceptable payback on the network.
2. The TSO/DSO could fix beforehand a limit in the payback effect (that could be dependent on the network node, time of the day and amount of power to be controlled). In such way, the aggregator knows which the payback's limit is and will offer its services accordingly.
3. The DSO/TSO, during technical verification process, checks if the payback lead to issues and informs the TSO/DSO about the power that will be controlled but also about the expected payback. In this case, the aggregator has to minimize the payback, in order for its service to be accepted.

8.2.2 The Energy Storage Systems

The rapid advances in energy storage technology and the growing interest of the industrial world and the scientific community have permitted such devices of reasonable size to be designed and commissioned successfully aiming at balancing any instantaneous mismatch in active power during abnormal operation of the power grid. At LV level, if coupled with PV generators, ESS should be used to maximize the self-consumption of PV production in order to reach the energy independence. Several projects are investigating on this topic, analysing the regulatory

environment, the most suitable technologies and size and test coupled solutions for the consumer in different pilot sites taking into account local parameters for optimization and using efficiency measures [19].

Electric vehicles belong to ESS category. Due to their charging pattern, they are going to impact on the distribution network, in terms of voltage dips and overcurrent. For this reason, it is important to find a suitable charging strategy in order to avoid stress condition on the LV network and maximize their benefits, giving support to the network.

8.2.3 Distributed Generation

Small-scale generating technologies (from renewable energy sources, or not) connected to the MV-LV level may determine technical and economic benefits (relieve contingencies, deferred investments for upgrades of facilities, reduced emissions of pollutants) but also create technical and safety problems like increasing fault currents, causing voltage oscillations. Generation from renewable sources like wind or PV cannot be controlled but it depends by the availability of the primary sources. However, the presence of smart inverters, with embedded communications and local intelligence to ensure that these functions are coordinated with distribution system operations and enabled only when appropriate to do so, allowing the management of the energy produced. Similar to PV with smart inverters, other distributed generation resources (such as CHP, fuel cells, diesel generators) can be enabled to provide automated or coordinated control to support grid conditions (e.g. reactive supply to achieve voltage control, operating and spinning reserves, network stability services).

8.3 DSI Strategies in LV Smart Distribution Network Operation

8.3.1 Methodologies

8.3.1.1 Distributed Vs. Centralized Control Systems

A first step for the development of a proper management system of the resources spread in the network is the identification of the type of control system to implement. It is recognized that, when a large number of elements are involved in a process, which requires a significant exchange of information between individuals, the centralized control system is not a suitable solution, since it requires computational resources and communication infrastructures, becoming an expensive solution. LV distribution networks fully embody this scheme, because they are characterized by many small entities with a noticeable information exchange among the parts. In

particular, the increasing utilization of EVs, their recharge systems, and small integrated generation (mostly photovoltaic) will cause contingencies like voltage limits violation and power flow congestions.

On the contrary, decentralized control systems are more suitable for a so-configured system, because the optimization problems can be performed at local level, resorting to a low exchange of information among the aggregator and the customers, with most of decisions made at customers level.

8.3.1.2 Multi-Agent System Approach

Decentralized control systems can be developed basing on different methodologies. One of the most promising techniques, used in several applications including diagnostics, power system restoration, market simulation, network control and automation [20], is the multi-agent system (MAS). MAS is a system composed of two or more agents with local goals corresponding to subparts of the object designed.

The agent is a software (or hardware), situated in some environment and able to react autonomously to changes in that environment (Fig. 8.2) [21]. Such intelligence is due to different characteristics:

1. Reactivity: the agent has the capacity to react to changes in its environment in a timely fashion, and it is capable to take actions based on those changes and the function it is designed to achieve.
2. Pro-activeness: the agent is goal-directed; it will dynamically change its behaviour in order to achieve its goals, "taking the initiative" [21].
3. Social ability: the agent is not a mean to exchange data between different software and hardware entities, but it has the ability to interact and negotiate in a cooperative manner with other agents, using an agent communication language (ACL), which allows agents to converse rather than simply pass data.

The above-mentioned characteristics of MAS make this system suitable for the operation of LV systems with distributed energy resources DER, developing a system that allows the direct control of customers for DSI policies. In this way it is possible to exploit existing LV assets (i.e. secondary substations, transformers and circuits) without limiting the electric energy consumption and the activation of new markets open to final consumers, which is becoming more and more necessary.

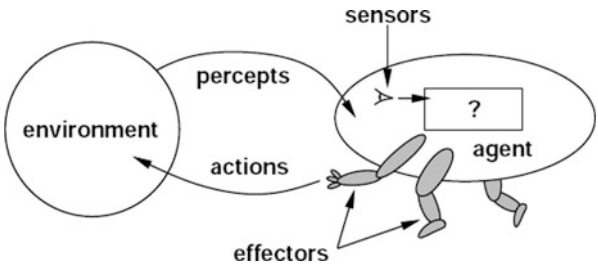

Fig. 8.2 Representation of an Intelligent Agent [38]

8.3.2 The Proposed MAS

The proposed MAS realizes a decentralized control system with a master-slave interaction that permits to find a global optimum without a direct control of each resource. The autonomous agents exchange information about the state of the system and develop strategies that enable the achievement of local and global objectives. In the proposed control system, the agents communicate directly with the master agent (MA), through a vertical communication, without exchange of information between the agents.

The MA broadcasts the data necessary for the agents to perform the local optimizations, gathers the results and requires new optimizations until an optimal and stable solution is reached. In order to achieve the global objective (i.e. an optimal DSI strategy by improving the voltage profile), each agent looks for the minimum of an OF, based on local information and on the average behaviour of the other agents in the system.

The MAS control system is developed with JADE (Java Agent Development Framework), an open source software framework, fully implemented in Java language, which allows the implementation of multi-agent systems through a middleware that complies with the FIPA specifications [22–24]. The communication among the agents (showed in Fig. 8.3) is made possible through three elements: (1) the agent management services (AMS) (i.e., the platform authority that gives the

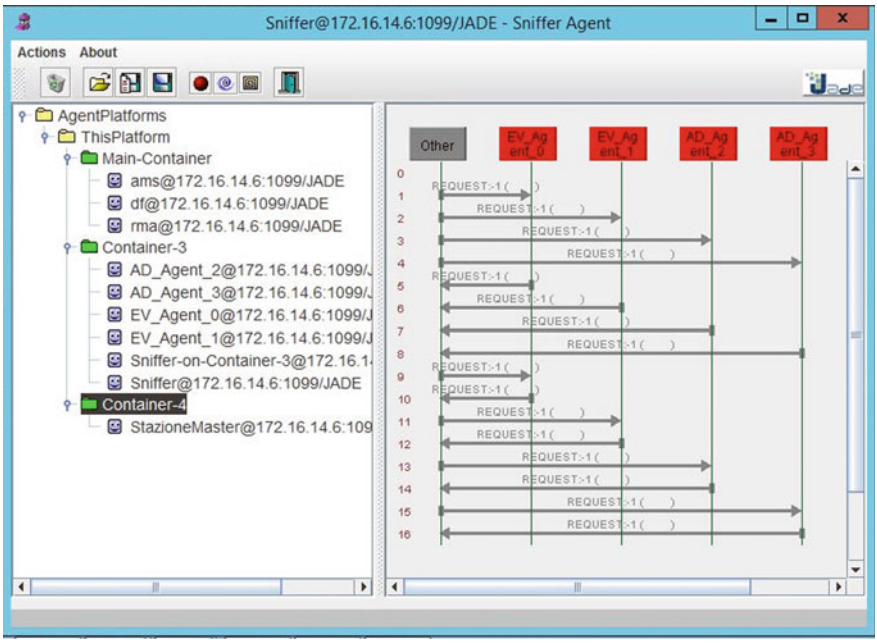

Fig. 8.3 The Sniffer Agent for messages between Master and Slaves

naming service); (2) the directory facilitator (DF), which acts as a yellow page service; and (3) the message transport system (MTS), responsible for delivering messages among agents. In order to simulate different agents located in different places, JADE allows creating an agent platform (indicated in Fig. 8.3) distributed across machines (identified as containers) to simulate. Moreover, it provides the ontologies (vocabulary and semantics for the content of the messages exchanged between the agents) support.

Figure 8.3 shows the communication among four agents (located on Container 3) and the master agent (located in Container 4), while on the Main Container are located the AMS, the DF and the RMA, the remote management agent. Such communication is showed through the sniffer agent (an agent that allows to "investigate" on agents' communication).

In Fig. 8.4 the structure of the control system proposed is presented and the software used for the implementation is shown.

The network model is simulated through the load flow calculations performed through OpenDSS, the electric power Distribution System Simulator developed by EPRI [25, 26]. NetBeans, a JAVA compiler, is used to implement the multi-agent system in the JADE environment. Once the starting data are known (i.e. the network parameters, the characteristics and needs of the DERs involved in the optimization process) and the initialization process is completed, the external iterative optimization process managed by the MA begins. The MA sends agents a message to start local optimization and provides them the virtual price and the tracking parameter.

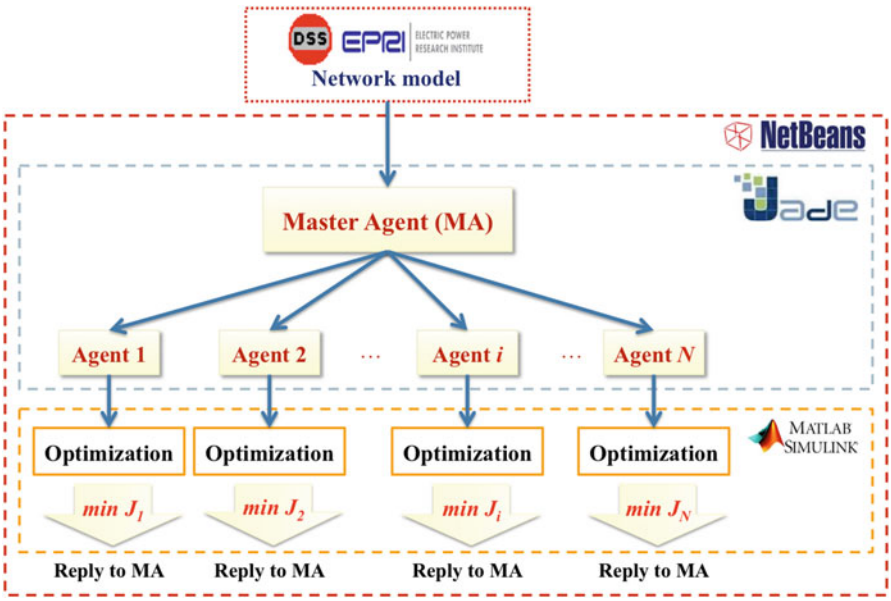

Fig. 8.4 Structure of the control system proposed

Each agent performs its own mono-dimensional optimization, by running a session of MATLAB. Once all agents have completed their local optimization, the strategy (e.g. charging/discharging strategy or the load profile) is returned to the MA that decides whether to accept or reject the programs and to repeat the algorithm varying the load profile, according to the strategies presented.

8.3.2.1 The Optimization Algorithm

The MAS optimization is performed through a weakly coupled game methodology, in which the agents know their own dynamics (i.e. maximum availability rate for the increase/reduction of load), the energy price and the average state of all other agents ("mass" behaviour). Therefore, each agent optimizes the local OF by using local information regarding its state and global information (i.e. the pricing strategy, the average behaviour of the other agents and the technical constraints) [27]. The DSI strategy depends on the virtual cost, $p(t, P_t)$, expressed by Eq. (8.1) [27]. Such cost is a linear function of the ratio between the total demand (the scheduled load demand and the demand of EVs, active loads and ESS) and the nominal power of the MV/LV transformer. The formulation of the virtual cost implies that the highest virtual prices occur at peak hours [28].

$$p(t, P_t) = f\left(\frac{D(t) + \sum_{i=1}^{N} \left(P_{\mathrm{EV},i}(t) + P_{\mathrm{AD},i}(t) + P_{\mathrm{ESS},i}(t)\right)}{P_{\mathrm{tr}}}\right) \tag{8.1}$$

$$P_t(t) = \sum_{i=1}^{N} P_i(t) = \sum_{i=1}^{N} \left(P_{\mathrm{EV},i}(t) + P_{\mathrm{AD},i}(t) + P_{\mathrm{ESS},i}(t)\right) \tag{8.2}$$

where

- $D(t)$ is the forecasted demand (excluding the demand of the elements involved in the optimization) of the MV/LV transformer at time t [kW].
- $P_{\mathrm{EV},i}(t)$ is the ith EV charging/discharging power at time t [kW].
- $P_{\mathrm{ESS},i}(t)$ is the ith ESS charging/discharging power at time t [kW].
- $P_{\mathrm{AD},i}(t)$ is the ith AD contribution (power reduction/increase) at time t [kW].
- $P_i(t)$ is the sum of the ith EV charging power at time t and the ith AD contribution (power reduction/increase) at time t [kW].
- P_t includes the total power of the elements involved in the optimization at time t [kW].
- P_{tr} is the nominal power of the MV/LV transformer [kW].
- t is the time interval.
- N is the effective number of agents participating to the MAS control. It is the sum of the EVs and ESS involved in the control system and the loads included in the AD programs.

The MA evaluates (8.1) and (8.2) and sends the value of the virtual cost $p(t, Pt)$ and Pt(t) to the agents that execute a quadratic mono-dimensional constrained optimization problem expressed in Eq. (8.3).

$$\min J_i(P_i, P_{-i}) = \sum_{t=0}^{T-1} \left\{ p(t, P_t) \cdot P_i(t) + \delta [P_i(t) - \text{avg}(P_t)]^2 \right\} \tag{8.3}$$

$$\text{avg}(P_t) = \frac{1}{N} \sum_{i=1}^{N} P_i(t) \tag{8.4}$$

subject to agent-specific technical constraints.

P_i indicates the ith agent power, P_{-i} is the power of other agents (excluding ith agent), avg.(P_t) is the average of the power controlled by Agents, t is the time at the beginning of each interval, T is the final time of the period (i.e. 0:00 a.m.) and δ is a tracking parameter with non-negative constant value [27].

This equation is constituted by two terms [27]. The first term is the virtual cost for purchasing energy from the system; the smaller is this cost, the bigger is the distance from the peak hours. The second term considers the deviations between the agent behaviour and mass behaviour of all agents; this term avoids the risk that all agents by moving far from the peak will form a new undesired peak in another hour. Indeed, each agent tries to maximize its own benefits but the deviation from the mean behaviour is a cost that guides the global optimization to a real (system) minimum. The technical constraints are agent specific and they are deeply described in the relevant sections; the constraints for all agents are linear or linearized with reference to the control variables. A MatLab quadratic optimization function, called "Quadprog" [29], is used to solve the optimization problem. *Quadprog* is capable to solve large-scale and medium-scale quadratic optimization problems, and it is appropriate to find the local minimum of the convex function (8.3). Since each local minimum is not a global minimum for the system, a global optimization is required. This result is achieved through a single-objective, non-cooperative, dynamic game, which converges to Nash equilibrium under the condition of weakly coupled agents. When all the agents have asynchronously performed local constrained optimizations, the feasible load profile is sent to the MA that recalculates (8.2) and (8.3). Equations (8.2) and (8.3) vary significantly in the first iterations and this is a measure of the distance from the global minimum. The smaller the changes between two subsequent iterations, the closer is the global minimum. From a theoretical point of view, this is the convergence to the unique Nash equilibrium. In fact, let us assume that $p(r)$ is continuous on the variable r, where r is the ratio of total demand divided by the nominal power of the MV/LV transformer that corresponds to the variables in Eq. (8.2). Then, it can be proved that the Nash equilibrium exists if $p(r)$ is continuously differentiable and strictly increasing on r, and the tracking parameter δ belongs to the interval defined by Eq. (8.5).

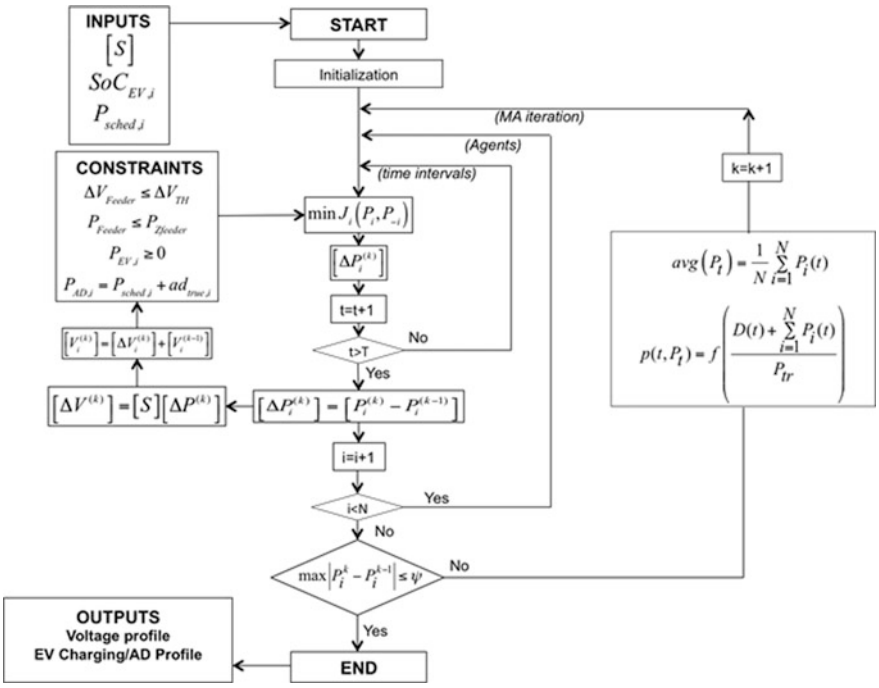

Fig. 8.5 Flowchart of the proposed MAS optimization algorithm [30]

$$\frac{1}{2c}\max_{r\in[r\min,\,r\max]}\frac{dp(r)}{dr}\leq\delta\leq\frac{a}{c}\min_{r\in[r\min,\,r\max]}\frac{dp(r)}{dr} \tag{8.5}$$

where $r_{\min}$ and $r_{\max}$ represent, respectively, the minimum and maximum r over the interval T, subject to the admissible control set, c is the total capacity of the secondary substation and a is a parameter in the range $0.5 \div 1$. Equation (8.5) is a sufficient condition for the convergence, as demonstrated in [28, 30–32].

The proposed MAS algorithm flow chart is depicted in Fig. 8.5. The MA receives the scheduled load and the voltage profile from the aggregator that gathers this information from market and/or DSO in order to participate to service markets. After performing initialization, an iterative optimization process managed by the MA starts ("k" iteration loop).

Once the agents receive the virtual price $p(t, Pt)$ *from the* MA, it starts optimizing the energy profile. Each agent performs the mono-dimensional optimization process described by Eq. (8.3), taking into account the given constraints and $p(t, Pt)$.

The agent's optimal pattern is given back to the MA that updates the requests, once all agents have completed the local optimization. Finally, the MA calculates the maximum load variation with respect to the previous iteration; if such variation is bigger than the acceptable threshold, the data are updated, and a new optimization is performed; otherwise the optimal schedule is found.

8.3.2.2 The Constraints

In the following, the constraints considered in the OF are described. Such constraints represent the inner characteristics of the active element involved in the optimization process and the technical limits of the assets of the network (nodal voltage and current limit).

The ESS and EV Charging Station Agent

For the modellization of this agent, two aspects have been taken into account: (1) the technical characteristics of the battery and the recharging station and (2) the customers' needs. The charging behaviour of the batteries is affected by different factors, such as the type of connection (unidirectional or bidirectional), their charging voltage and current levels, battery status and capacity, charging duration, etc. Thus the optimization problem to be solved by the ESS and EV charging station agents is subject to the constraints (8.6)–(8.8).

$$\mathrm{SOC}_i(T-1) = 1 \tag{8.6}$$

$$\sum_{t=0}^{T-1} P_i(t) = (1 - \mathrm{SOC}_i(t=0)) \cdot \frac{C_{\mathrm{bat}}}{C_{\mathrm{eff}}} \tag{8.7}$$

$$0 \leq P_i(t) \leq P_{\mathrm{plug}} \tag{8.8}$$

where SOC$i(t)$ is the ith battery state of charge at time t, T is the charging period, C_{bat} is the capacity of the battery, C_{eff} is the charging efficiency and P_{plug} is the maximum charging power of the charging infrastructure.

The optimal usage of storage depends not only on instantaneous data but also on the previous and future operation decisions (8.3). For this reason, the energy stored until the time t and the charging (or discharging) strategy proposed by the agent are considered in the optimization process (8.9).

$$\mathrm{SOC}_i(t) = \mathrm{SOC}_i(t=0) + \sum_{t'=t_{\mathrm{in}}}^{t} P_i(t') \tag{8.9}$$

Overcharging/discharging are avoided through inequalities constraints (8.10) and (8.11):

$$\mathrm{SOC}_i(t) \leq \mathrm{SOC}_{i,\max} = k_{i,\max} \cdot E_{i,\mathrm{nom}} \tag{8.10}$$

$$\mathrm{SOC}_i(t) \geq \mathrm{SOC}_{i,\min} = k_{i,\min} \cdot E_{i,\mathrm{nom}} \tag{8.11}$$

where $\mathrm{SOC}_{i,\ \mathrm{min}}$ and $\mathrm{SOC}_{i,\ \mathrm{max}}$ are the ith battery state of charge suggested to avoid battery degradation, respectively, $E_{i,\ \mathrm{nom}}$ is the nominal energy of the ith battery and

$k_{i,\ \max}$ and $k_{i,\ \min}$ are coefficients [0.0 ÷ 1.0]. If required, the EV charging station agent could also implement the vehicle-to-grid model (V2G), taking into account three factors: the current-carrying capacity of the wires connecting the charging station through the building to the grid, the stored energy in the vehicle (divided by the time it is used) and the rated maximum power of the vehicle's power electronics [33, 34].

The travel pattern of the EV vehicles is not directly modelled, but it is taken into account in the optimization process through the SOC of the battery: the initial SOC, which is the SOC when the vehicle is connected to the charging station, and the desired SOC of the battery at departure time. Other parameters considered in the optimization process are the desired charging period (the start and end time of the recharge).

The Active Demand Agent

Following the experiences made by other EU projects, the AD is expressed as a variation of load with respect to the scheduled profile, representing the load without any participation to demand side integration.

In the load model two aspects have been considered:

- **Level of participation of the consumer:** the acceptance model is necessary because every user is willing to modify his consumption profile in different ways. This depends on price signal, but also on available flexibility, willingness to reduce the comfort, etc. In particular the most crucial aspect is the price signal that significantly affects the degree of customer acceptance.
- **Payback effect** (as described in detail in Sect. 8.2.1.2).

Network Constraints

Customers and power system equipment have to operate within a range of voltage (usually ±5% of the nominal voltage). In the proposed methodology, the MA uses demand flexibility to offer system services such as voltage regulation and congestion relieves.

Regarding the constraints on voltage, in order to guarantee that in each feeder the voltage deviation is within the maximum allowed threshold ΔV_{TH} (in the flow chart in Fig. 8.5 constraint $\Delta V_{\mathrm{Feeder}} \leq \Delta V_{\mathrm{TH}}$), the voltage constraint for the Agent i in the network is expressed by Eq. (8.12):

$$\frac{\sum_{m=1}^{n} V_m^{(k-1)} + \sum_{m=1}^{n} \frac{\delta V_m}{\delta P_i} \left(P_i^{(k)} - P_i^{(k-1)} \right) \cdot \mathrm{KC}}{n} \geq (1 - \Delta V_{\mathrm{TH}}) \cdot V_n \qquad (8.12)$$

where

- n is the total number of agents in the same feeder of the ith agent of the LV network.
- m is the internal iteration index ($m = 1, 2, \ldots, n$), considering the voltage contributions of the other agents in the same feeder of agent i.
- k is the external iteration index ($k = 1, 2, \ldots, K$), managed by the master agent until the optimal agent strategy for the network is reached, where K is the iteration in which the stopping criterion is reached.
- $\sum_{m=1}^{n} V_m^{(k-1)}$ is the sum of the voltage in the agent buses [kV].
- $P_i^{(k)}$ is the contribution of the ith agent at the k-iteration [kW].
- $P_i^{(k-1)}$ is the contribution of the ith agent at the $(k-1)$ iteration [kW].
- KC is a coefficient greater than 1.
- ΔV_{TH} is the average variation on voltage admitted by the DSO [kV].
- V_n is the reference value of the voltage [kV].
- $\frac{\partial V_m}{\partial P_i}$ is the *sensitivity coefficient* of nodal voltage m with respect to the P_i injected power $\left[\frac{\mathrm{kV}}{\mathrm{kW}}\right]$.

The sensitivity coefficients are used in the algorithm to linearize the relationship between the nodal voltages and the nodal power injections so that constraints remain linear [28]. Since the aggregator does not know the network status, it is assumed that DSO calculates these coefficients.

The theory of the sensitivity is based on the Newton-Raphson formulation of the load flow calculation to directly assume the voltage sensitivity coefficients as sub-matrices of the inverted Jacobian matrix. This relationship is represented by the following expression (8.13):

$$\begin{bmatrix} [\Delta P] \\ [\Delta Q] \end{bmatrix} = \begin{bmatrix} \left[\frac{\partial P}{\partial \vartheta}\right] & \left[\frac{\partial P}{\partial V}\right] \\ \left[\frac{\partial Q}{\partial \vartheta}\right] & \left[\frac{\partial Q}{\partial V}\right] \end{bmatrix} \cdot \begin{bmatrix} [\Delta \vartheta] \\ [\Delta V] \end{bmatrix} \tag{8.13}$$

where $[\Delta V]$ is the nodal voltages magnitudes and $[\Delta \vartheta]$ is the nodal voltage phase variations corresponding to the nodal active or reactive power injections $[\Delta P]$ $[\Delta Q]$.

The matrix expression can be written as follows (8.14):

$$\begin{bmatrix} [\Delta P] \\ [\Delta Q] \end{bmatrix} = [J] \cdot \begin{bmatrix} [\Delta \vartheta] \\ [\Delta V] \end{bmatrix} \tag{8.14}$$

where $[J] = \begin{bmatrix} \left[\frac{\partial P}{\partial \vartheta}\right] & \left[\frac{\partial P}{\partial V}\right] \\ \left[\frac{\partial Q}{\partial \vartheta}\right] & \left[\frac{\partial Q}{\partial V}\right] \end{bmatrix}$ is the Jacobian matrix.

The sub-matrix $\frac{\partial Q}{\partial V}$ is usually adopted to express voltage variations as a function of reactive power injections when the ratio of longitudinal line resistance versus reactance is negligible. This assumption is not applicable to distribution systems that require in addition to take into account active power injections.

In a distribution system, characterized by N buses, the relationship between the voltage variation and the power injections can be expressed with Eq. (8.15).

$$[\Delta V] = [S] \cdot [\Delta P] \rightarrow \begin{bmatrix} \Delta V_1 \\ M \\ \Delta V_N \end{bmatrix} = \begin{bmatrix} \left[\frac{\partial V_1}{\partial P_1}\right] & K & \left[\frac{\partial V_1}{\partial P_N}\right] \\ M & 0 & M \\ \left[\frac{\partial V_N}{\partial P_1}\right] & K & \left[\frac{\partial V_N}{\partial P_N}\right] \end{bmatrix} \cdot \begin{bmatrix} \Delta P_1 \\ M \\ \Delta P_N \end{bmatrix} \tag{8.15}$$

where S is the sensitivity matrix ($N \times N$), ΔV is the vector of the voltages variations, $\gamma = \frac{\delta V_m}{\delta P_k}$ is the sensitivity coefficient and ΔP is the vector of the variations of power injection [28].

The KC parameter is fundamental since all loads in the network cause voltage variations but, when a single agent performs the local mono-dimensional optimization, the unique control variable is represented by the agents' controlled power, which might be not enough to improve voltage regulation. This is a clear interaction between the local agent optimization and the global goal of the DSI direct control system. The idea is to ask each agent to improve the voltage "pro quota", by assuming that each Agent can be responsible for its rated power capacity. With some algebraic manipulations of the linearized relationship between the agent power and the nodal voltages, this can be expressed with the coefficient KC, which, in the simplest case of equal rated power for all agents, is equal to the number of agents in the feeder.

Regarding the constraints on cable overloading, it has been assumed that the DSO passes the dynamic line rating of cables to the MA and agents use it as a constraint in the local optimization. In the flow chart of Fig. 8.5, the actual consumption of loads in each feeder P_{Feeder} must be within the rating of the feeder, $P_{\text{Feeder}} \leq P_{\text{Zfeeder}}$. The dynamic line rating considers the inelastic demand as well as the positive effect of AD.

Equation (8.16) formalizes the constraint at the kth iteration of the general optimization for the EV agent i and for the EV agent I, respectively,

$$\begin{aligned} P_{\text{EV},i}^{(k)}(t) &\leq \left(P_{\text{zfeeder}} - D_{\text{feeder}}(t) + \sum ad^{(k-1)} + \sum P_{\text{ESS}}^{(k-1)}\right) \cdot \frac{P_{\text{EV max},i}}{\sum_{j=1}^{N_v} P_{\text{EV max},j}} \\ P_{\text{ESS},i}^{(k)}(t) &\leq \left(P_{\text{zfeeder}} - D_{\text{feeder}}(t) + \sum ad^{(k-1)} + \sum P_{\text{EV}}^{(k-1)}\right) \cdot \frac{P_{\text{ESS max},i}}{\sum_{j=1}^{N_s} P_{\text{ESS max},j}} \end{aligned} \tag{8.16}$$

P_{zfeeder} is the dynamic line rating of the feeder, $D_{\text{feeder}}(t)$ is the demand (excluding those related to EVs and ESS) of the feeder, $\sum ad^{(k-1)}$ is the contribution of the AD agents to increase the available power capacity of the feeder and the ratio $\frac{P_{\text{EVmax},i}}{\sum_{j=1}^{Nf} P_{\text{EVmax},j}}$ leaves to EV (or to the ESS) agent the opportunity to use only a quota of the available capacity proportional to the maximum rated power, where $j = 1, 2, \ldots, N_{\text{v}}$ (or N_{s}) is the sum index, N_{v} is the number of EV agents in the feeder and N_{s} is the number of ESS agents in the feeder.

8.3.2.3 Stopping Criterion

The optimal strategy for the network is reached when the global scheduling does not significantly change after two consecutive iterations. For this reason, the stopping criterion of the iterative process is based on a threshold in the maximum variation between the agent power in the last and in the previous iteration in Fig. 8.5 as in (8.17).

$$\max \left| P_i^k - P_i^{k-1} \right| \leq \psi \tag{8.17}$$

where P_i^k is the power of the ith agent at the k-iteration, P_i^{k-1} is the power of the ith agent at the $(k-1)$ iteration and ψ is the threshold selected.

8.4 Application Examples

In the following, some examples of the application of the proposed methodology are proposed, in order to show its effectiveness. In the test cases, the MAS control system has been tested in representative Italian LV distribution networks, in the presence of DER. The representative urban networks used for the case study represent both the typical LV Italian topology (e.g. radial, constituted by four wires (neutral + three conductors)) and the typical load and the generation profiles, defined in the ATLANTIDE project [35, 36]. The DER involved in the optimization process are EV charging station (installed at residential side, with different customers' habits for EV recharging), residential customers that participate to AD programs following a time-based DR program (the price is defined in Eq. (8.1)) and ESS at domestic level. In the studies, in order to simulate real DSI policies, which leave the final customer the possibility to decide at what extent participating to the direct control of demand, each EV owner can override aggregator's suggestion and decide the time for completing the battery recharge and the desired level of SoC. In the studies, the behaviour of EV owners is stochastic, and the arrival and departure time as well as the SoC at arrival and departure (assuming that when the charge is completed the EV owner can leave the house) can be generated randomly.

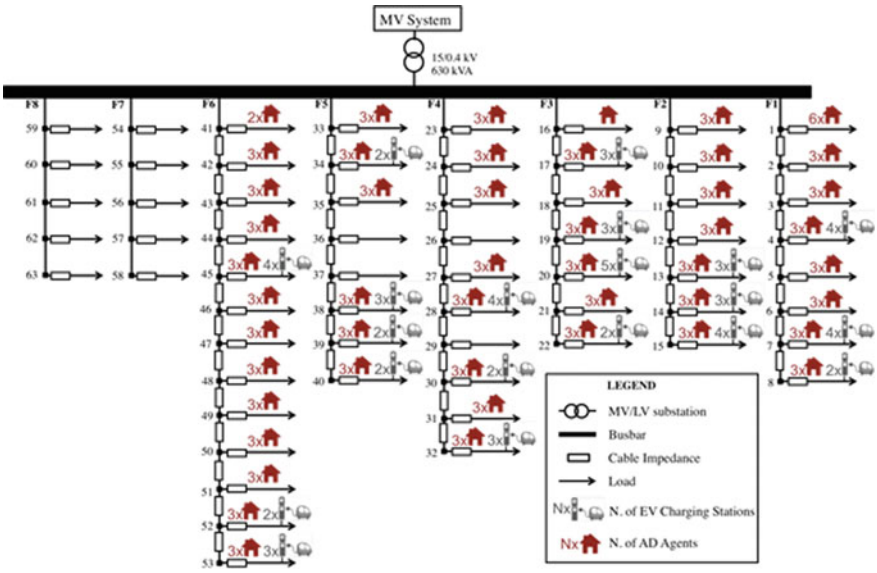

Fig. 8.6 The LV network [21]

8.4.1 MAS Application on EVs and AD in Active LV Networks

In [30], the MAS control system has been tested in an urban area with a plausible penetration of EVs connected to the distribution network. Figure 8.6 shows the LV network, supplied by one MV/LV secondary substation with a 15/0.4 kV 630 kVA transformer. Eight feeders, with 63 LV buses and 193 urban clients (residential, commercial and offices) constitute the network. The loads are both single-phase (175) and three-phase (18). The required average voltage threshold is 0.97 p.u., in order to satisfy the power quality service imposed by DSO ($\Delta V_{TH} = 3\%$).

All the residential loads (147) are involved in DSI through the aggregator, with different participation factors. The AD model parameters, taking into account the customer's level of participation and the payback effect, are $f_0 = 0.55$; $f_1 = 0.4$; and $f_2 = 0.05$.

EV charging stations are connected to the LV nodes as shown in Fig. 8.6, mostly at the end of the feeders in order to stress the studies with the worst scenario. The number of EVs in the test network is 59 (40% of the total residential loads in the AD programs).

In order to better analyse the direct control with the comparison of several cases studies, the arrival and departure times of the EVs have been considered fixed for each one of the two sets of EV (see Table 8.1). Finally, the EV $SoC_{arrival}$ is considered in the study equal to 30%, whereas the desired EV $SoC_{departure}$ is 100% of the total charging capacity, even if those parameters can be custom by each EV owner.

Table 8.1 Arrival and departure time for two different EV sets assumed in the test case

EV set	Number of EVs	% of total EVs	T_{in}	T_{out}
A	41	70	6:00 p.m.	7:00 a.m.
B	18	30	5:00 p.m.	11:00 p.m.

As in previous cases, the time granularity for simulations and for the load profiles is 1 h; the time window is 24 h wide since all simulations are devoted to day-ahead markets.

The results of simulations show that excessive voltage drop, and overloading of system elements can limit the allowable amount of EV charging load.

Different cases have been analysed to show the MAS:

- Case 0: Uncoordinated recharge of the EV batteries (*dumb charging*).
- Case 1: Intelligent recharge with a smart use of battery load profiles (EV SET A).
- Case 2: Intelligent recharge with a smart use of battery load profiles (EV SET B)
- Case 3: intelligent recharge with a smart use of battery load profiles with AD agent contribution in the MAS control.

In Case 0, with the *Dumb charging,* the EVs start charging at the home arrival: the peak load demand rises (Fig. 8.8a) and the voltage may be adversely affected (Fig. 8.8b). Figure 8.8a shows the excessive peak of power demand, which requires the refurbishment of a new transformer in the secondary substation and new conductors with a bigger cross-section to improve voltage regulation and to avoid overloads. Furthermore, by projecting the local situation on a large scale, it is worth to notice that the growth rate of the demand in the evening, when low support can come from renewables, stresses the traditional generation park that cannot follow too fast load rates.

In *Case 1*, when the EVs recharge, the average voltage profiles in the feeders (Fig. 8.7) are marked by an excessive voltage drop, mostly in feeder F3 between 17:00 and 21:30. The MAS direct control cannot succeed since the percentage of EV with late arrival time is significant and there is not enough time to spread the demand on a sufficient number of hours. This means that the coincidence factor cannot be reduced with optimal operation and network investments might be still necessary (i.e. resizing of feeder F3) in order to comply with the EVs request to be fully charged at departure time.

In *Case 2*, the relaxation of the $SoC_{departure}$ for the EV belonging to the Set B in Table 8.1 allows complying with all technical constraints. In this case, the MAS direct control is capable to give a solution only by accepting 80% of $SoC_{departure}$ for the vehicles included in Set B. Figure 8.9a shows that the agents shift EV demand to load profile valleys and limit the growth of demand in evening. The voltage remains within the regulation range (red curve in Fig. 8.9b) and no power congestions appear.

In Case 3, by introducing the AD agent contribution in the MAS control, the EVs can be fully charged. The curves in Fig. 8.10a, b show the positive effect on the

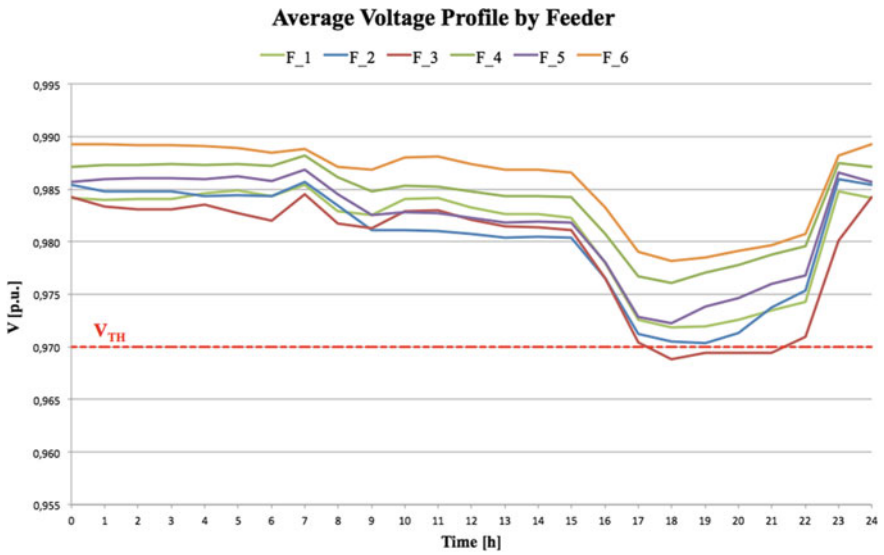

Fig. 8.7 Case 1—Average voltage profiles without AD support ($SOC_{departure}$=100%) [21]

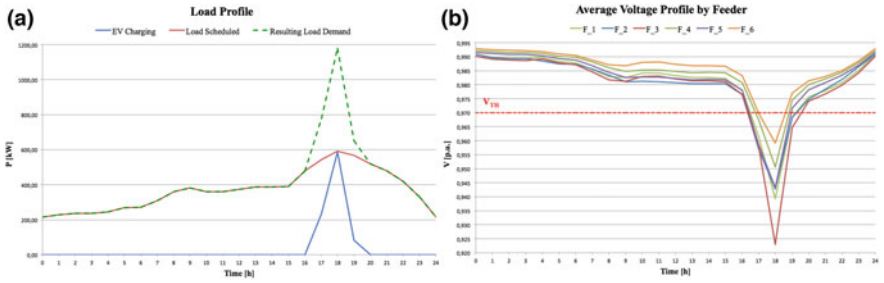

Fig. 8.8 (**a**) Load profiles with dumb charging (case 0). (**b**) Average voltage profiles with dumb charging (case 0) [30]

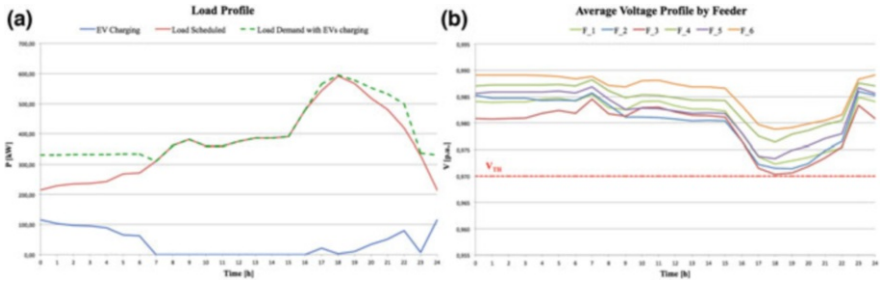

Fig. 8.9 (**a**) Case 2—Load profiles. (**b**) Average voltage profiles without AD support ($SOC_{departure}$ = 80%) [30]

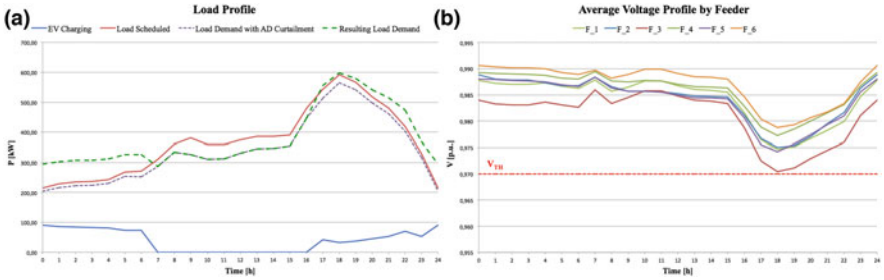

Fig. 8.10 (**a**) Case 3—Load profile with 85% AD ($SOC_{departure} = 100\%$). (**b**) Average voltage profiles by feeder with 85% AD ($SOC_{departure} = 100\%$) [30]

power and voltage profile, respectively. In fact, the reduced demand at the peak hours further improves the voltage profile compared with Case 2, for the benefit of power quality. It is worth to notice that this result is obtained with the participation of 85% of total responsive demand that means a sufficient margin to take into account possible overrides form customers.

Finally, the maximum allowable EV penetration in the test network by considering 100% AD available has been evaluated. By implementing the MAS control, the maximum allowable number of EVs without investment for network reinforcing is 55% of the total residential loads.

8.4.2 MAS Application on ESS and EVs in Active LV Networks

In [34], the proposed methodology has been applied to a portion of an urban Italian distribution network (the radial LV network depicted in Fig. 8.11), with a reasonable penetration of EVs connected to the distribution network. One MV/LV secondary substation with a 15/0.4 kV 630 kVA transformer supplies the test network. The network is constituted by three feeders, with 40 LV buses and 140 urban loads (136 single-phase, 4 three-phase), for a total amount of 489 kW installed. Different daily load curves characterize the 117 residential loads, 22 tertiary loads (commercial, offices, bars, garages, etc.) and 1 public lighting load. The network is characterized by the presence of 111 domestic PV systems and 20 tertiary PV installed in customer side, for a total amount of 620 kW.

As shown in Fig. 8.11, some residential PVs have been considered connected to an ESS, with different power rating (3 kW and 9 kW) for the different needs. The ESS-rated capacity is 10 kWh, the ESS charging efficiency is assumed to be equal to 97% and the discharging efficiency is 94% [34].

In addition, the network hosts 39 EV charging stations (30% of the total demand capacity), with different home arrival and departure times, different SoC of each

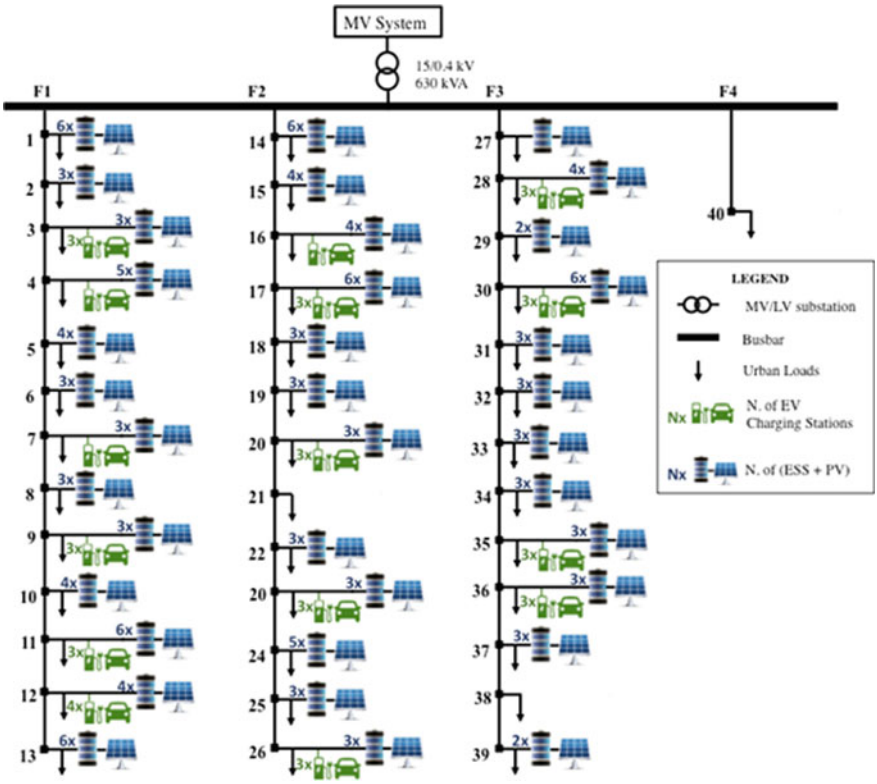

Fig. 8.11 The LV test network [34]

single battery (since different drivers can drive for different distances). The domestic charging stations manage EV charging from 5 p.m. to 9 p.m., while the public ones (garage) considers EV plug-in from 9 p.m. to 7 a.m. The charging and discharging efficiency for the EV batteries are assumed to be both equal to 95%. In order to stress the studies with the worst scenarios, the active elements are connected to the LV nodes as shown in Fig. 8.11. In order to satisfy the PQ service required by the Italian DSO, the average voltage threshold should be equal to 0.95 p.u. ($\Delta V_{TH} = 5\%$).

Different simulations with MAS have been performed, assuming time granularity of 1 hour for both simulations and load and generation profiles. The time window is 24 h.

CASE 0: The results of simulations show that the scheduled load demand (Fig. 8.12) causes voltage drops in the majority of feeders in the test network. In fact, during the evening when people come back home, the load demand increases due to the dumb charging of the EVs. This causes undervoltage exceeding the statutory limit in feeder F1, F2 and F3 (Fig. 8.13). Moreover, due to the presence of PV, small overvoltage occurs in the network during the central hours of the day.

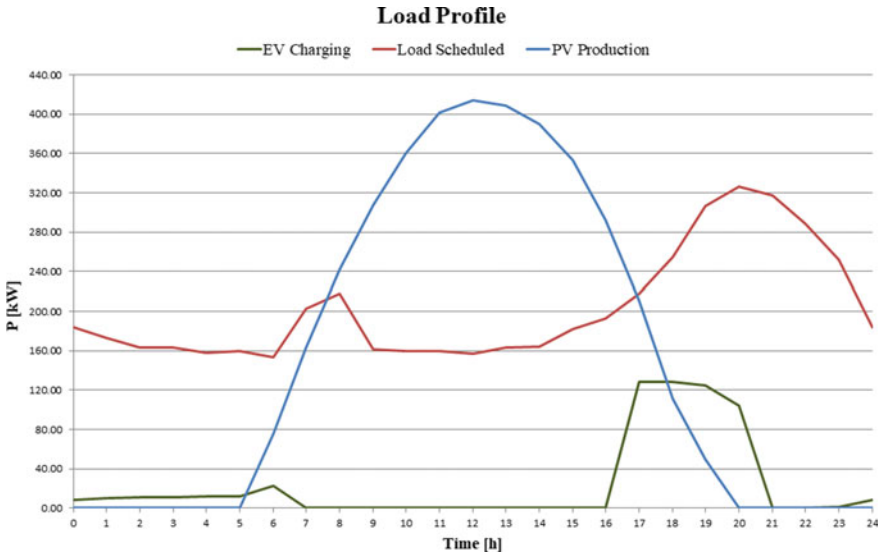

Fig. 8.12 The daily load curves [34]

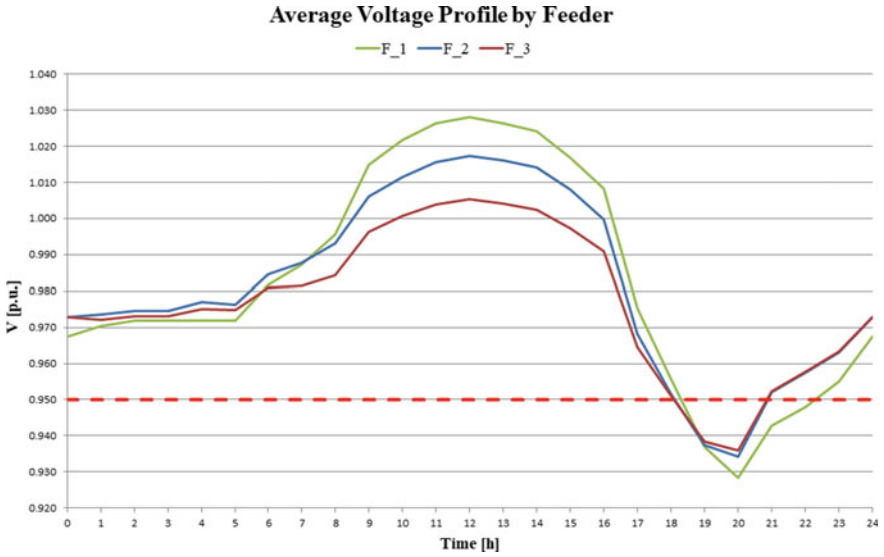

Fig. 8.13 Voltage profile without MAS strategy [34]

CASE 1: If all the EV charging stations in the network are involved in the MAS control strategy, it is not possible to solve the contingencies of the network and undervoltage occurs in some hours of the day, even if the EV recharge is limited to 65% of its full capacity.

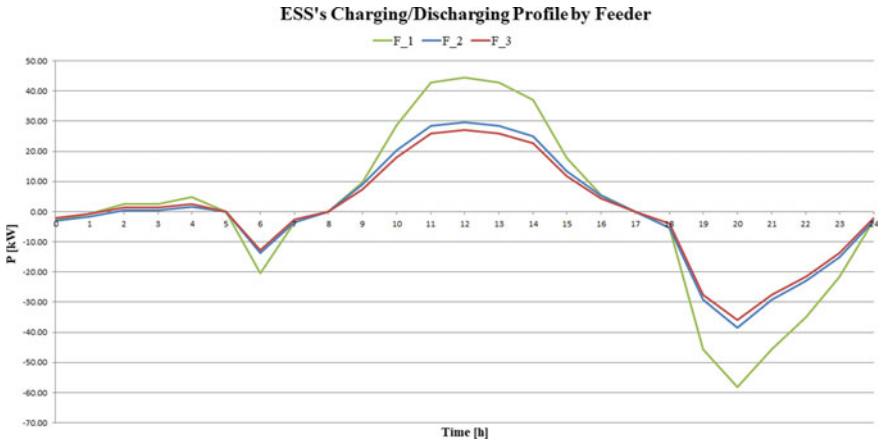

Fig. 8.14 Charging/discharging profile of ESS [34]

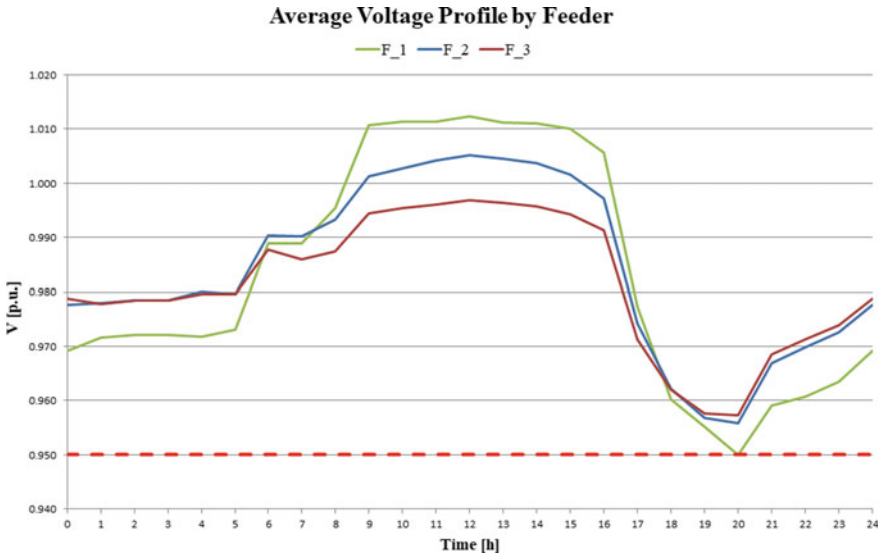

Fig. 8.15 Voltage profile with ESS and EV agents in the MAS strategy [34]

CASE 2: If also the ESS agents connected to PV systems participate to the MAS strategy, the voltage profile is improved. ESSs recharge during the central hours of the day and allow supplying home devices at peak electricity consumption hours (in the evening), reducing the peak demand (Fig. 8.14). Moreover, in Case 2 it is possible to fully recharge the EVs in the network without constraint violations (Fig. 8.15). The same positive results have been obtained by assuming that the aggregator owns the storage, concentrated in the middle and at the end of each feeder, to provide services to the customers included in its portfolio. This could be a good market opportunity in case it will be not economically viable for residential customers to purchase the ESSs.

CASE 3: Finally, by assuming a future scenario with strong incentives for ESS, each PV in the network (residential and garage) has been considered connected to an ESS. Then, the last simulation individuates the maximum percentage of EV that can be fully recharged with a wide distribution of ESS. As a result, the number of EV charging stations that can be integrated in the network thanks to the ESS diffusion and without constraint violations is 65 (50% of the total demand).

8.4.3 *MAS Application on EV for the Exploitation of V2G in Active LV Networks*

In [37], the MAS proposed has been applied to an urban area (representative of urban Italian distribution networks) with a reasonable penetration of EVs connected to the distribution network. The test network is supplied by one MV/LV substation with a 15/0.4 kV 630 kVA transformer (Fig. 8.16). Six feeders, with 53 LV buses and 189 urban loads, constitute the network.

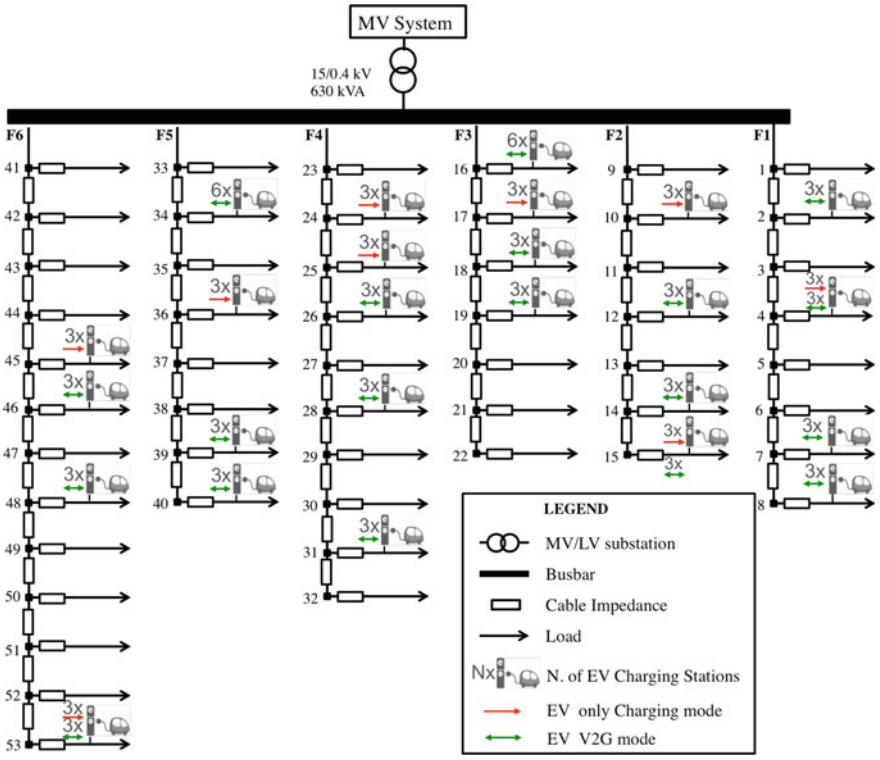

Fig. 8.16 The LV test network [36]

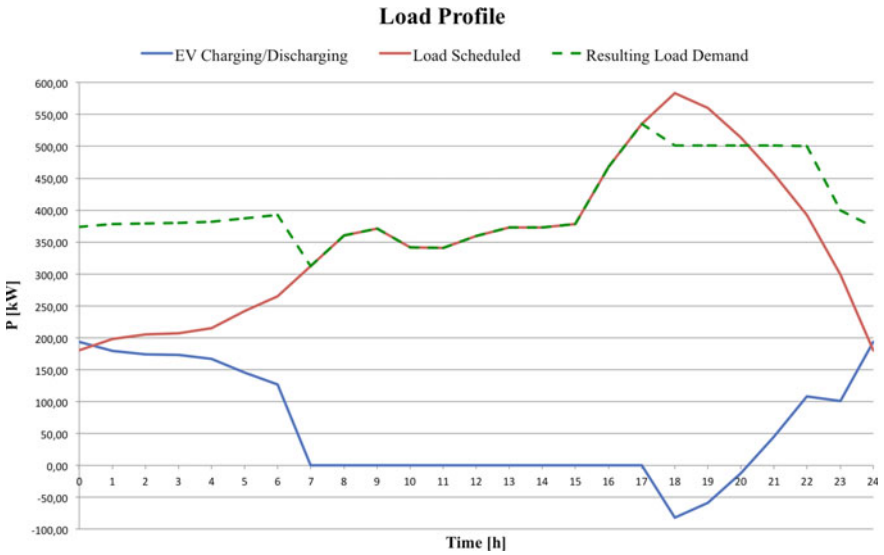

Fig. 8.17 The daily load curve [37]

There are residential loads and tertiary loads, characterized by different daily load curves. The average voltage threshold is required to be equal to 0.95 p.u., in order to satisfy the power quality service imposed by DSO ($\Delta V_{TH} = 5\%$). EV charging stations are connected to the LV nodes as shown in Fig. 8.16. The charging stations involved in the MAS direct control are 90 and manage different owners' needs (charging time and SOC). The percentage of the EVs that adopt the V2G technology is 70%.

The results of simulations show that the scheduled load demand (red line in Fig. 8.17) causes voltage drops in the majority of feeders in the test network (Fig. 8.18) between 6 p.m. and 8 p.m., limiting the allowable amount of EV charging load.

Considering only the charging mode available in the MAS control, the voltage profile is improved in some feeders, but some constraint violations still remain in some feeders because at the peak hours the voltages are already below the threshold, due to conventional loads. As a consequence, the EVs start charging after the desired plug-in time and cannot be fully charged at the plug-out time (11 p.m.). By introducing the charging/discharging strategy in the MAS control (blue line in Fig. 8.17) voltage regulation issues are fixed. Indeed, with V2G the MAS results in charging the EVs during the low demand period (green dashed line in Fig. 8.17), and the average voltage profile by feeder remains within the voltage threshold imposed by the DSO (red dashed line in Fig. 8.19). The MAS reduces the lines and transformer loading in the peak hours (respectively, 20% and 10%) because the EVs enabling V2G contribute through their discharging to reduce power flow, giving an economic alternative to network reinforcement (necessary without V2G).

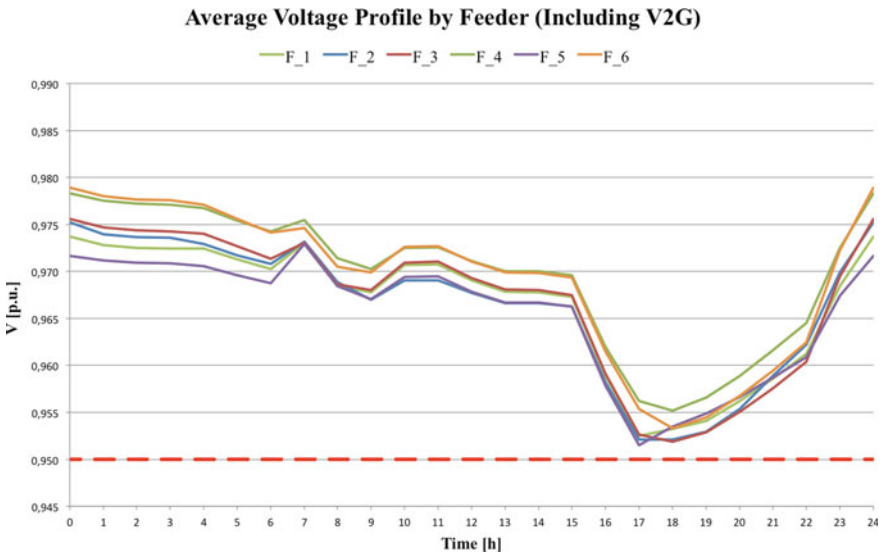

Fig. 8.18 The average voltage profiles by feeder [37]

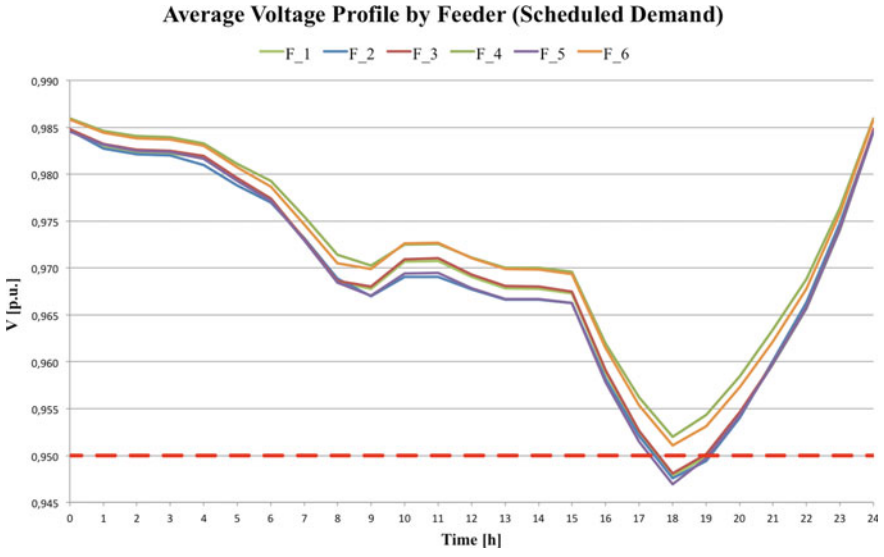

Fig. 8.19 The average voltage profile by feeder with V2G [36]

8.5 Conclusion

In the chapter, the importance of a proper management strategy of DERs (AD, ESS and EV charging station) has been discussed. Such strategy has been developed without the need of complex centralized optimization, but through a decentralized control based on MAS technology, characterized by a master agent (a modern aggregator of the resources spread in the LV distribution network) and several smart agents (responsible for the EV charging stations, domestic ESS and the AD). The agents are capable to optimize their own strategy taking into account global (network constraints like voltage and current limits, energy price) and local constraints (battery's limits, EV owners' needs). Moreover, the strategy proposed allows supporting the network operation (e.g., absorbing the surplus energy produced by PV and supplying energy during peak periods), reducing substation transformers and line loading and increasing hosting capacity and network efficiency.

The effectiveness of the method has been illustrated through simulations on typical Italian distribution networks, which allows showing the possible benefit of the smart strategy proposed.

The possible improvement showed are not possible if not supported by EU directives, national laws and regulation frameworks, which should promote innovation with output-based schemes following the path initiated by countries like Germany, Italy and the UK. New local markets for energy and services, possibly real time or almost real time, will allow distributed resources offering their contribution to adequacy and security.

Therefore, flexible demand must be promoted by eliminating regulatory barriers preventing customers, or aggregators, from using demand response—including ESS management—and taking part in electricity markets on the same level of generators.

Not only regulatory barriers should be removed, also technology improvements are needed.

Research project worldwide underlined the need of suitable and reliable communication infrastructures, which allow a secure exchange of information among the parties involved. Another aspect is related to the need to share the knowledge acquired during the research activity and pilot implementation, in order to guarantee high technical standard to all the parties involved (from utilities to small clients). Finally, users' accessibility should be increased, removing the fear from the end users about cyber-security and possible frauds.

References

1. European Commission, A Clean Planet for All a European Strategic Long-Term Vision for a Prosperous, Modern, Competitive and Climate Neutral Economy, 28/11/2018 [Online]. https://ec.europa.eu/clima/sites/clima/files/docs/pages/com_2018_733_en.pdf Last access: 8/03/2019
2. European Commission, Directive of the European Parliament and of the Council on common rules for the internal market in electricity (COM (2016) 864 final), Brussels, 23/2/2017

3. X. Wang, A. Palazoglu, N.H. El-Farra, Operational optimization and demand response of hybrid renewable energy systems. Appl. Energy **143**, 324–335 (2015)
4. O. Erdinc, N.G. Paterakis, T.D.P. Mendes, A.G. Bakirtzis, J. P. S. Catalão, Smart household operation considering bi-directional EV and ESS utilization by real-time pricing-based DR. IEEE Trans. Smart Grid **6**(3), 1281–1291 (2015)
5. F.S. Gazijahania, J. Salehi, Game theory based profit maximization model for microgrid aggregators with presence of EDRP using information gap decision theory. IEEE Syst. J. **99**, 1–9 (2018)
6. J. Soares, H. Morais, T. Sousa, Z. Vale, P. Faria, Day-ahead resource scheduling including demand response for electric vehicles. IEEE Trans. Smart Grid **4**(1), 596–605 (2013)
7. ADDRESS Project. [Online]. http://www.addressfp7.org/ Last access: 8/03/2019
8. R.J. Bessa, M.A. Matos, The role of an aggregator agent for EV in the electricity market, in *Proceedings of 7th MEDPOWER, Ayia Napa, Cyprus 7–10* November (2010)
9. F. Samadi Gazijahania, J. Salehi, Integrated DR and reconfiguration scheduling for optimal operation of microgrids using Hong's point estimate method. Int. J. Electr. Power Energy Syst. **99**, 481–492 (2018)
10. F. Samadi Gazijahania, J. Salehi, Reliability constrained two-stage optimization of multiple renewable-based microgrids incorporating critical energy peak pricing demand response program using robust optimization approach. Energy **161**, 999–1015 (2018)
11. H. Yang, T. Xiong, J. Qiu, D. Qiu, Z. Yang Dong, Optimal operation of DES/CCHP based regional multi-energy prosumer with demand response. Appl. Energy **167**, 353–365 (2016)
12. A.L. Dimeas, N.D. Hatziargyriou, Operation of a multiagent system for microgrid control. IEEE Trans. Power Systems **20**, 1447 (2005)
13. J.E.L. Karfopoulos, N.D. Hatziargyriou, A multi-agent system for controlled charging of a large population of electric vehicles. IEEE Trans. Power Syst **28**(2), 1196–1204 (2012)
14. L. Gan, U. Topcu, S.H. Low, Optimal decentralized protocol for electric vehicle charging. IEEE Trans. Power Syst. **28**(2), 940 (2013)
15. K. Mets, R. D'hulst, C. Develder, Comparison of intelligent charging algorithms for electric vehicles to reduce peak load and demand variability in a distribution grid. J. Commun. Netw. **14** (6), 672 (2012)
16. B. Asare-Bediako, W.L. Kling, P.F. Ribeiro, Multi-agent system architecture for smart home energy management and optimization, in *4th IEEE PES Innovative Smart Grid Technologies Europe (ISGT Europe), October 6–9, Copenhagen* (2013)
17. M. Biabani, M. A. Golkar, A. Sajadi, Operation of a multi-agent system for load management in smart power distribution system, in *Proceedings of 11th International Conference on Environment and Electrical Engineering (EEEIC), Venice, 18–25 May* (2012)
18. ENTSO-E, ENTSO-G, "TYNDP 2018 Scenario Report: Main Report". [Online]. https://docstore.entsoe.eu/Documents/TYNDP%20documents/TYNDP2018/Scenario_Report_2018_Final.pdf Last access: 8/03/2019
19. StoRES project. [Online]. https://stores.interreg-med.eu/ Last access: 8/03/2019
20. S.D.J. McArthur et al., Multi-agent systems for power engineering applications—Part I: Concepts, approaches, and technical challenges, IEEE Trans. Power Syst. Vol. 22, No. 4, November 2007 1743-1752
21. M. Wooldridge, *An introduction to MultiAgent system* (Wiley, Hoboken, 2002)
22. M. Nikraz, G. Caire, P.A. Bahri, A Methodology for the Analysis and Design of Multi-Agent Systems Using JADE [Online]. http://jade.tilab.com/doc/tutorials/JADE_methodology_website_version.pdf. Last access: 8/03/2019
23. JADE Programmer's Guide. [Online]. http://jade.tilab.com/doc/programmersguide.pdf Last access: 08/03/2019
24. The FIPA website. [Online]. http://www.fipa.org/ Last access: 08/03/2019
25. R.C. Dougan, T.E. McDermott, An open source platform for collaborating on smart grid research, in *2011 IEEE, Power and Energy Society General Meeting* (2011)
26. http://sourceforge.net/projects/electricdss. Last access: 8/03/2019

27. Z. Ma, D. Callaway, I. Hiskens, Decentralised charging control for large population of plug-in electric vehicles, in *Proceedings of 49th IEEE CDC Conference, Yokohama, Japan* (2010)
28. S. Mocci, N. Natale, S. Ruggeri, F. Pilo, Multi-agent control system for increasing hosting capacity in active distribution networks with EV, in *Proceedings of Energycon IEEE International Energy Conference 2014, Dubrovnik, 13–16 May* (2014)
29. Mathworks website [Online]. https://it.mathworks.com/help/optim/ug/quadprog.html. Last access: 08/03/2019
30. S. Mocci, N. Natale, F. Pilo, S. Ruggeri, Demand side integration in LV smart grids with multi-agent control system. Electr. Power Syst. Res. **125**, 23–33 (2015)
31. S. Mocci, N. Natale, F. Pilo, S. Ruggeri, Multi-agent control system to coordinate optimal demand response actions in active distribution networks, in *Proceedings of MEDPOWER 2014, Athens, 2–5 November* (2014)
32. S. Mocci, N. Natale, F. Pilo, S. Ruggeri, Multi-agent control system to coordinate optimal EV charging and demand response actions in active distribution networks, in *Proceedings of 3rd Renewable Power Generation Conference, Naples, 24–25 September* (2014)
33. W. Kempton, J. Tomić, Vehicle to grid power fundamentals: calculating capacity and net revenue. J. Power Sources **144**, 268 (2005)
34. S. Mocci, N. Natale, F. Pilo, S. Ruggeri, Exploiting distributed energy storage to increase network hosting capacity with a multi-agent control system, in *2016 AEIT International Annual Conference* (2016)
35. A. Bracale, R. Caldon, M. Coppo, D. Dal Canto, R. Langella, G. Petretto, F. Pilo, G. Pisano, D. Proto, S. Ruggeri, S. Scalari, R. Turri, Active management of distribution networks with the ATLANTIDE models, in *Proceedings of 8th Mediterranean Conference on Power Generation, Transmission, Distribution and Energy Conversion, MEDPOWER 2012, Cagliari, 1–3 October* (2012)
36. A. Bracale, R. Caldon, G. Celli, M. Coppo, D. Dal Canto, R. Langella, G. Petretto, F. Pilo, G. Pisano, D. Proto, S. Scalari, R. Turri, Analysis of the Italian distribution system evolution through reference networks, in *Proceedings of IEEE PES Innovative Smart Grid Technologies (ISGT) Europe Conference, Berlin, 14–17 Oct* (2012)
37. S. Mocci, N. Natale, F. Pilo, S. Ruggeri, Multi-agent control system for the exploitation of vehicle to grid in active LV networks, in *CIRED Workshop*, *14–15 June* (2016)
38. S. Russell, P. Norvig, Artificial intelligence: a modern approach, Prentice Hall, ISBN D-IH-IQBSOS-E (1995)

Chapter 9
Multi-Objective Optimization Model for Optimal Performance of an Off-Grid Microgrid with Distributed Generation Units in the Presence of Demand Response Program

Afshin Najafi-Ghalelou, Kazem Zare, Sayyad Nojavan, and Mehdi Abapour

Nomenclature

Sets

t Time period

Parameters

$C_{\text{Batt, Ch}}$, $C_{\text{Batt, Dch}}$	Charging and discharging costs of the battery
C_{Ue}, C_{Exe}	Cost of undelivered energy and excess generated energy
C_{WT}, C_{PV}, C_{FC}	Cost of produced power by the wind turbine, photovoltaic panel, and fuel cell unit
$E^{\max}$	Maximum allowed shifted load in the DRP
L_t	Electricity demand
$P_t^{\text{Batt,limit}}$	Limitation of stored energy in the battery
$P_t^{\text{Batt,dch,limit}}$, $P_t^{\text{Batt,ch,limit}}$	Discharging and charging limitations of the battery
$P_t^{\text{WT,limit}}$, $P_t^{\text{PV,limit}}$, $P_t^{\text{FC,limit}}$	Limitation of produced power by the wind turbine, photovoltaic panel, and fuel cell unit

A. Najafi-Ghalelou · K. Zare (✉) · M. Abapour
Faculty of Electrical and Computer Engineering, University of Tabriz, Tabriz, Iran
e-mail: afshin.najafi95@ms.tabrizu.ac.ir; kazem.zare@tabrizu.ac.ir; abapour@tabrizu.ac.ir

S. Nojavan
Department of Electrical Engineering, University of Bonab, Bonab, Iran
e-mail: sayyad.nojavan@bonabu.ac.ir

S. Nojavan, K. Zare (eds.), *Demand Response Application in Smart Grids*,
https://doi.org/10.1007/978-3-030-32104-8_9

Variables

Exe_t	Excess generated power
L_t^{New}	New electricity demand after implementation of DRP
$L_t^{\mathrm{shiftable}}$	Amount of shifted load by DRP
P_t^{Batt}	State of charge of the battery
$P_t^{\mathrm{Batt,ch}}$, $P_t^{\mathrm{Batt,dch}}$	Charging and discharging power of the battery
P_t^{WT}, P_t^{PV}, P_t^{FC}	Produced power by the wind turbine, photovoltaic panel, and fuel cell unit
Ue_t	Undelivered energy
X_t	Binary variable: Equal to 1 if the battery be in charging mode, otherwise 0
Y_t	Binary variable: Equal to 1 if the battery be in discharging mode, otherwise 0

9.1 Introduction

Recently, some new concepts such as microgrid have been appeared with the aim of handling various issues related to integration of renewable energy sources and increased demand of reliable electricity supply. So, some studies should be done not only to make such concepts technically feasible but also to be commercially attractive and viable.

9.1.1 Literature Review

Literature review about deterministic-based model of microgrid energy management has been provided as follows: to fairly distribute the bill costs among buildings, a novel residential microgrid model has been provided in [1]. Total operation cost of a residential microgrid has been minimized in the presence of solar thermal storage system in [2]. Performance of an islanded microgrid has been optimized in [3] which consists of wind turbine, photovoltaic panel, fuel cell, and battery. Compressed air energy storage-based model of a microgrid has been optimized under various uncertainties in [4].

Literature review about uncertainty-based model of microgrid energy management has been provided as follows: A novel robust load frequency control strategy has been provided in [5] for analyzing the operation of the islanded microgrid considering vehicle-to-grid constraints. Information gap decision theory approach-based model of a residential microgrid has been analyzed under market price uncertainty in [6]. The particle swarm optimization algorithm has been presented in [7] to optimize the microgrid performance in a real-time operation mode. Solar thermal storage-based model of a residential microgrid has been analyzed under

market price uncertainty in [8]. In order to investigate the charging effects of plug-in hybrid electric vehicles on the optimal operation of microgrid, a novel stochastic approach has been provided in [9]. Robust optimization approach has been utilized in [10] to minimize the operation cost of a compressed air energy storage-based microgrid under market price uncertainty. ROA-based residential model has been optimized under market price uncertainty in [11]. With the aim of optimizing the microgrid's operation cost in the presence of renewable energy sources, an additive and integrated net load forecast model has been presented in [12]. Short-term risk-based model of a smart residential microgrid has been analyzed under market price uncertainty in [13]. Market price uncertainty-based model of a hub system has been optimized using robust optimization approach in [14]. A genetic algorithm-based model of the hydrothermal model has been optimized in [15]. A novel robust optimization approach-based model of a novel microgrid has been studied under market price uncertainty in [16].

Literature review about microgrid energy management considering various objective functions has been provided as follows: with the aim of decreasing the operation cost and emission of microgrid, a multi-objective uniform water cycle approach has been provided in [17]. A renewable energy-based microgrid model has been studied from economic and environmental viewpoints considering compressed energy storage system and demand response program in [18]. A multi-objective framework has been presented in [19] to minimize the emission and the cost of a microgrid using normal boundary intersection technique. In order to mitigate the fluctuation of power flow, decrease energy cost, and reduce the emission of greenhouse gases, a novel multi-objective-based model of microgrid has been provided in [20]. A ε-constraint approach has been used in [21] for optimal scheduling of a novel hybrid energy system under economic and environmental factors. A multi-objective-based cost-emission model of a residential apartment building has been optimized using ε-constraint and weighted sum approaches in [22]. Finally, a multi-objective-based cost-emission model of a hybrid system is optimized utilizing weighted sum approach in [23].

9.1.2 Novelty of This Chapter

1. Minimizing the operation and energy not supplied costs at the same time under DRP constraints.
2. Using ε-constraint and fuzzy satisfying approaches to solve the proposed multi-objective problem and select the best compromise solution.

9.1.3 Chapter Organization

The chapter is structured as follows: The proposed multi-objective optimization model is formulated in Sect. 9.2. In Sect. 9.3, two different scenarios have been investigated with and without considering the effects of DRP. Finally, the conclusion is presented in Sect. 9.4.

9.2 Problem Formulation

9.2.1 Objective Function 1

The first objective function of the proposed chapter is minimization of the microgrid's operation cost:

$$Min\,\mathrm{OF}_1 = \sum_{t=1}^{24} \left(P_t^{\mathrm{WT}} \times C_{\mathrm{WT}} + P_t^{\mathrm{PV}} \times C_{\mathrm{PV}} + P_t^{\mathrm{FC}} \times C_{\mathrm{FC}} - P_t^{\mathrm{Batt,ch}} \times C_{\mathrm{Batt,Ch}} + P_t^{\mathrm{Batt,dch}} \times C_{\mathrm{Batt,Dch}}\right) \quad (9.1)$$

The first term of the proposed objective function (9.1) is related to the cost of produced power by the wind turbine. The second and third terms are related to the cost of produced power by the photovoltaic panel and the fuel cell unit. The cost of consumed power with the aim of charging the battery is presented in the fourth term. Finally, the cost of produced power through the discharge process of the battery is provided in the last term.

9.2.2 Objective Function 2

The second objective function is presented to minimize the energy not supplied cost in the microgrid.

$$Min\,\mathrm{OF}_2 = \sum_{t=1}^{24} \left(\mathrm{Ue}_t \times C_{\mathrm{Ue}}\right) \quad (9.2)$$

9.2.3 Constraints of the Wind Turbine, Photovoltaic Panel, and Fuel Cell

Produced power by the wind turbine, photovoltaic panel, and fuel cell are provided as follows:

$$P_t^{\mathrm{WT}} \leq P_t^{\mathrm{WT,limit}} \tag{9.3}$$

$$P_t^{\mathrm{PV}} \leq P_t^{\mathrm{PV,limit}} \tag{9.4}$$

$$P_t^{\mathrm{FC}} \leq P_t^{\mathrm{FC,limit}} \tag{9.5}$$

9.2.4 Constraints of the Battery

The technical constraints of the battery are formulated by Eqs. (9.6)–(9.12) [3]. The state of charge, charge and discharge limitations of the battery are expressed by Eqs. (9.6)–(9.8).

$$P_t^{\mathrm{Batt}} \leq P_t^{\mathrm{Batt,limit}} \tag{9.6}$$

$$P_t^{\mathrm{Batt,dch}} \leq P_t^{\mathrm{Batt,dch,limit}} \times X_t \tag{9.7}$$

$$P_t^{\mathrm{Batt,ch}} \leq P_t^{\mathrm{Batt,ch,limit}} \times Y_t \tag{9.8}$$

Equation (9.9) is presented to control the charge and discharge mode of the battery.

$$X_t + Y_t = 1 \tag{9.9}$$

Maximum limits of discharging and charging of the battery are presented in Eqs. (9.10) and (9.11), respectively.

$$P_t^{\mathrm{Batt,dch}} - P_{t-1}^{\mathrm{Batt}} \leq 0 \tag{9.10}$$

$$P_t^{\mathrm{Batt,ch}} + P_{t-1}^{\mathrm{Batt}} \leq P_t^{\mathrm{Batt,limit}} \tag{9.11}$$

Finally, Eq. (9.12) is presented to update the state of charge of battery.

$$P_t^{\mathrm{Batt}} = P_{t-1}^{\mathrm{Batt}} + P_t^{\mathrm{Batt,ch}} - P_t^{\mathrm{Batt,dch}} \tag{9.12}$$

9.2.5 Demand Response Program

The time-of-use (TOU) rates of demand response program are used in the chapter. TOU shifts the electricity demand from peak periods to flatten the load curve, improve the performance of microgrid, and decrease the operation cost of the microgrid. The utilized DRP can be formulated as follows:

$$L_t^{\text{New}} = L_t + L_t^{\text{shiftable}} \tag{9.13}$$

$$\left|L_t^{\text{shiftable}}\right| \leq E^{\max} \times L_t \tag{9.14}$$

$$\sum_{t=1}^{T} L_t^{\text{shiftable}} = 0 \tag{9.15}$$

It is noteworthy that it is assumed only 20% of the base load can be shifted at each period.

9.2.6 Power Balance Constraints

Power balance limitation can be formulated as follows:

$$P_t^{\text{WT}} + P_t^{\text{PV}} + P_t^{\text{FC}} + P_t^{\text{Batt,dch}} + \text{Ue}_t = L_t + P_t^{\text{Batt,ch}} + \text{Exe}_t \tag{9.16}$$

It should be mentioned that on the right side of Eq. (9.16), L_t^{New} should be replaced with L_t to consider the effects of the proposed DRP.

9.2.7 ε-Constraint Method

In this chapter, the proposed multi-objective optimization model is solved using the ε-constraint method. In order to create Pareto front, objective function (9.1) is minimized, while the second objective function is considered as a constraint. The mathematical formulation of mentioned statements can be expressed as follows [24]:

$$\begin{aligned} &\text{OF} = \max\left(\Phi_1\right) \\ &\text{s.t.} \\ &\begin{cases} \Phi_2 \leq \varepsilon \\ \text{Eqs.}(9.3) - (9.20) \end{cases} \end{aligned} \tag{9.17}$$

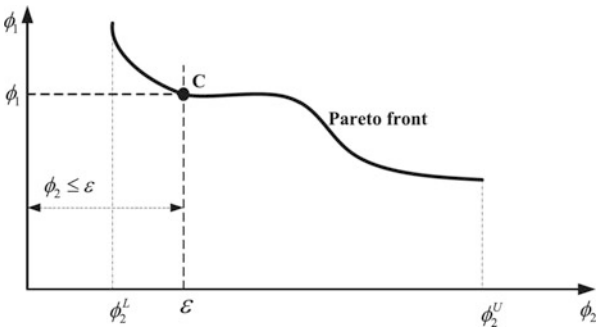

Fig. 9.1 Description of ε-constraint method

It can be observed from the Eq. (9.17) and Fig. 9.1 that the ε is limited by Φ_2. In this section, by increasing ε from Φ_2^{L} to Φ_2^{U}, the modified single objective function is solved. With comparing the obtained results for each value of ε, the optimal solutions like point C in Fig. 9.1 are obtained.

9.2.8 *Fuzzy Satisfying Method*

Min-max fuzzy method is one of the best methods for selecting the optimal solution from the obtained Pareto solutions. The linear membership function can be described as follows:

$$\mu_k^n = \begin{cases} 1 & f_k^n \le f_k^{\min} \\ \dfrac{f_k^{\max} - f_k^n}{f_k^{\max} - f_k^{\min}} & f_k^{\min} \le f_k^n \le f_k^{\max} \\ 0 & f_k^n \ge f_k^{\max} \end{cases} \tag{9.18}$$

In this equation, f_k^n is limited with minimum and maximum values of the kth objective function in Pareto optimal set. μ_k^n shows the optimality degree of nth solution of kth objective function. It should be mentioned that nth solution can be calculated as follows:

$$\begin{aligned} \mu^n &= \min\left(\mu_1^n, \ldots, \mu_N^n\right) \\ n &= 1, \ldots, N_P \end{aligned} \tag{9.19}$$

The maximum weakest membership function can be considered as the best strategy. Thus, the corresponding membership of solution ($\mu^{\max}$) can be calculated as follows:

$$\mu^{\max} = \max\left(\mu^1, \ldots, \mu^{N_{\mathrm{P}}}\right) \tag{9.20}$$

The general flow chart of the utilized approaches is illustrated in Fig. 9.2.

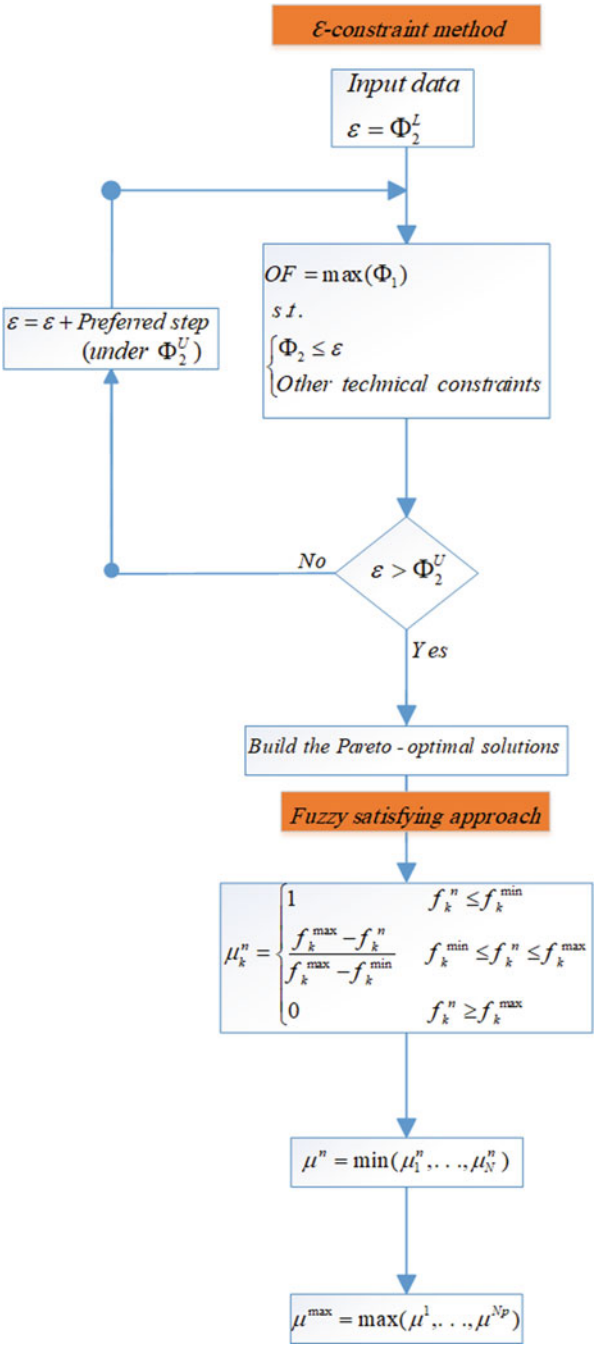

Fig. 9.2 Flow chart of the ε-constraint and min-max fuzzy approaches

9.3 Numerical Simulation

In the proposed chapter, an isolated microgrid in the Budapest Tech [25] is evaluated as a case study. As shown in Fig. 9.3, the proposed sample microgrid comprises of renewable energy sources such as wind turbine, photovoltaic panel, fuel cell, and battery storage.

9.3.1 Input Data

The types of used wind turbine, photovoltaic panel, and fuel cell are "Air-X 401," "DS 40," and "Flexiva" with the nominal power of 400 W at 11.5 m/s, 40 W, and 80 W, respectively. The output of the wind turbine and photovoltaic panel are provided in Figs. 9.4 and 9.5, respectively. Also, the estimated load profile is illustrated in Fig. 9.6. Notably the optimization problem is investigated under two load profiles. Parameters related to the costs of different units and their relevant limitations are presented in Table 9.1.

9.3.2 Simulation Results in Two Study Cases

In this chapter, two case studies are analyzed with the aim of evaluating the performance of the proposed model. The proposed model without considering the

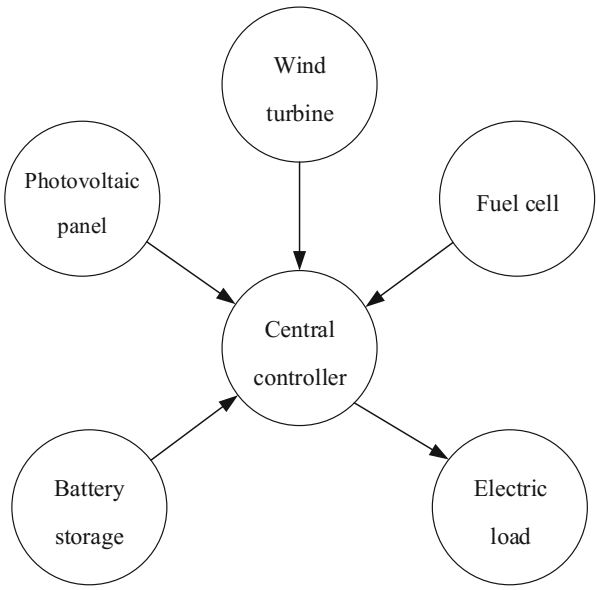

Fig. 9.3 Schematic of the proposed microgrid model

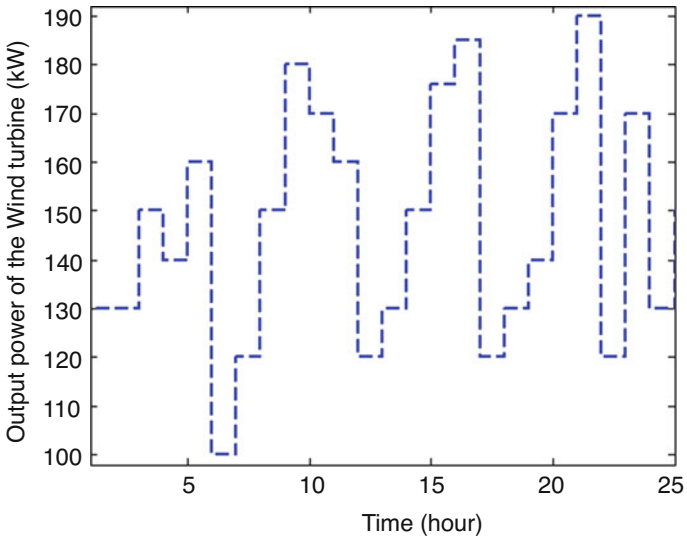

Fig. 9.4 Output power of wind turbine

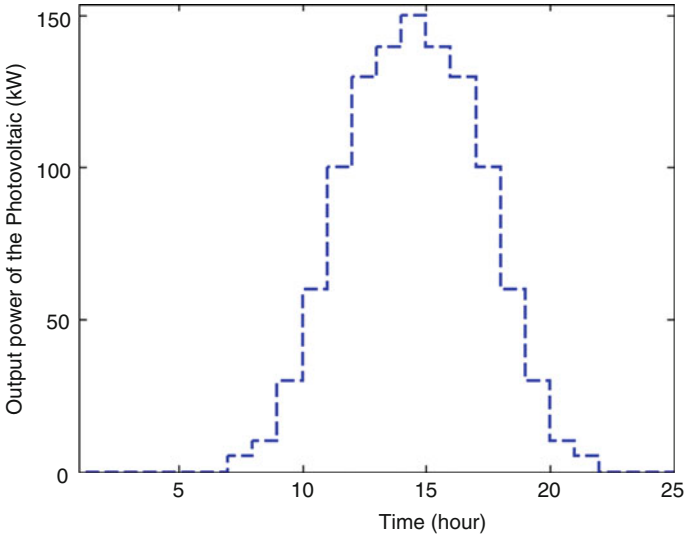

Fig. 9.5 Output power of photovoltaic system

DRP constraints has been analyzed in the first scenario and with considering the DRP constraints has been investigated in the second one.

The state of charge of battery and the charge and discharge rates of battery are illustrated in Figs. 9.7 and 9.8, respectively.

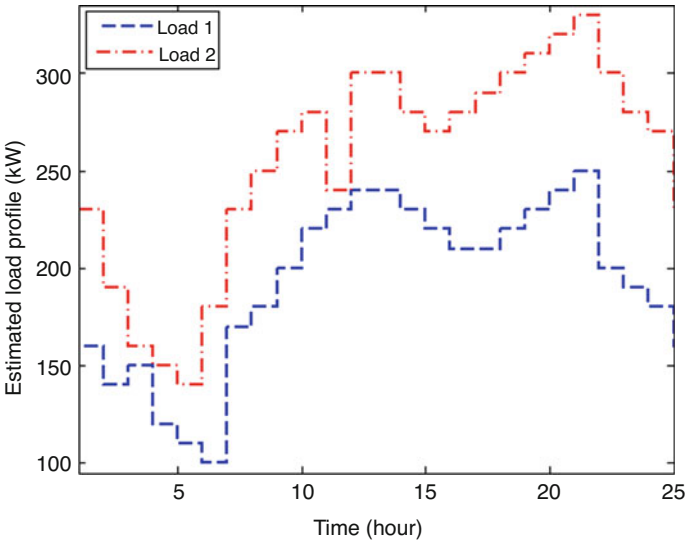

Fig. 9.6 Load profiles

Table 9.1 Costs of different units and their relevant limitations

Parameter	Unit	Value	Parameter	Unit	Value
C_{WT}	€/kWh	0.4	$P_t^{FC,limit}$	W	80
C_{PV}	€/kWh	0.4	$P_t^{Batt,limit}$	W	200
C_{FC}	€/kWh	0.9	$P_t^{Batt,dch,limit}$	W	50
$C_{Batt,\ Ch}$	€/kWh	0.4	$P_t^{Batt,ch,limit}$	W	200
$C_{Batt,\ Dch}$	€/kWh	0.6			
C_{Ue}	€/kWh	1.5			
C_{Exe}	€/kWh	Free			

By analyzing these two figures, it can be understood that without DRP, the state of charge of battery is 1995 kWh. Meanwhile, with considering the DRP, the state of charge of battery is 3423.56 kWh, and this means that with considering DRP, the state of charge of battery increases 1428.5644 kWh. Also amount of charge without DRP is 175 kWh and with DRP is 167 kWh, which means that the charge of battery decreases 8 kWh under the DRP. Furthermore, discharge rate without DRP is 275 kWh and with DRP is 98.36 kWh. So, the discharge rate of battery decreases 176.64 kW under the DRP. In general, it can be concluded that with considering the DRP, the charge and discharge rates of battery are decreased which makes the battery life to be increased and the operation cost of microgrid decreased.

The excess energy is illustrated in Fig. 9.9. According to the provided figure, it can be understood that without DRP, the excess energy is 266 kWh and with DRP is zero. Thus, the excess energy decreases 266 kWh and becomes zero under the DRP. In general, reduction of excess energy decreases the operation cost of the microgrid.

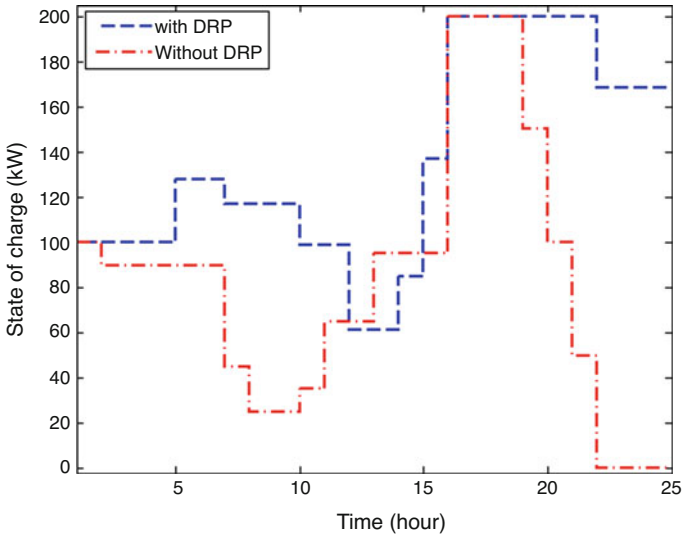

Fig. 9.7 State of charge of battery

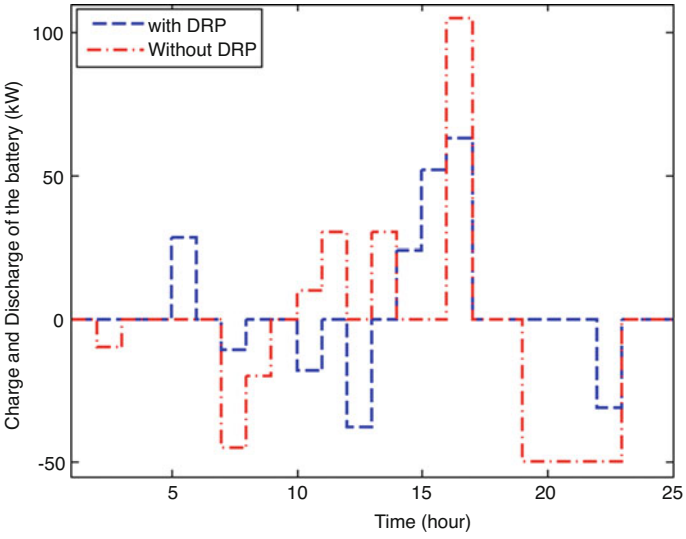

Fig. 9.8 Charge and discharge of battery

The energy not supplied is provided in Fig. 9.10. According to this figure, without considering DRP the undelivered energy is 163.017 kWh and with considering DRP is 67.64 kWh, which means that with considering DRP the undelivered energy decreases 95.377 kWh and this leads to the reduction of the operation cost. It should be mentioned that the output power of fuel cell without DRP is 1.98 kWh and with DRP is zero, and this low output power is due to high operation cost of the fuel cell.

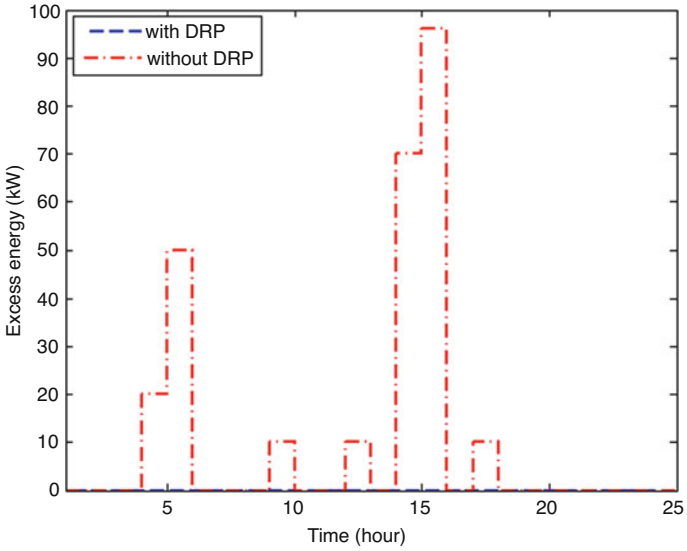

Fig. 9.9 Excess energy

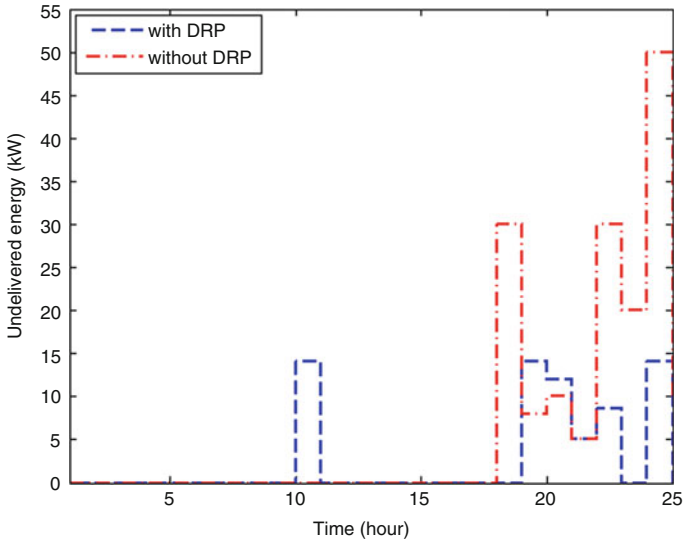

Fig. 9.10 Undelivered energy

Finally, the obtained Pareto solutions with and without DRP are summarized in Table 9.2. In the first scenario, by using min-max fuzzy method, solution#19 is selected as the trade-off solution in which the operation cost of microgrid is

Table 9.2 Pareto solutions with and without considering DRP

	Without demand response program					With demand response program				
	Operation cost (€)	Energy not supplied cost (€)	Φ_1 (p.u.)	Φ_2 (p.u.)	min (Φ_1, Φ_2)	Operation cost (€)	Energy not supplied cost (€)	Φ_1	Φ_2	min (Φ_1, Φ_2)
1	2252.400	0	0	1.000	0	1889.200	0	0	1.000	0
2	2098.518	2.304	0.353	0.997	0.353	1864.010	62.976	0.353	0.736	0.353
3	2089.969	16.552	0.373	0.980	0.373	1862.610	66.475	0.373	0.721	0.373
4	2081.420	30.801	0.392	0.962	0.392	1861.211	69.974	0.392	0.706	0.392
5	2072.871	45.049	0.412	0.944	0.412	1859.811	73.472	0.412	0.692	0.412
6	2064.322	59.297	0.431	0.927	0.431	1858.412	76.971	0.431	0.677	0.431
7	2055.773	73.546	0.451	0.909	0.451	1857.012	80.470	0.451	0.662	0.451
8	2047.224	87.794	0.471	0.892	0.471	1855.613	83.968	0.471	0.648	0.471
9	2038.675	102.042	0.490	0.874	0.490	1854.213	87.467	0.490	0.633	0.490
10	2030.125	116.291	0.510	0.856	0.510	1852.814	90.966	0.510	0.618	0.510
11	2021.576	130.539	0.529	0.839	0.529	1851.414	94.464	0.529	0.604	0.529
12	2013.027	144.788	0.549	0.821	0.549	1850.015	97.963	0.549	0.589	0.549
13	2004.478	159.036	0.569	0.804	0.569	**1848.615**	**101.462**	**0.569**	**0.574**	**0.569**
14	1995.929	173.284	0.588	0.786	0.588	1847.216	104.960	0.588	0.560	0.560
15	1987.380	187.533	0.608	0.768	0.608	1845.816	108.459	0.608	0.545	0.545
16	1978.831	201.781	0.627	0.751	0.627	1844.417	111.958	0.627	0.530	0.530
17	1970.282	216.029	0.647	0.733	0.647	1843.017	115.456	0.647	0.515	0.515
18	1961.733	230.278	0.667	0.716	0.667	1841.618	118.955	0.667	0.501	0.501
19	**1953.184**	**244.526**	**0.686**	**0.698**	**0.686**	1840.219	122.454	0.686	0.486	0.486
20	1944.635	264.412	0.706	0.674	0.674	1838.819	125.952	0.706	0.471	0.471
21	1936.086	285.784	0.725	0.647	0.647	1837.420	129.451	0.725	0.457	0.457
22	1927.537	307.157	0.745	0.621	0.621	1836.020	132.950	0.745	0.442	0.442
23	1918.988	328.529	0.765	0.594	0.594	1834.621	136.448	0.765	0.427	0.427
24	1910.439	349.902	0.784	0.568	0.568	1833.221	139.947	0.784	0.413	0.413

25	1901.890	371.275	0.804	0.542	0.542	1831.822	143.446	0.804	0.398	0.398
26	1893.341	392.647	0.824	0.515	0.515	1830.422	146.944	0.824	0.383	0.383
27	1884.792	414.020	0.843	0.489	0.489	1829.023	154.329	0.843	0.352	0.352
28	1876.243	435.392	0.863	0.462	0.462	1827.623	164.825	0.863	0.308	0.308
29	1867.694	456.765	0.882	0.436	0.436	1826.224	175.321	0.882	0.264	0.264
30	1859.145	478.137	0.902	0.410	0.410	1824.824	185.817	0.902	0.220	0.220
31	1850.596	499.510	0.922	0.383	0.383	1823.425	196.313	0.922	0.176	0.176
32	1842.047	520.882	0.941	0.357	0.357	1822.025	206.809	0.941	0.132	0.132
33	1833.498	542.255	0.961	0.331	0.331	1820.626	217.305	0.961	0.088	0.088
34	1824.949	595.882	0.980	0.264	0.264	1819.226	227.801	0.980	0.044	0.044
35	1820.400	810.000	1.000	0	0	1817.827	238.294	1.000	0	0

1953.184 € and the unsupplied energy cost is 244.526 €. In the second scenario, solution#13 is selected as the trade-off solution in which the operation cost of microgrid is 1848.615 € and unsupplied energy cost is 101.462 €. Consequently, the operation cost of the microgrid increases 5.36% and the cost of unsupplied energy reduces 58.51% under the DRP.

9.4 Conclusion

In this chapter, two conflicted objective functions of an off-grid microgrid, operation cost and energy not supplied, have been provided. To handle the provided multi-objective model, ε-constraint method is used. Then, fuzzy satisfying approach is employed to select the best compromise solution from the obtained solutions. According to the obtained results, the operation cost of microgrid is increased 5.36% and the cost of unsupplied energy is reduced 58.51% in the presence of DRP. So, it can be concluded that DRP can be employed to provide desired economic ideals. It should be noted that some new multi-microgrid models can be analyzed under various conditions as a future work.

References

1. A. Najafi-Ghalelou, K. Zare, S. Nojavan, Optimal scheduling of multi-smart buildings energy consumption considering power exchange capability. Sustain. Cities Soc. **41**, 73–85 (2018)
2. A. Najafi-Ghalelou, S. Nojavan, M. Majidi, F. Jabari, K. Zare, Solar Thermal Energy Storage for Residential Sector, in *Operation, Planning, and Analysis of Energy Storage Systems in Smart Energy Hubs* (Springer, 2018), pp. 79–101
3. H. Morais, P. Kadar, P. Faria, Z.A. Vale, H. Khodr, Optimal scheduling of a renewable micro-grid in an isolated load area using mixed-integer linear programming. Renew. Energy **35**, 151–156 (2010)
4. A.N. Ghalelou, A.P. Fakhri, S. Nojavan, M. Majidi, H. Hatami, A stochastic self-scheduling program for compressed air energy storage (CAES) of renewable energy sources (RESs) based on a demand response mechanism. Energy Convers. Manag. **120**, 388–396 (2016)
5. M.-H. Khooban, T. Niknam, F. Blaabjerg, P. Davari, T. Dragicevic, A robust adaptive load frequency control for micro-grids. ISA Trans. **65**, 220–229 (2016)
6. A. Najafi-Ghalelou, S. Nojavan, K. Zare, Heating and power hub models for robust performance of smart building using information gap decision theory. Int. J. Electr. Power Energy Syst. **98**, 23–35 (2018)
7. M. Elsied, A. Oukaour, H. Gualous, O.A.L. Brutto, Optimal economic and environment operation of micro-grid power systems. Energy Convers. Manag. **122**, 182–194 (2016)
8. A. Najafi-Ghalelou, S. Nojavan, K. Zare, Information gap decision theory-based risk-constrained scheduling of smart home energy consumption in the presence of solar thermal storage system. Sol. Energy **163**, 271–287 (2018)
9. A. Kavousi-Fard, A. Abunasri, A. Zare, R. Hoseinzadeh, Impact of plug-in hybrid electric vehicles charging demand on the optimal energy management of renewable micro-grids. Energy **78**, 904–915 (2014)

10. S. Nojavan, A. Najafi-Ghalelou, M. Majidi, K. Zare, Optimal bidding and offering strategies of merchant compressed air energy storage in deregulated electricity market using robust optimization approach. Energy **142**, 250–257 (2018)
11. A. Najafi-Ghalelou, K. Zare, S. Nojavan, Risk-based scheduling of smart apartment building under market price uncertainty using robust optimization approach. Sustain. Cities Soc. **48**, 101549 (2019)
12. A. Kaur, L. Nonnenmacher, C.F. Coimbra, Net load forecasting for high renewable energy penetration grids. Energy **114**, 1073–1084 (2016)
13. A. Najafi-Ghalelou, S. Nojavan, K. Zare, Robust thermal and electrical management of smart home using information gap decision theory. Appl. Therm. Eng. **132**(5), 221–232 (2018)
14. A. Najafi-Ghalelou, S. Nojavan, K. Zare, B. Mohammadi-Ivatloo, Robust scheduling of thermal, cooling and electrical hub energy system under market price uncertainty. Appl. Therm. Eng. **149**, 862–880 (2018)
15. M. Nazari-Heris, B. Mohammadi-Ivatloo, A. Haghrah, Optimal short-term generation scheduling of hydrothermal systems by implementation of real-coded genetic algorithm based on improved Mühlenbein mutation. Energy **128**, 77–85 (2017)
16. M. Nazari-Heris, B. Mohammadi-Ivatloo, G.B. Gharehpetian, M. Shahidehpour, Robust short-term scheduling of integrated heat and power microgrids. IEEE Syst. J. **13**(3), 3295–3303 (2018)
17. A. Deihimi, B.K. Zahed, R. Iravani, An interactive operation management of a micro-grid with multiple distributed generations using multi-objective uniform water cycle algorithm. Energy **106**, 482–509 (2016)
18. S. Nojavan, M. Majidi, A. Najafi-Ghalelou, K. Zare, Supply side management in renewable energy hubs, in *Operation, Planning, and Analysis of Energy Storage Systems in Smart Energy Hubs* (Springer, 2018), pp. 163–187
19. M. Izadbakhsh, M. Gandomkar, A. Rezvani, A. Ahmadi, Short-term resource scheduling of a renewable energy based micro grid. Renew. Energy **75**, 598–606 (2015)
20. J. Cai, F. Gao, X. Guan, K. Liu, N. Yao, X. Cheng, An economic dispatch model based on scenario tree in industrial micro-grid with solar power and storage, in *12th World Congress on Intelligent control and automation (WCICA), 2016* (IEEE, 2016), pp. 1594–1599
21. S. Nojavan, M. Majidi, A. Najafi-Ghalelou, M. Ghahramani, K. Zare, A cost-emission model for fuel cell/PV/battery hybrid energy system in the presence of demand response program: ε-constraint method and fuzzy satisfying approach. Energy Convers. Manag. **138**, 383–392 (2017)
22. A. Najafi-Ghalelou, K. Zare, S. Nojavan, Multi-objective economic and emission scheduling of smart apartment building. J. Energy Manage. Technol **3**(3), 41–53 (2019)
23. M. Majidi, S. Nojavan, N.N. Esfetanaj, A. Najafi-Ghalelou, K. Zare, A multi-objective model for optimal operation of a battery/PV/fuel cell/grid hybrid energy system using weighted sum technique and fuzzy satisfying approach considering responsible load management. Sol. Energy **144**, 79–89 (2017)
24. S.M. Mohseni-Bonab, A. Rabiee, B. Mohammadi-Ivatloo, S. Jalilzadeh, S. Nojavan, A two-point estimate method for uncertainty modeling in multi-objective optimal reactive power dispatch problem. Int. J. Electr. Power Energy Syst. **75**, 194–204 (2016)
25. P. Kádár, Energy on the roof, in *3rd Romanian-Hungarian Joint Symposium on Applied Computational Intelligence* (2006), pp. 343–352

Chapter 10
Optimal Operation of the Microgrid Considering Network Losses and Demand Response Programs Under Condition of Uncertainty

Kazem Zare and Saber Makhandi

10.1 Introduction

In recent years, for reasons such as increasing global demand for energy, efforts to reduce environmental pollution due to climate change, rising energy prices and traditional power grid, burn out the need to implement a sustainable, high-performance and secure smart network, sustainable and high-performance is felt more than ever. By modifying power grids to smart grids, MGs play an important role in providing electricity. MG usually contains set of distributed sources, energy storage system (ESS), and loads which can be exploited as a connection to the main grid or with an island performance. Regarding the type of load, MGs are divided into AC and DC types. The use of MG is an effective way to use distributed resources with a wide range of renewable energy sources to achieve goals such as improving power quality, increasing reliability, decreasing peak consumption, and improving energy efficiency [1, 2]. However MGs have disadvantages such as the complexity of network protection, absence of complete standards when reconnecting or separating these networks from the upstream network, increase high-frequency harmonics due to the use of power electronic devices, and voltage and frequency fluctuation. MG studies are usually divided into two groups:

- The studies are related to the construction of MGs, which is aimed at using technologies in the construction of MG.
- The studies relate to scheduling of MG operation aimed at providing optimal power generation program from various economic, environmental, and technical points of view to supply the load. Reliability, accountability, DRPs, network security, and losses are among the issues that are usually considered to be the optimal planning of unit production.

K. Zare (✉) · S. Makhandi
Faculty of Electrical and Computer Engineering, University of Tabriz, Tabriz, Iran
e-mail: kazem.zare@tabrizu.ac.ir

S. Nojavan, K. Zare (eds.), *Demand Response Application in Smart Grids*,
https://doi.org/10.1007/978-3-030-32104-8_10

The optimal power generation planning with the goal of minimizing operating cost under various constraints is most studied on the exploitation of MGs by researchers. In [3] for an MG equipped with CHP units, a multi-objective model is designed to minimize the cost of exploitation and emission. The MG used includes electric only, heat only, CHP units, and ESS and has the ability to exchange power with the upstream network. The optimal 24-h scheduling is done with the aim of finding the optimal point of energy resources to achieve maximum possible profits in [4]. The desired planning for a sample MG is done in two modes of operation. The characteristic efficiency, reliability, economic and environmental requirements for the proper operation of the MG are provided in [5]. Hence, an economic-environmental planning methodology in an MG in a connected mode has been formulated. The objective is to minimize the cost of operation and emission as well as the amount of electricity purchased from the main grid at high-cost hours. The presence of RESs along with many advantages, due to the random nature and uncertainty of their output power, is one of the most fundamental challenges. Electricity market price and load demand are other uncertain parameters. In various studies, some of these parameters with random nature are considered in the form of differences between predicted and exact values and using various methods to reduce its impact. In [6] a stochastic method based on the technique of producing different scenarios is presented for modeling uncertainty. In [7], which has been investigated for intelligent energy management, the fuzzy method has been used to model the predicted parameters. Using a robust optimization method to reduce the uncertainty effect in [8] is proposed for the problem MG energy planning under conditions of consumption and heat uncertainty as well as electricity prices.

On the other hand, due to limited energy resources and growing consumption, it is important to use the best available resources. In the new system, one of the solutions to cover load and RES fluctuations is the development of system infrastructure that requires high capital or the use of existing units at the point of non-optimal work. While in order to overcome these problems and optimize the operation of the new structure, one of the cheapest methods is to use the demand response (DR). The stochastic operation scheduling for energy and reserve in an intelligent system is addressed in [9]. A part of required reserve is to cover the volatility of WT power and load procurement by responsive load that are able to participate in energy and reserve planning. A multi-objective energy management system is introduced to improve the short-term performance of MG, considering the random behavior of RESs in [10]. In this planning, various residential, commercial, and industrial loads are able to participate in load response programs. These programs are implemented in the form of incentive tariffs and in the form of price, offering packages that are based on the roulette cycle method. In order to implement DR, Ref. [11] has used a new incentive method. This incentive-driven mechanism is in fact a two-way contract that is obtained between the owners of DGs and consumers in the bottom buses through secondary bid auctions. The DRPs of direct load control type in electricity markets are evaluated in [12] using a nonlinear exponential model.

It should be noted that we are faced with an optimization problem in solving the grid scheduling problem. Different techniques and methods have been introduced to solve the optimization problems. These techniques are divided into a multi-class

based on the type of the search space and target function. Simple linear programming, nonlinear programming method, and stochastic (dynamic) programming are examples of these methods. Although the numerical and mathematical methods are widely used in solving optimization problems, these methods require more computational process, which leads to unusual and uncertain results, due to the dimensions of the problem. Intelligent optimization algorithms such as genetic algorithms (GA) and particle swarm optimization (PSO) algorithms are among the smart methods that have been considered by researchers in recent years to solve optimization problems. References [13, 14] have applied a dynamic planning methodology for solving the optimization problem in an MG, taking into account the uncertainty of renewable sources and load. The goal is to maximize the benefit that a landlord can obtain from the energy business during a day from the grid.

The current paper focuses on the development and optimization of optimal operational planning of an MG equipped with diesel, wind, and storage units and in the upstream network connectivity mode with respect to different constraints. In this regard, the planning has been carried out in the uncertainty environment of the wind turbine, load, and electricity prices of the main network. Due to the importance of the problem and the type of grid, the technical losses related to the transmission line are also calculated and sought to reduce it. Then, using DRPs with an appropriate method and using a more accurate model, we are trying to optimize the operation of the production units and make them effective in the energy market. The impact of the implementation of these programs on the operating cost, the amount of losses, the amount of generators generated, the load profile, as well as the voltage profile and generally in the planning process are specifically answered. In order to solve the optimization problem resulting from planning, considering the type of problem and the advantage of heuristic and meta-heuristic methods, an intelligent method based on the PSO algorithm has been used.

The rest of this paper is organized as follows: In Sect. 10.2, the details of the modeling of uncertainty and DR as well as the formulation of the objective function and the constraints of the problem are expressed. Section 10.3 explains the method of PSO as a problem solution method. Section 10.4 presents simulation studies and discussions on the results. Finally, the conclusion is provided in Sect. 10.5.

10.2 Problem Formulation

10.2.1 Uncertainty Modeling

Wind turbine power output is dependent on wind speed and because wind speed is a random quantity, the wind turbine output will also be an uncertain quantity. Additionally, the amount of demand and energy price are also uncertain quantities. Therefore, exploitation of them is usually possible. In this paper, a stochastic programming formulation is used to model the uncertainty of these parameters. For this purpose, for wind power, the average wind velocity curve is extracted

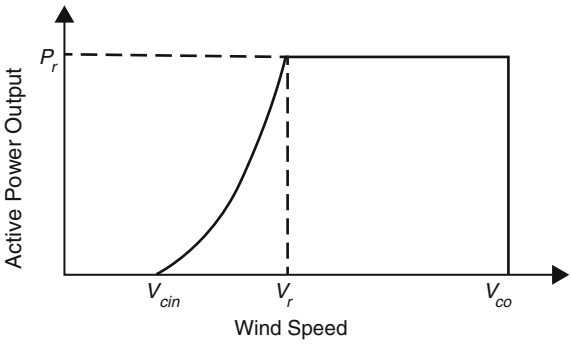

Fig. 10.1 The relationship between the input wind speed and output power for wind generators

from the past data of this parameter in [15]. Then, using the speed-power curve, according to Fig. 10.1, the wind turbine output power for the planning period is obtained. The main network electricity price is also assumed for the certain mode according to the prediction of Ref. [15]. In order to model the uncertainty and implement a stochastic programming formulation, the limited and random forecasted error is considered for the mean wind speed curve, electricity price, and load forecast curve.

The following expression can describe the relationship between the input wind speed and output power of a wind turbine:

$$\begin{cases} P_{\mathrm{WT}} = 0 & V \le V_{\mathrm{cin}} \;\; V \ge V_{\mathrm{co}} \\ P_{\mathrm{WT}} = P_{\mathrm{r}} \dfrac{V - V_{\mathrm{cin}}}{V_{\mathrm{r}} - V_{\mathrm{cin}}} & V_{\mathrm{cin}} \le V < V_{\mathrm{r}} \\ P_{\mathrm{WT}} = P_{\mathrm{r}} & V_{\mathrm{r}} \le V < V_{\mathrm{CO}} \end{cases} \tag{10.1}$$

where v is the randomly varying wind speed, V_0 is the location parameter, α is the shape parameter, and β is the scale parameter.

Considering the prediction error, the set of Eqs. (10.2) shows different scenarios and the probability associated with each of the wind turbine power parameters, the amount of consumption, and the energy price to investigate their uncertainty:

$$\begin{aligned} &S_{\mathrm{wind}} = \{(P_{\mathrm{wind},1}, \pi_{\mathrm{wind},1})\ (P_{\mathrm{wind},2}, \pi_{\mathrm{wind},2}) \ldots\} \\ &S_{\mathrm{load}} = \{(P_{\mathrm{load},1}, \pi_{\mathrm{load},1})\ (P_{\mathrm{load},2}, \pi_{\mathrm{load},2}) \ldots\} \\ &S_{\rho} = \{(\rho_{E,1}, \pi_{E,1})(\rho_{E,2}, \pi_{E,2}) \ldots\} \\ &\pi_s = \pi_{\mathrm{wind}} \times \pi_E \times \pi_{\mathrm{load}} \\ &\sum_{s=1}^{Ns} \pi_s = 1 \end{aligned} \tag{10.2}$$

10.2.2 Demand Response Modeling

In this paper, RTP method is used to implement responsive programs. The mathematical model presented in [16] is also used to transfer power consumption from high consumption times to lower load times by increasing the price at peak times and decreasing it at off-peak times. The following mathematical model is introduced:

10.2.2.1 Elasticity

The change in demand for a unit of electricity price change is load elasticity and indicated by the E symbol:

$$E = \frac{\rho_0}{d_0} \cdot \frac{\partial d}{\partial \rho} \tag{10.3}$$

10.2.2.2 Insider Elasticity

Changing the amount of load in the (i) time period due to the change in electricity prices in the same period (i):

$$E(i,i) = \frac{\rho_0(i)}{d_0(i)} \cdot \frac{\partial d(i)}{\partial \rho(i)} \tag{10.4}$$

10.2.2.3 Mutual Elasticity

The mutual elasticity of the period (i) relative to period (j) means the change in the load over time (i) due to the change in the electricity price during the period (j):

$$E(i,j) = \frac{\rho_0(j)}{d_0(i)} \cdot \frac{\partial d(i)}{\partial \rho(j)}, \quad i \neq j \tag{10.5}$$

For a constant period (i), the sensitivity to all other time periods (j) must be calculated. For the 24-h period of this research, the matrix of self and mutual elasticity is formed as Eq. (10.6):

$$\begin{bmatrix} \Delta d(1) \\ \Delta d(2) \\ \Delta d(3) \\ \vdots \\ \Delta d(24) \end{bmatrix} = \begin{bmatrix} E(1,1) & E(1,2) & \cdots & \cdots & E(1,24) \\ E(2,1) & E(2,2) & \cdots & \cdots & \cdots \\ \cdots & \cdots & E(i,j) & \cdots & \cdots \\ \cdots & \cdots & \cdots & \cdots & \cdots \\ E(24,1) & \cdots & E(24,j) & \cdots & E(24,24) \end{bmatrix} \times \begin{bmatrix} \Delta\rho(1) \\ \Delta\rho(2) \\ \Delta\rho(3) \\ \vdots \\ \Delta\rho(24) \end{bmatrix} \tag{10.6}$$

The elements on the main diameter represent the insider elasticity and non-diagonal elements representing the mutual elasticity (i, j). Regarding these equations, two types of responsive models can be extracted based on time tariffs:

First, the single-period model, which is only dependent on self-sensitivity and used for loads that cannot be transmitted to different periods (light loads). Second, the multi-period model is used for loads that can be moved in different periods; this means that consumption can be transmitted to mid-peak or off-peak times.

10.2.2.4 Final Demand Response Model

According to the presented explanation, the final demand response model based on the time tariff used in this paper is according to Eq. (10.7):

$$d(i) = d_0(i) \times \left\{ 1 + \frac{E(i,i) \cdot [\rho(i) - \rho_0(i)]}{\rho_0(i)} + \sum_{\substack{j=1 \\ j \neq i}}^{24} E(i,j) \cdot \frac{d_0(i)}{\rho_0(j)} [\rho(j) - \rho_0(j)] \right\} \tag{10.7}$$

10.2.3 Objective Function

The objective function minimizes the expected operating cost in an MG with the upstream network connection mode for the 24-h period. In this paper, a scenario-based stochastic method has been used to model wind turbine, load, and energy price

uncertainty. In other words, the WT power output, load, as well as the electricity price of the network vary from scenario to scenario. Also the cost of producing WT has been ignored.

$$\mathrm{OF} = \sum_{s=1}^{N_s} \pi_s \left\{ \sum_{t=1}^{T} \left[C_{\mathrm{grid}}(t,s) + \sum_{j=1}^{\mathrm{NDG}} \times \left(C_{\mathrm{DG}}(j,t) \times s_{j,t} + \mathrm{SU}(j,t) \times y_{j,t} + \mathrm{SD}(j,t) \times x_{j,t} \right) + C_{\mathrm{str}}(t) \right] \right\} \quad (10.8)$$

According to Eq. (10.8), the cost of operating consists of different costs, which is further computed as follows. As mentioned the formulation of the problem is stochastic and dependent on the scenario. Also π_s shows the probability of occurrence of each scenario.

$C_{\mathrm{DG}}(j,t)$: The fuel cost of the diesel generator (DG) j is in the time period t:

$$C_{\mathrm{DG}}(j,t) = \alpha(j) + \beta(j) \cdot P_{\mathrm{DG}}(j,t) + \gamma(j) \cdot P_{\mathrm{DG}}^2(j,t) \quad (10.9)$$

$C_{\mathrm{grid}}(t,s)$: Expresses the cost of purchasing electricity from the main network, depending on the amount and price of the purchase at time period t. The amount of power exchange with the upstream network varies from scenario to scenario:

$$C_{\mathrm{grid}}(t,s) = P_{\mathrm{grid}}(t,s) \cdot \rho_{\mathrm{E}}(t,s) \quad (10.10)$$

ρ_{E} is the hourly electricity price of the main grid for the next day market and an uncertainty parameter. Therefore, its amount depends on different scenarios. Also, the MG has the ability to exchange power with the main network in two ways. If economic conditions require that electricity can be sold from the grid to the upstream network in this case, C_{grid} is considered as a profit for the MG. This usually happens in peak times where prices are high and purchases from the main network has a lot cost to the MG operator.

Another important element of the grid, known as a virtual power plant, is the energy storage system, which is particularly useful when it comes to reducing electricity purchases from more expensive units at peak hours. In accordance with Ref. [17], the cost function of a storage device follows from Eq. (10.11):

$$C_{\mathrm{str}}(t) = A \cdot |P_{\mathrm{str}}(t)| + B \quad (10.11)$$

$P_{\mathrm{str}}(t)$ is the amount of power which the storage device receives from the network (charge) at the hour t or injects into the network (discharge). A and B, the constant coefficients of this function, are dependent on the storage factor, which is 0.1 and 0.35, respectively.

Also $\mathrm{SD}(j,t)$ and $\mathrm{SU}(j,t)$ indicate the costs of shutting down and starting up the DG which will be switched off and on again due to economic conditions.

Equation (10.12) indicates the amount of the losses of the MG in the total planning hours, which is dependent on the resistance and current of the MG lines, and is obtained by using the backward-forward power flow method and after calculating the lines current and buss voltage. The goal is to reduce the amount of these losses and its imposed cost.

$$P_{\text{loss,total}} = \sum_{t=1}^{24} \sum_{\text{line}=1}^{32} R_{\text{line}} \times I_{h,\text{line}}^2 \tag{10.12}$$

10.2.4 Constraints

Minimizing the objective function referred to in the previous section should be subject to a series of constraints, including network constraints, unit constraints, and technical constraints. In this section, the mathematical model of each of these constraints is discussed.

10.2.4.1 Power Balance Constraint

One of the most important constraints that must be considered when planning MG production in order to ensure the correct and complete load, and to avoid problems of frequency stability and increase reliability, is the balance between the amount of production and consumption per hour of planning, which is the problem in Eq. (10.13):

$$\begin{aligned} &P_{\text{grid}}(s,t) + \sum_{j=1}^{J} P_{\text{DG}}(j,t) + P_{\text{WT}}(s,t) + P_{\text{str}}(s,t) \\ &\quad = \text{Demand}(t) + P_{\text{loss}}(s,t) \end{aligned} \tag{10.13}$$

10.2.4.2 Wind, Diesel Generator, and Main Grid Power Limits in Each Hour

Each of the available distributed resources has a permissible range of power generation. Also, the transmission line between the MG and the main network has power constraints:

$$P_{\mathrm{DG}}^{\min}(j,t) \le P_{\mathrm{DG}}(t) \le P_{\mathrm{DG}}^{\max}(j,t) \tag{10.14}$$

$$0 \le P_{\mathrm{Wind}}(t) \le P_{\mathrm{Wind}}^{\max}(t) \tag{10.15}$$

$$-P_{\mathrm{grid}}^{\max}(t) \le P_{\mathrm{grid}}(t) \le P_{\mathrm{grid}}^{\max}(t) \tag{10.16}$$

10.2.4.3 Ramp Rate Constraint

The thermal unit has a specific rate to increase or decrease power from hour to hour, and these problems should be taken into account in the planning of hourly power generation:

$$P_{\mathrm{DG}}(t+1) - P_{\mathrm{DG}}(t) \le \mathrm{UR}, \quad \text{if} \quad P_{\mathrm{DG}}(t+1) > P_{\mathrm{DG}}(t) \tag{10.17}$$

$$P_{\mathrm{DG}}(t) - P_{\mathrm{DG}}(t+1) \le \mathrm{DR}, \ \text{if} \ P_{\mathrm{DG}}(t) > P_{\mathrm{DG}}(t+1) \tag{10.18}$$

10.2.4.4 Minimum Up/Down Time Constraint

Economic planning requires that the thermal unit be shut off and re-illuminated within hours of the planning period for one or several hours. But the shutdown or re-illumination of these units is conditional on a certain period of time remaining in the state before the change.

$$\left(T_{\mathrm{ON},i}^{t-1} - \mathrm{MUT}_i\right) \times \left(s_i^{t-1} - s_i^t\right) \ge 0 \tag{10.19}$$

$$\left(T_{\mathrm{OFF},i}^{t-1} - \mathrm{MDT}_i\right) \times \left(s_i^t - s_i^{t-1}\right) \ge 0 \tag{10.20}$$

s_i is binary variable related to the status of the unit's on or off.

10.2.4.5 Battery Limitation

The battery cannot be charged and discharged at any one time and has a limited charge and discharge range for 1 h, which two equations indicate:

$$P_{\text{str}}(t) < P_{\text{ch}}^{\max} \tag{10.21}$$

$$P_{\text{str}}(t) < P_{\text{dis}}^{\max} \tag{10.22}$$

The positive value P_{str} indicates the discharge mode and its negative value indicates the battery charge status.

Also, the storage space is limited and the amount of charge and discharge per hour is proportional to the capacity of the battery:

$$E_{\text{stor}}(t) = E_{\text{stor}}(t-1) - P_{\text{str}}(t) \tag{10.23}$$

$$E_{\text{stor}}^{\min} \leq E_{\text{stor}}(t) \leq E_{\text{stor}}^{\max} \tag{10.24}$$

10.3 Solution Method

The optimization problem presented in the previous section is mixed integer nonlinear programming (MINLP) type, and it's difficult to solve it with conventional and classical methods and it may not lead to the exact answer. Therefore, this paper uses the PSO method as one of the meta-heuristic methods for solving mixed-optimization problems.

PSO as a problem optimization technique is based on the intelligent motion of particles, which uses the concept of social behavior of some beings and stimulates them to solve optimization problems. This algorithm was introduced and developed in 1995 by James Kennedy and Russell Ebertard. Some of the benefits of this method make it different from other optimization techniques:

- Multi-point search algorithm.
- Easier implementation.
- Faster calculations than other meta-heuristic algorithms.
- Ability to solve objective functions with stochastic nature.
- No need for a good initial solution to start the repeat process.

10.3.1 Particles Describing Equations

The motion of the particle in order to find the optimal solution is modeled as the following equations (10.25) and (10.26):

$$v^i(t+1) = w \cdot v^i(t) + c_1 r_1 \cdot \left[x^{i,\text{best}}(t) - x^i(t)\right] + c_2 r_2 \cdot \left[x^{\text{gbest}}(t) - x^i(t)\right] \quad (10.25)$$

$$x^i(t+1) = x^i(t) + v^i(t+1) \quad (10.26)$$

where x^i is the particle position; v^i is the particle velocity; $x^{i,\text{ best}}$ is the best position experienced by the particle; x^{gbest} is the best position experienced among all particles (best particle); w, c_1, c_2 are the constant coefficients of PSO method; and r_1, r_2 are the stochastic values.

Binary PSO algorithm is introduced to address the deficiencies of the main algorithm of PSO and is used to solve the optimization problems with discrete search space. The equations for updating the velocity and position of each particle of this algorithm, which is also used in this paper with regard to the existence of binary variables, is according to the following Eqs. (10.27) and (10.28):

$$v_{i,d}^{k+1} = v_{i,d}^k + c_1 r_1 \left(p_{i,d}^k - x_{i,d}^k\right) + c_2 r_2 \left(p_{g,d}^k - x_{i,d}^k\right) \quad (10.27)$$

$$x_{i,d}^k = \begin{cases} 1 & r_3 < \text{sigmoid}\left(v_{i,d}^k\right) \\ 0 & \text{other} \end{cases} \quad (10.28)$$

In recent equations, $p_{i,d}^k$ expresses the best position of the ith particle in repeating k and in the search space as large as d. r_1, r_2, and r_3 are random numbers between 0 and 1 with uniform distribution. The sigmoid logic transform function is used to limit the velocity at a distance of [0,1] and is defined in the following equation (10.29):

$$\text{sigmoid}\left(v_{i,d}^k\right) = \begin{cases} \dfrac{2}{1+\text{e}^{-v_{i,d}^k}} - 1 & -v_{i,d}^k \geq 0 \\ 1 - \dfrac{2}{1+\text{e}^{-v_{i,d}^k}} & -v_{i,d}^k \leq 0 \end{cases} \quad (10.29)$$

According to the presented description, the flow chart of the method used in this research is to solve the MG scheduling optimization problem in accordance with Fig. 10.2. It is assumed that:

$i_{\max}$: The maximum number of PSO members
$k_{\max}$: Maximum PSO iteration
PF: Power flow
C_i : The 24-h cost of the ith member, taking into account the different wind power scenarios and the main electricity grid
$C_{pb,\ i}$: The best (lowest) cost of the ith member
C_{tb}:The best (lowest) cost of all particles
C_{gb}: The final optimal cost

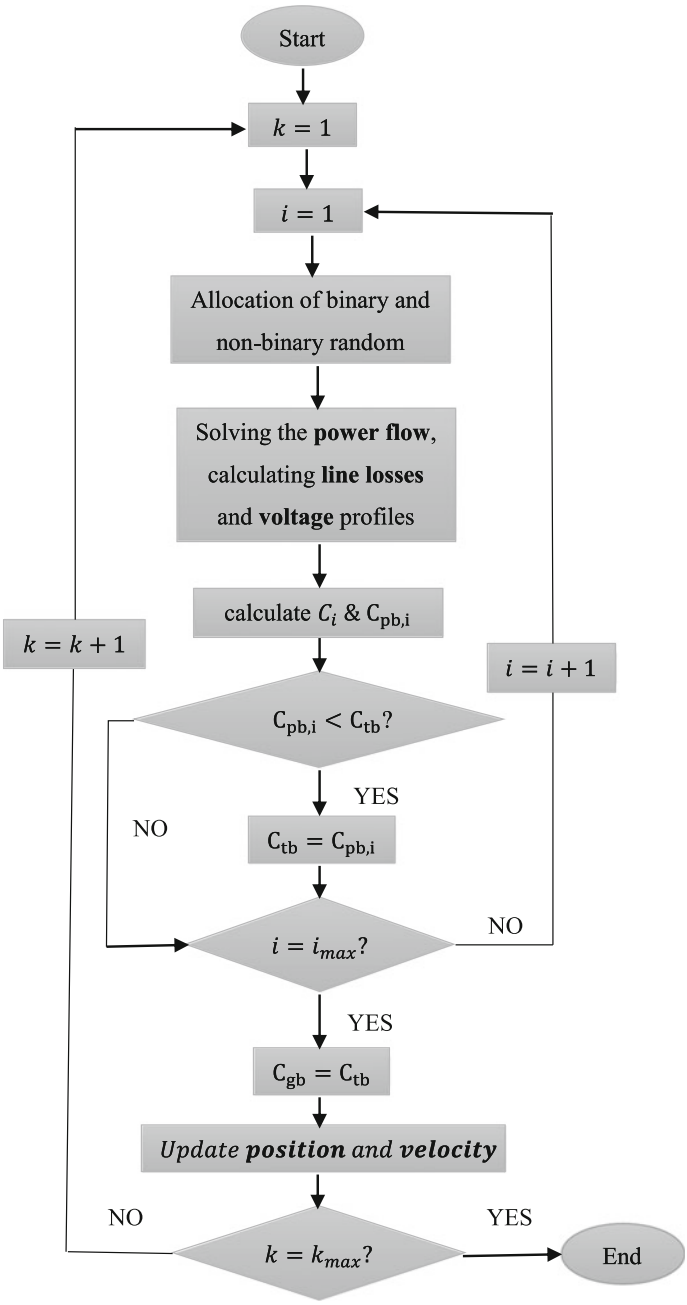

Fig. 10.2 The flow chart of the method used to solve the MG scheduling optimization problem

10.4 Simulation Result

In this section to examine the results of the performance of the model and the proposed method, the IEEE 33-bus test radial distribution network has been used. To convert the distribution system into an MG connected to the main grid after reducing the load scale and increasing the impedance of the grid lines, in such a way that the network voltage and load profiles are exactly the same as their previous and standard state, a series of distributed energy resources and storage equipment have been used. The technical and economic features of the distributed units used are shown in Table 10.1:

After installing each of the scattered resources, the MG is operated as follows (Fig. 10.3):

In the desired MG, the maximum consumption during the planning period is 371.5 kW and the minimum is 99.885 kW. The daily consumption forecast curve for this MG is as shown in Fig. 10.4:

Table 10.1 The technical and economic features of the distributed units

Unit	Cost coefficients and technical constraints					
Diesel	α	β	γ	P_{min}	P_{max}	RU
	0.221	0.142	0.0061	30	300	270
	RD	MUT	MDT	SU	SD	P_0
	250	2	2	0.21	0.21	290
Wind	P_{min}	P_{max}	V_{cin}	V_{co}	V_r	P_r
	0	100	3	25	12	100
Battery	P_{min}			P_{max}		
	−12			12		

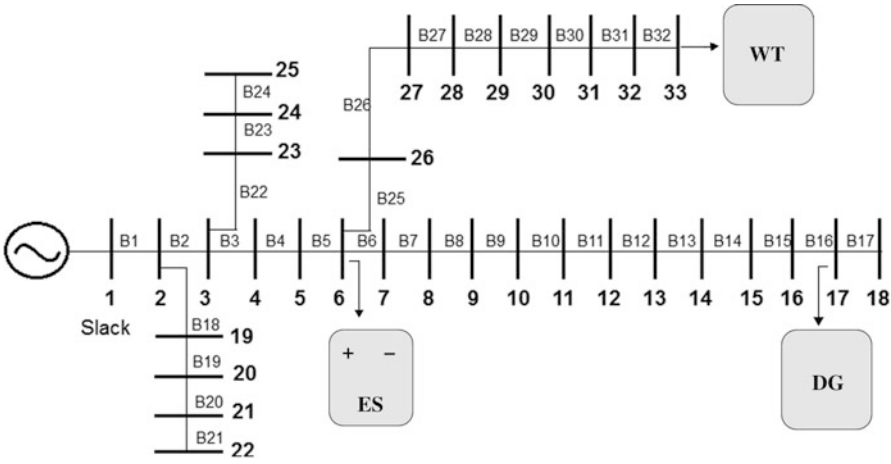

Fig. 10.3 IEEE 33-bus radial distribution system

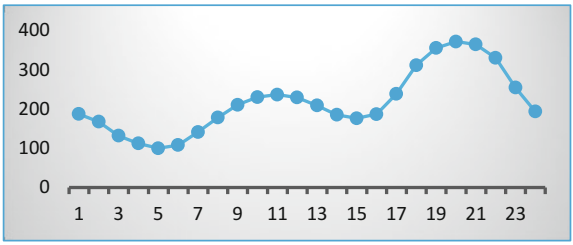

Fig. 10.4 The daily consumption forecast curve

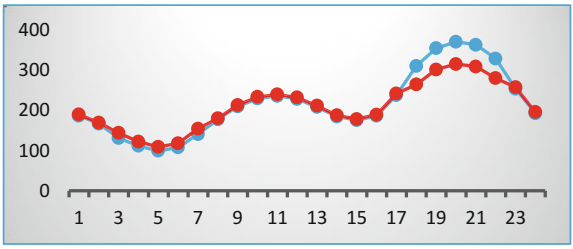

Fig. 10.5 The impact of DRPs on the load curve

Figure 10.5 shows the impact of DR programs on the load curve, assuming a maximum firm commitment of 30%.

As shown, the amount of power consumed at the peak time is reduced, and some amount of power is transferred to the off-peak time, which depends on the amount of the transfer to the price change at different times, the demand pull matrix, and the degree of participation in these programs. The effect of implementing these programs on the cost function, the planning of the power of distributed units, the amount of power exchange with the upstream network, the load profile, and the losses of the MG are the objectives of the implementation of these programs in this paper.

The predicted energy market price for a particular day, as predicted by Ref. [9], is given in Table 10.2. Also, the average wind speed curve for a particular day in the same reference is shown in Fig. 10.6.

In order to evaluate the results and performance of the proposed model and method, the simulation results are analyzed for the four scenarios (Sects. 10.4.1, 10.4.2, 10.4.3, and 10.4.4):

10.4.1 Utilization Planning Without Consideration of Uncertainty and DR

In this case, all predicted parameters such as wind speed, energy cost, and load are assumed definitively and loads are nonresponsive. Figure 10.7 shows the power distribution between distributed units, the amount and time of charge or discharge of the battery, and the way of power exchange with the main network for this state:

Table 10.2 The daily predicted energy market price

Hour	1	2	3	4
Price ($/KWh)	0.4747	0.3164	0.3165	0.326
Hour	5	6	7	8
Price ($/KWh)	0.4078	0.3864	0.7895	0.9414
Hour	9	10	11	12
Price($/KWh)	1.227	1.3229	1.4459	1.0849
Hour	13	14	15	16
Price ($/KWh)	1.064	0.6088	0.585	0.4875
Hour	17	18	19	20
Price ($/KWh)	0.8555	1.1242	2.7558	3.5772
Hour	21	22	23	24
Price ($/KWh)	2.3506	1.4718	0.6127	0.339

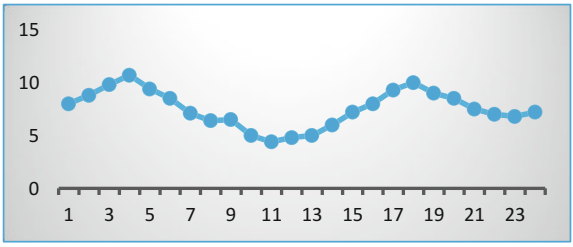

Fig. 10.6 The average wind speed curve

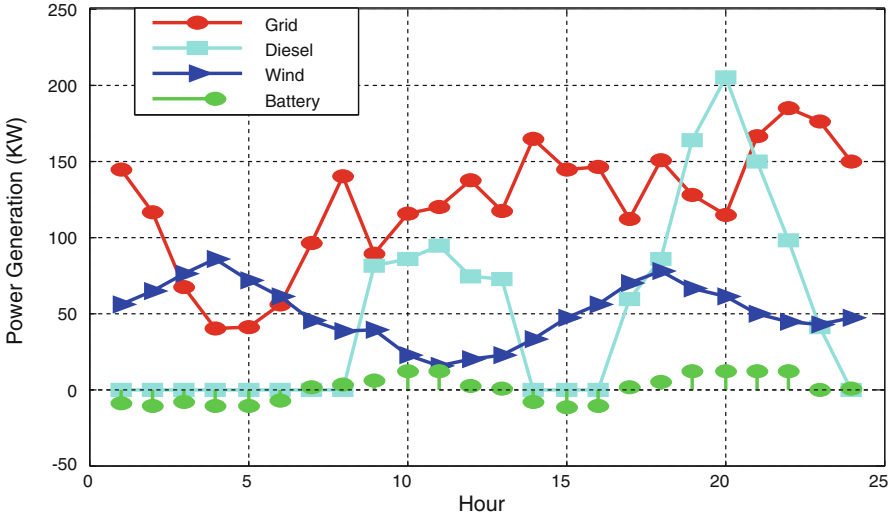

Fig. 10.7 Optimal power distribution of the MG resources in scenario A

Table 10.3 The daily optimal operation cost and loss

Optimal cost ($)	Loss (kWh)
4521.745	125.8791

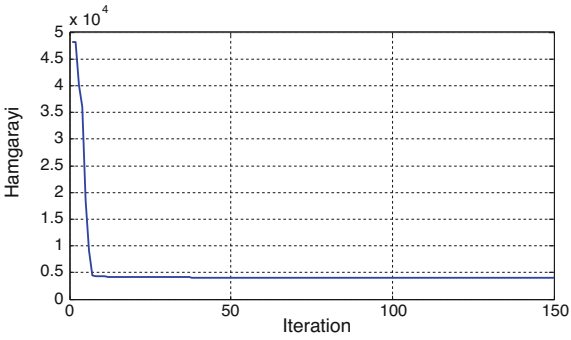

Fig. 10.8 The convergence of the proposed method

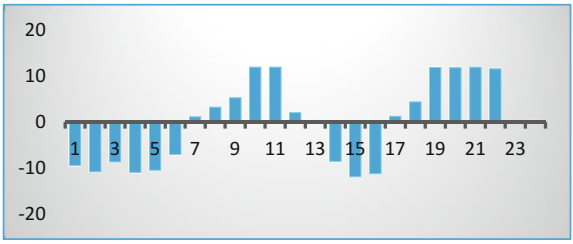

Fig. 10.9 The amount of charge or discharge power of the battery in scenario A

According to Fig. 10.7, in the early hours when the electricity price is lower than peak times, the diesel unit is turned off and power is generated by the network and the other unit, and during high-cost network hours, the diesel unit can be switched on and output, and the amount of purchase from the network has dropped due to its high price, and even the surplus of dispersed and storage units can be sold to the network. The optimal utilization cost for daily planning and the amount of loss during the planning period is presented in Table 10.3.

Figure 10.8 shows the convergence of the proposed method in finding the optimal cost after repeated repetitions.

It should be noted that in the different setup of the program using the MATLAB software and the method described, this value is very low tolerance and can be neglected, and this small amount is also due to the random nature of the method.

The battery used in this grid has a maximum charge and discharge power of 12 kW/h and can store up to 65 kWh and at least 5 kWh of energy. Figures 10.9 and 10.10, respectively, indicate the amount of charge or discharge power and the percentage of available energy of the battery as compared to its maximum storage space per hour of the scheduling period.

As shown in Fig. 10.9, the battery is charged at off-peak hours and discharged at peak times when the energy price is high and is considered as a source of production.

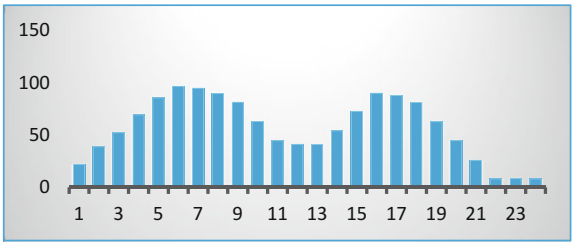

Fig. 10.10 The percentage of available energy of the battery in scenario

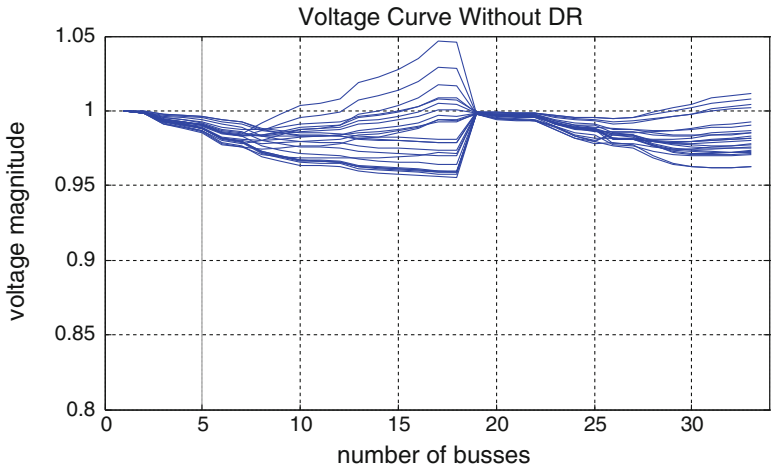

Fig. 10.11 The bass voltages per hour of the scheduling period in scenario A

As noted above, the planning has been carried out with due observance of different constraints. One of the important constraints in the planning of power output in the MG is to consider the non-violation of the voltage value as a technical limit is within the permissible range of 5% of the slack bass voltage. Figure 10.11 shows the bass voltages per hour of the scheduling period as prionite.

As shown in Fig. 10.11, the voltage curve has not exceeded the permissible limit in any of the 24-h scheduling periods.

10.4.2 Utilization Planning Without Consideration of Uncertainty and Presence of DR

In this case, consumers are sensitive to price changes at different times. As a result, with rising prices at peak hours, consumption is reduced during these hours or part of it is transferred to off-peak times. Figures 10.12 and 10.13, respectively, compare the cost of operation and the casualties of this mode with the operating mode without DR:

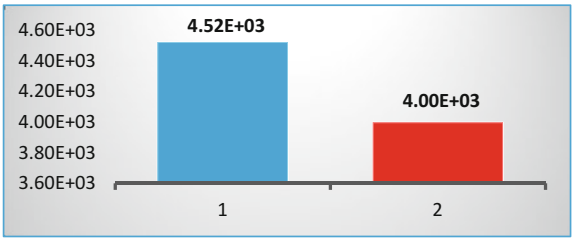

Fig. 10.12 Comparison of the cost of operation in the with and without DRPs (scenario A and B)

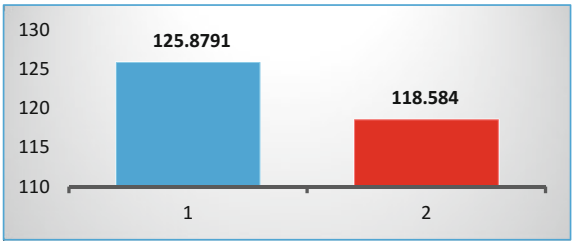

Fig. 10.13 Comparison of transmission line losses in the with and without DRPs (scenario A and B)

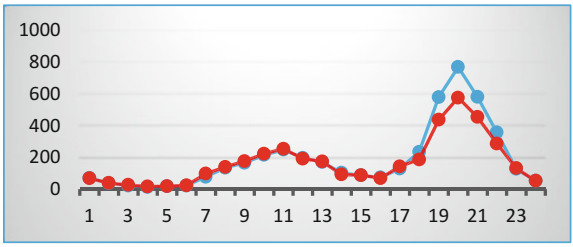

Fig. 10.14 Comparison of the operating cost per hour of the scheduling period with and without DRPs

It can be seen that the implementation of these programs reduces the cost of exploitation and losses of the MG lines.

The curve of Fig. 10.14 clearly shows that the cost of utilization in peak times during the implementation of load response programs has declined, and because of the price drop in peak hours and the shift in part of the consumption to these hours, the cost of these hours has gone up modestly.

In this case, optimal scheduling requires that the power transmission be carried out in such a way that, besides changing the values of the diesel unit and the battery, in the first priority, the purchase of the upstream network will be reduced due to its high price and this is seen in the following results. The status of charge and discharge of the battery and the amount of energy in the battery with the same previous information, with a slight increase in the charge amount at off-peak hours and increasing the amount of discharged at peak times, are in accordance with Figs. 10.15 and 10.16, respectively.

By implementing responsive programs and changing the load profile and distributing power between resources, new programming should not cause voltage curves to run out of range and Fig. 10.17 confirms this problem.

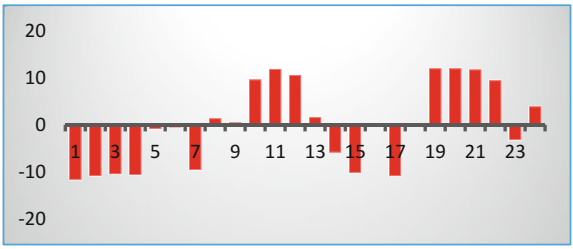

Fig. 10.15 The amount of charge or discharge power of the battery in scenario B

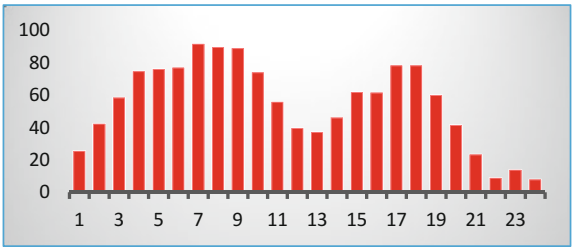

Fig. 10.16 The percentage of available energy of the battery in scenario B

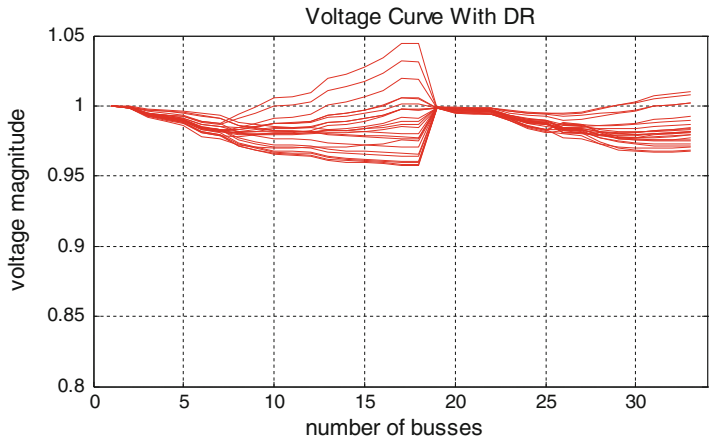

Fig. 10.17 The bass voltages per hour of the scheduling period in scenario B

10.4.3 Utilization Planning with Consideration of Uncertainty and Lack of DR

In this case, the results are based on the implementation of stochastic formulation. Each of the uncertainty parameters has a certain amount of predicted error relative to their values in the two previous states, which consider these errors leading to different scenarios of the values of these parameters. Eventually, the uncertainty is covered by providing randomized planning based on existing scenarios. Figure 10.18 shows the power distribution between the units available for this mode of operation.

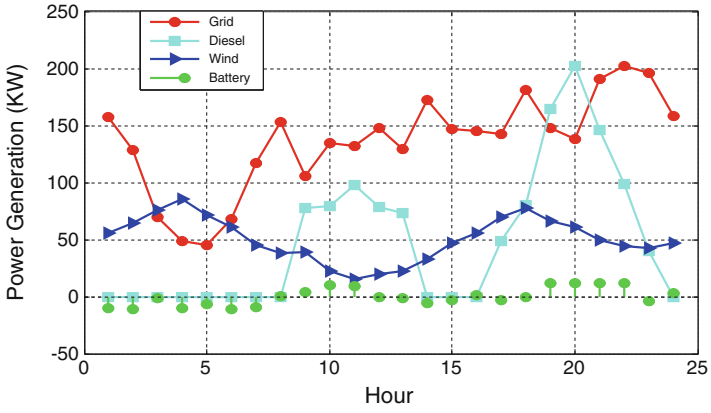

Fig. 10.18 Optimal power distribution of the MG resources in scenario C

Fig. 10.19 Comparison of the cost of operation in the definitive and stochastic programming

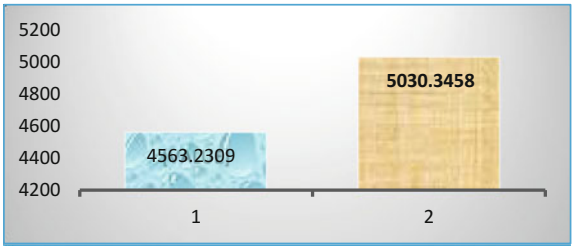

Fig. 10.20 Comparison of the transmission losses in the definitive and stochastic programming

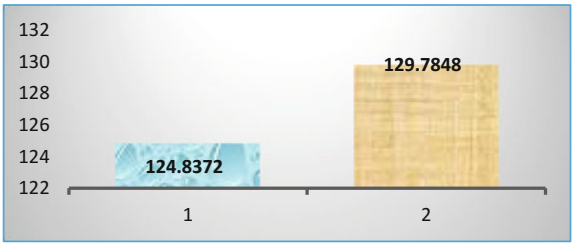

It can be argued that by applying this insufficiency, the amount of MG dependence has increased to buy power from the main grid. The reason for this increase in purchases from the main network and the relative decline in purchases from diesel generators can be seen at the high cost of generating diesel generator power due to higher fuel costs than the cost of purchasing power from the main network.

Figures 10.19 and 10.20 show the comparison of cost and casualties in two definitive and randomized operation models without considering the DR.

This increase is reasonable in a randomized operation model that is more stable and more reliable under conditions of uncertainty of renewable resources, load, and network costs. Also, the amount of grid losses in this case has also increased due to the relative increase in unit production due to wind power error and consumer load.

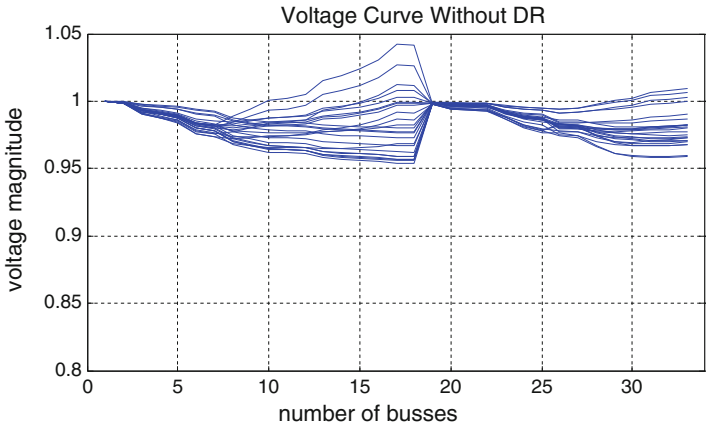

Fig. 10.21 The bass voltages per hour of the scheduling period in scenario C

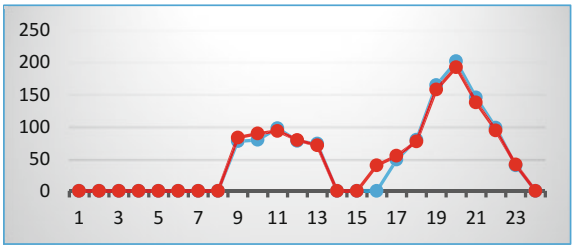

Fig. 10.22 The changes in the production capacity of a diesel unit in operation mode with and without DRPs

Stochastic operation under the conditions of different scenarios of the irregular parameters should not increase or drop excess network voltages, as shown in Fig. 10.21 of this claim.

10.4.4 Operational Planning with Consideration of Uncertainty and DR

In this case, by executing responsive programs, optimal cost utilization and losses changes, along with the coverage of uncertainty parameters, are investigated. Figures 10.22 and 10.23 show, respectively, the changes in the production capacity of a diesel unit and the main network in a random mode with presence of DRPs compared to a without DRPs mode.

According to these comparisons, at peak times, the dependence of the MG on the diesel unit is higher than the main grid because of its higher price, and the amount of purchase from the main grid at these times has significantly decreased. Also, due to lower prices during off-peak hours as a result of the implementation of these programs, the amount of injected power of the network is slightly increased and the

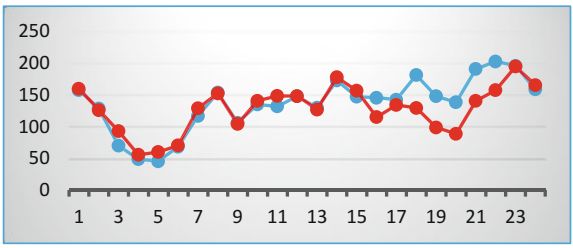

Fig. 10.23 The changes in the production capacity of a diesel unit in operation mode with and without DRPs

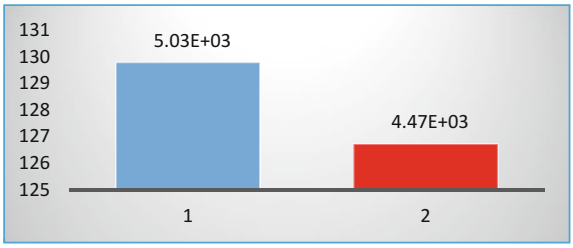

Fig. 10.24 Comparison of the cost of operation in the with and without DRPs (scenario C and D)

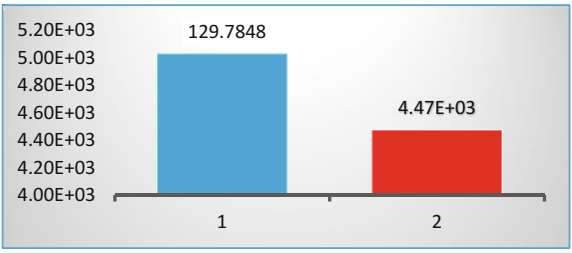

Fig. 10.25 Comparison of transmission line losses in state with and without DRPs (scenario C and D)

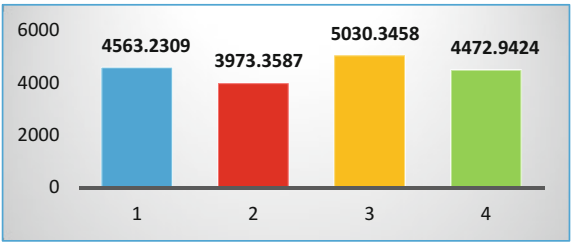

Fig. 10.26 Comparison of optimal cost of four different exploitation scenarios

diesel unit in these hours is off because of the high cost of fuel than to buy power from the main network. These changes in resource generation reduce the optimal cost as well as the network losses and Figs. 10.24 and 10.25 illustrate this issue, respectively.

Figures 10.26 and 10.27 show, respectively, optimal cost values and network losses in four different scenarios to determine the best operating conditions from the operator's perspective.

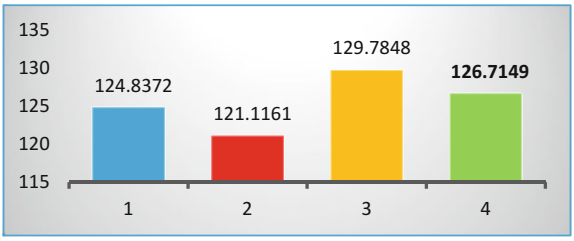

Fig. 10.27 Comparison of transmission losses of four different exploitation scenarios

As the figures show, running DRPs, both in certain mode operation and stochastic operation, leads to a reduction in optimal utilization costs and grid losses, and this shows the necessity of implementing these programs in the planning of this MG. On the other hand, while the definitive mode of operation, taking into account DRPs relative to random operation mode, is about 12.5% less cost and about 4.5% fewer casualties, but this is reasonable and justified way due to considering and covering the uncertainty of renewable energy sources, the amount of MG load, and network price, in stochastic mode. Therefore, planning with the consideration of DRPs and uncertainty is the most economical planning in real terms.

10.5 Conclusion

Considering the importance and development of MGs in the distribution network, it is important to develop and improve their utilization planning. In this regard, this paper presents optimal operational planning of an MG connected to the upstream network, taking into account the losses of transmission lines and the implementation of the demand response program, under the conditions of uncertainty of renewable resources, the amount of consumption, and the price of energy. The operator's goal is to reduce the cost of supplying power to feed the grid load, under the conditions of different constraints of production units, technical and network, also part of this cost related to the losses of transmission lines. The duration of the MG operation planning is 24 h. Also, the impact of the DRPs of the optimal utilization cost, the MG losses, and the planned power of the MG components is analyzed. To simulate and evaluate the results, four different scenarios of exploitation have been studied. Numerical results show that by executing the DRP, the cost of power supply and the losses of the MG are reduced. However, in the case of stochastic operation and under uncertainty conditions, the cost of exploitation and losses are more than definitive utilization mode and without considering the uncertainty. However, these increases seem to be reasonable, due to the consideration and coverage of these uncertainties. Finally, according to the results, it was suggested that from the operator's point of view, the most appropriate scenario is the planning of exploitation in the presence of the DRPs and taking into account the uncertainty.

References

1. R.H. Lasseter, P. Paigi, Microgrid: a conceptual solution. PESC Rec. IEEE Annu. Power Electron. Spec. Conf. **6**, 4285–4290 (2004)
2. J.D. McDonald, The next-generation grid: energy infrastructure of the future, Guest Editorial, IEEE Power & Energy Magazine, **7** (2009)
3. M. Gitizadeh, S. Farhadi, S. Safarloo, Multi-objective energy management of CHP-based microgrid considering demand response programs, in *Smart Grid Conference*, (2014), https://doi.org/10.1109/sgc.2014.7090870
4. M. Alipour, B. Mohammadi-Ivatloo, K. Zare, Stochastic scheduling of renewable and CHP-based microgrids. IEEE Trans. Ind. Informatics **11**(5), 1049–1058 (2015)
5. C. Deckmyn, T.L. Vandoorn, M. Moradzadeh, L. Vandevelde, Multi-objective optimization for environomic scheduling in microgrids, in *IEEE PES General Meeting Conference & Exposition* (2014), pp. 1–5
6. S. Mohammadi, S. Soleymani, B. Mozafari, Scenario-based stochastic operation management of MicroGrid including wind, photovoltaic, micro-turbine, fuel cell and energy storage devices. Int. J. Electr. Power Energy Syst. **54**, 525–535 (2014)
7. A. Chaouachi, R.M. Kamel, R. Andoulsi, K. Nagasaka, Multiobjective intelligent energy Management for a Microgrid. Aymen Chaouachi - academia. IEEE Trans. Ind. Electron. **60** (4), 1688–1699 (2013)
8. R. Wang, P. Wang, G. Xiao, A robust optimization approach for energy generation scheduling in microgrids. Energy Convers. Manag. **106**(2015), 597–607 (2015)
9. A. Zakariazadeh, S. Jadid, P. Siano, Stochastic operational scheduling of smart distribution system considering wind generation and demand response programs. Int. J. Electr. Power Energy Syst. **63**, 218–225 (2014)
10. G.R. Aghajani, H.A. Shayanfar, H. Shayeghi, Presenting a multi-objective generation scheduling model for pricing demand response rate in micro-grid energy management. Energy Convers. Manag. **106**(2015), 308–321 (2015)
11. H.S.V.S.K. Nunna, S. Battula, A. Sesetti, S. Doolla, Impact of incentive mechanism on demand response programs in smart microgrids with electric vehicles. Intell. Ind. Syst. **1**(3), 245–254 (2015)
12. S. Shams, S. Farahani, M. B. Tabar, H. Tourang, M. G. Naraghi, A. Javadian, Using exponential modeling for EDRP demand response programs. J. Basic Appl. Sci. Res. **10**, 1774–1779 (2011)
13. J.M. Guerrero, M. Chandorkar, T.-L. Lee, P.C. Loh, Advanced control architectures for intelligent microgrids, Part I: decentralized and hierarchical control. IEEE Trans. Ind. Electron. **60**(4), 1254–1262 (2013)
14. S. French, Uncertainty and imprecision: modelling and analysis. J. Oper. Res. Soc. **46**(1), 70–79 (1995)
15. M. Mazidi, A. Zakariazadeh, S. Jadid, P. Siano, Integrated scheduling of renewable generation and demand response programs in a microgrid. Energy Convers. Manag. **86**, 1118–1127 (2014)
16. H.A. Aalami, M.P. Moghaddam, G.R. Yousefi, Modeling and prioritizing demand response programs in power markets. Electr. Power Syst. Res. **80**(4), 426–435 (2010)
17. P. Karimyan, M. Abedi, R. Khatami, Stochastic approach to represent distributed energy resources in the form of a virtual power plant in energy and reserve markets. IET Gener. Transm. Distrib. **10**, 1792–1804 (2016)

Chapter 11
Techno-Economic Framework for Congestion Management of Renewable Integrated Distribution Networks Through Energy Storage and Incentive-Based Demand Response Program

Arya Abdolahi, Farhad Samadi Gazijahani, Navid Taghizadegan Kalantari, and Javad Salehi

Nomenclature

Sets and Indices

b	BES units index
c	CHP units index
i	Network busses index
l	Network lines index
n	WT units index
N_{B}	Set of busses
N_{BES}	Set of BES units
N_{CHP}	Set of CHP units
N_{L}	Set of lines
N_{PV}	Set of PV units
N_{WT}	Set of WT units
m	PV units index
t	Hour index

Variables

δ_i	Voltage angle of ith node
$\rho(t)$	Electricity price
$\rho_0(t)$	Primary electricity price

A. Abdolahi · F. S. Gazijahani (✉) · N. T. Kalantari · J. Salehi
Department of Electrical Engineering, Azarbaijan Shahid Madani University, Tabriz, Iran
e-mail: f.samadi@azaruniv.ac.ir

S. Nojavan, K. Zare (eds.), *Demand Response Application in Smart Grids*,
https://doi.org/10.1007/978-3-030-32104-8_11

θ_l	Admittance angle of lth line
$d(t)$	Consumption demand after executing DR program
$d_0(t)$	Primary consumption demand
$P_{t,l}^{\text{cap}}$	Maximum capacity of line l at time t
P_t^{DG}	Power generation of DG at tth hour
$P_{b,t}^{\text{ch}}$	The amount of charged power of bth BES at tth hour
$P_{b,t}^{\text{dis}}$	The amount of discharged power of bth BES at tth hour
P_i^{net}	Net active power of bus i
P_t^{load}	The amount of power consumption at tth hour
$P_{t,\ l}$	Active power flow of line l at tth hour
$P_{t,l}^{\text{loss}}$	Power losses of line l at tth hour
P_i^{net}	Net active power of bus i
$P_{m,t}^{\text{pv}}$	Power production of the mth PV at tth hour
P_t^{REST}	Power of net load at tth hour
$P_{n,t}^{\text{wind}}$	Power production of the nth WT at tth hour
Q_i^{net}	Net reactive power of bus i
$\text{SoC}_{b,\ t}$	State of charge of bth storage at tth hour
V_i	The amount of voltage of ith bus
Y_l	Admittance of lth line

Parameters

η_{ch}	The efficiency of charge
η_{dis}	The efficiency of discharge
Π_t^{ch}	Charging price at tth hour
Π_t^{dis}	Discharging price at tth hour
$\vec{a}$	Iteration step vector of GWO
$\vec{A}, \vec{C}$	Vectors of GWO factor
C	Scale factor of the Weibull PDF
G	Global solar radiation
G_{ING}, G_{STG}	Solar irradiance in standard and study condition
$\text{iter}_{\max}$	Maximum iteration number
k	Power temperature factor
K^{DG}	Operating coefficient of DG
K^{ESS}	Operating coefficient of BES
L	Non-dominated solutions number
NOCT	Normal operating cell temperature
$P^{\min}$, $P^{\max}$	Minimum and maximum active power of DGs
P_i^{rat}	Rated power of the WT installed in bus i
P_{STG}	Rated produced power by the PV under normal trial situation
$Q^{\min}$, $Q^{\max}$	Minimum and maximum reactive power of DGs

r_1, r_2	Random vectors of GWO
s	Shape factor of the Weibull PDF
$\mathrm{SoC}_b^{\min}$	Lower bound of SoC of bth BES
$\mathrm{SoC}_b^{\max}$	Upper bound of SoC of bth BES
T_a	Ambient temperature
T_C, $T_{C,\,\mathrm{ref}}$	Cell and air temperature of PV units
v	The speed of wind
$v_{\mathrm{c\,in}}$	Cut-in speed of WT
$v_{\mathrm{c\,out}}$	Cutout speed of WT
v_{rat}	Rate speed of the WT
$V^{\min}$, $V^{\max}$	Minimum and maximum ranges of voltage magnitude
$\vec{X}$	Location of the gray wolf
$\vec{X}_P$	Location vector of the hunt
Z_i, z_i	Maximum and minimum value of the ith objective function

11.1 Introduction

11.1.1 Background

With development of the power systems and growth in the demand of electricity, the need for production and electrical energy transmission has been increased. On the other hand, with the execution of deregulation in the power sector, the optimal and economical operation of power systems has become important. Free access systems, which lead to competing in production, permit consumers to choose their energy resources voluntarily. This reason causes the maximum capacity of the lines to be used more than ever [1].

Traditionally to meet the growth in demand, new substations and distribution lines have been designed and exploited. This raises the need for further generation because of increase in system losses, as well as more costs for distribution feeders/lines and equipment. In recent decades with increasing of the oil price and other fossil fuels, which are used in power plants for electricity production, the need for economic and optimal operation of power systems increased. With regard to the problems related to the distribution lines and environmental and legal issues, it is avoided from the expansion of new lines in the distribution network (DN) as far as possible and attempted to utilize the maximum capacity of the distribution lines [2, 3].

With the ever-increasing demand and advancement in technology, the electricity market has become deregulated condition from regulated condition. Congestion, spot prices mutation, reliability reducing, and market unbalancing are some of challenges in the deregulated power market. From the above challenges, they recently focus on the congestion management (CM). Congestion occurs when distribution lines have not sufficient capacity to transfer all the power according to

the market designs [4]. Congestion is defined as a line overloaded condition that causes unexpected outages, equipment failures, generators outages, a sudden increase in demand, and a lack of coordination between generation and transmission. This will prevent new contracts and the impossibility of existing contracts, causing damage to components of the system. Congestion may be partially managed by reserve units and congestion pricing and improved with some technical controls such as phase shift, change in transformer tap, reactive power control, and generation rescheduling [5].

The existence of a large number of renewable energy sources (RES) in DN increases the risk of the network capacity expansion more than ever. Therefore, the existing network expansion for congestion management leads to high investment costs in the power system. Demand response programs (DRPs) and energy storage systems (ESS) are a promising solution to deal with congestion without expansion [6].

11.1.2 Congestion in Power Systems

In the competitive power market, optimal operation in a direction that reduces costs and handles the maximum capacity of lines is very important. Participants in the power market try to gain more profit and deliver higher electrical power from distribution lines optimally. Therefore, the power systems often work near their marginal condition, and some of the lines may be overloaded, which are called congestion. Applying appropriate solutions for eliminating congestion is called CM that is one of the most important tasks of the distribution system operator (DSO). It is one of the most challenging issues in the electricity market and distribution networks [7].

11.1.3 Congestion Management in Power Systems

Recently increasing in electricity demand and preventing air contamination, it is essential to install a large capacity of RESs like solar cells, wind turbines (WT), and combined heat and power (CHP) generation systems in active distribution networks (ADN). Increasing penetration of distributed generation sources creates a series of technical problems such as overvoltage, line congestion, and harmonics, and in addition, increase in demand affects shortage of production capacity, outages, and increasing electricity prices [8].

With a steady increase in demand, additional costs are used to expand the existing DN and installation of new power stations and feeders. Thus these costs are just for power supply in some critical periods of a year. Therefore, we need to consider the appropriate methods to release the capacity of the lines, reducing network congestion during the peak hours. It is necessary to apply DRPs and ESSs to transfer the

inessential load demand from peak periods to off-peak periods with the goal of CM [9].

11.1.4 Literature Review

In recent years, several methods have been used for CM in [10]. For example, author in Ref. [11] presented a formulation for coordinating both FACTS device controllers and DRPs via constrained optimization method with the goal of CM at a lower operation cost. Moreover, the incentive and penalty terms are appended to the DR mathematical model to allow the ISO through the aggregator to have two factors to control the responsive demand capacity. These terms increase the number of DR participants at certain load buses that are important for the system security. A distribution congestion price (DCP)-based market approach is suggested in [12] to investigate the behavior of DRPs on CM in distribution systems in the day-ahead electricity market. Since the DCPs should determine the accurate cost of congestion, the theory of locational marginal pricing is utilized to specify the DCPs in the day-ahead electricity market by the distribution system operator. Reference [13] has been modeled the distribution locational marginal price (DLMP) as a quadratic programming for CM in ADNs.

Paper [14] presented a novel process for specifying the optimal busses and hours for the DRP execution based on power transfer distribution coefficients, available transfer capability (ATC), and dynamic DC-OPF as well as considering the effects of DRPs on ATC and line congestion alleviation. A new CM method is presented via DRPs [15]. In this scheme, optimal combination of generation scheduling and DRPs is used to alleviate the congestion of lines. Optimal congestion management is based on electricity power market mechanism presented in [16], where DRPs are implemented with considering retailer electricity provider. The author in Ref. [17] concentrates on solving congestion problem with generation rescheduling, emergency DRPs, and direct load control (DLC). In this article, a multi-objective CM is modeled due to solve the congestion phenomena; fuzzy multi-objective PSO algorithm considering Pareto frontier is suggested. The suggested model includes a kind of objective functions and practical concepts containing maximization of transmission lines loading with operation costs as first objective and minimization of air pollution as defined second objective function. A bi-level optimization model for the accurate evaluation of ATC has been discussed in [18].

11.1.5 Contributions

Because of the presence of various distributed energy resources (DERs) in ADNs, which have various rates and generation, loads are often able to supply their required power from cheaper and more reliable sources. The load consumption of consumers

has changed hourly and involves peak and off-peak hours. In peak hours, further loads enter the network and the total demand of the network increases, so in these periods, some lines become congested. The congestion of lines should be managed and reduced. For solve this problem, the available capacity of the network lines must be increased. In other words, existing lines must be expanded. This is not a good solution to solve the congestion problem because the development of the ADN has high investment cost and long-term exploitation. The proposed solution for solving the congestion problem is applied in the energy storage system (ESS) available in the ADN and demand response program (DRP). In the off-peak hours, the ESS purchase power from the upstream grid with a lower rate than the DERs and charged. Then, in the peak hours when the electricity rate is high, ESS can sell stored power to costumers, so that the congestion of lines alleviated and the operation cost minimized. Moreover, DRP manage the congestion of the system by altering the rate of electricity tariffs through different hours aimed at motivating consumers to change their energy usage patterns. The main goal of the proposed methodology is to manage the network congestion as well as minimize the operation costs with the use of ESS and DRP. This chapter attempts to provide the following contributions:

- Utilizing DR and ESS to manage the congestion and minimize the operation cost.
- Formulating the congestion problem as a cost-oriented model from the DSO perspective.
- Optimal decentralized energy management of dispatchable and non-dispatchable resources.
- Investigating the uncertainty of RESs generation using probabilistic modeling.
- Deploying a mixed integer nonlinear programming to model the problem and optimizing by gray wolf optimization (GWO) algorithm.

11.2 Problem Formulation

Equation (11.1) presents the sum of congestion and system operational cost equations, which is minimized by GWO algorithm in this chapter to reach the proposed goal include congestion and energy management of the system with implementing DR program, scheduling of BESS, and optimal planning of DERs.

$$\min F_{\text{Total}} = [F_1 + F_2] \tag{11.1}$$

11.2.1 Congestion Management

The proposed distribution network is active one and includes different kinds of private DERs. These private DERs sell their generation powers to the consumers at

locational marginal prices (LMPs). But because of the limitation of the network lines capacity, some DERs with low price cannot sell their maximum production. In this case, the LMPs will be increased in some nodes of network. In order to avoid this problem, BESS is used to store excess power generated by DERs at the off-peak hours and discharged it at the peak hours in the network. In addition to BESS, the DRPs have been applied to reduce the consumption load of system in critical hours.

The goal of CM is to alleviate the distribution lines congestion or, on the other hand, to decrease the value of power flow of distribution lines which is overloaded. For this aim, the difference between the active power transactive of lines and the maximum capacity of lines should be minimized. Equation (11.2) shows the difference between active power transmission and line capacity, which is considered with a cost coefficient until the equation converted from power to cost [19]. The congestion cost coefficient (K^{Con}) for all buses is determined by the difference of LMP between the first bus and desired buses which can be calculated as shown in Eq. (11.3).

$$F_1 = \sum_{t=1}^{T} \sum_{l=1}^{N_L} \left[\left(\left| P_{t,l} - P_{t,l}^{\text{cap}} \right| \right) \times K^{\text{Con}} \right] \tag{11.2}$$

In this paper, the suggested CM method is implemented in accordance with the practical and technical constraints given below.

$$P_l^{\min} \le P_l \le P_l^{\max}, \quad \forall l \in N_L, \forall t \in T \tag{11.3}$$

$$V_i^{\min} \le V_i \le V_i^{\max}, \quad \forall i \in N_{\text{B}}, \forall t \in T \tag{11.4}$$

$$P_{t,l}^{\text{loss}} = \left(RP_i^2 / V_i^2 \right), \quad \forall i \in N_{\text{B}}, \forall t \in T \tag{11.5}$$

$$P_{t,l} = V_i \times I_l^*, \quad \forall l \in N_{\text{L}}, \forall t \in T \tag{11.6}$$

$$P_i^{\text{net}} = \sum_{l=1}^{N_L} \sum_{i=1}^{N_{\text{bus}}} V_i V_{i+1} Y_l \cos\left(\delta_i - \delta_{i+1} - \theta_l\right), \quad \forall l \in N_{\text{L}}, \forall i \in N_{\text{B}}, \forall t \in T \tag{11.7}$$

Constraint (11.3) indicates the limitation of the transaction active power of the line l. Constraint (11.4) shows the minimum and maximum voltage magnitude limit of the bus i. Equation (11.5) shows the power losses of the line l at time t. The amount of power flow of lth line at tth hour is illustrated in Eq. (11.6). Equation (11.7) presents net active power of the ith bus at tth hour.

11.2.2 Operational Costs

Considering the balance between production and consumption and comparing market prices with the energy-generated price from local sources, the optimal

charging/discharging scheduling of BESS is carried out. Therefore, if the output of DERs and upstream network are higher than the consumption rate, the BESS will operate as a consumer and charges. Nevertheless, if the value of DERs and upstream network are less than the amount of consumption, the BESS will act as a generator into the network and provides loads.

$$F_2 = \sum_{t=1}^{T} \left[\sum_{b=1}^{N_{\text{BES}}} \left[\begin{array}{l} \left(K^{\text{PV}} \times P_t^{\text{PV}}\right) + \left(K^{\text{WT}} \times P_t^{\text{WT}}\right) + \left(K^{\text{CHP}} \times P_t^{\text{CHP}}\right) \\ + \left(\Pi_t^{\text{Ch}} \times P_{b,t}^{\text{Ch}}\right) + \left(K^{\text{BES}} \times P_{b,t}^{\text{Ch}}\right) + \sum_{l=1}^{N_L} \left(P_{t,l}^{\text{Loss}} \times K^{\text{Loss}}\right) \end{array} \right] + C^{\text{DR}} \right] \tag{11.8}$$

Equation (11.8) shows the operating cost of DGs including wind power turbines, PVs, and CHP units. Optimal scheduling of ESSs, optimal production of DGs, and applied DRP could manage the congestion of lines. It should be mentioned that the cost of DRP is defined as follows and the optimal amount of incentive is determined by the GWO algorithm.

$$\begin{aligned} C^{\text{DR}} = &\left(\text{Incentive cost} - \text{Reduced consumption cost}\right) \\ &\times \text{The amount of curtailed power by consumers} \end{aligned}$$

Different constraints are considered in the optimization problem, as shown below.

$$P_t^{\text{REST}} = P_t^{\text{load}} - P_t^{\text{DG}}, \quad \forall t \in T \tag{11.9}$$

$$P_t^{\text{DG}} = P_{n,t}^{\text{WT}} + P_{m,t}^{\text{PV}} + P_{c,t}^{\text{CHP}}, \quad \forall t \in T \tag{11.10}$$

$$P_{t,n}^{\text{WT, min}} \le P_{t,n}^{\text{WT}} \le P_{t,n}^{\text{WT, max}}, \quad \forall n \in N_{\text{WT}}, \forall t \in T \tag{11.11}$$

$$P_{t,m}^{\text{PV, min}} \le P_{t,m}^{\text{PV}} \le P_{t,m}^{\text{PV, max}}, \quad \forall m \in N_{\text{PV}}, \forall t \in T \tag{11.12}$$

$$P_{t,c}^{\text{CHP, min}} \le P_{t,c}^{\text{CHP}} \le P_{t,c}^{\text{CHP, max}}, \quad \forall c \in N_{\text{CHP}}, \forall t \in T \tag{11.13}$$

Equations (11.9) and (11.10) show the equilibrium equation of total power and the total production capacity of DERs at time t, respectively. Additionally, constraints (11.11–11.13) express the operating zone of DERs.

11.2.3 Battery Energy Storage System

Batteries are produced from compressed cells, which turn chemical energy to electrical energy. The level of the voltage and current of the batteries are obtained from the type of parallel connection or series of cells. The batteries are classified in terms of energy and power. Efficiency, lifetime, operating temperature, discharge depth, and energy density are some of the most critical parameters of the battery.

$$\mathrm{SoC}_{b,t+1} = \mathrm{SoC}_{b,t} + \left(P_{b,t}^{\mathrm{Ch}} \eta^{\mathrm{Ch}} - P_{b,t}^{\mathrm{Dis}} / \eta^{\mathrm{Dis}}\right), \quad \forall t \in T \tag{11.14}$$

$$\mathrm{SoC}_b^{\min} \leq \mathrm{SoC}_{b,t} \leq \mathrm{SoC}_b^{\max}, \quad \forall t \in T, \forall b \in N_{\mathrm{BES}} \tag{11.15}$$

$$0 \leq P_{b,t}^{\mathrm{Ch}} \leq P_b^{\mathrm{Ch,\,max}}, \quad \forall t \in T, \forall b \in N_{\mathrm{BES}} \tag{11.16}$$

$$0 \leq P_{b,t}^{\mathrm{Dis}} \leq P_b^{\mathrm{Dis,\,max}}, \quad \forall t \in T, \forall b \in N_{\mathrm{BES}} \tag{11.17}$$

Equation (11.14) shows the SoC of battery b at tth hour. Equation (11.15) indicates the maximum and minimum limit of SoC, and constraints (11.16) and (11.17) illustrate the maximum limits of charging and discharging, respectively.

11.3 DRP Implementation

Smart grid promises high efficiency in electric energy and it is one of the major components of DRP. DR is a unique energy contract with a utility or curtailment service provider. This financial arrangement is called for load shedding, when the network is in response to the price variations. Facility managers receive a notification from an event and take the necessary measures to reduce their energy consumption. In general, DRPs can be classified in incentive-based and time-based groups, where each mentioned group includes several programs as shown in Fig. 11.1 [20–22].

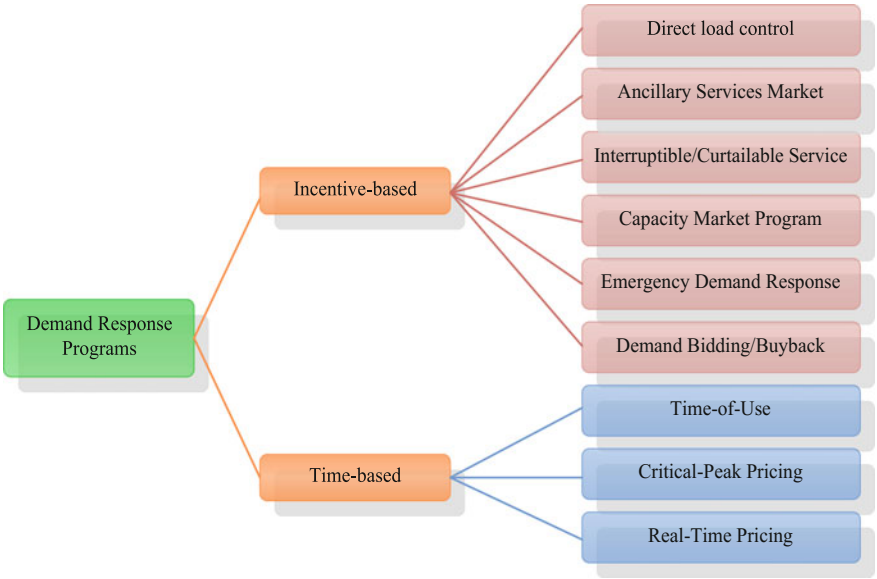

Fig. 11.1 Categories of DRPs

Elasticity is defined as the ratio of demand variation to the price variation as in (11.18) and (11.19):

$$E(t,t') = \frac{\rho_0(t')}{d_0(t)} \times \frac{\partial d(t)}{\partial \rho(t')} \tag{11.18}$$

$$\begin{cases} E(t,t') \leq 0, & \text{if} \rightarrow t = t' \\ E(t,t') \geq 0, & \text{if} \rightarrow t \neq t' \end{cases} \tag{11.19}$$

The daily amount of self-elasticity and cross-elasticity shown in (11.20) is named the price elasticity matrix.

$$\begin{bmatrix} \Delta d(1)/d_0(1) \\ \Delta d(2)/d_0(2) \\ \Delta d(3)/d_0(3) \\ \vdots \\ \Delta d(24)/d_0(24) \end{bmatrix} = \begin{bmatrix} E(1,1) & \cdots & E(1,24) \\ \vdots & \ddots & \vdots \\ E(24,1) & \cdots & E(24,24) \end{bmatrix} \times \begin{bmatrix} \Delta \rho(1)/\rho_0(1) \\ \Delta \rho(2)/\rho_0(2) \\ \Delta \rho(3)/\rho_0(3) \\ \vdots \\ \Delta \rho(24)/\rho_0(24) \end{bmatrix} \tag{11.20}$$

*J*th column from the price elasticity matrix shows the price variations. In this matrix, if the elements above the main diagonal are non-zero, it expresses that consumers want to transfer their consumption to hours other than hours at high prices. If the elements below the main diagonal are non-zero, it shows that consumers wait for hours with low price by postponing their consumption at hours with high price [14]. The net profit of consumers is presented in Eq. (11.21).

$$\text{NP}(d(t)) = B(d(t)) - [d(t) \times \rho(t)] \tag{11.21}$$

The derivative of Eq. (11.21) should be zero to maximize the net profit of consumers as in (11.22).

$$\frac{\partial \text{NP}(d(t))}{\partial d(t)} = \frac{\partial B(d(t))}{\partial d(t)} - \rho(t) = 0 \rightarrow \frac{\partial B(d(t))}{\partial d(t)} = \rho(t) \tag{11.22}$$

Taylor series of net profit equation is written as follows.

$$B(d(t)) = \left\{ B(d_0(t)) + \frac{\partial B(d_0(t))}{\partial d(t)} [d(t) - d_0(t)] + \frac{1}{2} \frac{\partial^2 B(d_0(t))}{\partial d^2(t)} [d(t) - d_0(t)]^2 \right\} \tag{11.23}$$

In order to reach the optimal consumption, consumers must get maximum profits as in (11.24).

$$B(d(t)) = \left\{ B(d_0(t)) + \rho_0(t)[d(t) - d_0(t)] + \frac{1}{2} \frac{\rho_0(t)}{E(t,t)d_0(t)} [d(t) - d_0(t)]^2 \right\} \tag{11.24}$$

Differentiating:

$$\frac{\partial B(d(t))}{\partial d(t)} = \rho_0(t) \left\{ 1 + \frac{d(t) - d_0(t)}{E(t,t)d_0(t)} \right\} \tag{11.25}$$

By combining (11.22) and (11.25), the single-period model is obtained as in (11.26):

$$d(t) = d_0(t) \left\{ 1 + \frac{E(t,t)[\rho(t) - \rho_0(t)]}{\rho_0(t)} \right\} \tag{11.26}$$

The multi-period model of responsive load is attained as in (11.27):

$$d(t) = d_0(t) + \sum_{\substack{t=1 \\ t' \neq t}}^{T} E(t,t') \times \frac{d_0(t)}{\rho_0(t')} \times [\rho(t') - \rho_0(t')] \tag{11.27}$$

In the end, the complete model of responsive load including the combination of the single and multi- period models is presented in Eq. (11.28).

$$d(t) = d_0(t) \left\{ 1 + E(t,t) \frac{[\rho(t) - \rho_0(t)]}{\rho_0(t)} + \sum_{\substack{t=1 \\ t' \neq t}}^{T} E(t,t') \frac{[\rho(t') - \rho_0(t')]}{\rho_0(t')} \right\} \tag{11.28}$$

11.4 Stochastic Problem Formulation

Regarding the uncertainties in load consumption, and RESs including wind and solar arrays, the scheduling of ADNs confronts with a main problem about specifying the location, capacity, and RES number. In this chapter, the uncertainties of wind, solar, and consumption load are considering applying scenario modeling. Monte Carlo simulation (MCS) is used to scenario generation for uncertain parameters [23]. The MCS is an option for modeling the behavior of the uncertain parameters that have

probabilistic nature. This implies that there exists a PDF that defines the behavior of these parameters. The main theory of the MCS approach is explained below:

Assume a multi-variable function, namely, y, $y = f(x_1, \ldots, x_n)$, in which x_1 to x_n are random variables with their own PDF. The question is, knowing the PDFs of all input variables, that is, x_1 to x_n, how the PDF of y can be achieved. The theory of MCS is getting the PDF of y_e using the PDFs of input variables x_i. In the end, the PDF of the output function, y, is considered as a normal PDF with a mean and standard deviation obtained from simulations. Discrete probability distribution sets for consumption load (B_{Dl}), wind production (B_{Gw}), and solar production (B_{Gs}) are written as below:

$$\begin{aligned} \mathrm{B}_{\mathrm{Dl}} &= \left\{ \left(\mathrm{Dl}^1, \beta_{\mathrm{Dl}}^1\right), \left(\mathrm{Dl}^2, \beta_{\mathrm{Dl}}^2\right), \ldots, \left(\mathrm{Dl}^{n\mathrm{Dl}}, \beta_{\mathrm{Dl}}^{n\mathrm{Dl}}\right) \right\} \\ \beta_E^1 &+ \beta_{\mathrm{Dl}}^2 + \cdots + \beta_{\mathrm{Dl}}^{n\mathrm{Dl}} = 1 \end{aligned} \tag{11.29}$$

$$\begin{aligned} B_{\mathrm{Gw}} &= \left\{ \left(\mathrm{Gw}^1, \beta_{\mathrm{Gw}}^1\right), \left(\mathrm{Gw}^2, \beta_{\mathrm{Gw}}^2\right), \ldots, \left(\mathrm{Gw}^n, \beta_{\mathrm{Gw}}^n\right) \right\} \\ \beta_{\mathrm{Gw}}^1 &+ \beta_{\mathrm{Gw}}^2 + \cdots + \beta_{\mathrm{Gw}}^n = 1 \end{aligned} \tag{11.30}$$

$$\begin{aligned} B_{\mathrm{Gs}} &= \left\{ \left(\mathrm{Gs}^1, \beta_{\mathrm{Gs}}^1\right), \left(\mathrm{Gs}^2, \beta_{Gs}^2\right), \ldots, \left(\mathrm{Gs}^n, \beta_{\mathrm{Gs}}^n\right) \right\} \\ \beta_{\mathrm{Gs}}^1 &+ \beta_{\mathrm{Gs}}^2 + \cdots + \beta_{\mathrm{Gs}}^n = 1 \end{aligned} \tag{11.31}$$

$$S = B_{\mathrm{Dl}} \cup B_{\mathrm{Gw}} \cup B_{\mathrm{Gs}} \tag{11.32}$$

$$\sum_{s \in S} \beta_{\mathrm{Dl}} \times \beta_{\mathrm{Gw}} \times \beta_{\mathrm{Gs}} = 1 \tag{11.33}$$

11.5 Providing an Overview of GWO Algorithm

In this chapter, in order to solve the suggested problem and find optimal solutions, gray wolf optimization algorithm is utilized as a new algorithm. The goal of employing this algorithm is its high convergence speed in comparison with other algorithms like genetic algorithm (GA) and particle swarm optimization algorithm (PSO). It also has great performance in convergence speed and provides better response than other optimizers. For this reason, the GWO algorithm is used in this chapter.

11.5.1 A Brief Description of GWO

GWO is a novel meta-heuristic algorithm presented in [24] and its main origin is gray wolves, which have a very dominant social hierarchy, as given in Fig. 11.2. A female and a male are chosen as the group leaders and called alpha (α). Alpha is

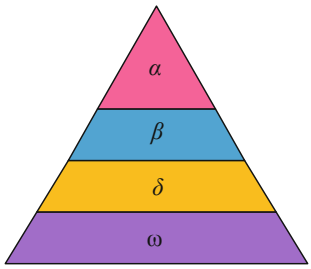

Fig. 11.2 Hierarchy of gray wolves

responsible for deciding on hunting, sleeping, and waking hours of other members. Beta (β) is the second level of the mentioned hierarchy that plays an adviser role for alpha and the best candidate to be alpha. The third and fourth level of the hierarchy are called delta (δ) and omega (ω), respectively. Omega plays the role of victim and should be obedient to other dominant wolves.

11.5.2 Mathematical Formulation of GWO Algorithm

The mathematical formulation of wolves' circling behavior through the target hunt is presented as follows.

$$\vec{D} = \left|\vec{C} \cdot \vec{X}_{\mathrm{P}}(e) - \vec{X}(e)\right| \tag{11.34}$$

$$\vec{X}(e+1) = \vec{X}_{\mathrm{P}}(e) - \vec{\mathrm{A}}.\vec{\mathrm{D}} \tag{11.35}$$

Coefficient vectors are determined as in (11.37) and (11.36).

$$\vec{A} = 2\vec{a} \cdot \vec{r}_1 - \vec{a} \tag{11.36}$$

$$\vec{C} = 2\vec{r}_2 \tag{11.37}$$

Vector A is linearly reduced from 2 to 0 over the iteration course and r_1 and r_2 shows random vectors in [0,1]. In order to simulate the mathematical behavior of gray wolves, we suppose that alpha, beta, and delta have a better knowledge from the potential hunting position. Therefore, we save best first three answers and force the other search agents (consist of omega wolves) to update their location due to the best search agents. This description is presented mathematically as follows.

$$\vec{D}_\alpha = \left|\vec{C}_1 \cdot \vec{X}_\alpha - \vec{X}\right|, \quad \vec{D}_\beta = \left|\vec{C}_2 \cdot \vec{X}_\beta - \vec{X}\right|, \quad \vec{D}_\delta = \left|\vec{C}_3 \cdot \vec{X}_\delta - \vec{X}\right| \tag{11.38}$$

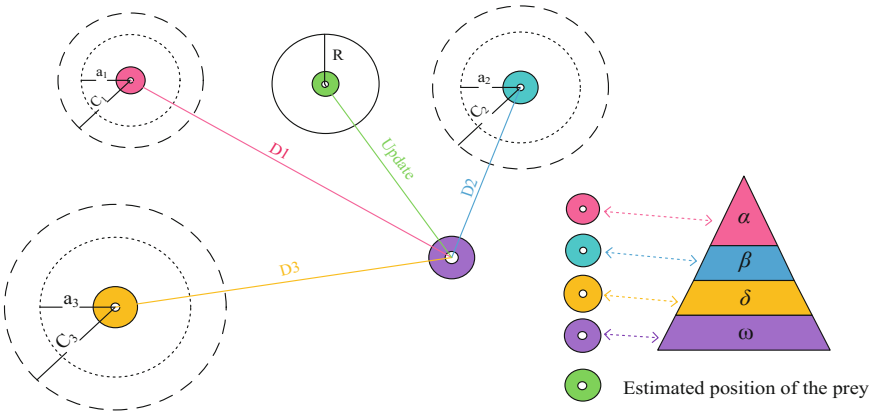

Fig. 11.3 Location updating of GWO algorithm

$$\vec{X}_1 = \vec{X}_\alpha - \vec{A}_1 \cdot \left(\vec{D}_\alpha\right), \quad \vec{X}_2 = \vec{X}_\beta - \vec{A}_2 \cdot \left(\vec{D}_\beta\right), \quad \vec{X}_3 = \vec{X}_\delta - \vec{A}_3 \cdot \left(\vec{D}_\delta\right) \tag{11.39}$$

$$\vec{X}(e+1) = \frac{\vec{X}_1 + \vec{X}_2 + \vec{X}_3}{3} \tag{11.40}$$

Figure 11.3 explains how an agent location in a two-dimensional search region depends on the hierarchy levels. The final location got at a random position in a circle is defined due to the alpha, beta, and delta position. In other words, alpha, beta, and delta evaluate hunting positions and other wolves update their position randomly around the hunt [25].

11.6 Case Study and Simulation Results

The case study is a modified IEEE 33-bus test system. In this network, we have assumed six BESSs and six DERs. The BESS and DERs are already available in network and are being exploited. The topology of the system to implement the proposed model is shown in Fig. 11.4. BESSs and DERs data are given in Tables 11.1 and 11.2, respectively [26]. The amount of LMP at different buses of 33-bus test system has been indicated in Table 11.3. The technical data of the network is presented in Table 11.4. Figure 11.5 shows the real-time market prices or the price of energy purchased from the upstream grid.

The hourly amount of demand is shown in Fig. 11.6 with different participation factors. As seen in Fig. 11.5, the DRP increases the amount of demand in off-peak periods and reduces it in peak periods. In addition, the effects of different participation factors are displayed and compared with each other.

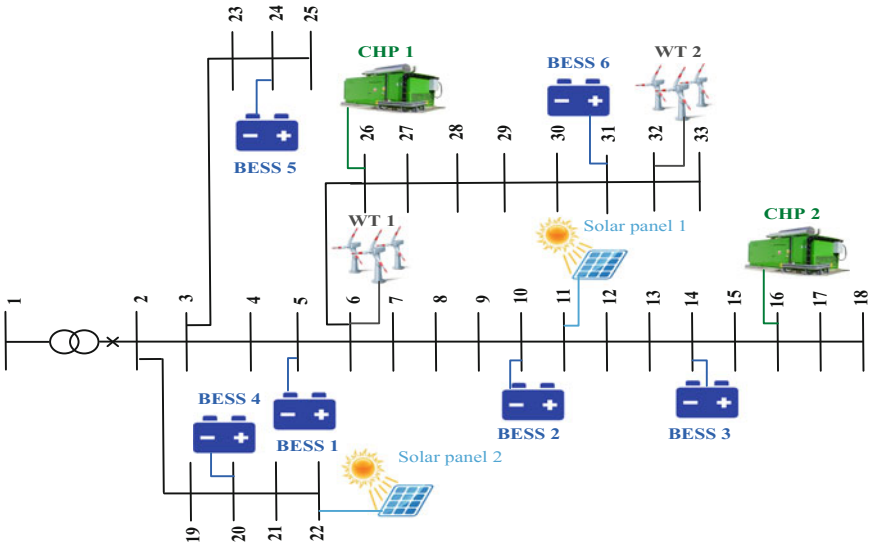

Fig. 11.4 Modified 33-bus IEEE test system with BESS and DERs

Table 11.1 Information of BESS

Number of BESS	Lower bound of SoC	Upper bound of SoC	Number of Bus	Price of charge ($/kWh)	Price of discharge ($/kWh)	η_{ch}	η_{dis}
1	150	700	5	0.10	0.20	0.90	0.90
2	100	800	10	0.15	0.22	0.90	0.90
3	150	800	14	0.10	0.20	0.75	0.75
4	100	1000	20	0.30	0.45	0.85	0.85
5	100	800	24	0.09	0.15	0.85	0.85
6	100	700	31	0.09	0.15	0.90	0.90

Table 11.2 Information of DG units

DG	Min production capacity (kWh)	Max production capacity (kWh)	Location in network	Cost coefficient ($/kWh)
1	200	600	6	0.02
2	200	500	11	0.05
3	150	450	16	0.01
4	100	400	22	0.05
5	200	700	26	0.01
6	200	600	32	0.02

Table 11.3 Amount of LMP at different buses of 33-bus test system

Bus no.	LMP ($/MVA-hr.)	Bus no.	LMP ($/MVA-hr.)	Bus no.	LMP ($/MVA-hr.)
1	20	12	22.427	23	20.674
2	20.096	13	22.66	24	20.885
3	20.559	14	22.738	25	20.992
4	20.807	15	22.796	26	21.659
5	21.056	16	22.853	27	21.739
6	21.597	17	22.925	28	22.03
7	21.671	18	22.949	29	22.239
8	21.871	19	20.111	30	22.347
9	22.106	20	20.215	31	22.495
10	22.325	21	20.234	32	22.526
11	22.362	22	20.251	33	22.534

Table 11.4 Comparison study on various approaches applied for CM problem

Ref.	Proposed method	Case study	Congestion reduction (%)
This chapter	DRP and optimal arbitrage of BESS including DERs	IEEE 33-bus system	45.43
[3]	DRP	IEEE 39-bus system	24.26
[6]	DRP along with FACT devices	IEEE 30-bus system	25.08
[7]	Rescheduling of GENCOs	IEEE 30-bus system	27.55
[10]	Rescheduling of generators along with load shedding	IEEE 118-bus system	29.41
[11]	Both DRP and distribution congestion prices	Danish 30-bus system	16.94
[13]	Rescheduling of conventional generators considering WTs	IEEE 30-bus system	31.66

The result of the BESS arbitrage is displayed in Fig. 11.7. As can be seen, the optimal charging and discharging of BESSs are determined by the proposed algorithm due to the equilibrium equation. Charging and discharging amount of BESSs depend on the production of DERs and load consumption every hour. So, if the answer of the equilibrium equation is positive, BESS is discharged. The BESSs are charged when the amount of P_{rest} is negative.

Figure 11.8 shows the optimal daily production of DERs in the presence of BESS and DRP. According to this figure, the production power of DERs depends on their capacity and location in the network, and optimal production of DERs is specified by BESS scheduling and the electricity market price in each hour. The PV units generate the power only when sun is available, i.e., 6 a.m. to 18 p.m.

In this paper, the well-known backward/forward algorithm has been used to execute power flow calculations [28]. It should be emphasized that with respect to

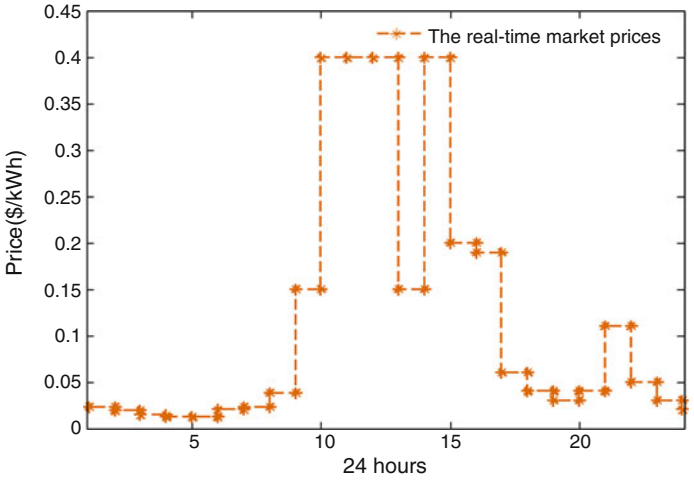

Fig. 11.5 Real-time market prices

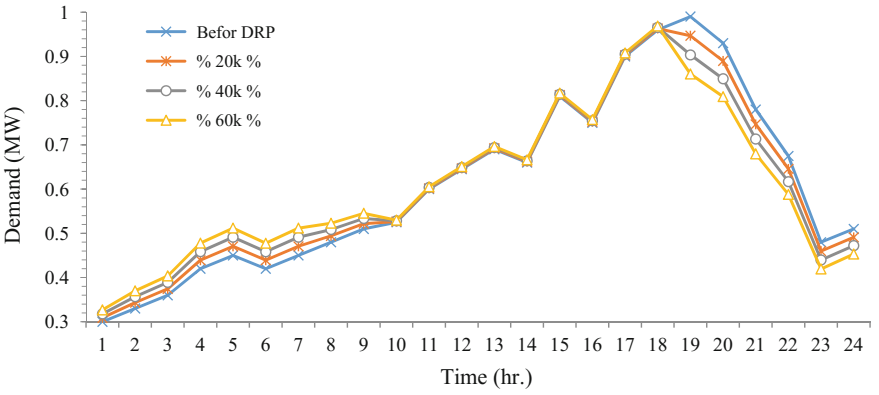

Fig. 11.6 Daily system's demand with and without DRP in different participation factors

features of proposed model which is a nonlinear, non-convex as well as non-smooth model (due to the implementation of the backward-forward load flow algorithm, considering complicating variables and constraints such as power mismatch constraints and prohibited operating zones of DER units and taking into account various objectives resulting in a NP-hard problem), it is not possible to solve it by exact methods such as CPLEX. Therefore, we had to use meta-heuristic algorithm to solve the problem. Accordingly, we studied various algorithms such as GWO, PSO, and GA, and finally with respect to obtained results, we have chosen GWO to solve the proposed congestion management problem. The optimal convergence curve obtained from GWO algorithm has been displayed in Fig. 11.9.

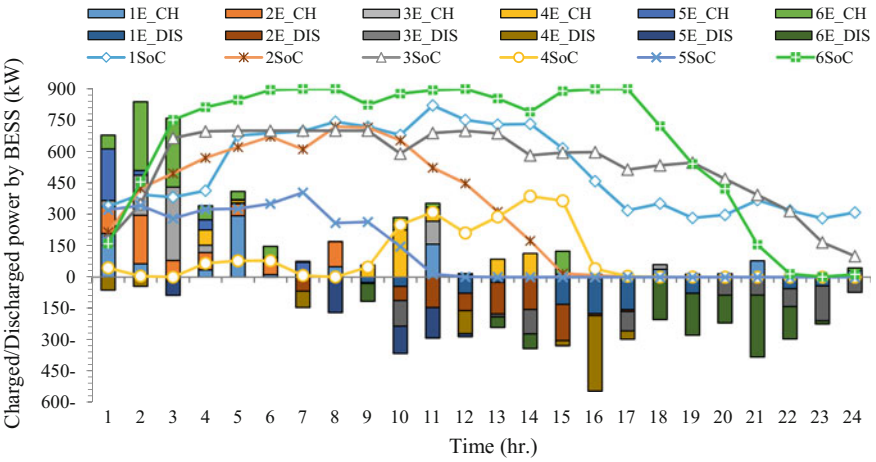

Fig. 11.7 Optimal day ahead arbitrage of BESS

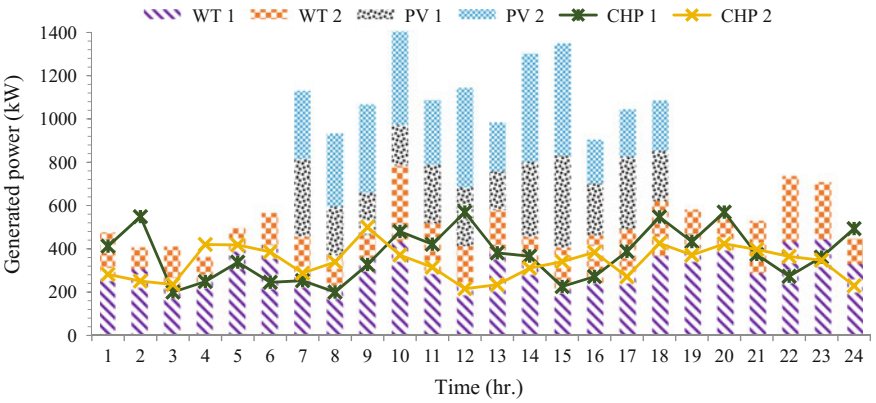

Fig. 11.8 Optimal production of DERs

The voltage profile of proposed system is presented in Fig. 11.10 in the presence of BESS, DERs, and DRP and compared with the initial case (without considering any sources). According to the figure, voltage profile of the system without considering any sources is not in acceptable range but with implementing the DRP, applying BESS, and optimal scheduling of DERs, it is limited in the allowable range. In other words, adding DRP, BESS, and DERs improve voltage profile compared with initial case. Figure 11.11 shows the 33-bus system power losses. As can be seen, the power losses of lines in the presence of the DRP have been dramatically reduced to the initial case (without DRP). In addition to the DRP, the effect of the BESS scheduling and the optimal planning of DERs is also not negligible in reducing the lines losses.

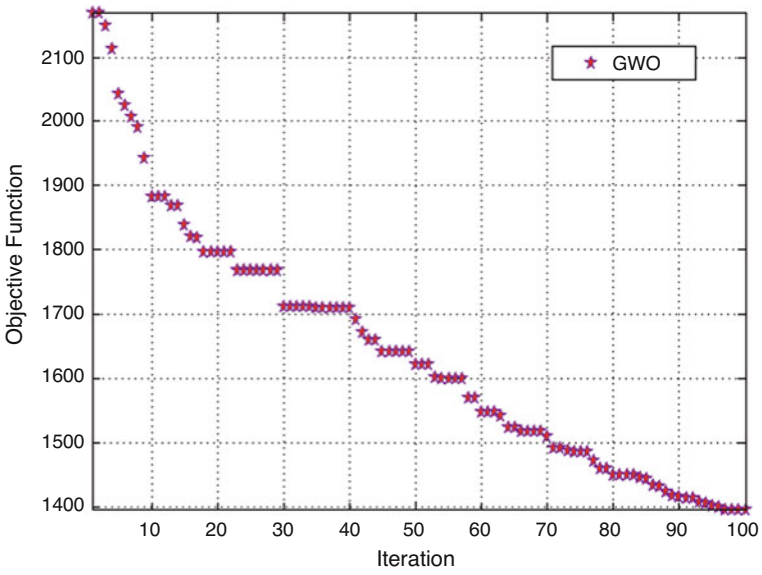

Fig. 11.9 Convergence curve obtained from GWO algorithm

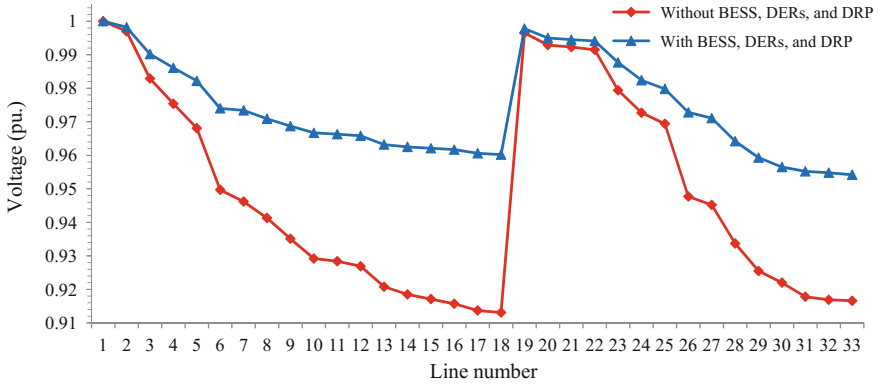

Fig. 11.10 Voltage profile of IEEE 33-bus system with and without DRP

The results of transaction powers through the lines in the presence of BESS, DERs, and DRP are illustrated in Fig. 11.12. As can be seen from the graph, the first column shows the initial transaction powers (without considering BESS, DERs, and DRP) through the lines, which is obtained from system optimal power flow, which is compared with the second column of this graph that indicates the value of power flow with proposed sources. By properly planning the DERs, optimal arbitrage of the BESS, and DRP implementation at appropriate hours, we were able to alleviate the active power flow of the lines significantly compared with the initial case (without these elements) and manage the congestion of lines as the goal of proposed problem.

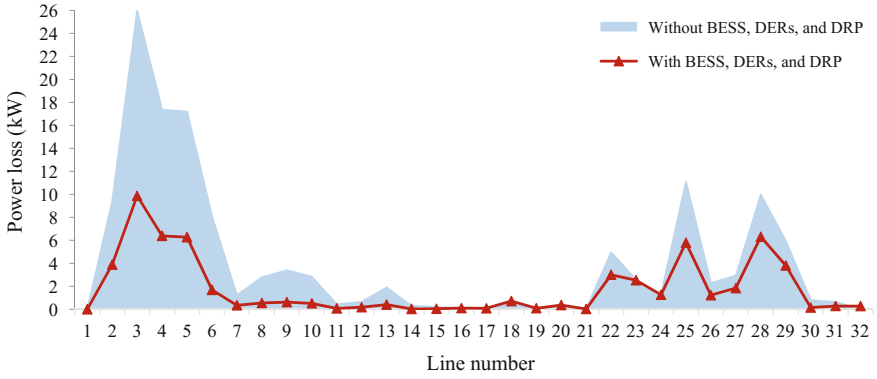

Fig. 11.11 Power losses of system with and without DRP

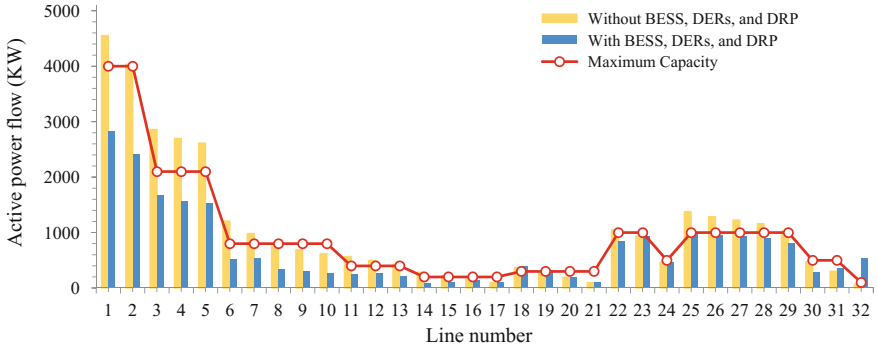

Fig. 11.12 Transaction powers through the lines in different cases

The LMP amount of each bus is presented in Fig. 11.13 and compared in two cases. As can be seen, the LMP amount in the presence of BESS, DERs, and DRP is significantly smooth compared to the initial case (without BESS, DERs, and DRP).

The amount of total active power flow (sum of all transaction powers in the lines) in the presence of DRP, BESS, and DERs with respect to the amount of total active power flow without these measures is equal to 45.43%. This value is obtained from Fig. 11.12 and written in the Table 11.4. All of the congestion reduction indexes have been calculated in the same way and compared in Table 11.4. As can be seen, DRP and optimal arbitrage of BESS along with DERs has significant effect on the congestion reduction compared to other conventional methods.

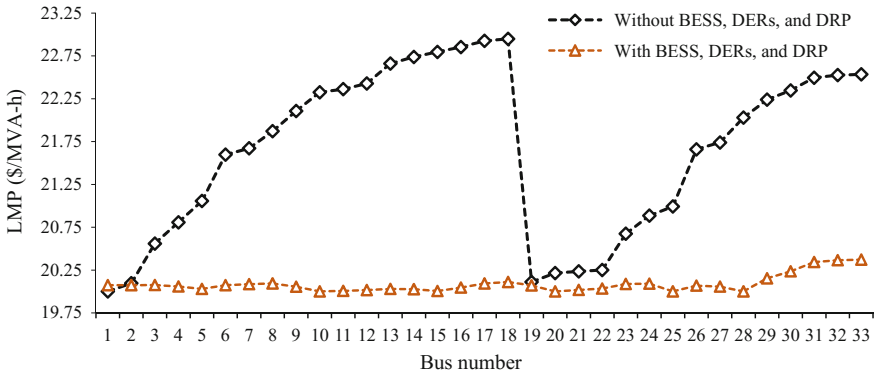

Fig. 11.13 The LMP amount at different buses

11.7 Conclusion

In this chapter, the optimal charging/discharging scheduling of BESS and incentive-based DRP execution was suggested with the goal of CM. In addition, the uncertainties pertaining to renewables were considered using the probabilistic model. Nonlinearity, non-convexity, and being non-smooth are features of the suggested problem that is why we applied the GWO algorithm to solve this problem. The arbitrage of BESS and incentive-based DRP as well as optimal production of DERs including WT, PV, and CHP systems are achieved in hourly scheduling. By utilizing the suggested method, the DSO is able to significantly decrease the overloading of lines as well as total power losses, and it can be used to improve some technical characteristic of the system like network security in dealing with overloading, voltage profile, and the network stability margin. Furthermore, results demonstrated that the BESS and DRP can decrease the curtailment energy of renewables, and it can relieve the negative impacts of uncertainties.

Appendix

The technical data of the 33-bus distribution network is given in Table 11.5.

Table 11.5 Technical data of the 33-bus test system [27] ($S_{base} = 1$ MVA, $V_{base} = 12.66$ kV)

Line no.	Sending node	Receiving node	R (Ohm)	X (Ohm)	P (kW)	Q (kVAR)
1	1	2	0.0922	0.0470	100	60
2	2	3	0.4930	0.2512	90	40
3	3	4	0.3661	0.1864	120	80
4	4	5	0.3811	0.1941	60	30
5	5	6	0.8190	0.7070	60	20
6	6	7	0.1872	0.6188	200	100
7	7	8	0.7115	0.2351	200	100
8	8	9	1.0299	0.7400	60	20
9	9	10	1.0440	0.7400	60	20
10	10	11	0.1967	0.0651	45	30
11	11	12	0.3744	0.1298	60	35
12	12	13	1.4680	1.1549	60	35
13	13	14	0.5416	0.7129	120	80
14	14	15	0.5909	0.5260	60	10
15	15	16	0.7462	0.5449	60	20
16	16	17	1.2889	1.7210	60	20
17	17	18	0.7320	0.5739	90	40
18	2	19	0.1640	0.1565	90	40
19	19	20	1.5042	1.3555	90	40
20	20	21	0.4095	0.4784	90	40
21	21	22	0.7089	0.9373	90	40
22	3	23	0.4512	0.3084	90	50
23	23	24	0.8980	0.7091	420	200
24	24	25	0.8959	0.7071	420	200
25	6	26	0.2031	0.1034	60	25
26	26	27	0.2842	0.1447	60	25
27	27	28	1.0589	0.9338	60	20
28	28	29	0.8043	0.7006	120	70
29	29	30	0.5074	0.2585	200	600
30	30	31	0.9745	0.9629	150	70
31	31	32	0.3105	0.3619	210	100
32	32	33	0.3411	0.5302	60	40

References

1. F.S. Gazijahani, J. Salehi, Game theory based profit maximization model for microgrid aggregators with presence of EDRP using information gap decision theory. IEEE Syst. J. **99**, 1–9 (2018)
2. S. Nojavan, B. Mohammadi-Ivatloo, K. Zare, Optimal bidding strategy of electricity retailers using robust optimisation approach considering time-of-use rate demand response programs under market price uncertainties. IET Gener. Transm. Distrib. **9**(4), 328–338 (2015)

3. A. Abdolahi et al., Probabilistic multi-objective arbitrage of dispersed energy storage systems for optimal congestion management of active distribution networks including solar/wind/CHP hybrid energy system. J. Renew. Sustain. Energy **10**(4), 045502 (2018)
4. A. Pillay, S.P. Karthikeyan, D.P. Kothari, Congestion management in power systems—a review. Int. J. Electr. Power Energy Syst. **70**, 83–90 (2015)
5. F.S. Gazijahani, J. Salehi, Reliability constrained two-stage optimization of multiple renewable-based microgrids incorporating critical energy peak pricing demand response program using robust optimization approach. Energy **161**, 999–1015 (2018)
6. M. Braun, Technological control capabilities of DER to provide future ancillary services. Int. J. Distrib. Energy Resour. **3**(3), 191–206 (2007)
7. P. Salyani et al., Chance constrained simultaneous optimization of substations, feeders, renewable and non-renewable distributed generations in distribution network. Electr. Power Syst. Res. **158**, 56–69 (2018)
8. F.S. Gazijahani, S. Najafi Ravadanegh, J. Salehi, Stochastic multi-objective model for optimal energy exchange optimization of networked microgrids with presence of renewable generation under risk-based strategies. ISA Trans. **73**, 100–111 (2018)
9. M. Majidi, S. Nojavan, K. Zare, Optimal stochastic short-term thermal and electrical operation of fuel cell/photovoltaic/battery/grid hybrid energy system in the presence of demand response program. Energy Convers. Manag. **144**, 132–142 (2017)
10. A. Kumar, S.C. Srivastava, S.N. Singh, Congestion management in competitive power market: A bibliographical survey. Electr. Power Syst. Res. **76**(1–3), 153–164 (2005)
11. A. Yousefi, T.T. Nguyen, H. Zareipour, O.P. Malik, Congestion management using demand response and FACTS devices. Int. J. Electr. Power Energy Syst. **37**(1), 78–85 (2012)
12. F.S. Gazijahani, J. Salehi, Robust design of microgrids with reconfigurable topology under severe uncertainty. IEEE Trans. Sustain. Energy **9**(2), 559–569 (2018)
13. S. Huang, Q. Wu, S.S. Oren, R. Li, Z. Liu, Distribution locational marginal pricing through quadratic programming for congestion management in distribution networks. IEEE Trans. Power Syst. **30**(4), 2170–2178 (2015)
14. E. Dehnavi, H. Abdi, Determining optimal buses for implementing demand response as an effective congestion management method. IEEE Trans. Power Syst. **32**(2), 1537–1544 (2017)
15. J. Hazra, K. Das, D.P. Seetharam, Smart grid congestion management through demand response, in: *2012 IEEE Third International Conference on Smart Grid Communications* (IEEE, 2012), pp. 109–114
16. M.H. Moradi, A.R. Reisi, S.M. Hosseinian, An optimal collaborative congestion management based on implementing DR. IEEE Trans. Smart Grid. **9**(5), 5323–5334 (2018)
17. F. Zaeim-Kohan, H. Razmi, H. Doagou-Mojarrad, Multi-objective transmission congestion management considering demand response programs and generation rescheduling. Appl. Soft Comput. **70**, 169–181 (2018)
18. J. Wu, B. Zhang, Y. Jiang, Optimal day-ahead demand response contract for congestion management in the deregulated power market considering wind power. IET Gener. Transm. Distrib. **12**(4), 917–926 (2017)
19. J. Hazra, A.K. Sinha, Congestion management using multiobjective particle swarm optimization. IEEE Trans. Power Syst. **22**(4), 1726–1734 (2007)
20. B.P. Bhattarai, M. Lévesque, B. Bak-Jensen, J.R. Pillai, M. Maier, D. Tipper, K.S. Myers, Design and cosimulation of hierarchical architecture for demand response control and coordination. IEEE Trans. Ind. Informatics. **13**(4), 1806–1816 (2017)
21. F.S. Gazijahani, J. Salehi, Integrated DR and reconfiguration scheduling for optimal operation of microgrids using Hong's point estimate method. Int. J. Electr. Power Energy Syst. **99**, 481–492 (2018 Jul 31)
22. S. Nojavan, K. Zare, B. Mohammadi-Ivatloo, Optimal stochastic energy management of retailer based on selling price determination under smart grid environment in the presence of demand response program. Appl. Energy **187**, 449–464 (2017)

23. F.S. Gazijahani, J. Salehi, Optimal bi-level model for stochastic risk-based planning of microgrids under uncertainty. IEEE Trans. Ind. Informatics **14**(7), 3054–3064 (2018)
24. S. Mirjalili, S.M. Mirjalili, A. Lewis, Grey wolf optimizer. Adv. Eng. Softw. **69**, 46–61 (2014)
25. M. Shamshirband et al., Decentralized trading of plug-in electric vehicle aggregation agents for optimal energy management of smart renewable penetrated microgrids with the aim of CO_2 emission reduction. J. Clean. Prod. **200**, 622–640 (2018)
26. F.S. Gazijahani, J. Salehi, Stochastic multi-objective framework for optimal dynamic planning of interconnected microgrids. IET Renew. Power Gener. **11**(14), 1749–1759 (2017)
27. A.M. Imran, M. Kowsalya, A new power system reconfiguration scheme for power loss minimization and voltage profile enhancement using fireworks algorithm. Int. J. Electr. Power Energy Syst. **62**, 312–322 (2014)
28. S. Mehdi et al., Look-ahead risk-averse power scheduling of heterogeneous electric vehicles aggregations enabling V2G and G2V systems based on information gap decision theory. Electr. Power Syst. Res. **173**, 56–70 (2019)

Chapter 12
Stochastic Optimal Preventive Voltage Stability Control in Power Systems under Demand Response Program

Morteza Nojavan, Heresh Seyedi, and Behnam Mohammadi-Ivatloo

Nomenclature

α_b	Maximum percentage of demand-side participation in DR programs at bus b
β_b	Percentage of bus b load, which is no allowed to be shed
$\delta_b(s)$	Voltage angle at bus b for scenario s
$\delta_j(s)$	Voltage angle at bus j for scenario s
$\widetilde{\delta}_b(s)$	Voltage angle of bus b at loadability limit point for scenario s
$\widetilde{\delta}_j(s)$	Voltage angle of bus j at loadability limit point for scenario s
$\lambda(s)$	Loading parameter of the system for scenario s
$\lambda_{\text{thershold}}$	Satisfied loading parameter of the system
μi	Mean value of variable x_i
μj	Mean value of variable x_j
$\phi(\cdot)$	The *PDF* of standard normal function
ρ_{0ij}	A component in the correlation matrix ρ_0 of standard normal random vector Y
σi	Variance of the variable x_i
σj	Variance of the variable x_j
τ_{CC}	Lead time of preventive control
θbj	Angle of element b–j of the system Y_{bus} matrix
AD_i	Cost of reduction of active power generation of unit i (\$/MWh)
AI_i	Cost of increase in active power generation of unit i (\$/MWh)
B	Index of buses
CC_b^{DR}	Cost of DR participation at bus b
CC_b^{LS}	Cost of ILC at bus b

M. Nojavan (✉) · H. Seyedi · B. Mohammadi-Ivatloo
Faculty of Electrical and Computer Engineering, University of Tabriz, Tabriz, Iran
e-mail: m.nojavan@tabrizu.ac.ir; hseyedi@tabrizu.ac.ir; bmohammadi@tabrizu.ac.ir

S. Nojavan, K. Zare (eds.), *Demand Response Application in Smart Grids*,
https://doi.org/10.1007/978-3-030-32104-8_12

d	Index of load buses
$\mathrm{DRC}_b^p(s)$	Active part of DR program at bus b participating for scenario s
$\mathrm{DRC}_b^Q(s)$	Reactive part of DR program at bus b participating for scenario s
$f_{X_iX_j}(x_i, x_j)$	The joint *PDF* of random variables x_i, x_j
$F_i(x_i)$	The corresponding cumulative distribution function
G	Set of generating units
G_{F}	Set of fast-response generating units
$\mathrm{LS}_b^p(s)$	Active part of involuntary load curtailment (ILC) at bus b for scenario s
$\mathrm{LS}_b^Q(s)$	Reactive part of involuntary load curtailment (ILC) at bus b for scenario s
n	Number of PV buses in zone j
$P_{b,r}^{\mathrm{w}}$	Rated power of wind turbine installed at bus b
P_{G_i}	Active power generation of unit i
$P_{\mathrm{G}_i}^0$	Economic scheduled value of active power generation of unit i
$P_{\mathrm{G}_i}^-$	Active power reduction of generation unit i
$P_{\mathrm{G}_i}^+$	Increase in active power generation of unit i
$P_{\mathrm{G}_i}^{\min}$	Minimum active power generation of unit i
$P_{\mathrm{G}_i}^{\max}$	Maximum active power generation of unit i
$\widetilde{P}_{\mathrm{G}_i}(s)$	Active power generation of unit i at loadability limit point for scenario s
$P_{\mathrm{L}_b}(s)$	Active power load of bus b for scenario s
$Q_{\mathrm{G}_i}^0$	Economic scheduled value of reactive power generation of unit i
$Q_{\mathrm{G}_i}^{\min}$	Minimum reactive power generation of unit i
$Q_{\mathrm{G}_i}^{\max}$	Maximum reactive power generation of unit i
$Q_{\mathrm{G}_i}(s)$	Reactive power generation of unit i for scenario s
$\widetilde{Q}_{\mathrm{G}_i}(s)$	Reactive power generation of unit i at loadability limit point for scenario s
$Q_{\mathrm{G}_i}^+(s)$	Increase in reactive power generation of unit i for scenario s
$Q_{\mathrm{G}_i}^-(s)$	Decrease in reactive power generation of unit i for scenario s
$Q_{\mathrm{L}_b}(s)$	Reactive power load of bus b for scenario s
$\mathrm{RD}_{\mathrm{G}_i}$	Ramp-down rate of generating unit i
RD_i	Cost of reduction of reactive power generation of unit i (\$/MVarh)
RI_i	Cost of increase in reactive power generation of unit i (\$/MVarh)
$\mathrm{RU}_{\mathrm{G}_i}$	Ramp-up rate of generating unit i
s	Index for scenarios
S_{n}	Total number of scenarios
v	Wind speed
$v_{\mathrm{in}}^{\mathrm{c}}$	Cut-in speed of wind turbine
$v_{\mathrm{out}}^{\mathrm{c}}$	Cutoff speed of wind turbine
$v_{\mathrm{rated}}^{\mathrm{c}}$	Rated speed of wind turbine
$V_b(s)$	Magnitude of bus b voltage for scenario s

$V_j(s)$	Magnitude of bus j voltage for scenario s
$\widetilde{V}_b(s)$	Magnitude of bus b voltage at loadability limit point for scenario s
$V_b^{\min}$	Minimum voltage magnitude of bus b
$V_b^{\max}$	Maximum voltage magnitude of bus b
$\widetilde{V}_b^{\min}$	Minimum voltage magnitude of bus b at loadability limit point
$\widetilde{V}_b^{\max}$	Maximum voltage magnitude of bus b at loadability limit point
$\widetilde{V}_j(s)$	Magnitude of bus j voltage at loadability limit point for scenario s
$\lvert Y_{bj}\rvert$	Magnitude of b–jth element of the system Y_{bus} matrix

12.1 Introduction

Voltage stability refers to the ability of a power system to maintain steady voltages at all buses in the system after being subjected to a disturbance from a given initial operating condition [1]. One of the main reasons of various blackouts all over the world is voltage instability. Therefore, various studies have been executed and different methods have been proposed to identify and prevent voltage instability. Researches in this subject can be classified into two categories:

1. Voltage stability indices: the scope of this category is to present stability indices to identify voltage instability or determine the voltage stability margin.
2. Preventive and corrective control facilities to prevent voltage instability: this group includes researches about optimal preventive or corrective control actions to ensure desirable load margin.

Facilities used to prevent voltage instability in the preventive control schemes include load shedding, re-dispatch of active and reactive powers of generators, and demand response. Load shedding is one of the most important and also costly countermeasures against voltage instability. Various papers have proposed optimal under-voltage load shedding methods to ensure voltage stability with minimum involuntary load curtailment [2–9].

An optimal under-voltage load shedding methodology to avoid voltage instability is presented in [2]. The candidate buses for load shedding are selected based on the sensitivity of minimum eigenvalue of load flow Jacobian matrix with respect to the dropped load. The algorithm for minimum load shedding is developed using differential evolution. A centralized under-voltage load-shedding scheme considering the load characteristics is presented in [3]. In this research, dimensions of the optimal problem are greatly simplified using the proposed indicator. A practical approach for determining the best location and the minimum amount of load to be shed for voltage collapse prevention is presented in [4]. A multistage method is proposed to solve the problem. The main idea of the proposed method is to solve the optimization problem, stage by stage, and to limit the load shedding to a small amount at each stage. An adaptive under-voltage load-shedding scheme is proposed in [5] to protect

power system against voltage instability. Adaptive combinational load shedding methods are used to enhance power system stability in [6–9]. In the proposed algorithms, load shedding is started from the locations with higher voltage decay for longer period of time. The speed, location, and amount of load shedding are changed adaptively depending on the disturbance location, voltage status of the system, and the rate of frequency decline.

Load curtailment could be undesirable and too costly for the customers and consequently for the system operators. On the other hand, re-dispatch of active and reactive powers of generators and demand response programs can be used as facilities to maintain system voltage stability with lower costs. Papers in the second category have used the mentioned control facilities to prevent voltage collapse.

In [10, 11], a new method is presented for power system protection against voltage collapse based on the difference between apparent power flows at the sending and the receiving ends of the transmission lines. Then, a triggering signal is sent to the reactive power sources to increase reactive power production. Comprehensive control framework to ensure loading margin of power systems is proposed in [12]. Demand response, load shedding and rescheduling of generating units are control facilities in [12]. Online diagnosis of capacitor switching to prevent voltage collapse based on the measurement of actual load powers and voltages is presented in [13]. Reactive power rescheduling is used as a facility to improve voltage stability in [14]. Using ranking coefficients, the generators are divided into "important" and "less-important" ones. At the next step, voltage stability margin is improved by decreasing and increasing reactive power generation at the less-important and important generators, respectively.

Impact of uncertain input variables on the output parameters is one of the major requirements in the power system planning and operation. Load and wind power are the important uncertain parameters in power systems. Hence, the load and wind power uncertainties must be considered in power system analysis. Several research papers have considered load uncertainty and stochastic wind power generation modeling. Optimum sizing of a hybrid wind–photovoltaic–battery system is formulated in [15] considering wind speed, solar radiation, and electricity demand. Influence of using solar and wind forecast and their uncertainties on the optimization of demand response of the economic dispatch of an isolated microgrid system is analyzed in [16]. In [17] the optimal sizing of distributed generation in a hybrid power system with wind and energy storage units is presented considering load demand and wind speed uncertainties. Correlated wind power for probabilistic optimal power flow is presented in [18]. Point estimate method is used for solving probabilistic optimal power flow. Biogeography-based optimization algorithm with weighted sum method is proposed in [19] to solve probabilistic multi-objective optimal power flow problem. Nataf transformation based on traditional point estimate method is utilized to handle the correlation of wind sources and load demands. A powerful tool for quantifying the impact of DG units on active loss and voltage profile is proposed which considers the unbundling rules. A method to carry the uncertainty of wind speed for optimal stochastic economic dispatch problem is presented in [20]. An effective approach for deriving robust solutions to the

security-constrained unit commitment problem, considering load and wind power uncertainties, is presented in [21]. An optimization-based real-time residential load management algorithm considering load uncertainty in order to minimize the energy payment for each user is presented in [22]. The proposed algorithm just requires some statistical estimates of the future load demand. A new method for corrective voltage control considering wind power generation and demand values uncertainties is proposed in [23]. Objectives of the proposed method are to ensure a desired loading margin while minimizing the corresponding control cost. It is supposed that all loads and wind powers increase or decrease at the same time. Then, the proposed method uses a simple and somewhat unreal modeling of load and wind power uncertainties.

Wind power and load are the important uncertain parameters in power systems. These uncertainties and correlation among them should be considered in power system modeling, especially voltage instability prevention problems. For this reason in this chapter, a new preventive voltage instability problem is presented considering correlated uncertain wind power and load, preventive actions cost, the complete nonlinear model of the system and demand response. The effect of these uncertainties and their correlation on voltage instability prevention costs is evaluated using a new scenario-based approach. The main contribution of this chapter is correlated wind and load uncertainties modeling in voltage stability control for first time.

The remainder of this chapter is organized as follows: Section 12.2 presents uncertain correlated wind power and load scenario generation steps. Section 12.3 indicates preventive voltage instability problem formulation. Simulation results are presented in Sect. 12.4. Finally, discussions and conclusions are presented in Sect. 12.5.

12.2 Uncertainty Sources

Main uncertainty sources are load and wind power generation in this chapter. Modeling of the correlation of these uncertain sources is presented in this section.

12.2.1 Modeling of Correlated Uncertain Wind Power Generations

The wind turbine's powers have correlation based on weather conditions and location. Hence, the correlation of wind powers must be considered to model the actual condition and real estimation of preventive voltage instability actions cost.

In this section, the wind power scenario generation method is presented. Wind power generation is an uncertain parameter. This parameter can be modeled

probabilistically using historical data of wind speed [23]. Variation of wind speed is modeled using Rayleigh probability density function (PDF):

$$\mathrm{PDF}(v) = \left(\frac{2v}{c^2}\right) \exp\left(-\left(\frac{v}{c}\right)^2\right) \tag{12.1}$$

The generated power of a wind turbine in terms of wind speed is estimated as follows [23]:

$$P_b^{\mathrm{w}}(v) = \begin{cases} 0 & \text{if } v \le v_{\mathrm{in}}^{\mathrm{c}} \text{ or } v \ge v_{\mathrm{out}}^{\mathrm{c}} \\ \dfrac{v - v_{\mathrm{in}}^{\mathrm{c}}}{v_{\mathrm{rated}}^{\mathrm{c}} - v_{\mathrm{in}}^{\mathrm{c}}} P_{b,r}^{\mathrm{w}} & \text{if } v_{\mathrm{in}}^{\mathrm{c}} \le v \le v_{\mathrm{rated}} \\ P_{b,r}^{\mathrm{w}} & \text{else} \end{cases} \tag{12.2}$$

The Cholesky decomposition is used for generation of correlated uncertain wind power scenarios. This method is explained in details in [24]. The components of correlation matrix can be calculated as the following:

$$\begin{aligned} \rho_{ij} &= \int_{-\infty}^{+\infty} \int_{-\infty}^{+\infty} \left(\frac{x_i - \mu_i}{\sigma_i}\right)\left(\frac{x_j - \mu_j}{\sigma_j}\right) f_{X_i X_j}(x_i, x_j)\, dx_i dx_j \\ &= \int_{-\infty}^{+\infty} \int_{-\infty}^{+\infty} \left(\frac{F_i^{-1}(\phi(y_i)) - \mu_i}{\sigma_i}\right)\left(\frac{F_i^{-1}(\phi(y_i)) - \mu_j}{\sigma_j}\right) \\ &\quad \times \phi_2(y_i, y_j, \rho_{0ij})\, dy_i dy_j \end{aligned} \tag{12.3}$$

where

$$\phi_n(y, \rho_0) = \frac{1}{\sqrt{(2\pi)^n \det(\rho_0)}} \exp\left(-\frac{1}{2} y^{\mathrm{T}} \rho_0 y\right) \tag{12.4}$$

If ρ and the marginal PDFs are known, ρ_0 can be determined completely by solving nonlinear Eqs. (12.3) and (12.4). Then, Choleskey decomposition is applied to ρ_0 as the following:

$$\rho_0 = L_0 {L_0}^{\mathrm{T}} \tag{12.5}$$

L_0 is the lower triangular matrix in Eq. (12.5). Afterwards, the mutually independent standard normal random vector $\boldsymbol{U}$ can be calculated as follows:

$$\boldsymbol{U} = {L_0}^{-1} Y \tag{12.6}$$

Finally, the correlated scenarios can be calculated as the following:

$$S = \mu + \boldsymbol{U} \tag{12.7}$$

where S and μ are the correlated wind power scenarios and mean values of wind power, respectively.

12.2.2 Correlated Uncertain Load Scenario Generation

The method of load scenarios generation is presented in this section, considering load uncertainty and correlation among loads. The electrical distances between buses are calculated in the first step. Then, the power system is divided into several areas based on these distances. In the next step, load correlation matrix is defined according to the identified zones. Finally, uncertain correlated load scenarios are generated based on the correlation matrix.

12.2.2.1 Electrical Distance Calculation

Electrical distance calculation is presented in details in [25]. The step-by-step method to obtain the electrical distance between two buses is given in the following:

1. The Jacobian matrix J is calculated and the submatrix $J_4 = [\partial Q/\partial V]$ is obtained.
2. J_4 ($B = J_4^{-1}$) is inverted. The elements of matrix B are written as $b_{ij} = \partial V_i/\partial Q_j$.
3. Attenuation matrix between all buses is calculated using the following equation:

$$\alpha_{ij} = b_{ij}/b_{jj} \tag{12.8}$$

4. Electrical distances, D_{ij}, between ith and jth buses are calculated:

$$D_{ij} = -\log\left(\alpha_{ij}.\alpha_{ji}\right) \tag{12.9}$$

5. The electrical distances are normalized as follows:

$$D_{ij} = D_{ij}/\mathrm{Max}(D_{i1}, \ldots, D_{iN}) \tag{12.10}$$

Partitioning of power system is presented in Sect. 12.2.2.2, based on these normalized electrical distances.

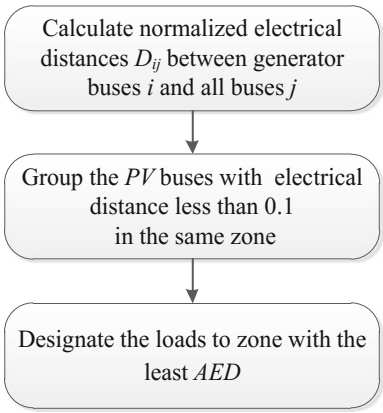

Fig. 12.1 Partitioning of power system

12.2.2.2 Partitioning of Power System

The normalized electrical distances D_{ij} between generator buses i and all other buses j are calculated according to descriptions presented in Sect. 12.2.1. Then, the PV buses are grouped in different zones as shown in the flow chart of Fig. 12.1. In this figure, the average of electrical distance for load i in zone j (AED_{ij}) is calculated as follows:

$$\text{AED}_{ij} = \frac{\sum_{k=1}^{n} D_{ik}}{n} \tag{12.11}$$

12.2.2.3 Generation of Correlation Matrix and Scenarios

In general, the loads in one zone are more influenced by common causes such as common weather or similar power-consuming behavior in comparison to the loads in other zones. Then, the correlation among loads in one zone is stronger than that of other zones. As a result, based on the above assumptions and the assumptions of [26], the correlation coefficients between loads are as follows:

- The correlation coefficients between loads at the same zone are assumed to be 0.8.
- The correlation coefficients between loads at neighboring zones are assumed to be 0.4.
- The correlation coefficients between loads at different zones are assumed to be 0.1.

The correlated load scenarios are generated based on the correlation matrix and Eqs. (12.3)–(12.7).

12.3 Preventing Voltage Instability Problem Formulation

The load margin is indicated by a simple *P–V* curve of bus. The load margin is defined as the distance between the system-operating point and voltage collapse point. This margin is shown in Fig. 12.2. In this figure, λ, B, and A are load margin, the system-operating point, and voltage collapse point, respectively. The load margin is indicated in details in [12].

In order to achieve the desired load margin, the generated active and reactive powers of power plants could either be decreased or increased. In the case of power decrease, opportunity cost should be paid, but in the case of power increase, electricity cost should be paid to the participant power plants. Figure 12.3 indicates this method. Considering this figure, $P^0_{G_i}$ is the economic scheduled generation, while $AI_i P_{Gi}{}^+$ and $AD_i{}^- P_{Gi}{}^-$ are costs, which should be paid to the units in case of increase or decrease with respect to their economic scheduled active power generation, respectively.

Demand response programs are presented in details in [12]. Direct load control (DLC) and interruptible/curtailable (I/C) programs are used in this chapter as different terms of objective function.

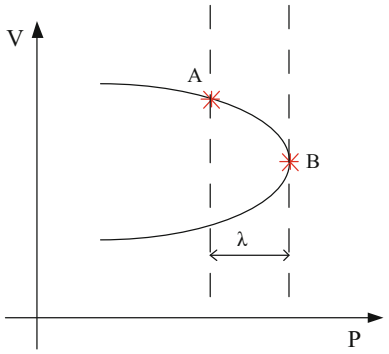

Fig. 12.2 The bus's *P–V* curve

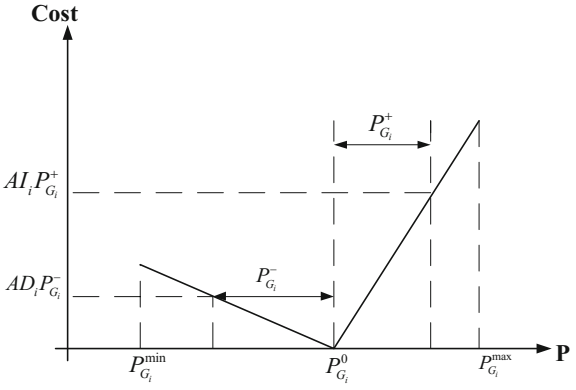

Fig. 12.3 The rule of paying cost to generators

Load shedding is considered as the last and most expensive control facility to prevent voltage instability. Hence, this facility is considered as the highest price term in the objective function.

The proposed facilities are classified into two different categories based on [23]. These categories are named here-and-now and wait-and-see. The values of wait-and-see facilities differ from one scenario to another, while values of here-and-now facilities are the same for all scenarios. Demand response, load shedding, and reactive power outputs of power plants are proposed as wait-and-see facilities, while active power outputs of power plants are proposed as here-and-now facilities [23].

Objective function of the proposed problem is presented as follows:

$$F = \sum_{i\in \mathrm{G_F}} \left(\mathrm{AD_i} P^{-}_{\mathrm{G}_i} + \mathrm{AI}_i P^{+}_{\mathrm{G}_i} \right) + \sum_{s=1}^{S_n} \left(\sum_{i\in \mathrm{G_F}} \left(\mathrm{RD}_i Q^{-}_{\mathrm{G}_i}(s) + \mathrm{RI}_i Q^{+}_{\mathrm{G_i}}(s) \right) \right.$$

$$\left. + \sum_{b\in d} \left(\mathrm{CC}^{\mathrm{DR}}_b \mathrm{DRC}^{p}_b(s) + \mathrm{CC}^{\mathrm{LS}}_b \mathrm{LS}^{p}_b(s) \right) \right) \Big/ S_n \tag{12.12}$$

This objective function contains the cost of preventive control facilities (generator active and reactive re-dispatch, load shedding, and demand response).

Considered constraints are formulated as the following:

$$\begin{aligned} &\sum_{i\in \mathrm{G_F}} P_{\mathrm{G}_i} - \left(P_{\mathrm{L}_b}(s) - \mathrm{DRC}^{p}_b(s) - \mathrm{LS}^{p}_b(s) \right) \\ &= \sum_{j\in B} V_b(s) V_j(s) \left| Y_{bj} \right| \cos\left(\delta_b(s) - \delta_j(s) - \theta_{bj} \right) \quad \forall b \in B \end{aligned} \tag{12.13}$$

$$\begin{aligned} &\sum_{i\in G} Q_{\mathrm{G}_i} - \left(Q_{\mathrm{L}_b}(s) - \mathrm{DRC}^{Q}_b(s) - \mathrm{LS}^{Q}_b(s) \right) \\ &= \sum_{j\in B} V_b(s) V_j(s) \left| Y_{bj} \right| \sin\left(\delta_b(s) - \delta_j(s) - \theta_{bj} \right) \quad \forall b \in B \end{aligned} \tag{12.14}$$

$$\mathrm{DRC}^{Q}_b(s) = 0.75 * \mathrm{DRC}^{p}_b(s) \quad \forall b \in B \tag{12.15}$$

$$\mathrm{LS}^{Q}_b(s) = 0.75 * \mathrm{LS}^{p}_b(s) \quad \forall b \in B \tag{12.16}$$

$$V^{\min}_b \le V_b(s) \le V^{\max}_b \tag{12.17}$$

$$0 \le P^{+}_{\mathrm{G}_i} \le \mathrm{RU}_{\mathrm{G}_i} \times \tau_{\mathrm{CC}} \quad i \in G_{\mathrm{F}} \tag{12.18}$$

$$0 \le P^{-}_{\mathrm{G}_i} \le \mathrm{RD}_{\mathrm{G}_i} \times \tau_{\mathrm{CC}} \quad i \in G_{\mathrm{F}} \tag{12.19}$$

$$P_{\mathrm{G}_i} = P^{0}_{\mathrm{G}_i} + P^{+}_{\mathrm{G}_i} - P^{-}_{\mathrm{G}_i} \quad i \in G_{\mathrm{F}} \tag{12.20}$$

$$P^{\min}_{\mathrm{G}_i} \le P_{\mathrm{G}_i} \le P^{\max}_{\mathrm{G}_i} \quad i \in G_{\mathrm{F}} \tag{12.21}$$

$$Q_{\mathrm{G}_i}(s) = Q^0_{\mathrm{G}_i} + Q^+_{\mathrm{G}_i}(s) - Q^-_{\mathrm{G}_i}(s) \quad i \in G \tag{12.22}$$

$$Q^{\min}_{\mathrm{G}_i} \le Q_{\mathrm{G}_i}(s) \le Q^{\max}_{\mathrm{G}_i} \quad i \in G \tag{12.23}$$

$$\begin{aligned}&\sum_{i\in G}\widetilde{P}_{\mathrm{G}_i} - \left(P_{\mathrm{L}_b}(s) - \mathrm{DRC}^p_b(s) - \mathrm{LS}^p_b(s)\right)(1+\lambda(s))\\ &= \sum_{j\in B}\widetilde{V}_b(s)\widetilde{V}_j(s)\left|Y_{bj}\right|\cos\left(\widetilde{\delta}_b(s) - \widetilde{\delta}_j(s) - \theta_{bj}\right) \quad \forall b \in B\end{aligned} \tag{12.24}$$

$$\begin{aligned}&\sum_{i\in G}\widetilde{Q}_{\mathrm{G}_i}(s) - \left(Q_{\mathrm{L}_b}(s) - \mathrm{DRC}^Q_b(s) - \mathrm{LS}^Q_b(s)\right)(1+\lambda(s))\\ &= \sum_{j\in B}\widetilde{V}_b(s)\widetilde{V}_j(s)\left|Y_{bj}\right|\sin\left(\widetilde{\delta}_b(s) - \widetilde{\delta}_j(s) - \theta_{bj}\right) \quad \forall b \in B\end{aligned} \tag{12.25}$$

$$\lambda(s) > \lambda_{\text{thershold}} \tag{12.26}$$

$$0 \le \mathrm{DRC}^P_b(s) \le \alpha_b P_{\mathrm{L}_b}(s) \tag{12.27}$$

$$0 \le \mathrm{DRC}^Q_b(s) \le \alpha_b Q_{\mathrm{L}_b}(s) \tag{12.28}$$

$$0 \le \mathrm{LS}^P_b(s) \le (1-\alpha_b-\beta_b)P_{\mathrm{L}_b}(s) \tag{12.29}$$

$$0 \le \mathrm{LS}^Q_b(s) \le (1-\alpha_b-\beta_b)Q_{\mathrm{L}_b}(s) \tag{12.30}$$

$$\widetilde{V}^{\min}_b \le \widetilde{V}_b(s) \le \widetilde{V}^{\max}_b \tag{12.31}$$

The power balance equations for active and reactive power are presented by (12.13) and (12.14). Equations (12.15) and (12.16) present constant power factor for necessary under-voltage load shedding and demand response. Bus voltage limit is indicated by (12.17). Equations (12.18) and (12.19) indicate ramp up and ramp down of power plants. Eqs. (12.21) and (12.23) state the capacity limit of the generators. Satisfied load margin is expressed by (12.26). Eqs. (12.27)–(12.30) indicate limitation of demand response and curtailed load of each bus. Equations (12.24), (12.25), and (12.31) are constraints for voltage collapse point.

12.4 Simulation Results

The proposed method is simulated on the large scale IEEE 118-bus test system. The costs of re-dispatching active and reactive powers of generating units AD_i, AI_i, RD_i, and RI_i are assumed to be 125, 25, 12.5, and 2.5% of the base-case locational marginal price (LMP) of buses connected to the generating units, respectively. The costs of load shedding and demand response at each bus are considered to be 100 and 10 times of LMP of that bus, respectively [12]. 150-MW turbines are connected at nodes17, 30, 59, 80, 92, and 100 [18]. The correlation is equal to 0.88 among the turbine pairs (17, 30), (59, 80), and (92,100) and is set to 0.48 for others [18].

Table 12.1 Grouping of generator buses

Group 1	G1(B1),G2(B4),G3(B6),G4(B8),G5(B10),G6(B12)
Group 2	G7(B15),G8(B18),G9(B19),G53(B113)
Group 3	G10(B24),G11(B25),G12(B26),G32(B72)
Group 4	G13(B27),G14(B31),G15(B32)
Group 5	G16(B34),G17(B36),G18(B40),G19(B42),G20(B46),G21(B49),G22(B54),G23 (B55),G24(B56),G25(B59),G26(B61),G27(B62),G28(B65),G29(B66),G30(B69), G54(B116)
Group 6	G31(B70),G33(B73),G34(B74)
Group 7	G35(B76),G36(B77),G37(B80)
Group 8	G38(B85),G39(B87),G40(B89),G41(B90),G42(B91),G43(B92)
Group 9	G44(B99),G45(B100),G46(B103),G47(B104),G48(B105),G49(B107), G50(B110), G51(B111),G52(B112)

The proposed algorithm is simulated in GAMS and MATLAB environments. The scenarios are generated in MATLAB environment, and voltage instability prevention problem is solved in GAMS software using NLP method.

12.4.1 Partitioning of the System

The IEEE 118-bus test system consists of 54 generating units and 186 transmission lines. The system data are presented in [12]. The proposed method for partitioning the system is applied to the IEEE 118-bus test system. This test system is divided into nine zones based on the algorithm presented in Fig. 12.1. Table 12.1 presents generators of each group. In this table, G7 (B15) means generator number 7 in bus number 15 as an example. Figure 12.4 shows different zones of the mentioned test system.

12.4.2 Scenario Generation and Analysis

Three cases are studied in this section as described in the following:

Case 1: Preventive voltage instability problem is solved under load and wind power generation uncertainties based on the method of references [23, 27] as a simple and unreal condition. Table 12.2 shows generated scenarios in this case.

Case 2: Preventive voltage instability problem is solved under uncorrelated load and wind power generation uncertainties for 20 scenarios.

Case 3: Preventive voltage instability problem which is assumed as a real condition is solved under correlated load and wind power generation uncertainties for 20 scenarios.

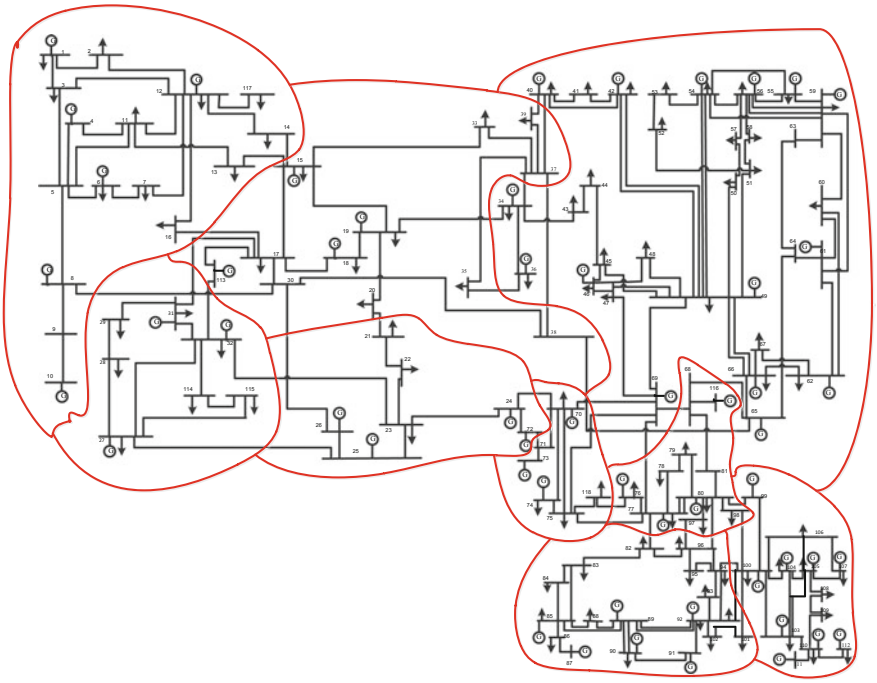

Fig. 12.4 Different zones of IEEE 118-bus test system

Table 12.2 Wind-load scenarios in Case 1

Scenario number	Load (%)	Wind (%)
S1	98	100
S2	100	100
S3	102	100
S4	98	50
S5	100	50
S6	102	50
S7	98	0
S8	100	0
S9	102	0

The number of proposed scenarios for wind power and loads are 4 and 5 in Cases 2 and 3, respectively. Hence, total 20 wind-load correlated scenarios are generated in this section based on the explanations provided in Sect. 12.2.

The total wind power scenarios and total load scenarios are shown in Figs. 12.5 and 12.6 for Cases 1, 2, and 3, respectively. Considering these figures, total load variation in Case 3 is greater than that of Case 2.

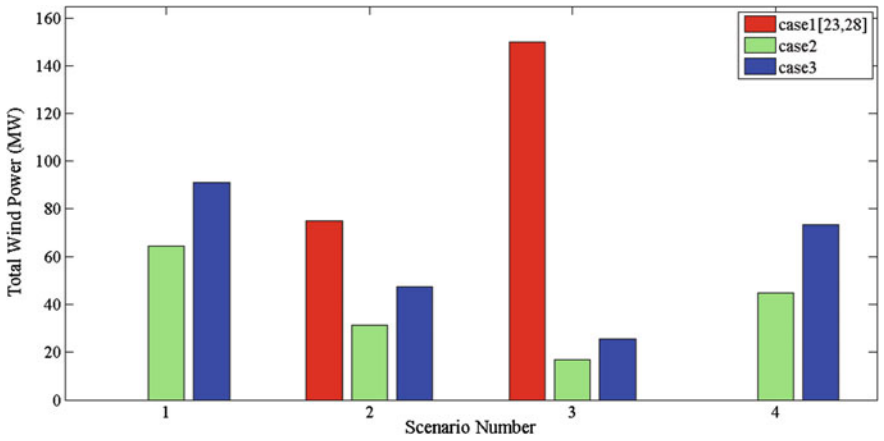

Fig. 12.5 Total wind power for each scenario in Cases 1, 2, and 3

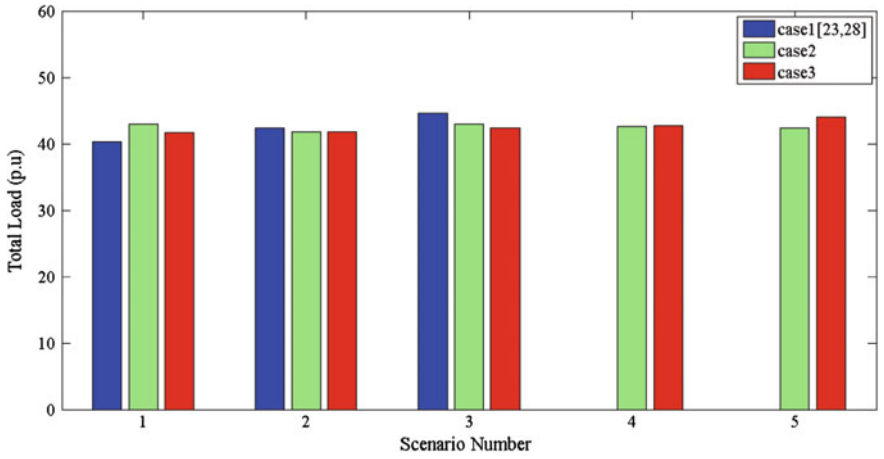

Fig. 12.6 Total load for each scenario in Cases 1, 2, and 3

The value of objective function is $4427.1 for Case 1. In this case, load shedding is not necessary. The value of demand response for nine scenarios is shown in Table 12.3 for Case 1. Objective function for 20 scenarios is $4896.4 for Case 2. Load shedding is not necessary in the 20 proposed scenarios. The value of demand response for 20 scenarios is shown in Table 12.4 for Case 2. In Case 3, objective function for 20 scenarios is $8178.7. In this case, load shedding is not necessary. The value of demand response for 20 scenarios is shown in Table 12.5 for Case 3.

The value of demand response for 9 scenarios in Case 1 and for 20 scenarios in Cases 2 and 3 are compared in Fig. 12.7. Considering this figure, for most scenarios, the value of demand response in Case 3 is greater than the value of demand response

Table 12.3 Values of demand response for 9 scenarios in Case 1

Scenario number	Demand response (p.u.)
1	0
2	0
3	0.7948
4	0
5	0
6	0.7766
7	0
8	0
9	0.7585

Table 12.4 Values of demand response for 20 scenarios in Case 2

Scenario number	Demand response (p.u.)	Scenario number	Demand response (p.u.)
1	0	11	0.062
2	0	12	0
3	0.0937	13	0.2846
4	0	14	0
5	0	15	0
6	0	16	0
7	0	17	0
8	0.1654	18	0
9	0	19	0
10	0	20	0

Table 12.5 Values of demand response for 20 scenarios in Case 3

Scenario number	Demand response (p.u.)	Scenario number	Demand response (p.u.)
1	0	11	0.1418
2	0	12	0
3	0	13	0
4	0	14	0
5	1.6424	15	1.7924
6	0.0822	16	0
7	0	17	0
8	0	18	0
9	0	19	0
10	1.7334	20	1.5844

in Cases 1 and 2. As a result, objective function in Case 3, as a real case, is greater than that in Cases 1 and 2.

Actual system loads and wind powers have correlation based on weather conditions and location. Hence, the correlation among loads and wind powers must be

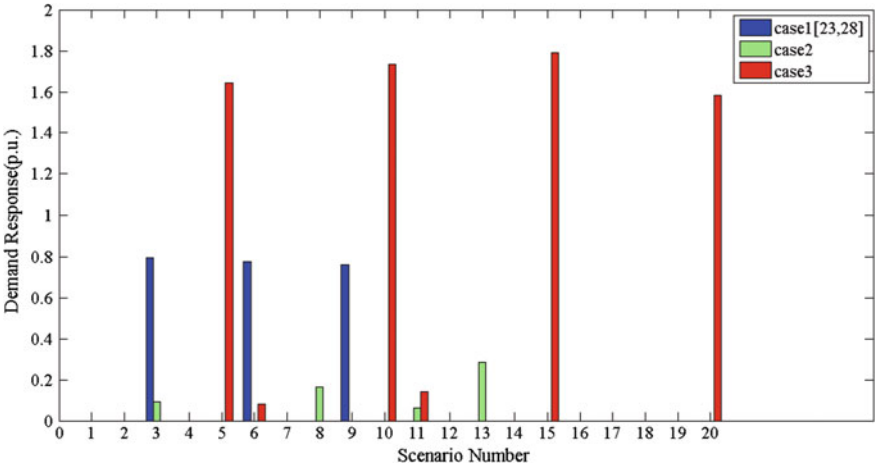

Fig. 12.7 Demand response value in Cases 1, 2, and 3

Table 12.6 Summary of the simulation results

	Total demand response (p.u.)	Objective function($)
Case 1 [23, 27]	2.328	4427.1
Case 2	0.6057	4896.4
Case 3	6.9766	8178.7

considered to model the actual condition. Considering these correlations, the cost of preventive actions is increased, based on the results of simulations. Therefore, if these correlations are not considered, the cost of preventive actions is underestimated. This fact illustrates the necessity of accurate load and wind power modeling in voltage stability evaluation.

12.4.3 Summary of Simulation Results

In this section, the simulation results are summarized to illustrate the necessity of correlation modeling. The results are presented in Table 12.6. According to Table 12.6, a noticeable difference in values of total demand response and objective function in Case 3 indicates the necessity of correlated load and wind power modeling in preventive voltage instability problem.

12.5 Conclusion

A new stochastic optimal preventive voltage stability control is presented in this chapter under correlated wind power and load uncertainties. Correlation matrix for wind turbine and loads are defined based on electrical distance and partitioning of the power system. Then, scenarios are generated and voltage instability prevention problem is solved. The control facilities in the proposed problem are classified into two categories. They are named here-and-now and wait-and-see. A new algorithm is presented to simulate real condition of power system. The proposed method is tested on the 118-bus IEEE standard test system. The system is simulated for three cases: wind and load uncertainties modeling based on previous research works, uncorrelated wind and load uncertainties, and correlated wind and load uncertainties. Case 3 is assumed close to the actual condition due to correlation among wind turbine powers and loads in real power systems. The analysis indicates higher cost of preventive actions for real conditions. In other words, to obtain realistic results for the cost of voltage instability prevention, both uncertainty and correlation among wind turbines powers and loads must be considered, according to the proposed method of this chapter.

References

1. IEEE/CIGRE Joint Task Force on Stability Terms & Definitions, ed. by P. Kundur (2002)
2. L.D. Arya, P. Singh, L.S. Titare, Differential evolution applied for anticipatory load shedding with voltage stability considerations. Int. J. Electr. Power Energy Syst. **42**(1), 644–652 (2012)
3. J. Deng, J. Liu, A study on a centralized under-voltage load shedding scheme considering the load characteristics, in *International Conference on Applied Physics and Industrial Engineering* (2012), pp. 481–489
4. Y. Wang, I.R. Pordanjani, W. Li, W. Xu, E. Vaahedi, Strategy to minimise the load shedding amount for voltage collapse prevention. IET Gener. Transm. Distrib. **5**(3), 307–313 (2011)
5. T. Amraee, A.M. Ranjbar, R. Feuillet, Adaptive under-voltage load shedding scheme using model predictive control. Electr. Power Syst. Res. **81**(7), 1507–1513 (2011)
6. A. Saffarian, M. Sanaye-Pasand, Enhancement of power system stability using adaptive combinational load shedding methods. IEEE Trans. Power Syst. **26**(3), 1010–1020 (2011)
7. H. Seyedi, M. Sanaye-Pasand, New centralized adaptive load-shedding algorithms to mitigate power system blackouts. IET Gener. Transm. Distrib. **3**(1), 99–114 (2009)
8. H. Seyedi, M. Sanaye-Pasand, Design of new load shedding special protection schemes for a double area power system. Am. J. Appl. Sci. **6**(2), 317–327 (2009)
9. M. Sanaye-Pasand, H. Seyedi, Centralized adaptive load shedding methods to enhance power system voltage stability margins. IEEJ Trans. Electr. Electron. Eng. **3**(6), 669–679 (2008)
10. G. Verbic, F. Gubina, A new concept of protection against voltage collapse based on local phasors, in *International Conference on Power System Technology* (2000), pp. 965–970
11. I. Šmon, M. Pantoš, F. Gubina, An improved voltage-collapse protection algorithm based on local phasors. Electr. Power Syst. Res. **78**(3), 434–440 (2008)
12. A. Rabiee, M. Parvania, M. Vanouni, M. Parniani, M. Fotuhi-Firuzabad, Comprehensive control framework for ensuring loading margin of power systems considering demand-side participation. IET Gener. Transm. Distrib. **6**(12), 1189–1201 (2012)

13. F. Karbalaei, M. Kalantar, A. Kazemi, On line diagnosis of capacitor switching effect to prevent voltage collapse. Energy Convers. Manag. **51**(11), 2374–2382 (2010)
14. H. Raoufi, M. Kalantar, Reactive power rescheduling with generator ranking for voltage stability improvement. Energy Convers. Manag. **50**(4), 1129–1135 (2009)
15. A. Maleki, M. Gholipour Khajeh, M. Ameri, Optimal sizing of a grid independent hybrid renewable energy system incorporating resource uncertainty and load uncertainty. Int. J. Electr. Power Energy Syst. **83**, 514–524 (2016)
16. D. Neves, M.C. Brito, C.A. Silva, Impact of solar and wind forecast uncertainties on demand response of isolated microgrids. Renew. Energy **87**(2), 1003–1015 (2016)
17. A.M. Abd-el-Motaleb, S. Kazem Bekdach, Optimal sizing of distributed generation considering uncertainties in a hybrid power system. Int. J. Electr. Power Energy Syst. **82**, 179–188 (2016)
18. C.S. Saunders, Point estimate method addressing correlated wind power for probabilistic optimal power flow. IEEE Trans. Power Syst. **29**(3), 1045–1054 (2014)
19. S. Shargh, B.K. Ghazani, B. Mohammadi-ivatloo, H. Seyedi, M. Abapour, Probabilistic multi-objective optimal power flow considering correlated wind power and load uncertainties. Renew. Energy **94**(1), 10–21 (2016)
20. A.H. Shahirinia, E.S. Soofi, D.C. Yu, Probability distributions of outputs of stochastic economic dispatch. Int. J. Electr. Power Energy Syst. **81**, 308–316 (2016)
21. B. Hu, W. Lei, M. Marwali, On the robust solution to SCUC with load and wind uncertainty correlations. IEEE Trans. Power Syst. **29**(6), 2952–2964 (2014)
22. P. Samadi, H. Mohsenian-Rad, W.W. Vincent, R. Schober, Tackling the load uncertainty challenges for energy consumption scheduling in smart grid. IEEE Trans. Smart Grid **4**(2), 1007–1016 (2013)
23. A. Rabiee, A. Soroudi, B. Mohammadi-Ivatloo, M. Parniani, Corrective voltage control scheme considering demand response and stochastic wind power. IEEE Trans. Power Syst. **29**(6), 2965–2973 (2014)
24. H. Li, L. ZhenZhou, X. Yuan, Nataf transformation based point estimate method. Chin. Sci. Bull. **53**(17), 2586–2592 (2008)
25. J. Zhong, E. Nobile, A. Bose, K. Bhattacharya, Localized reactive power markets using the concept of voltage control areas. IEEE Trans. Power Syst. **19**(3), 1555–1561 (2004)
26. W. Li, R. Billinton, Effect of bus load uncertainty and correlation in composite system adequacy evaluation. IEEE Trans. Power Syst. **6**(4), 1522–1529 (1991)
27. S.M. Mohseni-Bonab, A. Rabiee, B. Mohammadi-ivatloo, Voltage stability constrained multi-objective optimal reactive power dispatch under load and wind power uncertainties: a stochastic approach. Renew. Energy **85**(1), 598–609 (2016)

Index

S. Nojavan, K. Zare (eds.), *Demand Response Application in Smart Grids*,
https://doi.org/10.1007/978-3-030-32104-8